MODELING OF TRANSPORT PHENOMENA

IN REVERSE OSMOSIS MEMBRANES

by

© HUSSEIN MEHDIZADEH, M.A.Sc.

A Thesis

Submitted to the School of Graduate Studies

in Partial Fulfillment of the Requirements

for the Degree

Doctor of Philosophy

in

Chemical Engineering

McMaster University, CANADA

February, 1990

MODELING OF TRANSPORT PHENOMENA

IN REVERSE OSMOSIS MEMBRANES

DOCTOR OF PHILOSOPHY (1990)   McMaster University
(Chemical Engineering)   Hamilton, Ontario, Canada

TITLE: Modeling of Transport Phenomena
                            in Reverse Osmosis Membranes

AUTHOR: Hussein Mehdizadeh
                            B.Sc.   (Tehran Polytechnic)
                            M.A.Sc.   (University of Waterloo)

SUPERVISOR: Dr. James M. Dickson
                            (Chemical Engineering)

NUMBER OF PAGES: xxiii, 356

ABSTRACT

The present research investigates, both theoretically and experimentally, transport phenomena in reverse osmosis (RO) membranes.

In order to properly describe and predict RO membrane performance, and to properly design RO units, a good understanding of the fundamentals of the membrane transport is needed; this means that a strong transport model needs to be developed. This research is concerned with the development of such a model. As well, the effects of system pressure, concentration, and temperature on the performance of thin-film composite, aromatic polyamide RO membranes with sodium chloride and some other salts are examined both experimentally and theoretically.

The present research investigates the development of a powerful, novel transport model for reverse osmosis, which does not have the serious shortcomings of the previous models, and an experimental evaluation of this model. As a result, a mechanistic model, called the Modified Surface Force-Pore Flow (MD-SF-PF) model, has been developed. The model assumes that transport through the membrane takes place in very fine pores, and the pores are modeled as perfect cylinders. In this two-dimensional model, a balance of applied and frictional forces acting on the solute in a pore is given as a function of radial and axial positions. The model incorporates a potential field inside the membrane which is responsible for the partitioning effect (at the two sides of the membrane) and, in part, determines the membrane performance. A computer code has been developed, based on the "orthogonal collocation" method of weighted residuals, which has proven to be very efficient and precise to solve the complicated differential equations of the transport models.

Three models have been developed during the present research: i) the Modified Surface Force- Pore Flow (MD-SF-PF) model, briefly described above, which is appropriate for solvent-membrane affinity systems (such as salt-water systems); a temperature-extended version of this model has also been derived; ii) the Extended MD-SF-PF model (a generalized form of the MD-SF-PF model) which can be used to describe or predict any type of RO system, that is, both solvent-membrane affinity systems, such as sodium chloride-water system, and solute-membrane affinity systems, such as toluene-water system; and iii) the Modified Finely Porous Model (MD-FPM) which is a one-dimensional transport model, and can describe simple systems.

Experimental data are used to determine model parameters. Also, experimental data can be compared to model predictions. The following experimental plan was undertaken using aromatic polyamide (FilmTec) FT30 membranes: i) experiments with 2000 ppm aqueous solutions of sodium chloride (brackish water concentration) in the range 350-7000 kPa and 5-60°C (a few experiments at 25°C and 5000, 10 000, and 15 000 ppm sodium chloride solutions were also performed (Phase I)); ii) experiments with 2000 ppm potassium chloride, lithium chloride, and lithium nitrate at 25°C and 500-4000 kPa (Phase II); and iii) experiments with 35 000 ppm sodium chloride (sea water concentration) at 4000-7000 kPa and 5-60°C (Phase III).

Model parameters were determined from the data of Phase I at 25°C, using a nonlinear optimization routine. The average pore radii for the SW30HR and BW30 types of FT30 membranes were determined at about 1.0 and 1.2 nm, respectively. All the experimental data at other pressures and concentrations are well predicted by the MD-SF-PF model. Somewhat fortuitously, the MD-SF-PF model also predicts well for the other 1-1 electrolytes.

Temperature effects are reasonably predicted by the temperature-extended MD-SF-PF model. The apparent activation energies for pure water permeability for the SW30HR and BW30 membranes are about 25 400 and 22 500 kJ/kmol at 5-40°C, respectively, and about 18 100 and 13 000 kJ/kmol at 40-60°C, respectively. Compaction, which becomes more severe as temperature or pressure is increased, has no effect on predicting the membrane separation or flux ratio (the ratio of total solution flux to pure solvent flux). An empirical model for compaction has also been developed and used to correct the flux ratio to the absolute values of permeation fluxes.

The Extended MD-SF-PF model has been found to well describe the difficult case of strong solute-membrane affinity, in which solute molecules are attracted toward the membrane rather than being rejected. The model implies that once the solute is rapidly sorbed into the membrane the solute molecules creep slowly adjacent to the wall of the membrane pores.

Overall, the family of the MD-SF-PF models has been found to predict RO membrane performance over a wide range of operating conditions. The agreement between the experimental data and model predictions supports, but does not prove, the proposed transport mechanism. In principle, the family of the MD-SF-PF models can be used for different research purposes including membrane development and RO module design.

ACKNOWLEDGEMENT

Dedicated to the memory of my teachers:

Allammeh Tabatabaee

and

Ostad Motahharry

shall the peace be upon them.

TABLE OF CONTENTS

LIST OF FIGURES

LIST OF TABLES

LIST OF ABBREVIATIONS

BW30	Brackish-Water type FT30 membrane
dof	degrees of freedom (statistic)
ESD	Extended Solution- Diffusion (Model)
FPM	Finely Porous Model
FPM-3 (or 4)	The 3 (or 4)- parameter version of FPM
FT30	A commercial RO membrane (FilmTec Corporation)
GFD	Gallons per square feet per day (unit of flux)
IT	Irreversible Thermodynamics
IT-PT	Irreversible Thermodynamics - Phenomenological Transport (Model)
KS	Kedem-Spiegler (Model)
KSA	Kimura-Sourirajan Analysis
MD-FPM	Modified Finely Porous Model
MD-FPM-3 (or 4)	The 3 (or 4) - parameter version of MD-FPM
MD-SF-PF	Modified Surface Force-Pore Flow (Model)
ODE	Ordinary Differential Equation
ORR	Onsager Reciprocal Relationship
PDE	Partial Differential Equation
PS-CF	Preferential Sorption-Capillary Flow (Mechanism)
PT	Phenomenological Transport (Models)
RO	Reverse Osmosis
SD	Solution-Diffusion (Model)
SDI	Solution-Diffusion Imperfection (Model)
SEM	Scanning Electron Microscopy
SF-PF	Surface Force-Pore Flow (Model)
SSQ	Sum of the Squares (statistic)
SW30HR	Sea Water-High Rejection type FT30 membrane
TDS	Total Dissolved Solid
UF	Ultrafiltration
Var(Res.)	Variance of the Residuals (statistic)

CHAPTER 1

INTRODUCTION

The present chapter gives an introduction to the state-of-the-art area of mathematical modeling for the separation process reverse osmosis, which is, then, followed by a description of the objectives in this research. Finally, an outline of the dissertation is presented.

1.1   The Reverse Osmosis Separation Process

Invented about 30 years ago, reverse osmosis (RO) has become a standard unit operation in Chemical Engineering. Today, this membrane separation process has found a wide variety of applications such as: desalination of sea water and brackish water, treatment of municipal and industrial wastes, concentration of food products, recovery of protein in the dairy industry, production of ultra-pure water for many applications including the semi-conductor industry, and recovery of valuable materials in chemical and petrochemical industries (Applegate, 1984; Slater et al., 1983; Sourirajan, 1970, and 1977).

RO and other membrane processes, such as ultrafiltration (UF), are attractive because they are simple, can be applied to a variety of problems in different fields, are economically competitive, and require no phase change. The last feature is particularly important for solutions which are sensitive to heating, such as food products and pharmaceutical materials.

The beginning idea, which led to reverse osmosis, started in the early 1950's at the University of California at Los Angeles (UCLA), where Professor Samuel T.

Yuster conceived the idea of using the Gibb's adsorption equation as a guideline to find techniques for producing fresh water from brackish and sea water (Sourirajan, 1970, and 1986). According to Gibb's equation, a relatively pure water layer should exist at the interface of brine and air (or any other hydrophobic surface) which could be skimmed off and, hence, fresh water could be produced. At the beginning, the application of the idea was difficult and unsuccessful until solid-liquid (rather than liquid-gas) interface was examined. The original idea was to let pure water form at the solid-liquid interface and then skim the water off by forcing the interfacial water to flow, under a high pressure, through the pores of the solid. At this time, the first successful test was performed using a flat plastic film, supported by a porous plate, in 1958 at UCLA (Yuster et al., 1958; Loeb, 1981; Sourirajan, 1986). Independently, about the same time, Breton and Reid did the first successful RO tests using cellulose acetate membranes and sea water, at the University of Florida (Breton, 1957; Reid and Breton, 1959). However, at that time, the permeation flux of water was extremely low (about a few drops per week) and, therefore, the process was not practical for industrial and society needs. The breakthrough, which made reverse osmosis commercially attractive, happened around 1958 when Loeb and Sourirajan made the first asymmetric cellulose acetate membrane (Loeb and Sourirajan, 1962); the membrane was not a homogeneous (uniform) membrane as before but was made of a thin skin layer, which was as dense as the previous homogeneous membranes, and a porous support layer. In the Loeb-Sourirajan membrane, significant fluxes could be obtained since the flow resistance, in the asymmetric membranes, was much smaller than in the homogeneous membranes.

Today, the technology has flourished, from the lab scale, to large industrial plants, and more applications are discovered each year for RO in different academic, industrial, and research centres throughout the world.

In order to describe properly the performance of a RO membrane, mathematical models are needed which can later be used for proper design of RO units. This demand has led to the development of several transport models (Soltanieh and Gill, 1981; Dickson and Mehdizadeh, 1988, and 1989). The general purpose of a transport model is to relate the membrane performance, usually expressed as permeation flux and separation (i.e., percentage of solute removal from feed solution), to the operating conditions (such as pressure or feed concentration) or the driving forces (usually pressure and concentration gradients) through some coefficients (know as phenomenological transport coefficients) which include the model parameters. The coefficients, or the parameters, must be determined from experimental data. The success of a model can be measured in terms of the ability of the model to describe mathematically the data with coefficients (or parameters) that are reasonably constant over the range of operating conditions. Ultimately, the model with the determined transport coefficients (or parameters) can describe the performance of a membrane over a wide range of operating conditions. This ability to predict the performance is the true power of a transport model. This can be used, in part, to eliminate the high costs of experimentation. Combined with a research program in membrane making, this can lead to better design criteria for tailor making membranes, and combined with a process design program can lead to a more logical scaleup for RO systems.

1.2 Objectives

The present research has the following three objectives:

i) Development of a general transport model with fewer assumptions than those in the existing models which can achieve true predictions of RO membrane performance.

ii) Investigation and modeling of temperature effects on the performance of RO membranes.

iii) Development of an efficient and precise numerical code which can solve the complicated differential equations of membrane transport models.

The above objectives, aimed at a better understanding of transport phenomena in RO membranes, are achieved by a procedure which includes mathematical modeling, experimentation, model optimization, parameter estimation, model predictions (by a computer code), and comparisons between theory and experimental data.

1.3 Dissertation Outline

The present dissertation includes 7 Chapters and 6 Appendices. In Chapter 1, the objectives of the research are defined after a short introduction of RO separation process. Chapter 2 is a literature review of several fundamental aspects of the reverse osmosis separation process including: mass transfer, transport mechanisms, transport models, temperature effects, and the numerical technique of orthogonal collocation.

Chapter 3 presents the mathematical models derived, including the transport models of: Modified Surface Force-Pore Flow (MD-SF-PF), Extended MD-SF-PF, and Modified Finely Porous Model (MD-FPM). The modeling of temperature effects is discussed as well as the application of orthogonal collocation to the transport models.

Chapter 4 details the experimental plan in three parts: Phases I, II, and III. The RO testing equipment is described and the general experimental procedure is presented. The system parameters are defined and the procedures are outlined.

In Chapter 5, the experimental and the theoretical results obtained are discussed. The performance of each model is evaluated. The experimental data are compared with the models predictions where applicable.

And, finally, an overview of the final conclusions of the present research and some recommendations for future research are presented in Chapters 6 and 7, respectively.

Appendices A and B are devoted to some basic mathematical derivations in the Extended MD- SF-PF and MD-FPM models, respectively, for the interested reader. Appendices C, D, and E present the experimental data for all the experiments in Phases I, II, and III, respectively, and Appendix F presents the computer code for optimising the parameters for the MD-SF-PF model.

CHAPTER 2

LITERATURE REVIEW

This chapter is an introduction to the fundamentals of transport phenomena in reverse osmosis (RO) membranes. First, the basic concepts are described in Section 2.1. Then, an introduction is given to RO membranes in Section 2.2. The transport mechanisms and some important transport models are discussed in Section 2.3, and reverse osmosis system design is discussed, shortly, in Section 2.4.

In Section 2.5, temperature effects on RO membrane performance is reviewed, and, finally, the "orthogonal collocation" method of weighted residuals is discussed in Section 2.6.

2.1   Fundamentals of Membrane Mass Transfer

This section encompasses the basic definitions and concepts used frequently in RO literature and the present dissertation.

2.1.1   Osmosis, osmotic pressure, and reverse osmosis

When a semi-permeable membrane (i.e., one that is permeable to solvent but not to solute) is placed between two compartments, one containing pure solvent and the other containing a solution (the solvent plus a solute), the solvent permeates through the membrane to the solution side. This phenomenon, which is called "osmosis" (see Figure 2.1.a), happens because the system seeks thermodynamic equilibrium. The chemical potential of the pure solvent is higher than that of the solvent in the solution side so that solvent flows to the solution side to try to restore equilibrium.

6
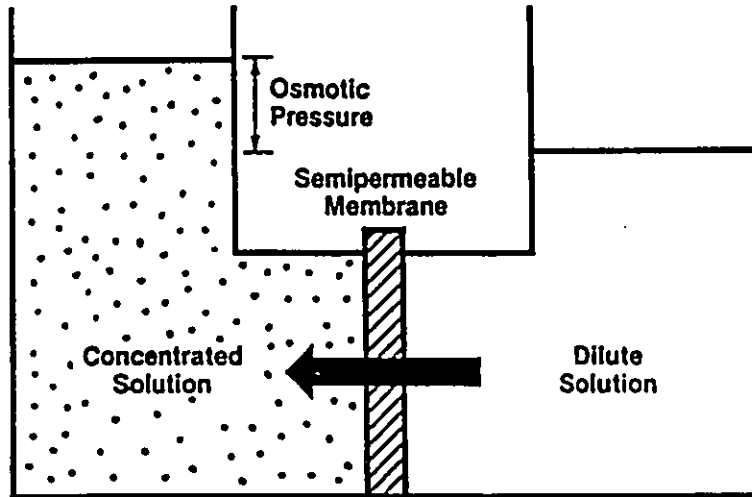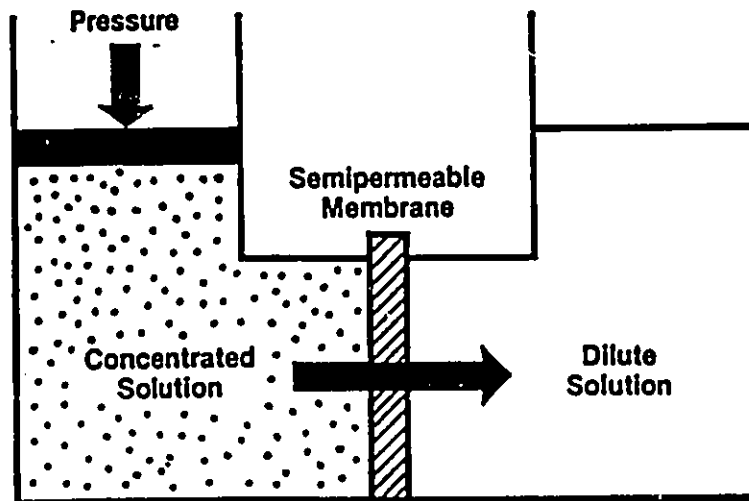
Figure 2.1:   (a) Osmosis, osmotic pressure, and (b) reverse osmosis (Applegate, 1984).

In an apparatus, such as depicted in Figure 2.1, the equilibrium is achieved when there is no net solvent flow through the membrane. The pressure head developed on the solution side is known as the "osmotic pressure" (Figure 2.1.a), which is a thermodynamic property of the solution and independent of the membrane. When a pressure greater than the osmotic pressure is applied to the solution side, increasing the chemical potential, the solvent flow reverses from the solution side to the pure solvent side; the phenomenon is known as "reverse osmosis" or RO as shown in Figure 2.1.b (Applegate, 1984). For a real membrane, some solute may be transported through the membrane and, therefore, the osmotic pressures of the solutions on both sides of the membrane should be considered in modeling. An "effective pressure driving force" across the membrane can be defined as the applied pressure difference, ΔP, minus the osmotic pressure difference, $\Delta \pi$, across the membrane. For most models, the solvent flux, N_B, is considered to be proportional to the effective pressure driving force, $(\Delta p - \Delta \pi)$.

The osmotic pressure of a solution, π, is related to the mole fraction and the partial molar volume of the solvent as (Daniels and Alberty, 1972):

$$\pi = - \frac{RT}{v_B} \ell n \, X_B \qquad (2.1)$$

For dilute solutions, Eqn.(2.1) simplifies to van't Hoff equation (e.g., Sourirajan, 1970; Daniels and Alberty, 1972):

$$\pi = C_A RT \qquad \text{for nondissociable solutes} \qquad (2.2a)$$

$$\pi = (v^+ + v^-)C_A RT \qquad \text{for dissociable solutes} \qquad (2.2b)$$

It is preferable to use experimental values of osmotic pressures, which can be found, for different solutions, in various references (e.g., Stoughton and Lietzke, 1965; Sourirajan, 1970; Weast, 1975).

2.1.2   Driving forces for reverse osmosis

In reverse osmosis, the main driving forces are pressure and concentration gradients which lead to permeation flux of solvent and solute, respectively. The cross influence of solute concentration driving force on solvent flux is represented by the osmotic pressure term in the solvent flux equation (see the "effective pressure driving force" in Section 2.1.1). The cross influence of pressure driving force on solute flux is often small, for high separation membranes, and is usually neglected; when included this effect is described by the Staverman (or reflection) coefficient, σ, (Staverman, 1951). When the Staverman coefficient is taken into account, the equation of solvent flux is written, in most models (e.g., Burghoff et al., 1980; Staverman, 1983), as:

$$N_B = A[\Delta P - \sigma(\pi_2 - \pi_3)] \tag{2.3}$$

where A is the solvent permeability coefficient.

The Staverman coefficient, σ, is a separation characteristic of the membrane which can hold values in the range $0 \leq \sigma \leq 1$. The closer the σ is to the unity, the higher the membrane separation; therefore, $\sigma = 0$ corresponds to a membrane with very little solute rejection, and $\sigma = 1$ corresponds to a membrane with complete solute rejection.

2.1.3   Membrane performance and concentration polarization

Membrane performance is usually characterized in terms of "permeation flux" and "separation". The flux is the rate of material transported per unit membrane area, and separation is the fractional concentration reduction of solute from feed stream (that is, the high-pressure side solution) as compared with permeate stream (that is, the low-pressure side solution).

Separation, f (which is sometimes called "rejection" or "retention" in the literature), is defined in terms of the feed bulk molality, m_{A1}, and the permeate molality, m_{A3}, (Sourirajan, 1970):

$$f = \frac{m_{A1} - m_{A3}}{m_{A1}} \tag{2.4}$$

For moderately dilute solutions, the molal concentration, m_{Ai}, can be approximated by molar concentration, C_{Ai}, and Eqn.(2.4) be written as:

$$f = \frac{C_{A1} - C_{A3}}{C_{A1}} \tag{2.5}$$

Alternatively, separation can be defined in terms of the concentration of the boundary-layer solution just outside the membrane on the high-pressure side, C_{A2}. This separation, f', called the "theoretical separation", is written, for moderately dilute solutions, as:

$$f' = \frac{C_{A2} - C_{A3}}{C_{A2}} \tag{2.6}$$

The boundary-layer concentration, C_{A2}, may differ from the feed bulk concentration, C_{A1}, due to a phenomenon called "concentration polarization". The polarization effect happens because as solute is rejected by the membrane the solute concentration increases near the membrane; this case, which is called the "solvent-membrane affinity" case, has been depicted in Figure 2.2. Compared to the solvent-membrane affinity case is the "solute-membrane affinity" case in which the solute molecules are attracted, rather than rejected, by the membrane; this case, discussed in Section 2.3.3, is depicted in Figures 2.3 and 2.4 for positive and negative separations, respectively. At steady state, C_{A2} does not vary with time and the "film theory" (Bird et al., 1960) is employed to describe the concentration polarization effect. A material balance for
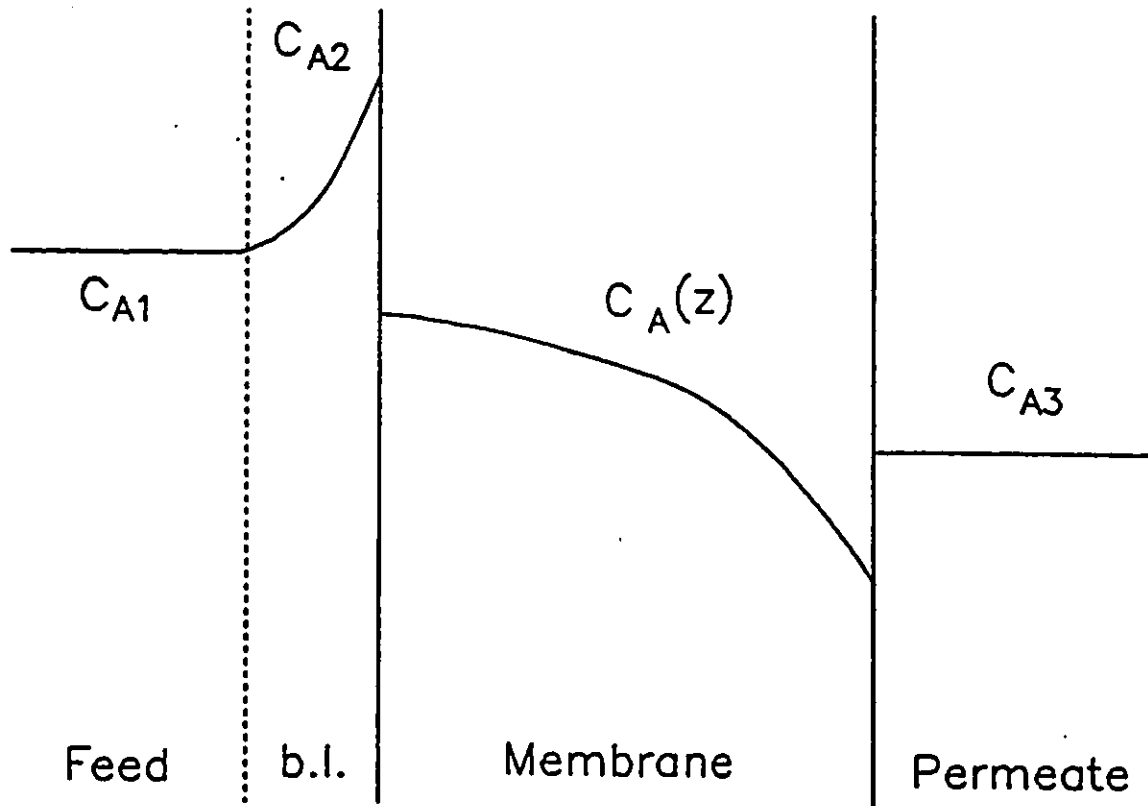
Figure 2.2:   Partitioning effect in a solvent-membrane affinity system (e.g.,
NaCl-water-cellulose acetate membrane).

$$C_A(z)$$

$$C_{A2}$$

$$C_{A1}$$

$$C_{A3}$$

Feed | b.l. | Membrane | Permeate
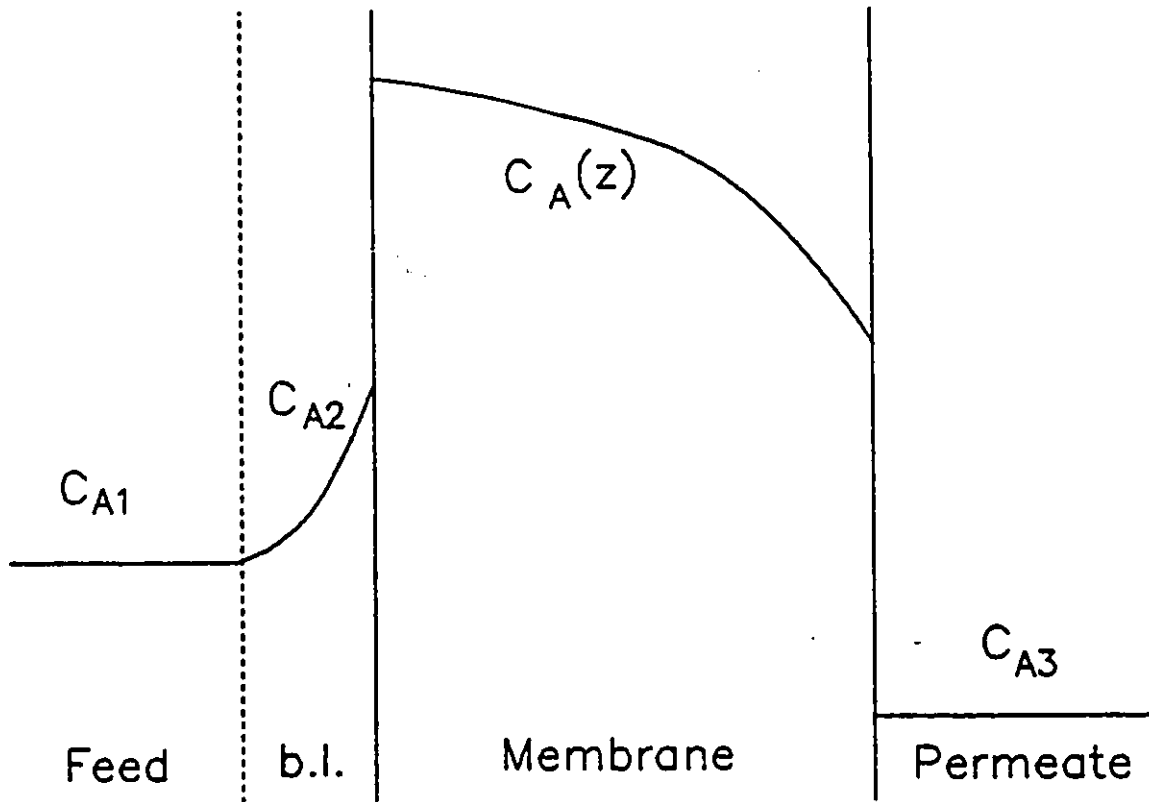
Figure 2.3: Partitioning effect in a solute-membrane affinity system with positive separation (e.g., toluene-water-cellulose acetate membrane).
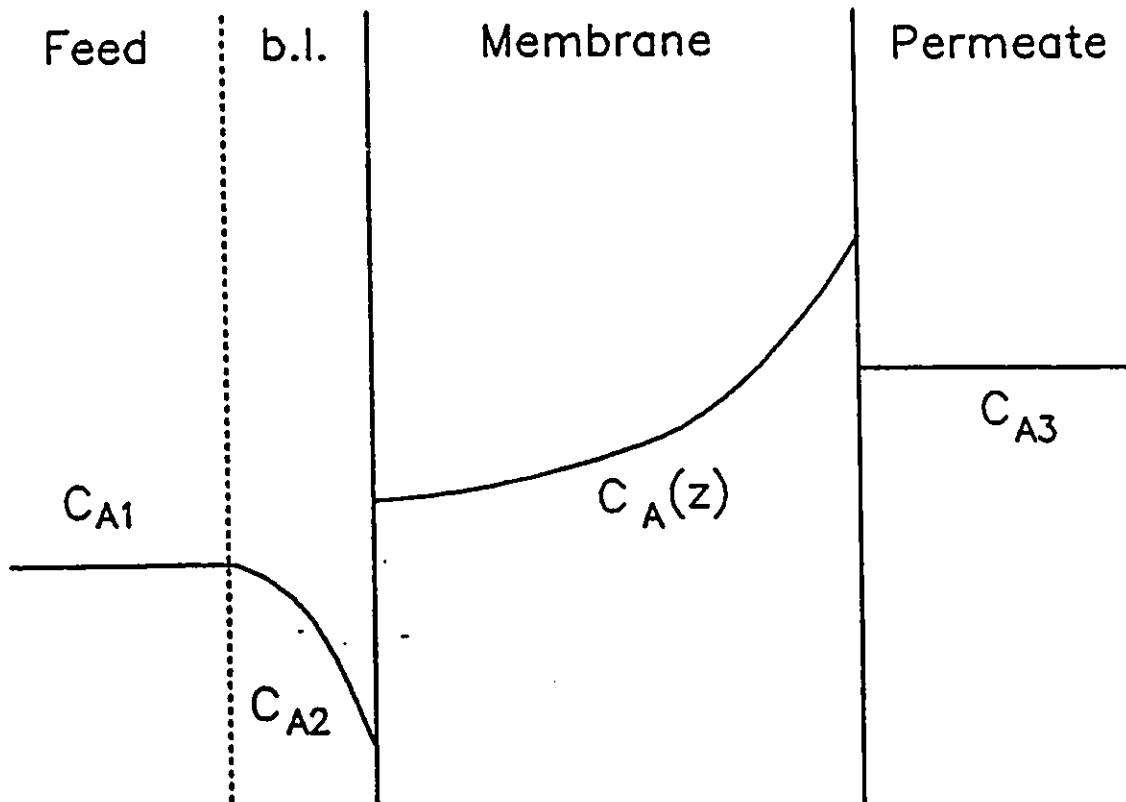
Figure 2.4:   Partitioning effect in a strong solute-membrane affinity system with negative separation (e.g., p-chlorophenol-water-cellulose acetate membrane).

solute across the membrane yields a form of Fick's first law which upon integration leads to:

$$C_{A2} = C_{A3} + (C_{A1} - C_{A3})e^{(J_v/k)}$$ (2.7)

where k is the mass transfer coefficient, a characteristic of the boundary layer (Sourirajan, 1970). As mixing on the high-pressure side of the membrane is increased, Equation (2.7) predicts that the mass transfer coefficient increases reducing the polarization effect (i.e., C_{A2} approaches C_{A1}). At infinite mixing (i.e., $k \to \infty$) f' approaches f; therefore, f' is the theoretical separation that would be measured with perfect mixing on the high-pressure side of the membrane (Sourirajan, 1970). Concentration polarization is an undesirable effect. As the polarization effect grows larger the boundary-layer concentration increases, the osmotic pressure increases, and, therefore, the effective pressure driving force $(\Delta P - \Delta \pi)$ decreases; hence the solvent flux decreases (see Eqn.(2.3)).

The mass transfer coefficient, k, is a function of feed flow rate, cell geometry, and solute system. Generalized correlations of mass transfer coefficient suggest that the Sherwood number, Sh, is related to the Reynolds, Re, and Schmidt, Sc, numbers (Sourirajan, 1970) as:

$$Sh = a' Re^{b'} Sc^{1/3}$$ (2.8)

where a' and b' are parameters to be determined experimentally.

For a fixed flow rate and cell geometry, Eqn.(2.8) implies that k varies as a function of solute diffusivity to the 2/3 power, since the Reynolds number cancels out and the Schmidt number is inversely proportional to the solute diffusivity. Rewriting Eqn.(2.8) with respect to a reference solute at the same experimental conditions gives (Sourirajan, 1970):

$$k = k_{ref} \left(\frac{D_{AB}}{D_{AB,ref}} \right)^{2/3}$$ (2.9)

Therefore, if k is known for a reference solute, then k for any other solute can be estimated using Eqn.(2.9) provided the operating conditions are the same.

An important relationship in RO transport theory, which is used in many transport models, is the relationship between the solute and solvent fluxes. These two fluxes are related to the permeate concentration by an overall material balance as:

$$C_{A3} = C \frac{N_A}{N_A + N_B} \qquad (2.10)$$

The equations shown above, Eqns.(2.2) to (2.10), are extensively referred to during the rest of this dissertation.

2.2   Reverse Osmosis Membranes and Membrane Modules

Original RO membranes were homogeneous (i.e., with an isotropically dense layer) so that water permeation flux was extremely low due to the large flow resistance produced by the homogeneous thickness of the membrane (Reid and Breton, 1959).

The success of the RO process is due to a large extent by the development of an "asymmetric membrane", originally developed by Loeb and Sourirajan (Loeb and Sourirajan, 1962). An asymmetric membrane is fabricated to give a relatively ultrathin, dense surface layer supported underneath by a much thicker, porous layer. The asymmetric structure is a direct consequence of the casting procedure used. When a polymer solution is cast on a flat surface, the evaporation of the solvent produces a surface skin. Subsequent gelation in cold water fixes the structure; the porous layer is formed by the replacement of the solvent by the nonsolvent water (e.g., Sourirajan, 1970). Scanning electron microscopy (SEM) indicates that three layers exist in an asymmetric membrane: a relatively dense surface skin, a transition layer, and a

porous support layer (Kesting, 1985). The transition layer is intermediate in both density and position with respect to the other two layers. Most of the resistance to mass transfer through the membrane exists in the surface skin. Therefore, it may be assumed that the membrane performance is dependent primarily on the chemical nature and physical structure of the surface skin.

A relatively new generation of membranes, which belong to the family of asymmetric membranes, are the "thin-film composite" membranes. These membranes have a similar structure to asymmetric membranes except that the two layers are fabricated separately: the porous support is fabricated first, from one polymer material, and a thin film of a different polymer is coated (often by interfacial polymerization) on the porous substrate (Cadotte and Petersen, 1980).

For the skin layer, the basic question is whether it is porous. SEM has indicated that Ultrafiltration membranes are clearly porous; but, when it comes to the very fine structure of RO membranes, no pores have been detected. The existence or absence of pores in RO membranes can not be determined by today's technology. This is the point where some transport models, to be discussed in Section 2.3.2, assume the membrane to be porous and some assume the membrane as non-porous; some models, which are usually based on irreversible thermodynamics, assume no specific membrane structure or transport mechanism.

One commercially successful type of thin-film composite membrane is the aromatic polyamide FT30 membranes manufactures by FilmTec Corporation (Cadotte et al., 1980; Cadotte and Petersen, 1980; Larson et al., 1981; Larson et al., 1983; Cadotte, 1985). The FT30 membrane consists of three parts: an ultrathin, skin layer of about 0.25 micrometers thick; a microporous support layer of polysulfone (about 50 micrometers thick); and a polyester carrier web with very large pores and a thickness

of about 125 micrometers. The chemical material of the skin layer is a crosslinked aromatic polyamide with some anionic functionality (i.e., negative charges). The skin layer in the FT30 membrane has a thickness several times that in other thin-film composite membranes (Cadotte et al., 1980); this makes the membrane much more resistant to mechanical and oxidizing damage. The membrane can be operated in a wide range of pH: about 3-11 for continuous operations and 1-13 for short-term operations. This allows the membrane to be cleaned with strong acid and base solutions at temperatures up to 50°C. Another important characteristic of FT30 membranes is the durability at high temperatures; studies have been done up to 85°C (Cadotte et al., 1980). The FT30 membranes have shown moderate resistance to chlorine attack, a test failed by most of the other noncellulosic RO membranes. The minimum rate of oxidation attack has been observed in the pH range of 5-6 for short periods of time (Cadotte, 1985). Constant exposure or high chlorine concentrations (above 5 ppm) will destroy FT30 membranes rapidly. Sea water tests (35 000 ppm TDS) have shown salt rejections of about 99.0 to 99.2 percent for spiral-wound elements of FT30 membranes at 5500 kPa (800 psi) pressure and 25°C temperature; the corresponding permeation fluxes of about 1.04×10^{-5} m3/m2 s (22 GFD) have been reported at these conditions (Larson et al., 1983). For brackish water solutions (2000 ppm TDS), fluxes of about 0.75×10^{-5} m3/m2 s (16 GFD) and salt rejections of about 96 percent have been reported for 1380 kPa (200 psi) pressure and 25°C temperature (Larson et al., 1983).

Two commercially important members of the family of FT30 membranes are the so-called SW30HR (Sea Water-High Rejection) and BW30 (Brackish Water) membranes. SW30HR is a high rejection membrane used for sea water desalination, and BW30 is used for brackish water desalination. These two membranes are

chemically similar but have different performance; the exact difference between these membranes is proprietary. Despite the high flux and high separation characteristics of thin-film composite membranes, including the FT30 membranes, little work has been done to determine the transport properties of these membranes.

Several technologies have been developed to put a large membrane area into a relatively small volume, for industrial use. The most popular of these designs are: spiral wound, hollow fibre, and tubular. The relative merits of each of these designs is dependent on the particular application. A review of the merits of the different designs is presented elsewhere (Applegate, 1984; Belfort, 1988).

2.3   Reverse Osmosis Transport Mechanisms and Models

In recent years, a large number of models and theories have been proposed to describe the transport mechanism of solute and solvent through RO membranes. Some reviews are in the literature (Sourirajan, 1977; Soltanieh and Gill, 1981; Dickson, 1988; Dickson and Mehdizadeh, 1988). The models have been usually proposed in an attempt to describe the transport mechanisms in RO processes (for those models which assume some sort of transport mechanism in the membrane). Nonetheless, general agreement exists about the mechanism. These models have been derived from two independent general approaches. The first group of models, called phenomenological, are usually based on irreversible thermodynamics (IT) where the membrane is treated as a black box in which relatively slow processes take place near equilibrium (Kedem and Katchalsky, 1958; Spiegler and Kedem, 1966). In these models, fluxes are linear combinations of forces in the system.

In the second group of models (which can be called the "mechanistic models"), some mechanism of transport is assumed and, accordingly, fluxes are related

to the driving forces that exist in the system. The mechanistic models may be subdivided into general and electrokinetic models. The general models may be applied to any kind of solute; however, the electrokinetic models apply only to electrolytic solution feeds. From another point of view, the mechanistic models may be subdivided into porous and non-porous membrane models. The transport models in the porous membrane group assume that the membrane is porous, and those in the non-porous membrane group supposes the membrane is dense and not porous.

2.3.1   Transport mechanisms

The mechanism of membrane transport in RO is still a matter of controversy. Several mechanisms have been suggested which are reviewed briefly here.

i)   Sieve mechanism: This very simple concept of sieve-filtration states that membrane separation occurs due to difference between the molecular sizes of solute and solvent; the membrane pore size should be between the two molecular sizes (Banks and Sharples, 1966). The mechanism is ruled out in RO since it can not describe systems such as sodium chloride-water in which the molecular sizes of the solute and water are about the same.

ii)   Wetted surface mechanism: Reid and Breton (1959), and later Orofino et al. (1969), realized that, due to wettability of membrane materials, water is sorbed into the membrane by hydrogen bonding. The long-chained water structure, obstructing the membrane pores, then prevents the solute transfer through the membrane. The water then permeates by diffusing from one wetted site to another.

iii)   Solution-diffusion (SD) mechanism: According to this mechanism, suggested by Lonsdale et al. (1965), the solute and solvent first dissolve in the dense skin layer of a membrane and then diffuse through the membrane; therefore, the solubilities and diffusivities of the solution component are of highest importance. Pore flow (i.e., convection) is ruled out in this mechanism. Later, Sherwood et al. (1967) extended the SD model by assuming some imperfections, or holes, on the membrane surface layer which contribute to the pore flow of solute and solvent, which is known as the Solution-Diffusion-Imperfection (SDI) model.

iv)   Preferential sorption-capillary flow (PS-CF) mechanism: On the contrary to the SD mechanism, above, the PS-CF mechanism, first suggested by Sourirajan (1963), assumes that the skin layer of the membrane is porous. According to this mechanism, the membrane transport is partly governed by surface phenomena, at the solution-skin layer interface, and partly by fluid transport through the micro-capillaries. The physicochemical nature of the solute-solvent-membrane surface system determines which constituent of solution is preferentially sorbed by the membrane. For example, for the system $NaCl$-water-cellulose acetate, in which the membrane has a low dielectric constant, the ions are repelled by the membrane and a solute-free layer of water is sorbed on to the membrane. The pure water layer is then forced to flow through the capillaries under the system pressure. Previously, Glueckauf (1965, and 1976) had estimated, using surface tension data, that the thickness of the pure water layer is about 0.35 nm.

2.3.2 Transport models

This section briefly reviews some important transport models of reverse osmosis. Details can be found in the literature (e.g., Soltanieh and Gill, 1981; Dickson, 1988; Dickson and Mehdizadeh, 1989a and 1989b).

2.3.2.1 Mechanism independent transport models

A few models have treated the membrane as a "black box" in which no mechanism has been assumed. Then, the principles of irreversible thermodynamics (IT) have been applied to derive equations for the membrane separation and flux. One of the principles of IT is that the system can be divided into small subsystems in which local equilibrium can exist and therefore thermodynamic quantities can be written for these subsystems. For systems that are not too far from equilibrium, IT suggests reasonable relationships between forces and fluxes.

Onsager (1931) suggested that the fluxes and forces could be expressed by the following linear equations:

$$J_i = L_{ii} F_i + \sum_{i \neq j} L_{ij} F_j \; ; \qquad i = 1, n \qquad (2.11)$$

where the fluxes, J_i, are related to the forces, F_j, by the phenomenological coefficients, L_{ij}. For membrane systems, the driving forces can be related to the pressure and concentration differences across the membrane, and the fluxes are solvent and solute permeate fluxes. Equation (2.11) can be simplified by assuming that cross coefficients are equal (Onsager, 1931):

$$L_{ij} = L_{ji} \qquad \text{for } i \neq j \qquad (2.12)$$

The above Onsager reciprocal relationship (ORR), Eqn.(2.12), is valid when the system is close to equilibrium, the linear laws (i.e., Eqn.(2.11)) are valid, and the correct choice of fluxes and forces has been made. For systems that are far from equilibrium,

as is often the case in reverse osmosis, Eqn.(2.12) may not be correct. The validity of the ORR has been discussed by Soltanieh and Gill (1981).

Two most important phenomenological transport models based on IT are briefly discussed below.

i)   Kedem and Katchalsky model: Kedem and Katchalsky (1958) used Eqns.(2.11) and (2.12) to derive what are known as the IT-PT relationship:

$$J_V = \ell_p (\Delta P - \sigma \Delta \pi) \tag{2.13}$$

$$N_A = \omega \Delta \pi + (1 - \sigma)(C_{AM})_{\ell n} J_V \tag{2.14}$$

where the adjustable parameters ℓ_p, ω, and σ are simple functions of the original phenomenological coefficients, L_{ij}. Equation (2.13) is identical to Eqn.(2.3). The Staverman coefficient acts to describe the effect of the pressure driving force on the flux of solute. For a high separation membrane this effect is small, as mentioned in Section 2.1.2, and σ approaches 1. For a low separation membrane the solute is significantly carried through the membrane by solvent flux and σ approaches zero so that the osmotic driving force becomes unimportant in Eqn.(2.13). Thus the Staverman (or reflection) coefficient represents the relative permeability of the membrane to the solute (Staverman, 1951).

Pusch (1977) has shown that Eqn.(2.14) can be rewritten to relate separation, f', and flux, J_v, as:

$$\frac{1}{f'} = \frac{1}{\sigma} + \left(\frac{\ell_\pi}{\ell_p} - \sigma^2\right)\left(\frac{\ell_p}{\sigma}\right)\pi_2\left(\frac{1}{J_V}\right) \tag{2.15}$$

The above equation predicts a linear relationship between $1/f'$ and $1/J_v$. The osmotic permeability, ℓ_π, is related to ω as:

$$\omega = \left(\frac{\ell_\pi}{\ell_p} - \sigma^2\right)(C_{AM})_{\ell n} \ell_p \tag{2.16}$$

The parameters in the model are the solvent and osmotic permeabilities, ℓ_p and ℓ_n, and the reflection coefficient, σ. These parameters can be determined for a given solute and membrane by applying Eqns.(2.13) and (2.15) simultaneously, using data collected at different operating conditions.

For reverse osmosis systems, the IT-PT equations have only been used to a limited extent for describing membrane transport for two reasons. First, the concentration differences across the membrane are often large enough that the linear laws are not valid. As a result the L_{ij} coefficients are concentration dependent (Onsager, 1931). However, for many systems, the coefficients ℓ_n, ℓ_p, and σ are nearly constant provided that the concentration changes are not too great. This assumption is relaxed in Kedem-Spiegler relationship, discussed below. Second, by considering the membrane as a "black box", the resulting analysis does not give any insight into the transport mechanism.

ii)   Kedem and Spiegler model: One critical assumption in the Kedem and Katchalsky model is that the linear laws were assumed to apply over the whole thickness of the membrane. Spiegler and Kedem (1966) resolved the problem by rewriting the original linear IT equations in differential form and then integrating them over the thickness of the membrane.

The equations in differential form for the solvent and solute flux, respectively, are:

$$J_V = p_B \left(\frac{dP}{dx} - \sigma \frac{d\pi}{dx} \right) \tag{2.17}$$

$$N_A = p_A \frac{dC_{AM}}{dx} + (1 - \sigma) C_{AM} J_V \tag{2.18}$$

where p_A is the solute permeability, p_B is the water permeability, and x is the coordinate direction perpendicular to the membrane.

If p_A, p_B, and σ are constant, Eqn.(2.17) can be integrated to give Eqn.(2.19), and Eqn.(2.18) can be integrated and combined with Eqns.(2.6) and (2.10) to give (Spiegler and Kedem, 1966; Soltanieh and Gill, 1981; Dickson, 1988) Eqn.(2.20), below:

$$J_v = \frac{p_B}{\Delta x} (\Delta P - \sigma \Delta \pi) \tag{2.19}$$

$$\frac{1}{f'} = \frac{1 - \sigma \exp[-(1 - \sigma)(\Delta x/p_A)J_v]}{\sigma\{1 - \exp[-(1 - \sigma)(\Delta x/p_A)J_v]\}} \tag{2.20}$$

The result is a three-parameter model described by Eqns.(2.19) and (2.20), similar to the previous phenomenological relationship but which should have coefficients that are independent of concentration and pressure. The three parameters in the Kedem-Spiegler relationship are $p_B/\Delta x$, $p_A/\Delta x$, and σ.

This model has been used by various researchers to describe reverse osmosis transport (Jonsson, 1978; Burghoff et al., 1980).

2.3.2.2   Mechanism dependent transport models

In this section, those transport models which assume some kind of membrane structure or transport mechanism are presented, briefly. First, the models which assume the membrane to be non-porous are discussed and then transport models based on the assumption of porous membrane are discussed. More details about the transport models can be found elsewhere (Soltanieh and Gill, 1981; Dickson, 1988; Dickson and Mehdizadeh, 1988).

Another group of models are those based on electrokinetic relationships for electrolytic solutions. The mathematical modeling of electrokinetic phenomena in porous media has been discussed by researchers such as Dresner (1963), Morrison and Osterle (1965), Gross and Osterle (1968), Fair and Osterle (1971), Jacazio et al. (1972), Neogi and Ruckenstein (1981), and Westermann-Clark and Anderson (1983). The basic formulation developed by Osterle and coworkers in the 1960's, referred to as a "space-charge" model, describes the transport of an electrolyte through a charged, cylindrical capillary pore. This model assumes the Gouy-Chapman model for the electric double-layer, the Nernst-Planck equation for ion fluxes, and Navier- Stokes equation for the viscous flow behaviour. Jacazio et al. (1972) and Neogi and Ruckenstein (1981) extended the classical model of Osterle and coworkers to the case of reverse osmosis. The works of Jacazio at el. (1972) and Neogi and Ruckenstein are briefly discussed in Section 2.3.2.2.3.

2.3.2.2.1 Non-porous transport models

Several models have been derived that specifically assume that the membrane surface skin is non-porous. These models are usually based on a solution-diffusion mechanism. Modifications of this model, such as the solution-diffusion imperfection and the extended solution diffusion relationships are discussed briefly.

I.   Solution-diffusion model: The solution-diffusion (SD) model was originally applied to reverse osmosis by Merten and coworkers (Lonsdale et al., 1965; Merten, 1966). The membrane surface layer is considered to be homogeneous and non-porous. Transport of both solvent and solute occurs by the molecules dissolving in the membrane phase and then diffusing through the membrane. The permeability of a species is equal to the product of the solubility and the diffusivity for that species.

Theoretically, the solubility and the diffusivity of the solute can be determined for a membrane material by performing equilibrium sorption and unsteady state sorption/desorption studies, respectively. The water flux is proportional to the solvent chemical potential difference (usually expressed as the effective pressure difference across the membrane), and the solute flux is proportional to the solute chemical potential difference (usually given as the solute concentration difference across the membrane). The solute and solvent are assumed to be transported across the membrane independently.

The solvent and solute fluxes, respectively are:

$$J_V = \frac{D_{BM} C_{BM} v_B}{RT \Delta x} (\Delta P - \Delta n) \tag{2.21}$$

$$N_A = \frac{D_{AM} K}{\Delta x} (C_{A2} - C_{A3}) \tag{2.22}$$

Note that Eqn.(2.21) is identical to Eqn.(2.3), except that A has been replaced by more physically meaningful terms. The group of parameters in Eqn.(2.21) is abbreviated as the hydraulic permeability coefficient, ℓ_p ($= D_{BM} C_{BM} v_B/RT \Delta x$). D_{AM} and D_{BM} are the diffusivities of the solute and the solvent in the membrane, respectively; C_{BM} is the membrane water content; v_B is the partial molar volume of water; and K is the partition coefficient defined as the following:

$$K = \frac{kg \, solute/m^3 \, membrane}{kg \, solute/m^3 \, solution} \tag{2.23}$$

K is a measure of the relative solute affinity to (K > 1.0) or repulsion from (K < 1.0) the membrane material.

As illustrated by Pusch (1977), Eqns.(2.21) and (2.22) may be combined with Eqns.(2.6) and (2.10) and rearranged to give:

$$\frac{1}{f'} = 1 + \left(\frac{D_{AM}K}{\Delta x} \right) \frac{1}{J_V} \qquad (2.24)$$

Equation (2.24) predicts a linear relationship between $1/f'$ and $1/J_V$. Equations (2.21) and (2.24) can be fit to experimental data to generate the two parameters ($D_{BM} C_{BM} v_B/RT \Delta x$) and ($D_{AM}K/\Delta x$), both of which are treated as single quantities. In order to resolve either of these terms into component parts, it is necessary to have an independent measure of some of the terms. One restriction of the SD model is that the separation obtained at infinite flux is always equal to 1.0. However, this limit is not reached for many solutes. For this reason, the SD model is appropriate for solute-solvent-membrane systems where the separation is close to 1.0. Notwithstanding this restriction, the SD model has been applied to many different inorganic and organic solute systems with different types of membranes (Pusch, 1977; Lonsdale et al., 1965; Merten, 1966). The primary advantage of this model is simplicity as only two adjustable parameters are required.

Several modifications to the original solution-diffusion model have been proposed and two of these are discussed here briefly.

I.i)   Solution-diffusion-imperfection (SDI) model: This model was derived by Sherwood et al. (Sherwood et al., 1967). The premise of this model is that during the membrane making process small defects in the membrane surface structure could result and these defects would lead to leakage of solution through the membrane. This mechanism would account for membranes that exhibited lower separation than the separation calculated based on solubility and diffusivity measurements. This model has been used successfully to describe the performance for a variety of solutes and membranes (Jonsson and Boesen, 1975).

I.ii)   Extended solution-diffusion (ESD) model: Both Burghoff et al. (1980) and Jonsson (1980) have pointed out that in the original solution-diffusion model, a pressure term in the solute chemical potential equation was neglected. Including this pressure term leads to a somewhat different form of the transport equations. The differences are primarily important for the situation when the solute partial molar volume is large and the solute-water separation is low. Burghoff et al. (1980) found good agreement between the ESD model and the observed performance for different organic solutes with cellulose acetate membranes. The negative separation observed for phenol was attributed to a large pressure contribution to the flux of solute.

2.3.2.2.2 Porous transport models

In this section, transport models in which it is specifically assumed that the membrane is porous are presented. Due to the importance of these models, each is discussed as a separate subsection.

2.3.2.2.3 Electrokinetic models

This section overviews the two electrokinetic transport models of Jacazio et al. (1972) and Neogi and Ruckenstein (1981) for reverse osmosis.

I.   Model of Jacazio et al. (1972): Jacazio et al. have extended the space-charge model of Osterle and his coworkers (Gross and Osterle, 1968; Fair and Osterle, 1971) to transport in reverse osmosis. The membrane is modeled as microporous, the pores are perfect cylinders having an average pore size and length, and the solute is considered

as a point (i.e., solute size is not included). The interior surface of the pores is assumed to acquire a net charge density when the membrane comes in contact with a saline solution and, therefore, an electrochemical double-layer is assumed to develop inside the pores. Then, the Poisson equation, which relates the double-layer potential to the surface charge density and the solute concentration in the pore, is used in conjunction with the Boltzmann equilibrium theorem, the Nernst-Planck equations of ion flux, the Poiseuille equation of solution velocity profile, and the condition of zero electrical current, to determine the performance of the RO membrane when a symmetrical electrolyte passes through the membrane. The boundary condition used for the Poisson equation is a constant wall potential case.

The model of Jacazio et al. (1972) has not been applied to a polymeric membrane, but has been used to describe the performance of a bed of clay which was used as a RO membrane.

The limitations of the above model are: i) the Poiseuille equation is used as the velocity profile, which may not be close to real situations under special circumstances (as discussed in Section 5.2.5); this implies that the electric field and the concentration field do not have any effect on the velocity profile, ii) the model is restricted to only symmetrical electrolytic feed solutions, iii) the model is restricted to the condition of constant wall potential of double-layer, and iv) the model is restricted to only small charged solute molecules where electrical effects are dominant (Born repulsion and van der Waals attraction are also important for large charged molecules of solute).

II.   Model of Neogi and Ruckenstein (1981): Neogi and Ruckenstein have applied the basic equations of electrokinetic transport, similar to the work of Osterle and coworkers (Gross and Osterle, 1968; Fair and Osterle, 1971) to reverse osmosis.

The model of Neogi and Ruckenstein, which assumes a microporous membrane with long cylindrical pores, uses the following transport equations: i) the Navier-Stokes equations of motion in radial and axial coordinates, ii) the equation of continuity, iii) the conservation of mass for the solute, iv) equilibrium in radial direction (or Boltzmann's equilibrium theorem), v) the Nernst- Planck equations of ion flux, vi) the Poisson-Boltzmann equation of electrical potential, and vii) the condition of zero electrical current.

The differences between the model of Neogi and Ruckenstein (1981) and that of Jacazio et al. (1972), discussed above, are: i) Neogi and Ruckenstein allow for viscoelectric effects on the solution velocity profile in the pore but Jacazio et al. assumed the Poiseuille velocity profile, ii) Neogi and Ruckenstein use both boundary conditions of constant wall potential of double-layer and constant surface charge density but Jacazio et al. use only the former boundary condition for the Poisson equation, and iii) Neogi and Ruckenstein allow for different ionic diffusivities while Jacazio et al. use an average diffusivity of the ionic solute. Due to the result of the above differences between the two models, separation values are overpredicted by Jacazio et al.'s model by 15%, compared to Neogi and Ruckenstein's model. The results of Neogi and Ruckenstein show that the solution velocity profile is affected by the electrical forces at all levels of the electrical potential; for potentials smaller than 35 mV the flow is decreased by about 10%, and for electrical potentials as high as 75 mV the flow is decreased as much as 90%.

2.3.2.3   Kimura-Sourirajan Analysis (KSA)

The Kimura-Sourirajan Analysis (KSA), (Kimura and Sourirajan, 1967; Sourirajan, 1970), was developed based on the "preferential sorption-capillary flow"

mechanism (see Section 2.3.1) proposed earlier by Sourirajan (1963). According to the KSA relationship, the membrane surface is microporous and transport occurs only through the pores. The membrane has a preferential attraction for solvent (usually water) and the resulting sorbed layer of almost pure water is forced through the membrane pores by pressure, in the case of solvent-membrane affinity. Therefore solute separation and flux are determined both by physicochemical interaction between the solute-solvent-membrane system and by the number, size, and size distribution of pores.

The solvent flux is viscous in nature and therefore the driving force for solvent transport is given by the effective pressure as in Eqn.(2.3) when σ equals unity:

$$N_B = A \left[\Delta P - (\pi_2 - \pi_3) \right] \tag{2.25}$$

The solute flux is diffusive in nature and is driven by the concentration gradient:

$$N_A = \frac{D_{AM} K}{\tau} (C_{A2} - C_{A3}) \tag{2.26}$$

Equations (2.6), (2.7), (2.10), (2.25), and (2.26) together make up the Kimura-Sourirajan analysis. For dilute solutions these equations can be combined to give the following relationship between f' and J_v:

$$\frac{1}{f'} = 1 + \left(\frac{D_{AM} K}{\tau} \right) \frac{1}{J_V} \tag{2.27}$$

Note that this equation is functionally the same as Eqn. (2.24) for the SD model. The two parameters are A (from Eqn.(2.25)) and $D_{AM}K/\tau$. Even though Eqn.(2.27) is similar to Eqn.(2.24) for the SD model, the coefficients are interpreted differently. In the KSA model, D_{AM} is the diffusivity of the solute in the membrane pore rather than in the polymer material; K is the partition coefficient defined based on the amount of solute in the pores rather than in the membrane material; and τ is the effective length of a pore, rather than the actual thickness of the membrane surface, Δx. As in the SD

model, Eqn.(2.27) predicts that f' approaches 1.0 for infinite flux. This characteristic is not realistic for the many solutes that do not approach perfect separation at high solvent flux rates.

2.3.2.4   Finely Porous Model (FPM)

The Finely Porous Model (FPM) developed by Merten (1966), is based on a balance of applied and frictional forces, as first proposed by Spiegler (1958), in a one-dimensional pore. A complete derivation of the model is given by Jonsson and Boesen (1975) and by Soltanieh and Gill (1981).

The general form of this model relates the volume flux, J_v, and the separation, f', as follows:

$$\frac{1}{f'} = \frac{1 - (1 - K_3/b) \exp[-(\tau/\epsilon D_{AB})J_V]}{(1 - K_2/b) - (1 - K_3/b) \exp[-(\tau/\epsilon D_{AB})J_V]} \qquad (2.28)$$

The solvent flux is represented by Eqn.(2.3). The parameters in the relationship are the pure water permeability, A, the partition coefficients on the high and low pressures sides of the membrane, K_2 and K_3, respectively, the friction parameter, b, the effective membrane thickness, τ, and the fractional pore area of the membrane surface, ϵ.

The partition coefficients, K_2 and K_3, are defined in a manner similar to that given earlier in Eqn.(2.23), with one difference. In this case, the concentration of solute in the membrane is interpreted as the concentration of solute in the membrane pore. The friction parameter, b, is defined (Jonsson and Boesen, 1975) as:

$$b = \frac{X_{AM} + X_{AB}}{X_{AB}} \qquad (2.29)$$

where X_{AB} represents friction between the solute and solvent and X_{AM} represents friction between the solute and membrane material. Therefore, b can be thought of as

the ratio of the total friction of the solvent plus membrane upon the solute to the friction between solute and solvent. The frictional forces are inversely proportional to the diffusivity of solute within the membrane pore, D_{AM}, and the diffusivity of the solute in the free solvent, D_{AB}, so that Eqn.(2.29) can also be expressed as:

$$b = D_{AB}/D_{AM} \tag{2.30}$$

The friction parameter can be estimated based on the Faxen equation,

$$b = (1 - 2.104\,\lambda + 2.09\,\lambda^3 - 0.95\,\lambda^5)^{-1} \tag{2.31}$$

as discussed in the literature (Bean, 1972; Satterfield et al., 1973; Anderson and Quinn, 1974; Jonsson and Boesen, 1975; Dickson, 1985). The Faxen equation is an analytical solution of the hydrodynamic drag problem for a solute at the pore centerline.

The effective thickness of the membrane, τ, is a product of the actual thickness of the membrane surface layer (membrane "skin" layer) multiplied by the tortuosity of the membrane pore. The tortuosity factor corrects the actual membrane skin thickness to an effective thickness that includes the nonlinearity of the pore geometry. ε is the fractional pore area of the membrane surface. For an asymmetric membrane, the value of ε is much less than that calculated from the water content of the whole membrane.

The Finely Porous Model as represented by Eqns.(2.3) and (2.28), is a four parameter model; the four grouped parameters are A, b/K_2, K_3/K_2, and τ/ε which can be obtained by fitting experimental reverse osmosis data to the model. The parameter, τ/ε, is a measure of the size and number of pores only, and should be a constant for a given membrane sample. The four-parameter model is sometimes called the FPM-4 relationship.

In principle, K_2 and K_3 may be different, but it is often assumed (Jonsson and Boesen, 1975; Pusch et al., 1976; Burghoff et al., 1980) that $K_2 = K_3 = K$. In order for this to be true, K should be independent of concentration, pressure, and membrane structure. When the above assumption is made, Eqn.(2.28) reduces to:

$$\frac{1}{f'} = \frac{1 - (1 - K/b) \exp[-(\tau/\varepsilon D_{AB})J_V]}{(1 - K/b)\{1 - \exp[-(\tau/\varepsilon D_{AB})J_V]\}} \qquad (2.32)$$

which is a three-parameter model. The three parameters are A, b/K, and τ/ε. The three-parameter model is sometimes called the FPM-3 relationship.

Several authors (Merten, 1966; Jonsson and Boesen, 1975; Jonsson, 1978; Burghoff et al., 1980) have successfully used this model (usually in the three-parameter form) to describe the transport of various electrolyte and non-electrolyte solutes through reverse osmosis membranes.

As discussed in Section 3.4, there exist some mistakes in this model which are corrected, in that section, and a corrected form, called the Modified Finely Porous Model (MD-FPM) is derived (Mehdizadeh and Dickson, 1989e).

2.3.2.5 Surface Force-Pore Flow (SF-PF) model

Several authors have considered transport of solute and solvent in 2-dimensional right cylindrical pores. The advantage of using a model of this type is that the model should more accurately describe the transport in a porous membrane. The disadvantages are that the models are considerably more complex (usually involving advanced numerical techniques to solve the governing equations) and the models are still considerable simplifications of the real situation. Nonetheless these models can be useful and therefore a description is given here.

The original work in this area was concerned with the transport in electrodialysis membranes so that electrical potential driving force and current flux were also considered in the model. Some of these early electrokinetic models are given

elsewhere (Fair and Osterle, 1971; Westermann-Clark and Anderson, 1983). This work was modified and applied to ultrafiltration membranes by Anderson and Malone (1974) and to reverse osmosis by Neogi and Ruckenstein (1981) and Jacazio et al. (1972). Subsequently, Sourirajan and coworkers (Matsuura and Sourirajan, 1981; Matsuura et al., 1981) developed the "Surface Force-Pore Flow" (SF-PF) model which was based on the earlier models. The advantage of this model over the previous models is that the effect of solute size, solute-membrane friction, and solute-membrane interaction (by a potential function) were all included in a manageable set of equations. Approaches similar to the SF-PF model can be found in previous literature (Spiegler, 1958; Merten, 1966; Jonsson and Boesen, 1975). Briefly, the model can be described as follows. The membrane is assumed to be microporous and the pores are modeled as perfect cylinders, with or without a pore size distribution. A two dimensional approach is used (i.e., radial and axial coordinates) in which solute velocity and concentration in the pore vary in both the radial and axial directions. A balance of applied and frictional forces acting on the solute in the pore is given as a function of the radial and axial positions. The solute-membrane interactions are expressed by a Sutherland-type potential function, ϕ, which represents the net body force acting on the solute by the pore wall. This potential, whose type (i.e., repulsion or attraction) and magnitude depends upon the membrane wall material, solute type, and the system conditions (such as the concentration and temperature), can be positive, indicating that the solute is repulsed, or negative, indicating that the solute is attracted by the pore wall. In this model, the potential is only assumed to be a function of radial position inside the pore. A friction parameter, $b(\rho)$, which is the ratio of solute diffusivity in free solution to solute diffusivity inside a pore, is used to describe the hydrodynamic drag on the solute by the pore wall. Initially, Matsuura and Sourirajan suggested that the friction parameter was a function of radial position

(Matsuura and Sourirajan, 1981); however, in their subsequent papers, they treated b as a constant (Matsuura et al., 1981; Chan et al., 1982).

The final equations derived in this model are presented, briefly, as follows.

Fluid velocity profile is given as:

$$\left(\frac{d^2 a(\rho)}{d\rho^2} + \frac{1}{\rho} \frac{d\,a(\rho)}{d\rho} \right) + \frac{\beta_2}{\beta_1'} - \frac{1}{\beta_1'}(1 - C_A(\rho))(1 - e^{-\Phi(\rho)})$$

$$- \frac{1}{\beta_1'} a(\rho)\,C_A(\rho)\,(b(\rho) - 1) = 0 \qquad (2.33)$$

subject to the boundary conditions:

$$a(\rho) = 0 \qquad \text{at } \rho = 1 \qquad (2.34)$$

$$da(\rho)/d\rho = 0 \qquad \text{at } \rho = 0 \qquad (2.35)$$

where,

$$\rho = r/R_W \qquad (2.36)$$

$$a(\rho) = \frac{u_B(\rho)\,\tau}{D_{AB}} \qquad (2.37)$$

$$\beta_2 = \frac{\Delta P}{C_{A2}\,RT} \qquad (2.38)$$

$$\beta_1' = \frac{\eta}{\chi_{AB}\,R_W^2\,C_{A2}} \qquad (2.39)$$

$$C_A(\rho) = \frac{C_{A3}(\rho)}{C_{A2}} = \frac{\exp[a(\rho)]}{1 + b(\rho)\,[\exp(a(\rho)) - 1]\exp(\Phi(\rho))} \qquad (2.40)$$

and $\Phi(\rho)$ is a dimensionless form of the potential, ϕ, defined as:

$$\Phi(\rho) = \frac{\phi(\rho)}{RT} \qquad (2.41)$$

Separation is determined from Eqn.(2.6), where:

$$C_{A3} = \frac{\int_0^1 C_{A3}(\rho)\, \alpha(\rho)\rho\, d\rho}{\int_0^1 \alpha(\rho)\rho\, d\rho} \qquad (2.42)$$

Solution permeation flux is given by:

$$N_T = N_P \left(\frac{16\, \beta_1'}{\beta_2} \right) \int_0^1 \alpha(\rho)\, \rho\, d\rho \qquad (2.43)$$

where the pure solvent flux, N_P, is:

$$N_P = A\, \Delta P = \frac{C\, R_W^2}{8\, \eta\, (\tau/\varepsilon)}\, \Delta P \qquad (2.44)$$

For the potential function, the SF-PF model considers the potential between a point and a flat wall. For electrolytes, the relationship is:

$$\Phi(\rho) = \begin{cases} A/d & \text{when: } \rho < 1 - \lambda \\ \infty & \text{when: } \rho \geq 1 - \lambda \end{cases} \qquad (2.45)$$

and, for organic non-dissociable solutes, the relationship is:

$$\Phi(\rho) = \begin{cases} -B/d^3 & \text{when: } \rho < 1 - \lambda \\ \infty & \text{when: } \rho \geq 1 - \lambda \end{cases} \qquad (2.46)$$

where A and B are the corresponding potential parameters, and λ is defined as the ratio of solute molecular radius to the average pore radius:

$$\lambda = R_A / R_W \qquad (2.47)$$

The above two equations are then used inside the cylindrical pore.

For the friction function, b, Matsuura and Sourirajan have used a modified form of the Faxen equation:

$$b = \begin{cases} b_{Faxen} & \text{when: } \lambda \leq 0.22 \\ (44.57 - 416.2\lambda + 934.9\lambda^2 + 302.4\lambda^3) & \text{when: } \lambda > 0.22 \end{cases} \qquad (2.48)$$

where b_{Faxen} is the value of friction function given by the Faxen equation in Eqn.(2.30). The Faxen equation was modified by fitting a large amount of experimental reverse osmosis data to the form in Eqn.(2.48) for large λ values. Although the friction function should be a function of radial position, the Faxen equation has been

found to be a reasonable approximation (e.g., Lane and Riggle, 1959; Jonsson and Boesen, 1975).

As discussed in Section 3.1, there exist serious mistakes in this model and a corrected model, called the Modified Surface Force-Pore Flow (MD-SF-PF) model is derived in Section 3.1 (Mehdizadeh and Dickson, 1989a and 1989b).

2.3.2.6 Summary and comparison of transport models

It is interesting to note that several of the models presented or discussed above have similar mathematical forms; particularly in terms of the predicted relationship between flux and separation. For instance, both the solution-diffusion model and the Kimura-Sourirajan analysis, on one hand, and the irreversible thermodynamics-Kedem Spiegler model and the Finely Porous Model, on the other hand, are mathematically identical. Some of these similarities have been discussed previously (Jonsson and Boesen, 1975; Soltanieh and Gill, 1981; Dickson, 1985; Dickson, 1988). Yet each of these models is based on substantially different assumptions. What this tells us is that simple agreement between experimental data and a model is not proof that the model is correct. In this light, care must be exercised in interpreting model parameters calculated from these models. For a membrane maker, using a porous model will give information about the porous nature of the membrane, and using a solution diffusion model will give information about the diffusion and solubility coefficients in the membrane. Until the nature of the membrane structure is resolved the decision of which model to use is, in part, a matter of personal choice.

For the person who is only interested in the application of a membrane, using the following equation (originally suggested, in this form, by Soltanieh and Gill (1981)) is a reasonable compromise:

$$\frac{1}{1 - f'} = E_1 - E_2 \exp(-E_3 J_v) \tag{2.49}$$

This equation is mathematically equivalent to the Kedem-Spiegler and the Finely Porous Model, Eqns.(2.20) and (2.28) respectively. The coefficients, E_1, E_2, and E_3 can then be treated as empirical parameters that must be determined for each new solute and membrane system.

2.3.3   Strong solute-membrane affinity case

It is well known that the reverse osmosis performance for certain low molecular weight organics in water, such as toluene, benzene, and phenol derivatives, is markedly different than those for simple aqueous salt solutions (Lonsdale et al., 1967; Matsuura and Sourirajan, 1973a and 1973b; Anderson et al., 1972; Burghoff et al., 1980). This anomalous behaviour, referred to as "solute-membrane affinity", is associated with a strong affinity between the organic solute and the membrane material such that the uncharged organic molecules are sorbed into the membrane rather than the usual case, in reverse osmosis, of being rejected by the membrane.

The characteristic behaviour for a strong solute-membrane affinity system can be summarized by the followings: i) increasing the operating pressure decreases the membrane separation, ii) permeate flux is usually much less than pure water flux even when osmotic effects are small, iii) partition coefficients are much larger than unity, and iv) separation can be positive, zero, or negative, depending on specific operating conditions (Matsuura and Sourirajan, 1971; Matsuura et al., 1974; Dickson et al., 1979; Dickson et al., 1983; Dickson, 1985; Connell, 1986). Typical concentration behaviours are shown in Figures 2.3 and 2.4.

Among the available transport models, only the (4-parameter) Finely Porous Model (Merten, 1966; Jonsson and Boesen, 1975), which assumes membranes to be porous, has been able to describe the peculiar case of solute-membrane affinity (Dickson, 1985). No non-porous transport model or any model based on irreversible thermodynamics has been able to predict such behaviour (Dickson, 1985).

A generalized form of the MD-SF-PF model, developed in Section 3.2, has shown (see Section 5.4) to reasonably describe and predict this challenging case.

2.4 System Design

The transport equations discussed in this chapter are useful for relating the membrane performance (flux and separation) in terms of the operating variables and some transport parameters. However, these models all assume that the amount of permeate collected is small compared to the feed rate (i.e., zero recovery). In a membrane module or membrane plant, the permeate is a significant fraction of the feed rate (i.e., finite recovery). The transport equations are valid at any point within the membrane module, but to describe the overall module (or system) behaviour it is necessary to integrate this solution over the length of the membrane system.

In general the problem is handled by first assuming a model to describe the membrane mass transfer, and then the model is integrated over the length of the membrane system. This ultimately relates the choice of membrane module, number and arrangement of modules, and the operating conditions to the system performance in terms of permeate recovery and separation (Dickson and Mehdizadeh, 1988).

2.5 Temperature Effects

It has been widely noted that temperature has significant effects on the performance of reverse osmosis membranes (Lonsdale et al., 1965; Govindan and Sourirajan, 1966; Agrawal and Sourirajan, 1969; Ohya and Taniguchi, 1974; Burghoff and Pusch, 1976; Saltonstall, 1976; Brandon and Samfield, 1978; Cadotte et al., 1980; Kimura and Nomura, 1981; Chen et al., 1983; Dale and Okos, 1983; Kurihara et al., 1983). FilmTec Corporation has also noticed that, in the field, temperature has a large effect on the flux and separation of FT30 polyamide membranes (Cadotte et al., 1980).

In order to properly evaluate these effects, it is important to have data that have been collected under carefully controlled laboratory conditions for comparison.

Studying temperature effects in reverse osmosis is important in several aspects:

i)   It provides a better understanding of transport mechanism in membranes.

ii)   It provides information about the optimum conditions at which membranes should be applied. One may exploit the advantages of operating at higher temperatures. Usually, increasing temperature increases the permeation flux of membranes. However, increasing temperature may also increase the rate of compaction (as discussed in the next section) and hence the flux declines with time. The high temperature and salinity of sea water in several locations where fresh water is in short supply are important factors in the design of RO plants (Kurihara et al., 1983).

iii)   High-temperature reverse osmosis and ultrafiltration are being evaluated for recycle of both water and chemicals in industrial effluents (e.g., textile industry). However, membrane deterioration rates are affected by operating pressure, temperature, pH, and cleaning regiments. Operating conditions increasing flux rates, namely high pressures and temperatures, also accelerate membrane deterioration.

2.5.1   Modeling of temperature effects

The fluxes of solvent and solute have been expressed, by previous researchers, in terms of an Arrhenius-type equation (e.g., Saltonstall, 1976),

$$N_i = A_i \exp\left(-\frac{E_i}{RT}\right) \tag{2.50}$$

where E_i is the apparent activation energy for transport of species i through the membrane. The magnitude of this energy for solvent (water) appears to vary from

19 250 kJ/kmol for membranes with little salt rejection to nearly 25 120 kJ/kmol for membranes with salt rejections in the order of 99% for cellulose acetate membranes (Saltonstall, 1976). These values are independent of pressure, solute identity, and solute concentration. At the same time, the corresponding values of the energy for solute (sodium chloride) transport varied from 20 100 kJ/kmol to more than 29 300 kJ/kmol and were always greater than the apparent activation energies of water. These values, stated above, imply that the diffusion through the membrane is hindered. A hindered diffusion process could be the consequence of molecular steric effects, interactions between solute, solvent, and membrane, and/or some form of flow obstruction.

This idea, that solute and solvent have to gain a minimum energy (apparent activation energy) in order to pass through the membrane, has been obtained by analogy with the idea of activation energy in chemical reactions. Therefore, Eqn.(2.50) states a mechanism for transport of solute and solvent through membrane in a phenomenological manner similar to the transport of material from reactant state to product state in chemical reactions.

In Eqn.(2.50), the effect of temperature on solute and solvent flux was modeled by an Arrhenius type equation. A theoretically more satisfying approach is to describe the effect of temperature on the model parameters.

For example, the parameters of the Kimura-Sourirajan Analysis (discussed in Section 2.3.2.3), A and $D_{AM}K/\tau$, have been expressed as a function of temperature as (Sourirajan, 1970),

$$A \, \eta_B = \text{constant} \tag{2.51}$$

$$\left(\frac{D_{AM} K}{\tau} \right) = \left(\frac{D_{AM} K}{\tau} \right)_{ref} \exp\left[0.005 \, (T-T_{ref})\right] \tag{2.52}$$

for cellulose acetate membranes (referred to as CA-NRC-18 in reference (Sourirajan, 1970)), 0.5-2.0 molar sodium chloride solutions, and 5-36°C. Similarly, Connell and

Dickson (1988) correlated the temperature dependencies of the parameters in the Finely Porous Model using Arrhenius equations for the separation of toluene from water with cellulose acetate membranes.

In general, the effects of temperature on any parameter, U, can be modeled by an Arrhenius equation normalized about temperature T_{ref} as (Connell and Dickson, 1988),

$$U = U_{ref} \exp\left[-\frac{E}{R}\left(\frac{1}{T} - \frac{1}{T_{ref}} \right) \right]$$

(2.53)

where E is the apparent activation energy associated with parameter U. Equation (2.53) can be rewritten as:

$$\ell n\, U = \ell n\, U_{ref} - \frac{E}{R}\left(\frac{1}{T} - \frac{1}{T_{ref}} \right)$$

which implies that $\ell n\, U$ varies linearly with $1/T$. For example, Eqn.(2.52) can be rearranged to the same form as Eqns.(2.53) or (2.54).

From a generalized mass transfer correlation the variation of k with temperature is predicted by (Sourirajan, 1970; Connell and Dickson, 1988),

$$\frac{k}{k_{ref}} = \left(\frac{D_{AB}}{D_{AB,ref}} \right)^{2/3} \left(\frac{\eta}{\eta_{ref}} \right)^{0.04} \left(\frac{\rho_{ref}}{\rho} \right)^{0.04}$$

(2.55)

An additional effect of temperature is the increased plastic creep of the membrane polymeric structure observed at higher temperatures (Merten et al., 1968; Sourirajan, 1970). This phenomenon, known as "compaction effect" causes a reduction in the permeation flux through the membrane. Therefore, at higher temperatures there is both increased flux and increased compaction. These two effects must both be considered in analyzing data at different temperatures. Modeling of compaction effect has been discussed in Section 3.3.1.

2.6 Orthogonal Collocation: An Advanced Numerical Technique

Consider the following general differential equation,

$$\pounds^V(y) = 0 \text{ in } V \tag{2.56}$$

where $\pounds$ is a linear or nonlinear differential operator defined over the volume V, and the general boundary conditions,

$$\pounds^S(y) = 0 \text{ on } S \tag{2.57}$$

where S is the boundary containing the volume V.

The dependent variable y is approximated by a series expansion $Y_N(x)$ containing N undetermined parameters and N trial functions p_N. The dependent parameters are then determined by applying the following equations at each of the N selected points,

$$\pounds^V(Y_N) = R^V \text{ in } V \tag{2.58}$$

$$\pounds^S(Y_N) = R^S \text{ on } S \tag{2.59}$$

where R^V and R^S are the residuals in the regions V and S, respectively, and by setting the residuals equal to zero at the N interior collocation points. The crucial step is now the selection of the collocation points. In "orthogonal collocation" method, it is the orthogonality of the trial functions that determines the collocation points, and hence the name "orthogonal" (Villadsen and Stewart, 1967). The orthogonal trial functions have been discussed elsewhere (Villadsen and Michelsen, 1978; Chihara, 1978).

For example, consider the following second order linear or nonlinear ordinary differential equation,

$$\pounds(y) = 0 \tag{2.60}$$

where $\pounds$ is a linear or nonlinear differential operator defined over the normalized interval $x \in [0,1]$, subject to the boundary conditions,

$$dy/dx + a_1 y = a_2 \quad \text{at } x = 0 \tag{2.61}$$

$$dy/dx + b_1 y = b_2 \quad \text{at } x = 1 \tag{2.62}$$

A suitable choice of the approximation function is (Villadsen and Stewart, 1967; Villadsen and Michelsen, 1978),

$$Y_N(x) = m^* + n^*x + x(1 - x) \sum_{i=1}^{N} q_i \, p_{i-1}(x) \qquad (2.63)$$

The expression in Eqn.(2.63) contains $(N + 2)$ constants. Two constants are to be determined from the boundary conditions (2.61) and (2.62) and the remaining constants by setting the residuals $Y_N(x)$ equal to zero at the N interior collocation points. The approximation function, Eqn.(2.63), which is a polynomial of degree $(N + 1)$ in x, can be written as,

$$Y_N(x) = \sum_{i=0}^{N+1} y_i \, x^i \qquad (2.64)$$

and x_i can be expressed as a linear combination of the orthogonal polynomials p_k ($k = 0, 1, ..., i$), so that,

$$Y_N(x) = \sum_{i=0}^{N+1} \delta_i \, p_i(x) \qquad (2.65)$$

where δ_i ($i = 0, 1, ..., N + 1$) are constants. Since the residual $\pounds Y_N(x)$ is set to zero at N interior collocation points, then this residual function either vanishes everywhere or contains a polynomial,

$$F_N(x) = \prod_{i=1}^{N} (x - x_i) \qquad (2.66)$$

whose zeros are the collocation points. Then, by analogy to Galerkin's method (Finlayson, 1980), which states that the residual be orthogonal to all the trial functions, the orthogonal collocation method selects the collocation points by specifying that $F_N(x)$ be orthogonal to all the $p_i(x)$ in Eqn.(2.65), over the interval $x \in$ [0,1]. This is automatically satisfied by taking $F_N(x)$ and $p_i(x)$ from a set of orthogonal polynomials, defined as,

$$\delta_{i,N} = \frac{\displaystyle\int_0^1 p_i(x) \, p_N(x) \, dx}{\displaystyle\int_0^1 p_N^2(x) \, dx} \qquad (2.67)$$

that is by collocating at the zeros of Legendre polynomials, $P_N^{(0,0)}(x)$, for the interval $x \varepsilon [0,1]$, where the (general) Jacobi polynomials, $p_N^{(\alpha,\beta)}(x)$, have been defined by the formula (Chihara, 1978),

$$p_N^{(\alpha,\beta)}(x) = (-2)^{-N} (N!)^{-1} (1-x)^{-\alpha} (1+x)^{-\beta} \frac{d^N}{dx^N} \left[(1-x)^{N+\alpha} (1+x)^{N+\beta} \right]$$

(2.68)

for: $\alpha > -1$ and $\beta > -1$

Therefore, let x_1, x_2, ..., x_N be the roots of $P_N^{(0,0)}(x)$ and $x_0 = 0$ and $x_{N+1} = 1$ the interval end points, and let y_i ($i = 0, 1, ..., N+1$) be the function ordinates at the collocation points x_i ($i = 0, 1, ..., N+1$). Then, Eqn.(2.65) can be written as (Villadsen and Michelsen, 1978),

$$Y_N(x) = \sum_{i=0}^{N+1} \ell_i(x) y_i$$

(2.69)

where $\ell_i(x)$ is the Lagrange interpolation polynomial, defined as,

$$\ell_i(x) = \prod_{j=0}^{N+1} \frac{(x - x_j)}{(x_i - x_j)} \qquad \text{for } j \neq i$$

(2.70)

Equations (2.69) and (2.70) are very useful if an efficient algorithm is available for the computation of the Lagrange interpolation polynomials and their first and second derivatives at the collocation points. Such an algorithm is available (Villadsen and Michelsen, 1978). Then, from Eqn.(2.69), the first and second derivatives can be determined (Villadsen and Michelsen, 1978; Finlayson, 1980),

$$\left(\frac{dY}{dx} \right)\bigg|_{x=x_i} = \sum_{j=0}^{N+1} A_{i,j} Y_j$$

(2.71)

$$\left(\frac{d^2Y}{dx^2} \right)\bigg|_{x=x_i} = \sum_{j=0}^{N+1} B_{i,j} Y_j$$

(2.72)

where,

$$A_{i,j} = \ell_j^{(1)}(x_i)$$

(2.73)

and,

$$B_{i,j} = \ell_j^{(2)}(x_i)$$

(2.74)

The above results have been applied to the differential equations in the present research in Section 3.5, and some of the results are discussed in Section 5.2.5.

2.7   Concluding Remarks

Fundamentals of mass transfer through reverse osmosis (RO) membranes were given. After a short introduction of RO membranes, possible transport mechanisms were discussed. Based on different transport mechanisms, a variety of transport models were briefly reviewed. The transport models were classified as mechanism-independent and mechanism-dependent models, with the latter group classified as non-porous, porous, and electrokinetic transport models. The finely porous model (FPM) and the Surface Force-Pore Flow (SF-PF) model, from the porous-transport models group were reviewed separately due to their importance.

An introduction to the effects of temperature on RO membrane performance was given. This was followed by an introduction to the numerical technique of "orthogonal collocation" for solving differential equations.

In the present research, some of the important limitations and mistakes in the SF-PF model are removed and a new model is derived called the Modified Surface Force-Pore Flow (MD-SF-PF) model which, mathematically, looks quite different from the SF-PF model. In general, the difference between the original and the modified models can have great effects on the results predicted. The MD-SF-PF model has been presented, in detail, elsewhere (Mehdizadeh and Dickson, 1989a and 1989b).

It is realized that the continuum theory is used in the development of the models, in the present dissertation. The problem of applying continuum equations to the very fine pores of RO membranes is a controversial matter. Iberall and Schindler (1973) suggested that the Navier-Stokes equations of motion, with appropriate boundary conditions, may be valid to pore diameters as small as 1.5 nm. The fact is that the exact pore size (in synthetic or biological membranes) below which the continuum theory breaks down is a matter of controversy (e.g., Quinn et al., 1972; Beck and Schultz, 1972; Levitt, 1973) because the pore size has to be determined from the very equations whose validity is under question. Regarding these facts, and in the absence of a sound molecular theory, researchers have applied the equations of continuum theory to the molecular level transport in reverse osmosis (e.g., Merten, 1966; Jacazio et al., 1972; Neogi and Ruckenstein, 1981; Matsuura and Sourirajan, 1981).

In the rest of this Section, for deriving the MD-SF-PF model, first the radial component of the solute flux and then the axial component of the solute flux together with the equation of continuity are examined. The above changes result in changes in the velocity profile of the SF-PF model. Finally the equations required to describe the overall flux and separation are presented.

3.1.2 Radial component of solute flux

In general, a solute in a cylindrical pore (see Figure 3.1) can have a net velocity in both the axial (z) and radial (r) directions. However, the flux of solute $J_{A,r}$ is zero at the pore wall and because the pore length is much larger than the pore radius ($R_W \ll \tau$), it is reasonable to assume that radial equilibrium exists (Anderson and Malone, 1974) so that:

$$J_{A,r} = 0 \tag{3.1}$$

Considering the solute flux in the radial direction to be proportional to the chemical forces plus the potential forces acting on the solute and setting the radial flux to zero (as in Eqn.(3.1)) gives (Anderson and Malone, 1974):

$$\frac{\partial C_A(r, z)}{\partial r} + \frac{C_A(r, z)}{RT} \frac{\partial \phi(r)}{\partial r} = 0 \tag{3.2}$$

where the surface wall potential, $\phi(r)$, represents the net body force acting on the solute by the pore wall; the potential decays to zero in solutions far outside the membrane. $\phi(r)$ can be positive, indicating the solute is repulsed by the pore wall or negative indicating the solute is attracted by the pore wall. In Eqn.(3.2), $\phi(r)$ has been assumed to be independent of axial position, z. $\phi(r)$ is determined by the electrical double-layer potential for the case of electrolyte solutes, or by dispersion or van der Waals forces in the case of uncharged organic solutes.

Integrating Eqn.(3.2), according to the shown boundary conditions, at a specified axial position,

$$\int_{C_A(0, z)}^{C_A(r, z)} \frac{\partial C_A(r, z)}{C_A(r, z)} + \frac{1}{RT} \int_{\phi(0)}^{\phi(r)} \frac{\partial \phi(r)}{\partial r} dr = 0 \tag{3.3}$$

leads to the well-known Boltzmann distribution:

$$C_A(r, z) = C_A(0, z) \exp\left[- \frac{\phi(r) - \phi(0)}{RT} \right] \tag{3.4}$$
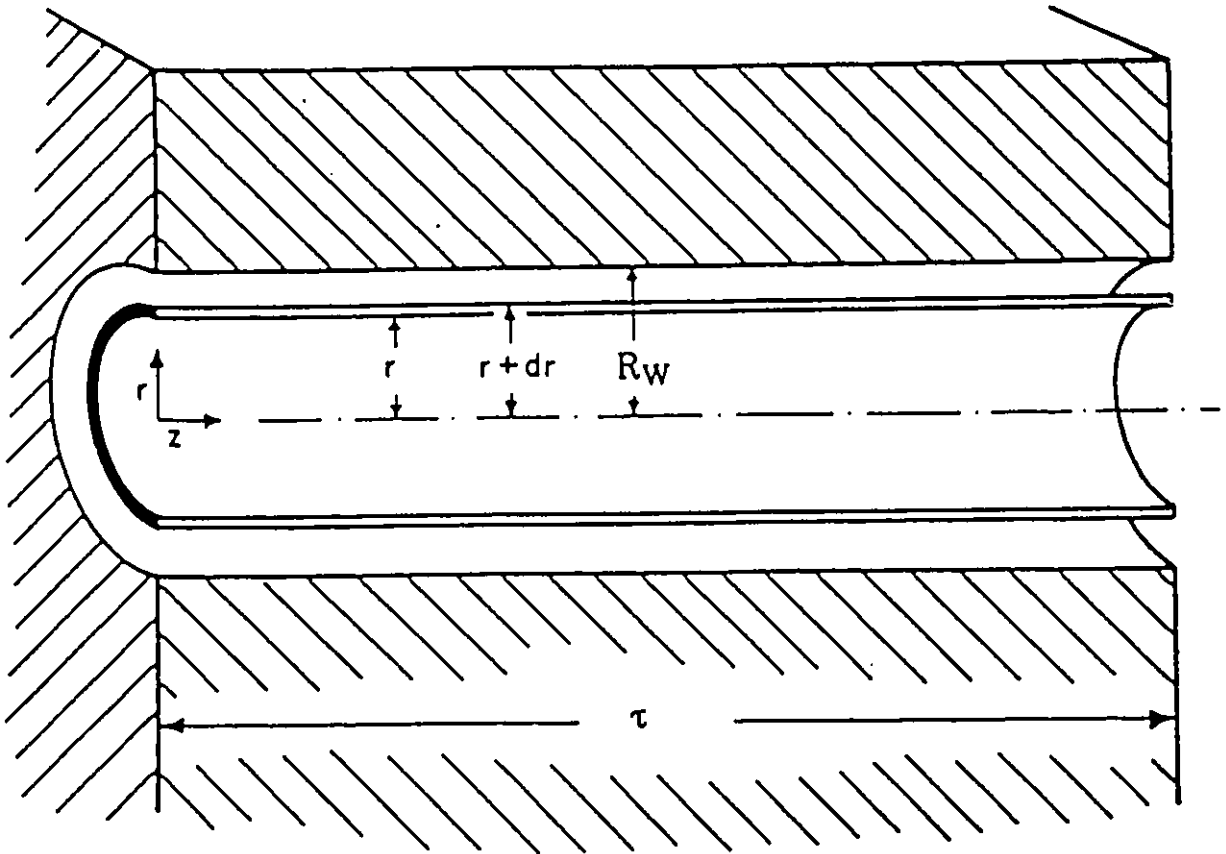
Figure 3.1:   The cylindrical coordinate system in a membrane pore.

The first major difference between our derivation and the derivation originally suggested by Matsuura and Sourirajan (1981) is in the application of Eqn.(3.4) at the outlet boundary of the pore. Setting $z = 0$ in Eqn.(3.4) gives:

$$C_A(r, 0) = C_{A2} \exp\left[-\frac{\phi(r)}{RT} \right] \tag{3.5}$$

where,

$$C_{A2} = C_A(0, 0) \exp\left[\frac{\phi(0)}{RT} \right] \tag{3.6}$$

which agrees with the SF-PF model. However, at the pore exit (where $z = \tau$),

$$C_A(r, \tau) = C_{A3} \exp\left[-\frac{\phi(r)}{RT} \right] \tag{3.7}$$

and,

$$C_{A3} = C_A(0, \tau) \exp\left[\frac{\phi(0)}{RT} \right] \tag{3.8}$$

The relationships between the concentrations just inside and just outside the pore, Eqns.(3.6) and (3.8), are further justified elsewhere (Appendix A of: Mehdizadeh and Dickson, 1989a); the justification is not shown in the present dissertation since similar derivations are shown for the Extended MD-SF-PF model in **Appendix A, part A.I.**

Equations (3.5) and (3.7) are consistent with those derived by others (Fair and Osterle, 1971; Anderson and Malone, 1974; Koh and Anderson, 1975; Neogi and Ruckenstein, 1981; Sasidhar and Ruckenstein, 1981; Westermann-Clark and Anderson, 1983). However, in the work of Matsuura and Sourirajan (1981) a radial dependency is given to C_{A3} so that Eqn.(3.7) is given as:

$$C_A(r, \tau) = C_{A3}(r) \exp\left[-\frac{\phi(r)}{RT} \right] \tag{3.9}$$

which is inconsistent both with the inlet boundary condition and with the form of Eqn.(3.4) from which the boundary conditions are derived.

The above results for the MD-SF-PF model can also be interpreted in terms of a radial dependent partition coefficient. The partition coefficient, K, is usually

defined as the ratio of concentration in the membrane over the concentration in the neighboring bulk solution at equilibrium. In this case, K is a function of radial position in the pore because of the radial dependent potential function, so that:

$$K(r) = \frac{C_A(r, 0)}{C_{A2}} = \frac{C_A(r, \tau)}{C_{A3}} = \exp\left[-\frac{\phi(r)}{RT}\right]$$

(3.10)

The partition coefficient is the same function at the pore inlet and pore outlet because of the earlier assumption that $\phi(r)$ is independent of axial position.

3.1.3   Axial component of solute flux and the equation of continuity

Since the pore is relatively long, the velocity profile is assumed to be fully developed and therefore a function of the radial position only. Then, similar to the SF-PF model, the axial component of the solute flux equation is obtained, from a force balance on the solute in the pore, as:

$$J_{A,z}(r) = -\frac{RT}{X_{AB}\, b(r)}\, \frac{\partial C_A(r, z)}{\partial z} + \frac{C_A(r, z)\, u_B(r)}{b(r)}$$

(3.11)

where;

$$X_{AB} = -\frac{F_{AB}}{u_A(r, z) - u_B(r)} = \frac{RT}{D_{AB}}$$

(3.12)

$$b(r) = \frac{X_{AB} + X_{AM}(r)}{X_{AB}} = \frac{D_{AB}}{D_{AM}(r)}$$

(3.13)

Equation (3.11) is true for the case of non-electrolytes. However, in order to properly include the osmotic effects for the case of strong electrolytes, the equation of salt flux has been derived in terms of osmotic pressure, rather than molar concentration (see Appendix B in: Mehdizadeh and Dickson, 1989a) as:

$$J_{A,z}(r) = \frac{1}{b}\left[-\frac{1}{X_{AB}}\, \frac{\partial \pi(r, z)}{\partial z} + \frac{\pi(r, z)\, u_B(r)}{RT}\right]$$

(3.14)

where π is the osmotic pressure of the solution in the pore. Similar derivation is shown for the Extended MD-SF-PF model in **Appendix A**, part A.II. Derivation of equations in terms of osmotic pressure is preferable since it properly accounts for the osmotic effects that dissociating species produce; in this way, the equations derived based on osmotic pressure, rather than concentration, are still valid for non-dissociating solute systems.

The correct way of using the above differential flux equation is to write the differential material balance in the pore, substitute in the flux equation and solve the resulting 2nd order differential equation with the two Boltzmann boundary conditions. The differential material balance states that the divergence of solute flux vector at steady state is zero:

$$\nabla \cdot \mathbf{J_A} = 0 \tag{3.15}$$

where ∇ is the del vector differential operator.

In cylindrical coordinates the angular component of the material balance is zero and the radial component is usually small compared to the axial component so that Eqn.(3.15) becomes:

$$\partial J_{A,z} / \partial z = 0 \tag{3.16}$$

Combining Eqns.(3.11) (or (3.14) for electrolytes) and (3.16) gives the following 2nd order differential equations:

$$\frac{\partial^2 C_A(\rho, \xi)}{\partial \xi^2} - \alpha(\rho) \frac{\partial C_A(\rho, \xi)}{\partial \xi} = 0 \quad \text{(for non–electrolytes)} \tag{3.17}$$

$$\frac{\partial^2 \pi(\rho, \xi)}{\partial \xi^2} - \alpha(\rho) \frac{\partial \pi(\rho, \xi)}{\partial \xi} = 0 \quad \text{(for electrolytes)} \tag{3.18}$$

where ρ and $\alpha(\rho)$ are defined by Eqns.(2.36) and (2.37), and:

$$\xi = z / \tau \tag{3.19}$$

subject to the boundary conditions, Eqns.(3.5) and (3.7). Equation (3.18) is equivalent to Eqn.(3.17) for dilute solutions of electrolytes. Equation (3.17) has been solved analytically (see Appendix C in: Mehdizadeh and Dickson, 1989a) to give the concentration profile in the pore, for the MD-SF-PF model, as:

$$C_A(\rho, \xi) = \left[C_{A2} - (C_{A2} - C_{A3}) \frac{e^{\alpha(\rho)\xi} - 1}{e^{\alpha(\rho)} - 1} \right] e^{-\Phi(\rho)} \tag{3.20}$$

where $\Phi(\rho)$ is the dimensionless potential function defined by Eqn.(2.41).

Similar derivation is shown for the Extended MD-SF-PF model in Appendix A, part A.III. Substituting the concentration profile into the solute flux Eqn.(3.11) gives an explicit expression for the solute flux in terms of the velocity profile, $\alpha(\rho)$, (see Appendix B in: Mehdizadeh and Dickson, 1989a),

$$J_{A,z}(\rho) = \frac{1}{\tau X_{AB} b(\rho)} \alpha(\rho) \left(n_2 + \frac{n_2 - n_3}{e^{\alpha(\rho)} - 1} \right) e^{-\Phi(\rho)} \tag{3.21}$$

The relationship describing the velocity profile is derived in the next section.

The above approach can be compared to that used in the original SF-PF model. Matsuura and Sourirajan (1981) used the following material balance in the pore:

$$J_{A,z}(r) = C_{A3}(r) u_B(r) \tag{3.22}$$

This Eqn.(3.22) was combined with Eqn.(3.11) to give a 1st order differential equation, which was solved using the boundary Eqn.(3.5). The resulting equation was substituted into the second boundary Eqn.(3.7) and rearranged to give an expression for $C_{A3}(r)/C_{A2}$ in the SF-PF model, as shown (see Appendix C in: Mehdizadeh and Dickson, 1989a).

The problems with the above method are as follows:

i.   Equation (3.22) ignores the diffusive contribution to solute flux and considers only the convective contribution. This violates the physical facts in Eqn.(3.11).

ii.   Equation (3.22) ignores the distinction between concentrations inside and outside the pore; a velocity inside the pore is combined with a concentration outside the pore.

iii. C_{A3} is considered to be a function of radial position as discussed in Section 3.1.2.

In essence, Matsuura and Sourirajan have assumed that the concentration profile as a function of radial position just inside the end of the pore (at $z = \tau$) and in the permeate, $C_{A3}(r)$, are the same (which violates Eqn.(3.9) in their model). Instead, in the MD-SF-PF model, the permeate concentration is considered constant, C_{A3}, and is related to the concentration inside the pore by the Boltzmann distribution and by material balance. In mathematical language, Matsuura and Sourirajan treated the problem as a parabolic one (i.e., one of the two boundaries is free and the other one is constrained) while the proper approach is to treat the problem as an elliptic one (i.e., both boundaries are constrained), as given by Eqns.(3.5) and (3.7) in the MD- SF-PF model. The result of these errors is that the SF-PF model calculates the concentration and concentration gradients in the pore incorrectly. In the original paper Matsuura and Sourirajan (1981) did not show the equation for the concentration profile in the pore. However, the derivation of concentration profile in SF- PF model is straightforward and has been shown elsewhere (see Appendix C in: Mehdizadeh and Dickson, 1989a) as:

$$C_A(\rho, \xi) = C_{A3}(\rho)\, b(\rho) + [C_{A2}\, e^{-\Phi(\rho)} - C_{A3}(\rho)\, b(\rho)]\, e^{\alpha(\rho)\xi} \qquad (3.23)$$

3.1.4 Derivation of the velocity profile

The differential equation expressing the velocity profile inside the pore can be obtained by a force balance in the z direction on the fluid element in the annular region between z and z + dz and between r and r + dr, as illustrated in Figure 3.1. The detailed derivation (presented in Appendix D of: Mehdizadeh and Dickson, 1989a) leads to the following differential equation:

$$\left(\frac{d^2 a(\rho)}{d\rho^2} + \frac{1}{\rho} \frac{d\, a(\rho)}{d\rho} \right) + \frac{1}{\beta_1} \left[\Delta P - \Delta \Pi (1 - e^{-\Phi(\rho)}) \right]$$

$$- \frac{1}{\beta_1} \left(1 - \frac{1}{b(\rho)} \right) a(\rho) \left[1 + \frac{\Delta \Pi}{e^{a(\rho)} - 1} \right] \; e^{-\Phi(\rho)} = 0 \tag{3.24}$$

where,

$$\beta_1 \;=\; \frac{\eta D_{AB}}{R_W^2 \, \pi_2} \tag{3.25}$$

$$\Delta P \;=\; \frac{\Delta P}{\pi_2} \tag{3.26}$$

$$\Delta \Pi \;=\; \frac{\pi_2 - \pi_3}{\pi_2} \tag{3.27}$$

The boundary conditions for Eqn.(3.24) are given by Eqns.(2.34) and (2.35). Equation (3.24) reduces the Poiseuille flow velocity profile for the case of zero potential, zero osmotic pressure, and b = 1,

$$a(\rho) = \frac{\Delta P \, R_W^2}{4 \eta D_{AB}} \, (1 - \rho^2) \tag{3.28}$$

Another special case is when the solute is completely rejected ($\Phi = \infty$ and b = 1) so that Eqn.(3.24) reduces to:

$$a(\rho) = \frac{(\Delta P - \pi_2) R_W^2}{4 \eta D_{AB}'} \, (1 - \rho^2) \tag{3.29}$$

The differential equation derived in the original SF-PF model is given in Eqn.(2.33), for comparison.

There are three reasons why the differential momentum balance for the original and modified models are different:

i.   In the original model the incorrect equation for solute flux is used, as discussed in Section 3.1.3.

ii.   The osmotic pressure is accounted for incorrectly in the original model. For instance, for a dissociated electrolyte the osmotic pressure at relatively low concentrations should be:

$$\pi = (v^+ + v^-)C_A \, RT \tag{3.30}$$

so that, for example, for $NaC\ell$ the osmotic pressure is estimated as 1/2 of the correct value in the original model. Instead, in the modified model the osmotic pressure is accounted for explicitly in the force balance on the solute (as illustrated in Appendix B of: Mehdizadeh and Dickson, 1989a).

iii.   The permeate concentration C_{A3} is used instead of $C_{A3}(r)$ as discussed in Section 3.1.2 on the Boltzmann boundary conditions.

3.1.5   Relationships for the solute and solvent fluxes through the membrane

In order to use the equations developed so far it is necessary to integrate solute and solvent fluxes over the area of a single pore and then to generalize for the flux over the surface area of the membrane.

The average velocity of the solvent in a single pore is found by integrating the solvent velocity profile over the cross-sectional area of the pore:

$$u_B = \frac{\displaystyle\int_0^{R_W} u_B(r)\, r\, dr}{\displaystyle\int_0^{R_W} r\, dr} = 2\left(\frac{RT}{\tau X_{AB}}\right) \int_0^1 a(\rho)\rho\, d\rho \tag{3.31}$$

Then, the average solvent flux is:

$$J_B = u_B C = 2\left(\frac{CRT}{\tau X_{AB}}\right) \int_0^1 a(\rho)\rho\, d\rho \tag{3.32}$$

The average solute flux is found by averaging the solute flux profile over the pore cross-sectional area as:

$$J_A = \frac{\displaystyle\int_0^{R_W - R_A} J_{A,z}(r)\, r\, dr}{\displaystyle\int_0^{R_W} r\, dr} = \frac{2}{\tau\, X_{AB}} \int_0^{1-\lambda} a(\rho)\left(n_2 + \frac{n_2 - n_3}{e^{a(\rho)} - 1}\right)\frac{e^{-\Phi(\rho)}}{b(\rho)}\,\rho\, d\rho \tag{3.33}$$

where λ is the dimensionless solute molecular radius defined by Eqn.(2.47).

In the above integration, the solute molecule is assumed to be no closer than one solute radius from the pore wall.

The permeate concentration, C_{A3}, is related to the solute and solvent fluxes as:

$$C_{A3} = C\,\frac{J_A}{(J_A + J_B)} \tag{3.34}$$

Upon substituting for the average fluxes in Eqn.(3.34), from Eqns.(3.32) and (3.32), the following relationship is found between C_{A3} and two definite integrals:

$$C_{A3} = C\left[1 + CRT\,\frac{\ell_1}{\ell_2}\right]^{-1} \tag{3.35}$$

where ℓ_1 and ℓ_2 are defined as the following two integrals:

$$\ell_1 = \int_0^1 a(\rho)\rho\, d\rho \tag{3.36}$$

$$\ell_2 = \int_0^{1-\lambda} a(\rho)\left(n_2 + \frac{n_2 - n_3}{e^{a(\rho)} - 1}\right)\frac{e^{-\Phi(\rho)}}{b(\rho)}\,\rho\, d\rho \tag{3.37}$$

In order to relate an average flux through a single pore to the flux through a membrane, N_i, the fractional pore area, ε, is used:

$$N_A = \varepsilon J_A = \frac{2}{X_{AB}} \left(\frac{\varepsilon}{\tau} \right) \int_0^{1-\lambda} \frac{a(\rho)}{b(\rho)} \left(\pi_2 + \frac{\pi_2 - \pi_3}{e^{a(\rho)} - 1} \right) e^{-\Phi(\rho)} \rho \, d\rho \tag{3.38}$$

$$N_B = \varepsilon J_B = \frac{2}{X_{AB}} \left(\frac{\varepsilon}{\tau} \right) CRT \int_0^1 a(\rho) \, \rho \, d\rho \tag{3.39}$$

Then, the total flux is given by:

$$N_T = (N_A + N_B) = \frac{2}{X_{AB}} \left(\frac{\varepsilon}{\tau} \right) (\ell_1 + \ell_2) \tag{3.40}$$

For pure solvent moving freely, the velocity profile in Eqn.(3.24) reduces to the Poiseuille velocity profile in Eqn.(3.28) and the solvent flux, N_B, in Eqn.(3.38) reduces the pure solvent flux, N_P, as:

$$N_P = A \, \Delta P \tag{3.41}$$

where,

$$A = \frac{CR_w^2}{8\eta \, (\ell/\varepsilon)} \tag{3.42}$$

The above analysis assumes that all the pores on the membrane surface have the same radius. If a pore size distribution is needed then the solute and solvent fluxes J_A and J_B need to be integrated across all the possible pore sizes. Methods of doing this are presented in the literature (e.g., Matsuura and Sourirajan, 1981).

3.1.6 The potential function

The potential function used in the original SF-PF model considers the potential between a point and a flat wall, as discussed in Section 2.3.2.5. For electrolyte solutes and non-dissociable organic solutes, the potential functions are given by Eqns.(2.45) and (2.46). These relationships are then used inside the cylindrical pore. In this form, the equations are inconsistent with the cylindrical pore geometry and as

such are not a good representation of the solute-pore wall interaction. One consequence of this inconsistency is that the radial gradient of the potential is non-zero at the pore centerline. This result can be calculated by taking the derivative of the potential and evaluating this at $\rho = 0$; for example, for the case of electrolytes,

$$\left. \frac{d\Phi(\rho)}{d\rho} \right|_{\rho=0} = \frac{A}{R_W} \neq 0 \tag{3.43}$$

The potential function in Figure 3.2 illustrates that the potential function comes to a peak at the pore centerline instead of the expected smooth function.

Strictly speaking the method for correcting this problem is to examine the potential function between the solute and pore wall and to write this expression in cylindrical coordinates. This approach is complex and should be examined in future research. For now, an empirical equation which is both consistent with the cylindrical geometry and has approximately the correct shape is proposed. Because this equation is empirical it can be applied to any solute (which is soluble in solvent) and membrane (charged or uncharged); for the case of attractive organic solutes, a different form of potential function is proposed in Section 3.2.6. The preliminary potential equation, for the case of solvent-membrane affinity, in the MD-SF-PF model is:

$$\Phi(\rho) = \begin{cases} \dfrac{\theta_1}{R_W} e^{\theta_2 \rho^2} & \text{when: } \rho < 1-\lambda \\ \infty & \text{when: } \rho \geq 1-\lambda \end{cases} \tag{3.44}$$

which has two fitting parameters, θ_1 and θ_2. θ_1 affects the centerline potential and θ_2 affects the radial slope of the potential curve. The radial gradient at the pore centerline is zero for this function. Figure 3.3 illustrates an example of this potential function. As discussed in Section 5.2.4, θ_2 is always close to 1/2 for the membranes tested during the present research, so that the MD-SF-PF model becomes a three-parameter model: R_W, θ_1, and τ/ε. The first two parameters (i.e., R_W and θ_1) are
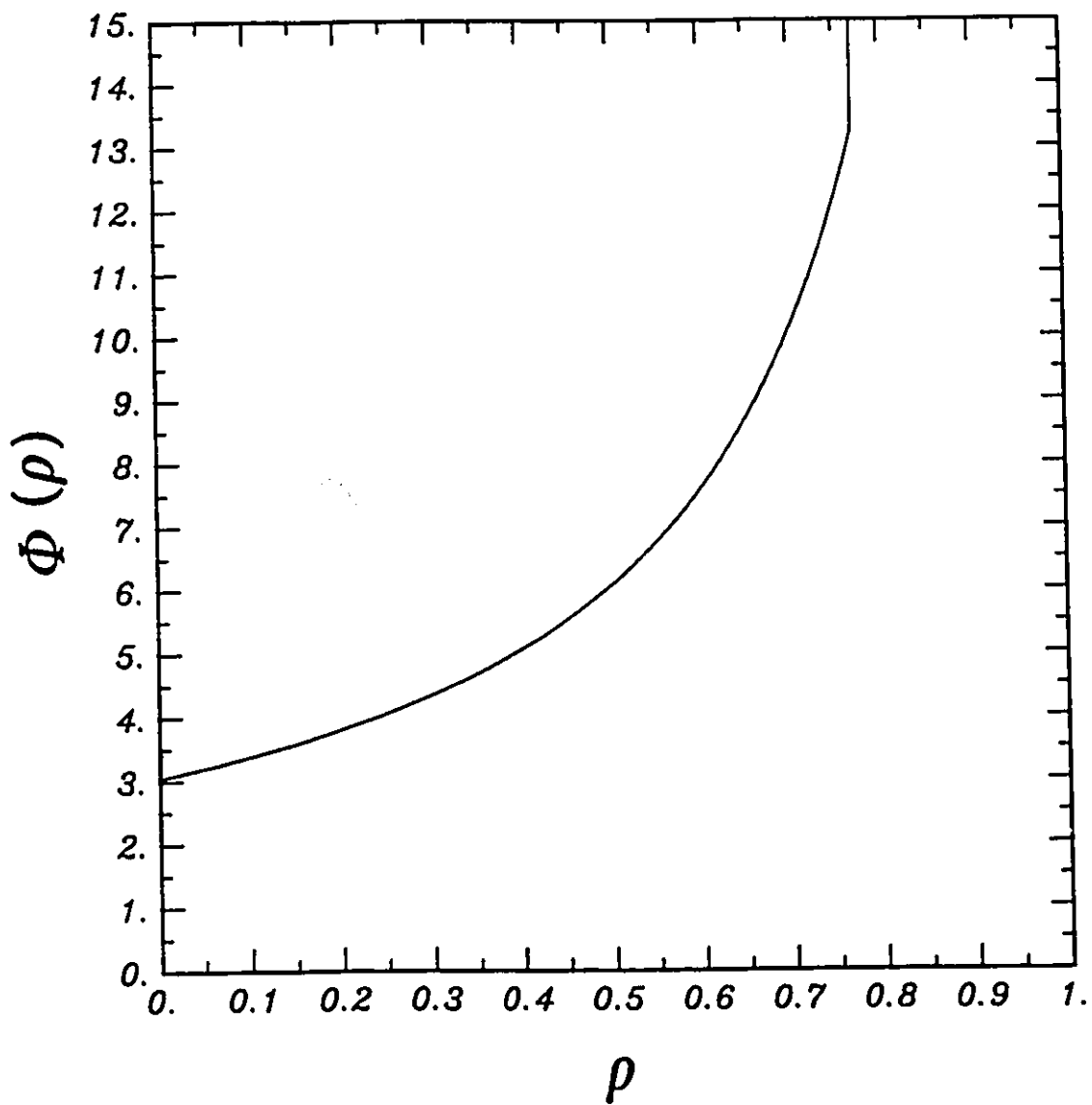
Figure 3.2:   Typical potential curve as a function of dimensionless radial position, ρ, in SF-PF model for the case of electrolytes: NaCℓ-water, $A = 21 \times 10^{-10}$ m, and $R_W = 6.9 \times 10^{-10}$ m.
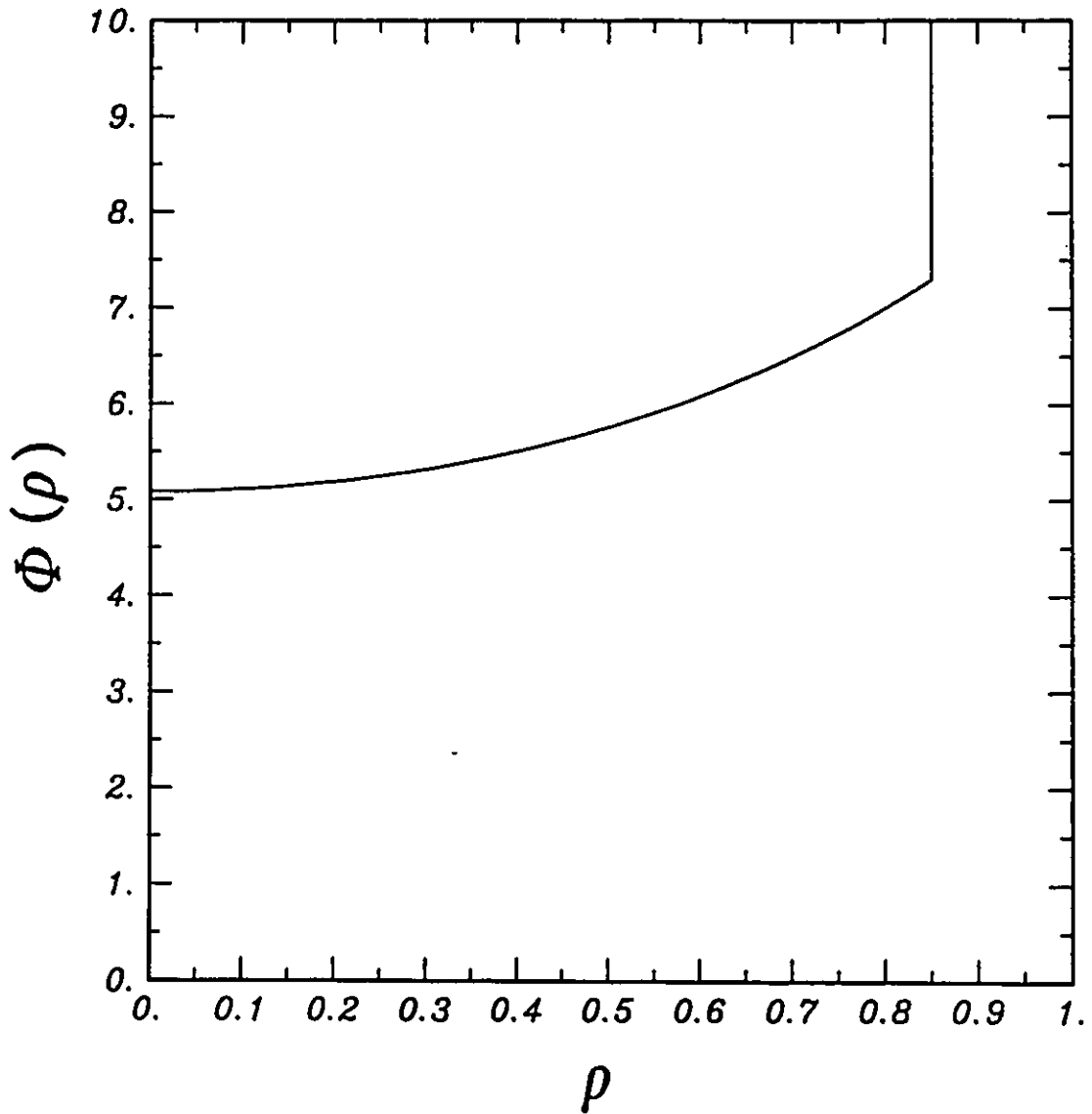
Figure 3.3:   Typical potential curve as a function of dimensionless radial position, ρ, in MD-SF-PF model for the case of electrolytes: NaCℓ-water, $\theta_1 = 54.4 \times 10^{-10}$ m, $\theta_2 = 0.49$, and $R_W = 10.7 \times 10^{-10}$ m.

necessary and enough to determine the separation, f', and the flux ratio, N_T/N_P, by the MD-SF-PF model. To calculate the absolute values of the fluxes (i.e., N_T and N_P) the third parameter, τ/ε, is also needed.

3.1.7   The friction function

An expression is required, in either the SF-PF or MD-SF-PF model, which describes the friction between the solute and the pore wall. This friction is the result of the hydrodynamic drag for a solute molecule moving in a small pore. Matsuura and Sourirajan have suggested using an empirical relationship for the friction function, b, in their first paper (Matsuura and Sourirajan, 1981). In later papers (Matsuura et al., 1981; Chan et al., 1982) they use a modified form of the Faxen equation, given by Eqn.(2.48).

Although the friction function should be a function of radial position, the Faxen equation (given by Eqn.(2.31)) is a reasonable approximation (e.g., Jonsson and Boesen, 1975) and is used in the MD-SF-PF model.

3.2   Development of the Extended MD-SF-PF Model

3.2.1   Introduction

In this section, the original MD-SF-PF model is reformulated and extended to a more general form to include the more difficult case of strong solute-membrane affinity (discussed in Section 2.3.3).

The model, called the Extended MD-SF-PF model, hereafter, differs in the following three aspects from the original MD-SF-PF model (Mehdizadeh and Dickson, 1989c):

i) The chemical potential of solute takes into account the effect of the pressure-induced solute transport. This additional term may be important for solutes with high partial molar volumes and membranes that have relatively low solute-water separation.

ii) The membrane surface potential function is assumed to be concentration dependent so that the surface potential varies as a function of both radial and axial positions inside the membrane. In the original MD-SF-PF model, the potential function varies only with radial direction, so that the partition coefficients on the high and low pressure sides of the membrane become equal. However, the partition coefficient may vary with concentration, membrane structure, temperature, and possibly pressure. In this work, a model for the variation of the potential function with radial and axial positions, inside the membrane, is proposed; as a result, the partition coefficients at the ends of the membrane may be different.

iii) The hydrodynamic friction function between the solute and the membrane, b, is assumed to vary in the radial direction inside the membrane. In the original MD-SF-PF model, this function is given by the Faxen equation which assumes the friction function is a constant (i.e., independent of radial position).

In this section, the extended MD-SF-PF model is derived in a manner paralleling the MD-SF-PF model, discussed in Section 3.1. First, the radial component of the solute flux and then the axial component of the solute flux together with the equation of continuity are examined. Finally, the equations required to describe the overall flux and separation are presented.

3.2.2   Radial component of solute flux

Following the assumption of radial equilibrium (Anderson and Malone, 1974), the radial component of the solute flux in a pore is:

$$J_{A,r} = \frac{\partial C_A(r, z)}{\partial r} + \frac{C_A(r, z)}{RT} \frac{\partial \phi(r,z)}{\partial r} = 0 \tag{3.45}$$

Now, the pore wall potential, $\phi(r,z)$, is allowed to vary along the pore length. As usual (see Section 3.1), a positive value for the potential means solute-membrane repulsion and a negative value means solute-membrane attraction.

Integration of Eqn.(3.45), according to the following boundary conditions, and at a specified axial position,

$$\int_{C_A(0,z)}^{C_A(r,z)} \frac{\partial C_A(r, z)}{C_A(r, z)} + \frac{1}{RT} \int_{\phi(0,z)}^{\phi(r,z)} \frac{\partial \phi(r,z)}{\partial r} \, dr = 0 \tag{3.46}$$

leads to the following Boltzmann distribution equation:

$$C_A(r, z) = C_A(0, z) \exp\left[-\frac{\phi(r,z) - \phi(0,z)}{RT} \right] \tag{3.47}$$

Setting $z = 0$ (i.e., at the pore entrance) in Eqn.(3.47) gives:

$$C_A(r, 0) = C_{A2} \exp\left[-\frac{\phi(r,0)}{RT} \right] \tag{3.48}$$

where,

$$C_{A2} = C_A(0, 0) \exp\left[\frac{\phi(0, 0)}{RT} \right] \tag{3.49}$$

Similarly, at $z = \tau$ (i.e., at the pore exit) Eqn.(3.47) reduces to:

$$C_A(r, \tau) = C_{A3} \exp\left[-\frac{\phi(r, \tau)}{RT} \right] \tag{3.50}$$

where,

$$C_{A3} = C_A(0, \tau) \exp\left[\frac{\phi(0,\tau)}{RT} \right] \tag{3.51}$$

The relationships between the concentrations just inside and just outside the pore, Eqns.(3.49) and (3.51), are further justified in **Appendix A**. Equations (3.45) to (3.51)

are similar to Eqns.(3.2) to (3.8) in the MD-SF-PF model; the only difference is that the potential can now vary with axial position.

The above results, Eqns.(3.48) and (3.50), can also be interpreted in terms of the radial dependent partition coefficients on the high and low pressure sides of the membrane:

$$K_2(r) = \frac{C_A(r, 0)}{C_{A2}} = \exp\left[-\frac{\phi(r,0)}{RT}\right] \qquad (3.52)$$

$$K_3(r) = \frac{C_A(r, \tau)}{C_{A3}} = \exp\left[-\frac{\phi(r,\tau)}{RT}\right] \qquad (3.53)$$

The partition coefficients are different since the potential functions are different at the ends of a pore. For convenience, in the following analysis, Eqns.(3.48), (3.50), (3.52), and (3.52) are rewritten as:

$$C_A(\rho, 0) = C_{A2} K_2(\rho) \qquad (3.54)$$

$$C_A(\rho, 1) = C_{A3} K_3(\rho) \qquad (3.55)$$

$$K_2(\rho) = \exp\left[-\phi(\rho, 0)\right] \qquad (3.56)$$

$$K_3(\rho) = \exp\left[-\phi(\rho, 1)\right] \qquad (3.57)$$

where,

$$\Phi(\rho, \xi) = \frac{\phi(r, z)}{RT} \qquad (3.58)$$

and ρ and ξ are the dimensionless radial and axial coordinates defined by Eqns.(2.36) and (3.19). The average partition coefficients, K_2 and K_3, are obtained by integrating Eqns.(3.56) and (3.57) over the pore radius available to the solute molecules (i.e., from $\rho = 0$ to $\rho = 1 - \lambda$),

$$K_2 = \frac{\int_0^{1-\lambda} K_2(\rho)\, \rho\, d\rho}{\int_0^1 \rho\, d\rho} = 2 \int_0^{1-\lambda} e^{-\Phi(\rho,0)}\, \rho\, d\rho \qquad (3.59)$$

$$K_3 = \frac{\int_0^{1-\lambda} K_3(\rho)\, \rho\, d\rho}{\int_0^1 \rho\, d\rho} = 2 \int_0^{1-\lambda} e^{-\Phi(\rho,1)}\, \rho\, d\rho \qquad (3.60)$$

where λ is the dimensionless solute radius (Eqn.(2.47)). Knowing the potential function, $\Phi(\rho,\xi)$, one can determine the partition coefficients from Eqns.(3.59) and (3.60).

3.2.3 Axial component of solute flux and the equation of continuity

The total driving force of solute is given by the solute chemical potential gradient inside the pore (Anderson and Malone, 1974):

$$F_A(r, z) = -\frac{\partial \mu_A(r, z)}{\partial z} \qquad (3.61)$$

where the solute chemical potential is:

$$\mu_A = \mu_A^o + RT\, \ell n\, a_A + v_A P \qquad (3.62)$$

The $v_A P$ term is included in Eqn.(3.62) to account for the transport of solute molecules by pressure forces. Assuming the solution to be ideal, so that the activity can be replaced with mole fraction, the gradient of the solute chemical potential can be written as:

$$\frac{\partial \mu_A (r, z)}{\partial z} = \frac{1}{C_A (r, z)} \frac{\partial [RT\, C_A (r, z)]}{\partial z} + v_A \frac{\partial P (r, z)}{\partial z} \qquad (3.63)$$

so that Eqn.(3.61), upon using van't Hoff's equation for solution osmotic pressure (given by Eqn.(2.2)), becomes:

$$F_A(r, z) = - \frac{RT}{n(r,z)} \frac{\partial n(r, z)}{\partial z} - v_A \frac{\partial P(r, z)}{\partial z} \tag{3.64}$$

This equation is used in a force balance on solute inside the pore, as shown in **Appendix A**, to derive the axial component of the equation of solute flux as:

$$J_{A,z}(\rho) = \frac{1}{\varsigma X_{AB} b(\rho)} \left\{ - \frac{\partial n(\rho, \xi)}{\partial \xi} - v_A \frac{n(\rho, \xi)}{RT} \frac{\partial P(\rho, \xi)}{\partial \xi} + a(\rho) n(\rho, \xi) \right\} \tag{3.65}$$

where the friction coefficient X_{AB} is defined as:

$$X_{AB} = - \frac{F_{AB}(\rho, \xi)}{[u_A(\rho, \xi) - u_B(\rho)]} \tag{3.66}$$

and $b(\rho)$ and $a(\rho)$ are the friction function and fluid velocity defined by Eqns.(2.29) and (2.37).

The equation of continuity, Eqn.(3.15), or the reduced form, Eqn.(3.16), is now combined with the equation of solute flux, Eqn.(3.65), to yield the following differential equation for osmotic pressure inside the pore:

$$\frac{\partial^2 n(\rho, \xi)}{\partial \xi^2} + \frac{v_A}{RT} \frac{\partial}{\partial \xi} \left\{ n(\rho, \xi) \frac{\partial P(\rho, \xi)}{\partial \xi} \right\} - a(\rho) \frac{\partial n(\rho, \xi)}{\partial \xi} = 0 \tag{3.67}$$

which upon being solved (see **Appendix A**) results in the profiles of osmotic pressure and concentration:

$$n(\rho, \xi) = \left\{ n_2 - [n_2 - K^*(\rho) \, n_3] \frac{e^{[a(\rho) + \omega(\rho)]\xi} - 1}{e^{[a(\rho) + \omega(\rho)]} - 1} \right\} e^{-\Phi(\rho, 0)} \tag{3.68}$$

$$C_A(\rho, \xi) = \left\{ C_{A2} - \left[C_{A2} - K^*(\rho) C_{A3} \right] \frac{e^{[a(\rho) + \omega(\rho)]\xi} - 1}{e^{[a(\rho) + \omega(\rho)]} - 1} \right\} e^{-\Phi(\rho, 0)} \tag{3.69}$$

where $K^*(\rho)$ is the ratio of the radial partition coefficients at the ends of the pore,

$$K^*(\rho) = \frac{e^{-\phi(\rho, 1)}}{e^{-\phi(\rho, 0)}} \tag{3.70}$$

and $\omega(\rho)$ represents the solute velocity induced by pressure forces, defined as:

$$\omega(\rho) = \frac{v_A}{RT} \left\{ \Delta P - [\sigma_2(\rho) n_2 - \sigma_3(\rho) n_3] \right\} \tag{3.71}$$

Therefore, Eqn.(3.71), which is similar to the equation of solvent flux (see Eqn.(2.3)), represents the solute flow as contributed by pressure forces. This solute flux is ignored in the MD-SF-PF model, discussed in Section 3.1. The $\sigma_2(\rho)$ and $\sigma_3(\rho)$ in Eqn.(3.71) are defined as:

$$\sigma_2(\rho) = 1 - e^{-\phi(\rho, 0)} \tag{3.72}$$

$$\sigma_3(\rho) = 1 - e^{-\phi(\rho, 1)} \tag{3.73}$$

It is interesting to note that the $\sigma_2(\rho)$ and $\sigma_3(\rho)$ are local Staverman (or reflection) coefficients at each side of the membrane; Staverman coefficients were discussed in Section 2.1.2. The v_A/RT coefficient, in Eqn.(3.71) is compared to the solvent permeability coefficient, A, in Eqn.(2.3). The larger the partial molar volume of the solute, v_A, and/or the higher the operating pressure, ΔP, the larger is the pressure-induced transport of the solute.

Equation (3.69) is very interesting, illustrating the phenomenon of solute repulsion or attraction is highly dependent on the values of the potential function across the membrane. That is, if the potential function is such that the ratio $K^*(\rho)$ so that $K^*(\rho) C_{A3}$ becomes smaller than C_{A2}, then concentration decreases along the pore length and, therefore, positive separation is calculated. On the other hand, if the potential is such that the ratio $K^*(\rho)$ so that $K^*(\rho) C_{A3}$ becomes larger than C_{A2}, then concentration increases along the pore length and, therefore, negative separation is calculated; in this case, solute is attracted by the membrane and the permeate stream becomes enriched with the solute (i.e., negative separation). The case of negative separation was shown in Figure 2.4, in Chapter 2. It is also possible for the potential function to have negative values (i.e., solute attraction) when $K^*(\rho) C_{A3}$ is smaller than C_{A2}; in this case (shown in Figure 2.3 in Chapter 2), solute is still attracted to the

membrane but positive separation occurs due to low mobility of solute molecules inside the pores. Some real examples of solute-membrane affinity, for both negative and positive separation systems, are presented and further discussed from the physical point of view in Section 5.4.2.

Finally, substituting Eqn.(3.68) into Eqn.(3.65) gives an explicit expression for the solute flux, as shown in **Appendix A**, to be:

$$J_{A,2}(\rho) = \left[\frac{a(\rho) + \omega(\rho)}{\tau X_{AB} b(\rho)} \right] \left\{ n_2 + \frac{n_2 - K^*(\rho) n_3}{e^{[a(\rho) + \omega(\rho)]} - 1} \right\} e^{-\Phi(\rho, 0)} \qquad (3.74)$$

This useful equation is used, in the following sections, to determine membrane separation and flux.

3.2.4 Derivation of the velocity profile

A force balance in the z direction on the fluid element, in the annular region between z and z+dz and between r and r+dr (Figure 3.1), yields the differential equation for the fluid velocity profile inside the pore as shown in **Appendix A**. The result is:

$$\left(\frac{d^2 a(\rho)}{d\rho^2} + \frac{1}{\rho} \frac{d a(\rho)}{d\rho} \right) + \frac{1}{\beta_1} \left\{ \frac{\Delta P}{n_2} - \frac{n_2 \sigma_2(\rho) - n_3 \sigma_3(\rho)}{n_2} \right\}$$

$$- \frac{1}{\beta_1} \left[1 - \frac{1}{b(\rho)} \right] [a(\rho) + \omega(\rho)] \left\{ 1 + \frac{1 - (n_3/n_2) K^*(\rho)}{e^{[a(\rho) + \omega(\rho)]} - 1} \right\} e^{-\Phi(\rho, 0)} = 0 \qquad (3.75)$$

where $a(\rho)$ has been defined by Eqn.(2.37). The boundary conditions are the same as those in the MD-SF-PF and SF-PF models, that is, Eqns.(2.34) and (2.35). The above velocity profile correctly reduces to the form in the original MD-SF-PF model, Eqn.(3.24), when the potential function becomes only a function of radial position (i.e., $K_2(\rho) = K_3(\rho)$) and v_A is negligible.

3.2.5 Solvent and solute fluxes through the membrane and the criterion of separation

The solvent and solute fluxes through a single pore are integrated over the area of the pore and then generalized for the fluxes over the surface area of the membrane as follows.

The average velocity of the solvent in a single pore is given by Eqn.(3.31), and the average solvent flux is given by Eqn.(3.32).

Using Eqn.(3.74), the average solute flux over the pore area is:

$$J_A = \left(\frac{2}{\tau X_{AB}}\right)\ell_3 \tag{3.76}$$

where,

$$\ell_3 = \int_0^{1-\lambda} [\alpha(\rho) + \omega(\rho)] \left\{\pi_2 + \frac{\pi_2 - K^*(\rho)\,\pi_3}{e^{[\alpha(\rho)+\omega(\rho)]}-1}\right\} \frac{e^{-\Phi(\rho,0)}}{b(\rho)}\, \rho\, d\rho \tag{3.77}$$

The above average fluxes over the pore area, J_A and J_B, are related to permeation fluxes through the membrane, N_A and N_B, using the fractional pore area, ε. The equation for N_B is given in Eqn.(3.39), and N_A is:

$$N_A = \varepsilon J_A = \frac{2}{X_{AB}}\left(\frac{\varepsilon}{\tau}\right)\ell_3 \tag{3.78}$$

Therefore, the total permeation flux through the membrane, N_T, is:

$$N_T = (N_A + N_B) = \frac{2}{X_{AB}}\left(\frac{\varepsilon}{\tau}\right)(CRT\,\ell_1 + \ell_3) \tag{3.79}$$

where ℓ_1 has been defined by Eqn.(3.36).

The material balance on the solute flux across the membrane, given by Eqn.(2.10) determines the permeate concentration. Upon substituting the average fluxes into Eqn.(2.10), from Eqns.(3.39) and (3.78), the following relationship is obtained for the permeate concentration:

$$C_{A3} = C\left[1 + CRT\left(\frac{\ell_1}{\ell_3}\right)\right]^{-1} \tag{3.80}$$

which is similar to Eqn.(3.35) in the original MD-SF-PF model. Finally, the separation achieved by a membrane is determined from Eqn.(2.6).

3.2.6 Forms of the potential and friction functions

In the original MD-SF-PF model, Eqn.(3.44) describes the form of the potential function for the case of solute repulsion by a membrane. This equation still holds in the Extended MD-SF-PF model, for the case of dissociable solutes, such as electrolytes, in which the potential function (and, therefore, the partition coefficient) is almost independent of feed concentration so that equal partition coefficients, on the two sides of the membrane, are expected (Lonsdale et al., 1965). However, strong solute-membrane affinity systems are usually associated with different partition coefficients on the two sides of the membrane (e.g., Connell, 1986). This implies that, in this case, the potential field may depend on other factors such as the solute concentration.

A first approximation to modeling of the concentration dependency may be as the following:

$$\phi(\rho, \xi) = \frac{\theta_1}{R_w} e^{\frac{1}{2}\rho^2} f\{C_A(\rho, \xi)\} \tag{3.81}$$

where $f\{C_A(\rho,\xi)\}$ is some relationship between the potential and the concentration inside the pore. However, whatever the $f\{C_A(\rho,\xi)\}$ should be, the concentration, $C_A(\rho,\xi)$, needs to be determined from the potential function (see Eqn.(3.69)) and the solution velocity which depends on the potential function (see Eqn.(3.75)). Therefore, the governing equations are highly coupled and formidable to solve. In order to avoid such difficult trial and error procedure, it may be possible to break down the $f\{C_A(\rho,\xi)\}$ term into separated feed and permeate concentration and some axial dependency, in

an empirical manner. One such correlation, which has been found in the present research to well represent the data (discussed in Section 5.4), is:

$$\phi(\rho, \xi) = \begin{cases} \dfrac{\theta_1}{R_w} e^{\frac{1}{2}\rho^2} e^{\gamma\xi} \left[1 + \dfrac{\ln C_{A2}}{\ln C_{A3}} \right] & \text{when } \rho < 1 - \lambda \\ \\ \infty & \text{when } \rho \geq 1 - \lambda \end{cases}$$

(3.82)

for dilute feed solutions of non-dissociable organic solutes (i.e., $X_{A1} \ll 1.0$). In the above equation, θ_1 and γ are the two empirical parameters required to know the potential function. The separation of variables done from Eqn.(3.81) to Eqn.(3.82) decouples the problem and simplifies the solution of the model. The concentration dependency suggested in Eqn.(3.82) implies that as the feed concentration of the uncharged organic solute is increased the potential function becomes less attractive, and, therefore, the separation should increase as expected (e.g., Dickson, 1985). The γ parameter empirically models the axial variation of the potential inside the pore. The axial dependency in Eqn.(3.82) suggests that as the solute molecules move through the pore they feel a stronger attraction potential, and the potential function at the pore end is, therefore, stronger than that at the pore inlet; this means that the partition coefficient at the pore exit is larger than the partition coefficient at the pore inlet, for the case of uncharged organic solutes, which means $K^*(\rho) > 1$ (see Eqn.(3.70)).

Equation (3.82), has been selected from several possibilities, but a better correlation may be found for the model, in the future.

The friction parameter, $b(\rho)$, which is given by the Faxen equation, Eqn.(2.31), in the MD-SF-PF model, is now allowed to vary in the radial direction inside the pore, in the Extended MD-SF-PF model. Originally, Matsuura and Sourirajan (1981) suggested an exponential radial dependency for $b(\rho)$ but later used an average b value given by Eqn.(2.48). Satterfield et al. (1973), who have studied the

problem of using an average b value, have found that the Faxen equation was not able to describe their experimental data for effective diffusivities of aromatic and paraffinic hydrocarbons in silica-alumina catalysts, and suggested an empirical correlation for the friction factor. Several other researchers have also found that the Faxen equation could not describe their experimental data (Anderson and Quinn, 1974; Deen et al., 1981). Anderson and Quinn (1974), who studied the problem of restricted diffusion in pores, agree with Bean (1972) that the radial dependence of b should be taken into account.

In the light of the discussion made by Dickson (1985) that concluded that the Faxen equation might not be adequate for solute-membrane affinity case, the following relationship, as suggested by Dickson (1985), is used in the Extended MD-SF-PF model:

$$b(\rho) = \begin{cases} b_{Faxen} \exp\left[\dfrac{E/R_w}{1-\rho}\right] & \text{when } \rho < 1 - \lambda \\[2mm] \infty & \text{when } \rho \geq 1 - \lambda \end{cases} \tag{3.83}$$

where E is an adjustable parameter. Equation (3.83) allows the friction function to vary markedly along the radial position inside the pore; the equation reduces to the Faxen equation when E becomes zero or far from the pore wall where the exponential term approaches 1.0 in large pores.

Equation (3.83) implies that when the parameter E is of the same (or larger) order of magnitude as (than) the pore size, R_w, very small diffusivities for the solute molecules are predicted (see Eqn.(2.30)). This result is consistent with the mechanism that, due to the strong attraction potentials inside the pore, the solute molecules diffuse very slowly through the pore.

3.3   Modeling of Temperature Effects

Temperature can have significant effects on the performance of RO membranes as discussed in Section 2.5. Most transport models available in the literature are isothermal. Only a few researchers have tried to model temperature effects; these models can be grouped into two classes, as described in Section 2.5, neither of which is useful in shedding light on the mechanism of transport. In this section, a third, more sound approach to modeling of temperature effects is offered. Briefly, the method is to incorporate, a priori, temperature effects directly in to an appropriate model and obtain a temperature-extended model based on the temperature dependencies of the physical properties of the system. The model used is the MD-SF-PF model (see Section 3.1) as described below.

.

3.3.1   Development of the temperature-extended MD-SF-PF model

In this section, the MD-SF-PF model, developed in Section 3.1, is extended into a temperature-dependent form (Mehdizadeh and Dickson, 1989d). The MD-SF-PF model has three adjustable parameters: the membrane pore size, R_W; a potential parameter to characterize the solute-membrane interactions, θ_1; and the parameter τ/ε which characterizes the physical structure of the membrane in terms of the effective membrane thickness, τ, and the relative surface pore area, ε. The model includes physical properties of solution such as density, viscosity, osmotic pressure, and solute diffusivity. Recall, from Section 3.1.6, that knowing only the values of R_W and θ_1, and the physical properties of the solution, allows prediction of membrane performance in terms of the theoretical separation, f', and the ratio of solution flux to pure solvent (water) flux, N_T/N_P (called the flux ratio). In order to determine the absolute values of the fluxes (i.e., N_T and N_P), requires the third parameter, τ/ε.

The MD-SF-PF model can be converted into a temperature-extended model by incorporating the temperature dependencies of all the model parameters and the physical properties. Temperature dependencies of the physical properties of aqueous solutions can be found in the literature (e.g., Stoughton and Lietzke, 1965; Korosi and Fabuss, 1968; Sourirajan, 1970; Weast, 1975; Reid et al., 1977). In the present research, it has been assumed that the membrane pore size, R_W, and the potential parameter, θ_1, are independent of temperature and the values determined at 25°C can be used at any temperature.

The assumption that θ_1 is temperature independent implies that the dimensionless potential function, $\Phi(\rho)$, is assumed to be independent of temperature. This implies the potential field, expressed by the potential function $\phi(\rho)$, varies linearly with temperature.

$$\Phi(\rho) = \frac{\phi(\rho)}{RT} \tag{2.41}$$

Is this a reasonable approximation for the potential inside the cylindrical pore? As a rough evaluation of this approximation, a simpler case can be considered in which a potential field, due to an electrochemical double-layer, exists between two infinite parallel plates. The surface potential can be expressed in terms of an "interaction energy", U, which is the energy of the potential field per unit area of electrochemical double-layer and is defined as the amount of work needed to bring the two flat plates from infinity to a finite distance (Chapter V in: Verwey and Overbeek, 1948).

The interaction energy has been derived for the case of constant-charge density, for the two flat plates system; for the special case of small double-layer potentials, the interaction energy is given as (Usui, 1973),

$$U = \left(\frac{16\, n^2 \sigma^2}{\epsilon_r \epsilon_o \kappa} \right) \left\{ \coth(\kappa h) - 1 \right\} \tag{3.84}$$

where κ is the reciprocal of Debye length:

$$\kappa = \left\{ \frac{e^2 \sum_i z_i^2 n_i}{\varepsilon_r \varepsilon_o k_o T} \right\}^{1/2}$$

(3.85)

For the above special case (Eqns.(3.84) and (3.85)), as temperature is increased both the Debye length, $1/\kappa$, and $\coth(\kappa h)$ increase, so that the interaction energy increases in a somewhat non-linear manner for temperatures up to 60°C . Now, for the case of a cylindrical pore, the situation is more complex and no equation for interaction energy of double-layer has yet been derived. However, by analogy with the case of the flat plates, the assumption that the potential function increases with temperature is reasonable.

Based on these assumptions, the temperature-extended model may be employed to describe or predict RO membrane performance as a function of temperature.

3.3.1.1 Modeling of compaction effect

One important phenomenon in high-temperature reverse osmosis is the compaction effect, described in Section 2.5. RO membranes usually exhibit a decrease in permeability due to compaction of the membrane as either pressure or temperature is increased. The following description of membrane compaction is appropriate for the aromatic polyamide FT30 membranes (for the membranes, see Section 2.2) but a similar approach should work for other membranes. The compaction effect can be modeled by considering the equation of pure solvent flux, given by Eqns.(3.41) and (3.42). These two equations can be combined to give:

$$\frac{v/c}{R_w^2} = \frac{C}{8\eta} \left(\frac{1}{A} \right) = \frac{C}{8\eta} \left(\frac{\Delta P}{N_p} \right)$$

(3.86)

Temperature dependency of the right-hand side in Eqn.(3.86) can be determined from pure solvent experimental data, which, in turn, determines the temperature dependency of the left-hand side, $(\tau/\varepsilon)/R_W^2$.

On the other hand, compaction is also a function of pressure, at a fixed temperature. Previously, the compaction effect was shown to vary with pressure in an Arrhenius-type manner (Sourirajan, 1970). However, other dependencies of pressure on compaction are possible. In the present research, a linear function is used (Mehdizadeh et al., 1989):

$$A = A^o - m\,\Delta P \tag{3.87}$$

where A^o is the pure solvent permeability coefficient in the absence of compaction, obtained by extrapolation to zero pressure and m is called the "compaction coefficient". The compaction coefficient might vary with temperature in a non-linear manner; this variation can be expressed by a polynomial (Mehdizadeh and Dickson, 1989d):

$$\ell n\, m = a_0 + a_1\, \ell n\, T + a_2 (\ell n\, T)^2 \tag{3.88}$$

where the a_i's are coefficients to be determined from experimental curves of $\ell n\, m$ versus $\ell n\, T$. The compaction-free permeability coefficient, A^o, may then follow an Arrhenius-type of relationship, similar to Eqn.(2.53), as:

$$A^o = A^o_{ref}\, exp\left\{ -\frac{E}{R}\left(\frac{1}{T} - \frac{1}{T_{ref}}\right)\right\} \tag{3.89}$$

where A^o_{ref} is the value of A^o at a reference temperature, T_{ref}, and E is the apparent activation energy for solvent passage through the membrane. Therefore, Eqns.(3.86) to (3.89) can be used to describe the compaction effect, once the coefficients in Eqn.(3.88) and the activation energy E in Eqn.(3.89) are known.

Since it is assumed, in the present research, that the pore size, R_W, does not change with temperature then all the compaction effect, determined for the $(\tau/\varepsilon)/R_W^2$ parameter in Eqn.(3.86), is contributed by the change in the τ/ε parameter. This

means that, when the number of pores and the average pore size remain constant with respect to temperature (or ε = constant), the compaction effect happens only because of changes in the membrane effective thickness, τ.

Alternatively, if the coefficients in Eqn.(3.88) and the apparent activation energy in Eqn.(3.89), E, are unknown, one may assume an Arrhenius-type of relationship for the τ/ε parameter, as:

$$\left(\frac{\tau}{\varepsilon}\right) = \left(\frac{\tau}{\varepsilon}\right)_{ref} \exp\left[-\frac{E_t}{R}\left(\frac{1}{T} - \frac{1}{T_{ref}}\right)\right] \tag{3.90}$$

where E_t is the apparent activation energy for changes in τ/ε with respect to temperature. Then, using the assumption that R_W is temperature independent, $\ell n\,[(\tau/\varepsilon)/R_W^2]$ can be plotted versus $1/T$, using Eqns.(3.86) and (3.90) and the experimental N_P data, to determine the apparent activation energy. This approach is taken in the present research, and the results are discussed in Sections 5.3.3 and 5.3.5.

Either of the above approaches is less than optimum theoretically, as an empirical Arrhenius equation is employed. A more correct method would be to model the behaviour of the material properties of the polymeric membrane at different temperatures and to interpret these results from a material science approach (such as: polymer elasticity and plasticity, and stress-strain relationships). The material science characteristics of the membrane should be related to the size and structure of the assumed membrane pores. This approach needs further research and is not addressed in the present dissertation. Finally, once the temperature dependency for τ/ε is known the temperature variation of solution flux can be determined from Eqn.(3.40).

3.4   Development of the MD-FPM Relationship

The Finely Porous Model (FPM) was proposed originally by Merten (1966). In this model, discussed in Section 2.3.2.4, transport of solute and solvent occurs in small one dimensional pores. A balance of applied and frictional forces is used to describe the flow of solute inside the pores, as proposed by Spiegler (1958). In principle, the solute partition coefficient (K) can be different on the high-pressure side and low- pressure side of the membrane. This form is known as FPM-4, implying that the model has four parameters. Often the partition coefficient is assumed to be the same on each side of the membrane ($K_2 = K_3 = K$) to give a three parameter model (FPM-3). A complete derivation of the model (FPM) has been given by Jonsson and Boesen (1975) and by Soltanieh and Gill (1981).

In this section, the theoretical aspects of the FPM-3 and FPM-4 relationships are examined. Some important limitations and mistakes in these models are removed and the new modified models, called the modified FPM-3 (MD-FPM-3) and the modified FPM-4 (MD-FPM-4) relationships, are derived. The mathematical formulation of the model is done for the general case of the MD-FPM-4 relationship, and then the MD-FPM-3 relationship is derived from the general relationship.

First, the equation of solute flux together with the equation of solute material balance are examined. Then, the equation of fluid velocity through the pores are derived, and, finally, the equations required to describe the overall flux and separation are presented.

Since the FPM models assume that the pores are one-dimensional then conditions vary only with axial position through the pore. Compared to a two-dimensional model, these conditions at any axial position represent the radially

averaged values. For instance, $C_A(z)$ represents the radially-average concentration of A in the pore at position z.

3.4.1   The equations of solute flux and solute material balance

Since the pore is relatively long (i.e., with respect to its radius), the solution velocity profile is assumed to be fully developed. Then, similar to the FPM, the equation of solute flux is obtained, from a force balance on the solute in the pore (Jonsson and Boesen, 1975), as:

$$J_A = -\frac{RT}{X_{AB}b}\frac{dC_A(z)}{dz} + \frac{C_A(z)u}{b} \tag{3.91}$$

where,

$$X_{AB} = -\frac{F_{AB}}{u_A - u_B} = \frac{RT}{D_{AB}} \tag{3.92}$$

$$b = \frac{X_{AB} + X_{AM}}{X_{AB}} = \frac{D_{AB}}{D_{AM}} \tag{3.93}$$

Equation (3.91) is true for the case of non-electrolytes. However, for the case of strong electrolytes, the equation of salt flux is derived, in **Appendix B** (Eqn.(B.I.7)), as:

$$J_A = \frac{1}{b}\left[-\frac{1}{X_{AB}}\frac{d\pi(z)}{dz} + \frac{\pi(z)u_B}{RT}\right] \tag{3.94}$$

where $\pi(z)$ is the osmotic pressure of the solution at position z inside the pore. The one-dimensional Eqn.(3.94) is comparing to Eqn.(3.14) in the two-dimensional MD-SF-PF model. As in the MD-SF-PF model, the conversion from concentration to osmotic pressure, in Eqn.(3.94), is done in order to properly include the osmotic effects for systems with dissociating solutes.

The correct way of using the above differential flux equation is to write the differential material balance in the pore, substitute in the flux equation, and solve the resulting 2nd order differential equation subject to boundary conditions at the pore inlet and outlet.

The general boundary conditions are given by the definition of the solute partition coefficient:

i)   At the pore inlet:

$$C_A(z=0) = C_{A2} K_2 \tag{3.95}$$

ii)   At the pore outlet:

$$C_A(z=\tau) = C_{A3} K_3 \tag{3.96}$$

The equation of continuity, Eqn.(3.15), is used as the differential material balance. In one-dimensional form, Eqn.(3.15) becomes:

$$\frac{dJ_A}{dz} = 0 \tag{3.97}$$

Then, combining Eqn.(3.91), or Eqn.(3.94) for electrolytes, with Eqn.(3.97) gives the following 2nd order differential equations:

$$\frac{d^2 C_A(\xi)}{d\xi^2} - a\frac{dC_A(\xi)}{d\xi} = 0 \tag{3.98}$$

$$\frac{d^2 n(\xi)}{d\xi^2} - a\frac{d n(\xi)}{d\xi} = 0 \tag{3.99}$$

where a is the dimensionless fluid velocity defined as:

$$a = \frac{u\tau X_{AB}}{RT} = J_v\left(\frac{\tau}{\varepsilon}\right)\frac{X_{AB}}{RT} \tag{3.100}$$

which represents the ratio of convection to molecular diffusion forces, and ξ is the dimensionless axial position defined by Eqn.(3.19). Equation (3.99) is equivalent to Eqn.(3.98) for dilute solutions of electrolytes. Equation (3.98) has been solved analytically, in **Appendix B**, to give the concentration profile in the pore, in the MD-FPM-4 relationship, as:

$$C_A(\xi) = \left\{ C_{A2} - \left(C_{A2} - \frac{K_3}{K_2} C_{A3} \right) \left[\frac{1 - \exp(\alpha\xi)}{1 - \exp(\alpha)} \right] \right\} K_2 \qquad (3.101)$$

Now, substituting the concentration profile, from Eqn.(3.101), into the solute flux Eqn.(3.91), or Eqn.(3.94), gives an explicit expression for the solute flux in terms of the dimensionless velocity and the partition coefficients:

$$J_A = \frac{\alpha}{\tau X_{AB} b} \left[\Pi_2 + \frac{\Pi_2 - (K_3/K_2)\Pi_3}{\exp(\alpha) - 1} \right] K_2 \qquad (3.102)$$

as derived in **Appendix B**.

The above approach can be compared to that used in the Finely Porous Model (FPM). In the FPM, the following material balance in the pore has been proposed:

$$J_A = C_{A3} u \qquad (3.103)$$

This equation was then combined with Eqn.(3.91) to give a 1st order differential equation (and, therefore, needs only one boundary condition), which was solved using the boundary condition at the pore inlet, Eqn.(3.95). The resulting equation was substituted into the second boundary condition, Eqn.(3.95), and rearranged to give an expression for separation, f'. The relationship between f' and α, in the FPM-4 relationship, has been derived in **Appendix B** as:

$$f' = \frac{(1 - K_2/b)\exp(\alpha) - (1 - K_3/b)}{[\exp(\alpha) - 1] + K_3/b} \qquad (3.104)$$

The problems with the above method (i.e., the Finely Porous Model) are as follows:

i)   Equation (3.103) ignores the diffusive contribution to solute flux and considers only the convective contribution. This violates the physical facts in Eqn.(3.91).

ii)   Equation (3.103) ignores the distinction between concentrations inside and outside the pore; a velocity inside the pore is combined with a concentration outside the pore.

As a result of these errors the Finely Porous Model calculates the concentration and concentration gradient in the pore incorrectly (note that the same mistake exists in the Surface Force-Pore Flow model, as discussed in Section 3.1.3). The equation of concentration profile in the pore (in FPM) has not been shown in the literature; however, its derivation is straightforward and is shown in **Appendix B**.

3.4.2   Fluid velocity profile in MD-FPM

As a first step, the Poiseuille expression of fluid velocity is modified for the pore fluid to include the frictional force between the solute and the pore wall (Jonsson and Boesen, 1975),

$$J_V = \frac{\varepsilon R_W^2}{8\eta}\left[-\frac{dP(z)}{dz} - X_{AM} u_A C_A(z)\right] \tag{3.105}$$

where,

$$J_V = \varepsilon u \tag{3.106}$$

and ε is the fractional pore area which corrects the fluid velocity in a single pore to the volumetric permeation flux for a whole membrane.

Within a pore, the flux and the velocity of solute are related as:

$$J_A = u_A C_A(z) \tag{3.107}$$

and J_A is given by Eqn.(3.102). On the other hand, the pressure gradient term, $-dP/dz$, can be well approximated by:

$$-\frac{dP(z)}{dz} = \frac{1}{\tau} \{\Delta P - \pi_2(1-K_2) + \pi_3(1-K_3)\} \tag{3.108}$$

which is similar to that in the FPM (Jonsson and Boesen, 1975), and ΔP is the pressure difference across the membrane. Then, using Eqns.(3.106) to (3.108) together with Eqn.(3.102), Eqn.(3.105) can be used to derive an implicit equation for α:

$$\alpha = \frac{R_W^2}{8\eta}\left(\frac{X_{AB}}{RT}\right)\left\{\Delta P - \pi_2(1-K_2) + \pi_3(1-K_3)\right.$$

$$\left.-\alpha\left(\frac{K_2}{b}\right)(b-1)\left[\pi_2 + \frac{\pi_2 - (K_3/K_2)\pi_3}{\exp(\alpha)-1}\right]\right\} \tag{3.109}$$

Under the special case of $\alpha \ll 1$, where:

$$\exp(\alpha) \approx \alpha + 1 \tag{3.110}$$

is valid, α can be derived from Eqn.(3.109) as:

$$\alpha = \frac{\left(\dfrac{R_W^2}{8\eta}\right)\left(\dfrac{X_{AB}}{RT}\right)\{\Delta P - (1-K_2/b)\pi_2 + (1-K_3/b)\pi_3\}}{1 + \left(\dfrac{R_W^2}{8\eta}\right)\left(\dfrac{X_{AB}}{RT}\right)\left(\dfrac{K_2}{b}\right)(b-1)\pi_2} \tag{3.111}$$

If this condition (i.e., Eqn.(3.110)) is not met then α has to be determined by trial and error using Eqn.(3.109).

3.4.3 Solute and solvent fluxes through the membrane and the equation of separation in MD-FPM

The solute and solvent fluxes through the membrane are related to the corresponding fluxes through a single pore as:

$$N_A = \varepsilon J_A \tag{3.112}$$

$$N_B = \varepsilon J_B \tag{3.113}$$

where J_A is given by Eqn.(3.102); and,

$$J_B = u_B C = \left(\frac{CRT}{\tau X_{AB}}\right)\alpha_B \tag{3.114}$$

where the dimensionless solvent velocity, a_B, is defined as:

$$a_B = \frac{u_B \, \tau X_{AB}}{RT} \tag{3.115}$$

The total permeation flux through the membrane is,

$$N_T = (N_A + N_B) = \varepsilon(J_A + J_B) \tag{3.116}$$

Using Eqns.(3.102) and (3.114), Eqn.(3.116) becomes:

$$N_T = \frac{1}{X_{AB}}\left(\frac{a}{\tau/\varepsilon}\right)\left\{\left[\pi_2 + \frac{\pi_2 - (K_3/K_2)\pi_3}{\exp(a)-1}\right]\frac{K_2}{b} + CRT\left(\frac{a_B}{a}\right)\right\} \tag{3.117}$$

However, from Eqn.(3.100),

$$J_V = \frac{a}{(\tau/\varepsilon)(X_{AB}/RT)} \tag{3.118}$$

And, by definition:

$$N_T = C J_V \tag{3.119}$$

Then using Eqns.(3.118) and (3.119), Eqn.(3.117) is employed to determine the ratio of solvent to solution velocities as:

$$\frac{a_B}{a} = 1 - \frac{1}{CRT}\left\{\pi_2 + \frac{\pi_2 - (K_3/K_2)\pi_3}{\exp(a)-1}\right\}\frac{K_2}{b} \tag{3.120}$$

Now, using Eqns.(3.102), and (3.114), Eqn.(2.10) becomes:

$$C_{A3} = C\left\{1 + \frac{CRT(a_B/a)}{\left[\pi_2 + \dfrac{\pi_2 - (K_3/K_2)\pi_3}{\exp(a)-1}\right]\dfrac{K_2}{b}}\right\} \tag{3.121}$$

Finally, substituting for a_B/a, from Eqn.(3.120) in Eqn.(3.121), the following relationships are derived for separation:

$$f' = \begin{cases} \dfrac{(1-K_2/b)\exp(a)-(1-K_3/b)}{[\exp(a)-1]+K_3/b} & \text{for non-dissociating solutes} \\[2em] \dfrac{[1-(v^+ +v^-)K_2/b]\exp(a)-[1-(v^+ +v^-)K_3/b]}{[\exp(a)-1]+(v^+ +v^-)K_3/b} & \text{for strong electrolytes} \end{cases} \tag{3.122}$$

The above equation, which is valid only under the restriction of Eqn.(3.110), is comparable to that in the FPM relationship, given by Eqn.(3.104); the two equations are identical only for non-dissociating solutes.

To determine the numerical value of separation in the above equations, the value of a is needed which can be determined from Eqn.(3.109), or Eqn.(3.111) if Eqn.(3.110) holds; however, in these equations the value of n_3 (and therefore f') is needed. Therefore, these equations are coupled and can be solved by a trial and error technique.

It is interesting to note that because $\exp(a) - 1$ is always greater than zero then:

$f' > 0$ (positive separation) when:

    $K/b < 1$ (for non-dissociating solutes)

    $K/b < 1/(v^+ + v^-)$ (for strong electrolytes)

$f' < 0$ (negative separation) when:

    $K/b > 1$ (for non-dissociating solutes)

    $K/b > 1/(v^+ + v^-)$ (for strong electrolytes)

and,

$f' = 0$ (no separation) when:

    $K/b = 1$ (for non-dissociating solutes)

    $K/b = 1/(v^+ + v^-)$ (for strong electrolytes)

Therefore, this modified model, MD-FPM, can predict positive, negative, or zero separations, which is consistent with experimental results. For instance, negative separation is found for solutes such a phenol with cellulose acetate membranes (Matsuura and Sourirajan, 1972), as discussed in Section 2.3.3.

3.4.4 The equation of fluid velocity in FPM

The volumetric flux of permeation in FPM-3 is (Jonsson and Boesen, 1975):

$$J_V = \frac{\varepsilon R_W^2}{8\eta} \left[\frac{1}{1 + R_W^2 X_{AM} C_{A3}/8\eta} \right] \frac{\Delta P - \Delta \pi(1-K)}{\tau} \tag{3.126}$$

and for FPM-4 is (Merten, 1966):

$$J_V = \frac{\varepsilon R_W^2}{8\eta} \left[\frac{1}{1 + R_W^2 X_{AM} C_{A3}/8\eta} \right] \frac{\Delta P - (1-K_2)\pi_2 + (1-K_3)\pi_3}{\tau} \tag{3.127}$$

Then, using Eqn.(3.100), Eqn.(3.127) can be rearranged in terms of the dimensionless fluid velocity, a,

$$a = \frac{(R_W^2/8\eta)(X_{AB}/RT)[\Delta P - (1-K_2)\pi_2 + (1-K_3)\pi_3]}{1 + (R_W^2/8\eta)(X_{AB}/RT)(b-1)C_{A3}RT} \tag{3.128}$$

Equation (3.128) can be compared directly to Eqn.(3.111) in the MD-FPM model. First, Eqn.(3.111), in the MD-FPM-4, holds when the approximation in Eqn.(3.110) is valid. The partition coefficient in Eqn.(3.128) are comparing to the coefficients divided by b in Eqn.(3.111), and the $C_{A3}RT$ term in Eqn.(3.128) is replaced by $\pi_2 K/b$ in Eqn.(3.111). These differences lead to different predictions under different operating conditions.

3.4.5 The MD-FPM-3 relationship

The MD-FPM equations discussed so far are for the general case (i.e., the MD-FPM-4 relationship) in which partition coefficients are allowed to vary from the pore inlet to the pore outlet. However, frequently the partition coefficient is assumed constant,

$$K_2 = K_3 = K \tag{3.129}$$

Making this above assumption generates the MD-FPM-3 which is then a three-parameter model. When Eqn.(3.129) holds, the MD-FPM-4 Eqns.(3.101), (3.109),

(3.111), (3.117), (3.120), (3.121), and (3.122) reduce to the following forms for the MD-FPM-3 relationship, respectively:

$$C_A(\xi) = \left\{ C_{A2} - \left(C_{A2} - C_{A3} \right) \left[\frac{1 - e^{a\xi}}{1 - e^a} \right] \right\} K \tag{3.130}$$

$$a = \frac{R_W^2}{8\eta} \left(\frac{\chi_{AB}}{RT} \right) \left[\Delta P - \Delta\pi(1-K) - a\left(\frac{K}{b} \right)(b-1)\left(\pi_2 + \frac{\Delta\pi}{\exp(a)-1} \right) \right] \tag{3.131}$$

$$a = \frac{(R_W^2/8\eta)\,(\chi_{AB}/RT)\,[\Delta P - \Delta\pi(1-K/b)]}{1 + (R_W^2/8\eta)\,(\chi_{AB}/RT)\,(K/b)(b-1)\pi_2} \tag{3.132}$$

$$N_T = \frac{1}{\chi_{AB}} \left(\frac{a}{v/\varepsilon} \right) \left\{ \left[\pi_2 + \frac{\Delta\pi}{\exp(a)-1} \right] \frac{K}{b} + CRT\left(\frac{a_B}{a} \right) \right\} \tag{3.133}$$

$$\frac{a_B}{a} = 1 - \frac{1}{CRT} \left(\pi_2 + \frac{\pi_2 - \pi_3}{e^a - 1} \right) \frac{K}{b} \tag{3.134}$$

$$C_{A3} = C \left\{ 1 + \frac{CRT\,(a_B/a)}{\left[\pi_2 + \dfrac{\Delta\pi}{\exp(a)-1} \right] \dfrac{K}{b}} \right\}^{-1} \tag{3.135}$$

$$f' = \begin{cases} \dfrac{(e^a - 1)(1 - K/b)}{(e^a - 1) + K/b} & \text{for non--electrolytes} \\[4ex] \dfrac{(e^a - 1)[1 - (v^+ + v^-)\,K/b]}{(e^a - 1) + (v^+ + v^-)\,K/b} & \text{for electrolytes} \end{cases} \tag{3.136}$$

3.5 Orthogonal Collocation: Formulation of A Strong Computer Code

In this section, the principles of orthogonal collocation method, discussed in Section 2.6, are applied to the MD-SF-PF model (developed in Section 3.1). The same principles apply to the other members of the MD-SF-PF family group (i.e., the Extended MD-SF-PF model, developed in Section 3.2, and the temperature-extended MD-SF-PF model, developed in Section 3.3.1).

In the MD-SF-PF model, the ordinary differential equation (ODE) to be solved is the equation of fluid velocity profile in the pore, given by Eqn.(3.24). This equation can be solved by collocating the zeros of $P_N^{(0,0)}(\rho)$ over the interval $\rho \, \varepsilon \, [0,1]$, hence converting the ODE to a set of nonlinear algebraic equations that have to be solved numerically (Mehdizadeh and Dickson, 1989f). Therefore, Eqn.(3.24) is discretized as the N independent equations,

$$\left(\sum_{j=1}^{N+2} B_{i,j} a_j + \frac{1}{\rho_i} \sum_{j=1}^{N+2} A_{i,j} a_j \right) + \frac{1}{\beta_1} \left[\Delta P - \Delta \pi \, (1 - e^{-\Phi_i}) \right]$$

$$- \frac{1}{\beta_1} (1 - \frac{1}{b}) a_i \left[1 + \frac{\Delta \pi}{e^{a_i} - 1} \right] e^{-\Phi_i} = 0 \qquad (3.137)$$

$$\text{for:} \quad i = 2, \dots, N + 1$$

Note that $i = 1$ and $i = N + 2$ are at the interval end points $\rho = 0$ and $\rho = 1$, respectively. The boundary conditions, Eqns.(2.34) and (2.35), are discretized as:

$$a_{N+2} = 0 \qquad (3.138)$$

$$\sum_{j=1}^{N+2} A_{1,j} a_j = 0 \qquad (3.139)$$

One efficient way to solve the set of Eqns.(3.137), subject to the boundary conditions Eqns.(3.138) and (3.139), is to add a time-transient term, $da(\rho)/dt$, to the velocity profile of Eqn.(3.24), discretize the resulting partial differential equation

(PDE) to a set of ODE's, and, finally, integrate this set of ODE's, with respect to time, until steady state ($t \rightarrow \infty$) is reached; this is the solution to Eqn.(3.137).

To simplify the solution, Eqn.(3.139) is expanded and combined with Eqn.(3.138) to give the velocity at the centerline of the pore, a_1:

$$a_1 = -\frac{1}{A_{1,1}} \sum_{j=2}^{N+1} A_{1,j} a_j \tag{3.140}$$

And, Eqns.(3.138) and (3.140) are then used in the set of ODE's, discussed in the previous paragraph, to derive the following manageable set of ODE's:

$$\frac{da_i}{d\Theta} = \sum_{j=2}^{N+1} C_{i,j} a_j + \frac{1}{\beta_1} \left[\Delta P - \Delta\pi (1 - e^{-\Phi_i'}) \right]$$

$$- \frac{1}{\beta_1} (1 - \frac{1}{b}) a_i \left[1 + \frac{\Delta\pi}{e^{a_i} - 1} \right] e^{-\Phi_i} \tag{3.141}$$

$$\text{for:} \quad i = 2, \ldots, N + 1$$

where Θ is the dimensionless time, defined as:

$$\Theta = \frac{\eta\, t}{\rho\, R_W^2} \tag{3.142}$$

$$C_{i,j} = B_{i,j}^* + A_{i,j}^* / \rho_i \tag{3.143}$$

$$B_{i,j}^* = B_{i,j} - B_{i,1}(A_{1,j}/A_{1,1}) \tag{3.144}$$

$$A_{i,j}^* = A_{i,j} - A_{i,1}(A_{1,j}/A_{1,1}) \tag{3.145}$$

Equation (3.141) represents the main set of ODE's (in the MD-SF-PF model) to be solved, numerically, subject to the initial condition that the velocity is zero at all collocation points at time zero (Mehdizadeh and Dickson, 1989f).

The computer code to optimize and solve the MD-SF-PF model is presented in **Appendix F**, and some of the results of using the orthogonal collocation method are discussed in Section 5.2.5.

3.6   Concluding Remarks

The family of Modified Surface Force-Pore Flow models were derived. The family includes the following two-dimensional, porous transport models: the Modified Surface-Force Pore Flow (MD-SF-PF) model, the Extended MD-SF-PF model, and the temperature-extended MD-SF-PF model. The Extended MD-SF-PF model is a generalization of the MD-SF-PF model which can be employed to describe or predict the RO membrane performance for any kind of RO system (i.e., solute rejection or solute attraction). The temperature-extended MD-SF-PF model is a version of the MD-SF-PF model which can describe or predict the RO membrane performance as a function of system temperature.

In addition, the Modified Finely Porous Model (MD-FPM), which is based on the correction of the finely porous model, was derived. The one-dimensional MD-FPM relationship was shown, mathematically, to be different from the finely porous model.

CHAPTER 4

EXPERIMENTAL

The whole experimental plan in this dissertation is divided into three parts, called: Phase I, Phase II, and Phase III.

Four FT30 polyamide membranes have been examined: two SW30HR (Sea Water, High-Rejection) and two BW30 (Brackish Water) membranes, manufactured by FilmTec Corporation (Cadotte et al., 1980; Larson et al., 1983; Cadotte, 1985). The membranes, which are called SW30-1, SW30-2, BW30-1, and BW30-2, were cut from flat sheets and compacted for 16 hours at 25°C temperature, 8500 kPa pressure (all pressures reported are gauge pressures), and 2000 ppm concentration of NaCℓ in water solution, before starting the experiments. The FT30 membranes are described in Section 2.2.

The effective surface area of each membrane was 15.08 cm². The pH of feed and permeate solutions, in all the Phases, were measured for some experiments. Free chlorine was checked for some feed samples, in each Phase, using the quick method of "Hach Free Chlorine Test Cube". The water used as the solvent, in all the Phases, was distilled and deionized.

In the following, first, the RO testing equipment is described in Section 4.1, and second, the experimental plan for each Phase is described in Sections 4.2, 4.3, and 4.4.

4.1   Reverse Osmosis Equipment

The reverse osmosis testing system, as shown in Figure 4.1, consists of a feed reservoir, a diaphragm metering pump, an accumulator, high/low pressure protector, six radial-flow test cells (shown by "RO Cell"), a pressure gauge, a pressure regulator, and a temperature controlling section which consists of a refrigeration system, a heating system, and a WEST-Model 2070 microprocessor based temperature controller. The feed solution is heated or cooled in a heat exchanger before entering the flow cells. Most of the equipment is contained in an insulated chamber (as illustrated in Figure 4.1) which is outfitted with heat exchangers for heating and cooling the system. The system allows independent control of temperature, pressure, feed flow rate, and feed concentration. Four of the six test cells were used for the four membranes tested.

The concentration of the solute (sodium chloride) in water solutions was measured by a YSI-Model 31 Conductivity bridge (with a Beckman pipette conductivity cell) and using a calibration curve which correlates conductances (μmho) to concentrations (ppm) at 25°C temperature. Samples were warmed or cooled to 25 ± 0.1°C before analysis.

Photographs of the testing equipment and the RO cell are shown in Figures 4.2 and 4.3, respectively.

4.2   Phase I Experimental Plan (Brackish Water Concentrations)

First the independent and dependent variables of the system are defined in Section 4.2.1, and then the experimental plan is described in Section 4.2.2.
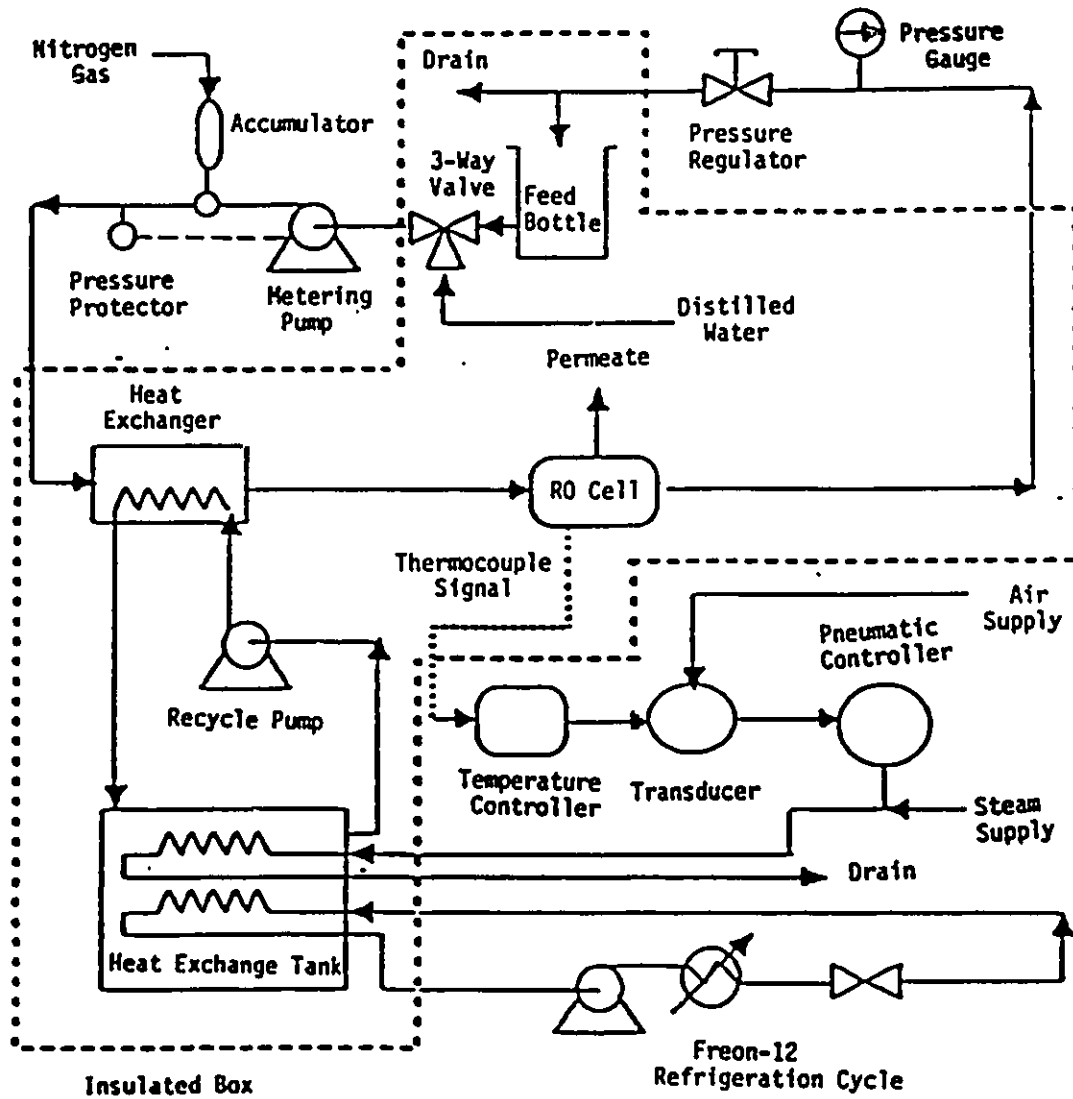
Figure 4.1:   Schematic diagram of the reverse-osmosis testing equipment.
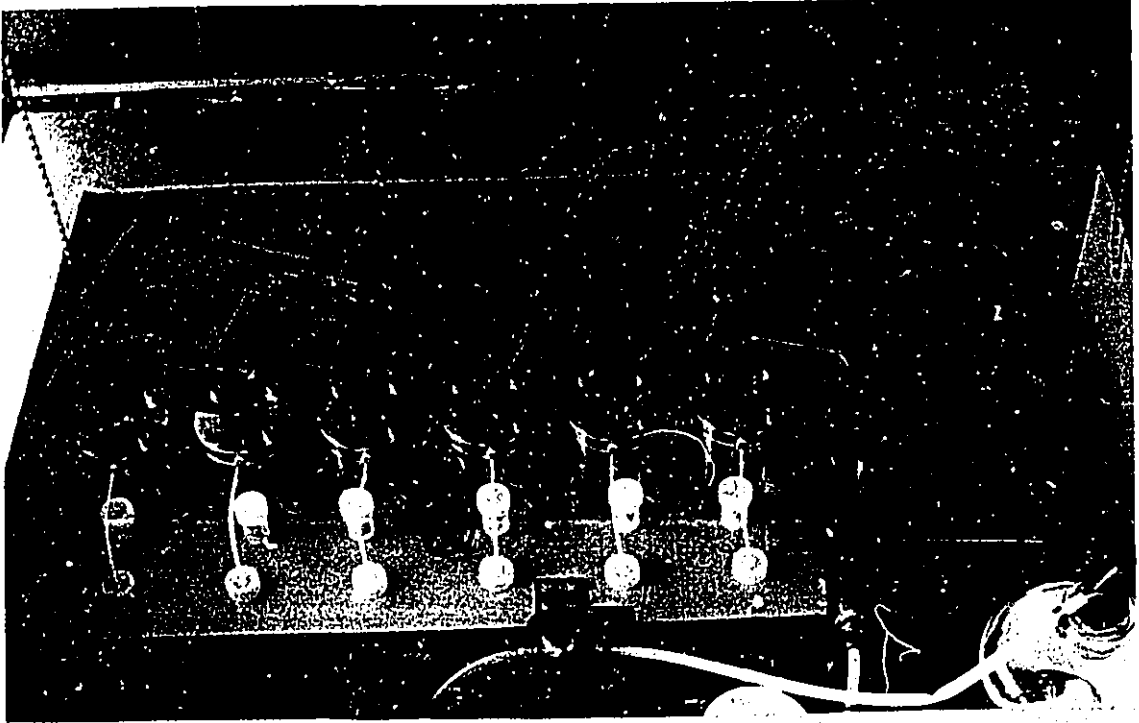
Figure 4.2:   The reverse osmosis testing equipment
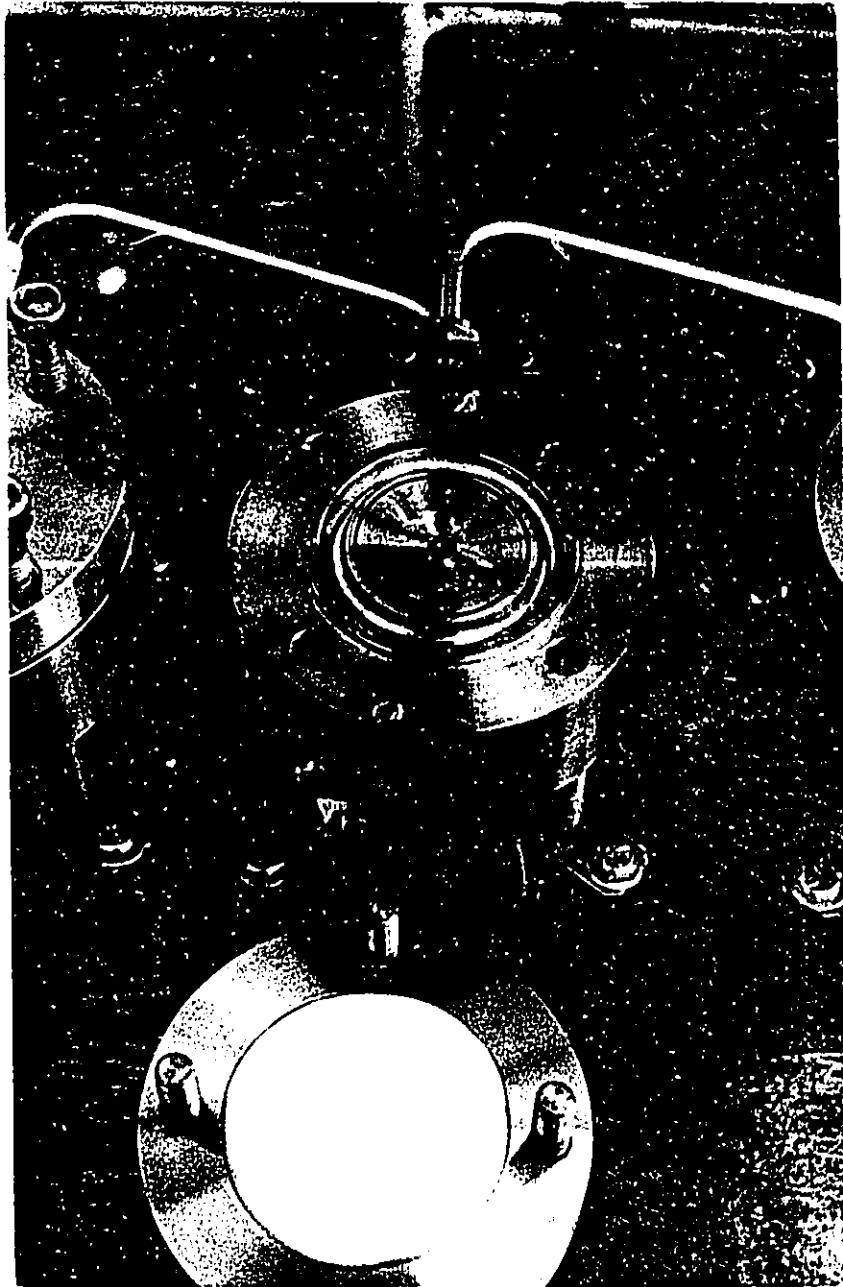
Figure 4.3:   The reverse osmosis cell

4.2.1 System parameters

The independent variables which were set for an experiment were the solvent (water), the solute (Analytical Reagent sodium chloride), solute concentration, feed flow rate, pressure and temperature.

The dependent variables which were measured are the permeate concentration, pure solvent (water) permeation flux, and permeation flux of the solution. The pH of feed and permeate solutions were measured for some experiments.

The range of each operating variable and the experimental error are:

- Pressure: 350 - 7000 kPa $\pm$0.2%

- Temperature: 5 - 60°C $\pm$0.2°C for each cell

  $\pm$0.25°C over all cells

- Feed flow rate: 1000 ml/min $\pm$1.0%

- Feed concentration: 2000 ppm $\pm$1.0%

4.2.2 Reverse osmosis experiments

The following series of experiments were designed to evaluate the performance of the thin-film composite aromatic polyamide membranes at different temperatures and pressures. Experiments which were more likely to damage the membranes were done last. Therefore, the earlier results could still be compared even if the membranes were damaged later on. The order of experiments in each section were randomized to reduce the interference of any systematic change in the membrane on the observed results.

Experiments with pure water feed have been performed before and after each NaCℓ-H_2O experiment. Some NaCℓ experiments, designated as "standard experiments", have been repeated to monitor any membrane changes over the time

period of the experimental plan. The "standard experiment" was operated at: 25°C, 1500 kPa, and 2000 ppm NaCℓ in water solution.

The experimental plan was as follows:

i)   Membrane compaction at 25°C, 8500 kPa and 2000 ppm aqueous NaCℓ solutions for 16 hours (until the permeate flux and concentration became stable)

ii)   Standard experiment.

iii)   Experiments at 25°C and at each of the following pressure (randomized): 350, 500, 1500, 4000, and 7000 kPa.

iv)   Standard experiment.

v)   Experiments at 5000, 10 000 and 15 000 ppm, 25°C, and 1500 kPa.

vi)   Experiments at pressures in the range of 350 - 7000 kPa and at temperatures in the range of 5 - 25°C. After each set of experiments at a fixed temperature, the standard experiment is repeated.

vii)   Experiments at several pressures in the range of 350 to 7000 kPa and at the temperatures of 30, 35, and 40°C. Standard experiment is repeated after each set of experiments at a fixed temperature.

viii)   Step (vi) repeated at 45, 50, and 60°C, followed by standard experiment after each set of experiments.

A single experiment consists of measuring the pure water flux at the appropriate conditions, switching to the electrolyte (i.e., NaCℓ-H$_2$O in Phase I) solution and after steady state is achieved, measuring the concentration of the feed, C_{A1}, the concentration of the permeate, C_{A3}, and the solution flux, n_T. Finally the pure water flux is again measured. The reported np value is the average pure water flux.

4.3 Phase II Experimental Plan (Other 1-1 Electrolytes)

The Phase II experiments were performed with 1-1 electrolytes other than sodium chloride, including: potassium chloride, lithium chloride, and lithium nitrate. The experimental conditions are as the following.

4.3.1 System parameters and reverse osmosis experiments

For a fixed set of operating conditions (which are: pressure, solute, feed concentration, feed flow rate, and temperature) the following dependent variables were measured: the permeate flux and concentration, the pH, and the pure solvent (water) permeation flux. Pure water fluxes were measured immediately before and after each solution experiment to monitor membrane change and to determine an appropriate average water flux. The change in solvent flux was small, usually < 1%. For each solute, the order of experiments were randomized to reduce the interference of any systematic change in the membrane results.

The range of each operating variable and the experimental error are (Mehdizadeh and Dickson, 1989g):

- Pressure: 350 - 4000 kPa   ±0.2%

- Temperature: 25°C   ±0.2°C for each cell

                                        ±0.25°C over all cells

- Feed flow rate: 1000 ml/min   ±1.0%

- Feed concentration: 2000 ppm   ±1.0%

- Solute: $KC\ell$, $LiC\ell$, and $LiNO_3$ (all Analytical Reagent)

The procedure for a single experiment is the same as described in Section 4.2.2.

4.4 Phase III (Sea Water Concentrations)

The membrane samples examined are the same membranes used in Phases I and II; these are four FT30 polyamide membranes: two SW30HR and two BW30 membranes, which are called SW30-1, SW30-2, BW30-1, and BW30-2. The solute used in all the 30 experiments was Analytical Reagent sodium chloride.

4.4.1 System parameters

The independent variables which were set for an experiment are the solvent (water), the solute (sodium chloride), solute concentration, pressure, temperature, and feed flow rate.

The dependent variables which were measured are the permeate concentration, pure solvent (water) permeation flux, and permeation flux of the solution. The pH of feed and permeate solutions were measured for some experiments.

The range of each operating variable and its experimental error are (Mehdizadeh and Dickson, 1989h):

- Pressure: 4000 - 7000 kPa   ±0.2%

- Temperature: 5 - 60°C   ±0.2°C for each cell

                                                   ±0.25°C over all cells

- Feed concentration: 35 000 ppm   ±1.0%

- Feed flow rate: 1000 ml/min   ±1.0%

4.4.2 Reverse osmosis experiments

The experimental plan is similar to that in Phase I. The schedule has been to perform experiments which might change or damage the membranes

structures last. Therefore, the earlier results could still be compared even if the membranes were damaged later on. The order of experiments in each section (i.e., fixed temperature and different pressures) are randomized to reduce the interference of any systematic change in the membrane on the observed results.

Experiments with pure water have been performed before and after each NaCℓ-H$_2$O experiment. Standard experiments, defined in Section 4.2.2, have been repeated to monitor any membrane changes.

The experimental plan was as follows:

i)   Standard experiment.

ii)   Experiments with 35 000 ppm NaCℓ in water solution at 25°C and at each of the following pressures (randomized): 4000, 5000, and 7000 kPa.

iii)   Standard experiment.

iv)   Same as step ii) but at 5°C.

v)   Standard experiment.

vi)   Same as step ii) but at 15°C.

vii)   Standard experiment.

viii)   Same as step ii).

ix)   Standard experiment.

x)   Same as step ii) but at 35°C.

xi)   Standard experiment.

xii)   Same as step ii) but at 45°C.

xiii)   Standard experiment.

xiv)   Same as step ii) but at 60°C.

xv)   Standard experiment.

The procedure for a single experiment is the same as described in Section 4.2.2.

4.5   Concluding Remarks

Three classes of experiments (called Phase I, Phase II, and Phase III) were done with four thin-film composite, aromatic polyamide, FT30 reverse osmosis membranes. Phases I and III were with brackish water and sea water concentrations of sodium chloride in water, respectively. The temperature range in Phases I and III was 5-60°C; the pressure ranges were: 350-7000 kPa for Phase I, and 4000-7000 kPa for Phase III. Phase II experiments were done with brackish water concentration of aqueous solutions of potassium chloride, lithium chloride, and lithium nitrate. The system temperature was 25°C, and the range of operating pressure was 500-4000 kPa.

The system temperature for all the experiments was controlled within a narrow range of error.

CHAPTER 5

RESULTS AND DISCUSSION

The major results obtained during the present research are presented in this Chapter. First the experimental results are discussed in Section 5.1. Then, the methods to solve the transport models (developed in Chapter 3) are described in Section 5.2. Simulation and prediction results for the MD-SF-PF and SF-PF models are presented in Section 5.3, which also includes predictions of temperature effects by the temperature extended MD-SF-PF model, under the operating conditions of Phases I and III. Section 5.4 presents some of the results with the Extended MD-SF-PF model for strong solute-membrane affinity systems, such as toluene-water and cumene-water systems. Finally, simulation results are presented for the MD-FPM and FPM relationships in Section 5.5.

5.1   Experimental Results

The experimental results for the Phases I, II, and III are presented in the following Sections 5.1.1, 5.1.2, and 5.1.3, respectively. The raw data for these experiments are tabulated in **Appendices C, D, and E**. The free chlorine tests have shown that, for all the Phases, the amount of free chlorine in feed sample was less than detectable (less than 0.5 ppm), and therefore the membranes were not exposed to the free chlorine attack.

105

5.1.1 Phase I (Brackish water concentrations)

In this section, the data obtained are presented and interpreted with attention to the effects of temperature on membrane performance.

5.1.1.1 Analysis of raw data

To determine the experimental performance of each membrane, the simple equations of concentration polarization, Eqn.(2.7), and solvent flux, Eqn.(2.25), have been employed. The pure solvent flux can be obtained, from Eqn.(2.25), in the form of Eqn.(3.41). The mass transfer coefficient, k, which characterizes the boundary layer at the feed side of the membrane, can be determined from the film-theory in Eqn.(2.7) or the following equivalent equation:

$$N_T = (N_A + N_B) = C \, k \, \ell n \left(\frac{C_{A2} - C_{A3}}{C_{A1} - C_{A3}} \right) \qquad (5.1)$$

By mass balance, the solute and solvent fluxes are related to permeate concentration by Eqn.(2.10), and separations can be determined via Eqns. (2.5) and (2.6).

The raw data for all the 79 experiments, in Phase I, have been processed by a computer program in the following manner:

i)   obtain molar fluxes, N_A, N_B, and N_T from experimental mass fluxes and the permeate concentration, and then Eqn.(3.41) gives A from the pure water flux, N_P,

ii)   obtain C_{A2} from Eqn.(2.25) using C_{A3}, A, and N_B from step i), and, the known relationship between concentration and osmotic pressure,

iii)   calculate the mass transfer coefficient, k, from Eqn.(5.1) using N_T, C_{A1}, C_{A2}, and C_{A3} from steps i) and ii).

The results of the above calculations are presented in **Appendix C**.

The pH values for feed and permeate streams, measured for some experiments, were all in the range 5.6 to 5.8, which is within the normal range expected for pure unbuffered water of 5 to 7; therefore, no attempts were made to adjust for the pH of the feed solutions.

5.1.1.2 Mass transfer coefficients

For relatively low concentration feed solutions the difference between pure water flux, N_P, and solution flux, N_T, is small which leads to a relatively large error in determining n_2 and hence C_{A2} from Eqn.(2.25). Subsequently, there is a larger error in calculating k from Eqn.(5.1). Therefore, even small experimental errors in the measurements of N_P, N_T, C_{A1} or C_{A3} can have a large effect on the k values; hence the wide variation of these values for the experiments at the same temperature, presented in Figures 5.1 and 5.2. Nonetheless, the k values at 25°C and 1500 kPa were averaged and used as k_{ref} in Eqn.(2.55). The k values calculated by the procedure in step iii) above and those predicted by the generalized mass transfer correlation (Eqn.(2.55)) are plotted in Figures 5.1 and 5.2. Given the expected error in calculating k for low concentration experiments, the agreement between trends of the data and Eqn.(2.55) is good.

To check the k_{ref} values used above, a few experiments at 25°C, 1500 kPa, and concentrations of 5,000, 10 000, and 15 000 ppm were performed. At higher concentrations the differences between N_P and N_T become larger, giving a more accurate value of C_{A2}, and therefore a more accurate estimate of k. These k values for each cell were reasonably constant and agreed with k_{ref} by a maximum deviation of 14%.

108
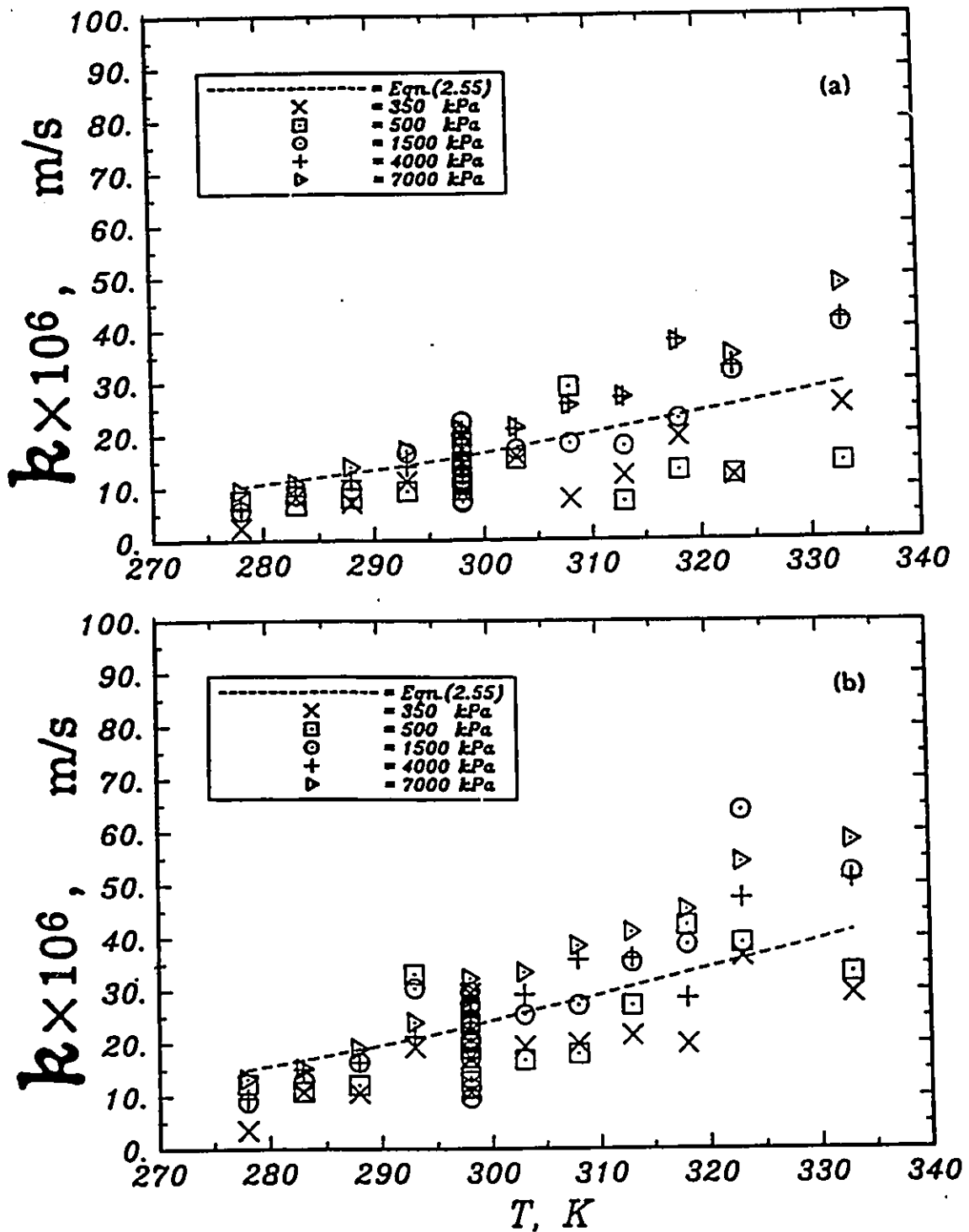
Figure 5.1:   Mass transfer coefficients versus temperature for the (a) SW30-1, and (b) SW30-2 membranes. The reference k values (obtained at 25°C and 1500 kPa) are: 15.35×10^{-6} m/s for the SW30-1 membrane, and 22.49×10^{-6} m/s for the SW30-2 membrane.
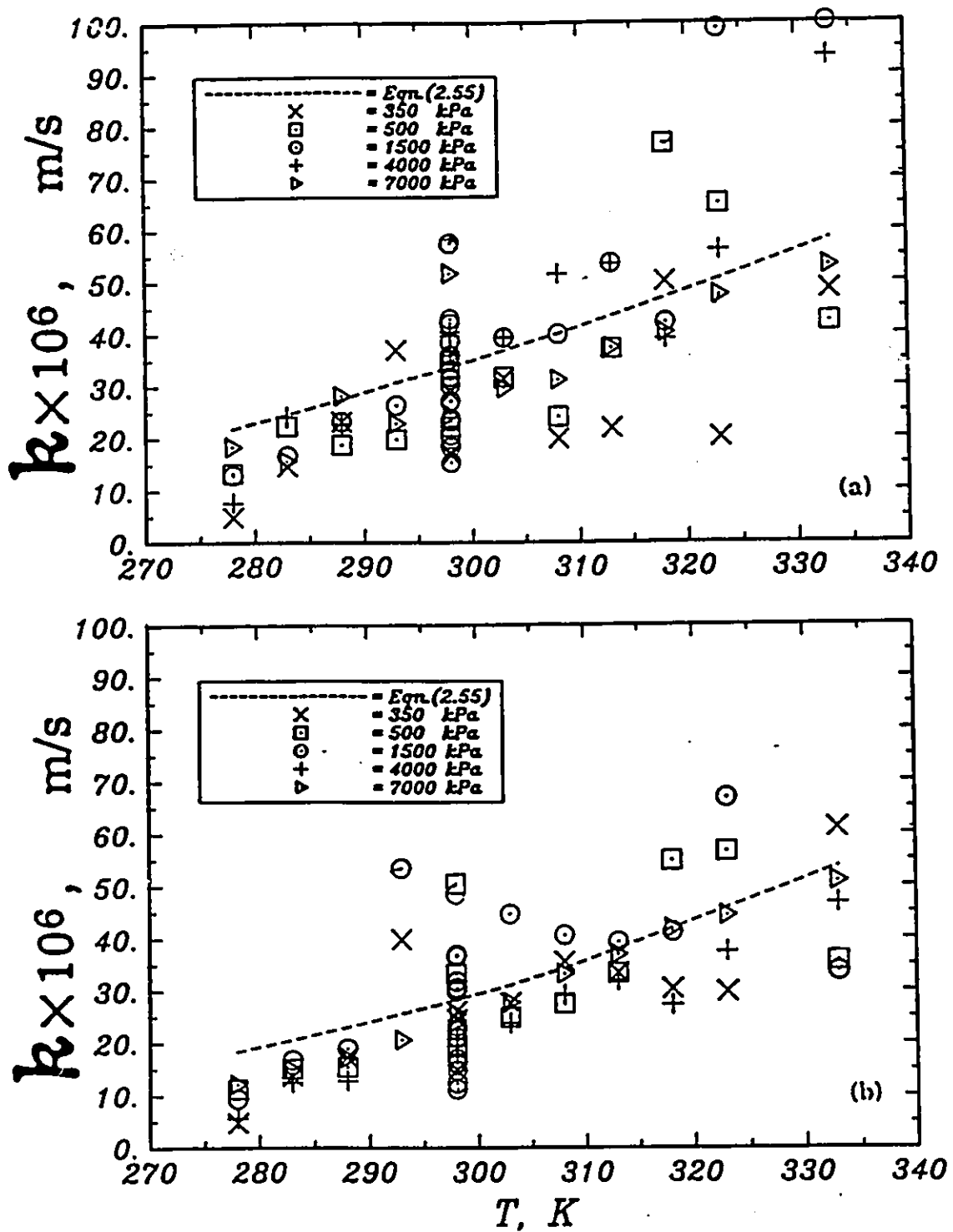
Figure 5.2: Mass transfer coefficients versus temperature for the (a) BW30-1, and (b) BW30-2 membranes. The reference k values (obtained at 25°C and 1500 kPa) are: 32.84×10^{-6} m/s for the BW30-1 membrane, and 27.65×10^{-6} m/s for the BW30-2 membrane.

The k values predicted by Eqn.(2.55) are used to recalculate C_{A2} (from Eqn.(5.1)), and f'. The effect of using the corrected mass transfer coefficients on f' is small (less than 3%).

5.1.1.3　Standard experiments

The results obtained for the standard experiments at different times are presented in Figures 5.3 and 5.4. Run number is used to approximate time. Run number represents the order in which the experiments were performed, with each run taking about one work day, and the system was shut off overnight between runs. Figure 5.3.a illustrates how separation, f, varies with time (as represented by run number) for the SW30-1 and SW30-2 membranes. The separation remains essentially constant over the time of testing. The average separation for each membrane is presented as the dashed lines for the SW30-1 and SW30-2 membranes, respectively. The values are 97.7% and 96.7%, respectively. Similar results are presented for the BW30 membranes in Figure 5.3.b. The separation for the BW30-1 membrane is constant (96.4%) as a function of time. However, the separation for the BW30-2 membrane oscillates above and below the results for the BW30-1 membrane, but has about the same separation as the BW30-1 membrane, on average (i.e., 96.4%). Perhaps the BW30-2 membrane sample has some surface defects or is otherwise not completely representative of BW30 membranes. By comparison, the SW30 membranes have higher separations than the BW30 membranes, as expected.

The variation of the pure water flux for all four membranes as a function of run number is presented in Figure 5.4. Up to run number 152 the flux for each of the membranes is constant. After run number 152 the flux for each membrane decreases slowly over the remaining experiments. The change in the flux corresponds to the first
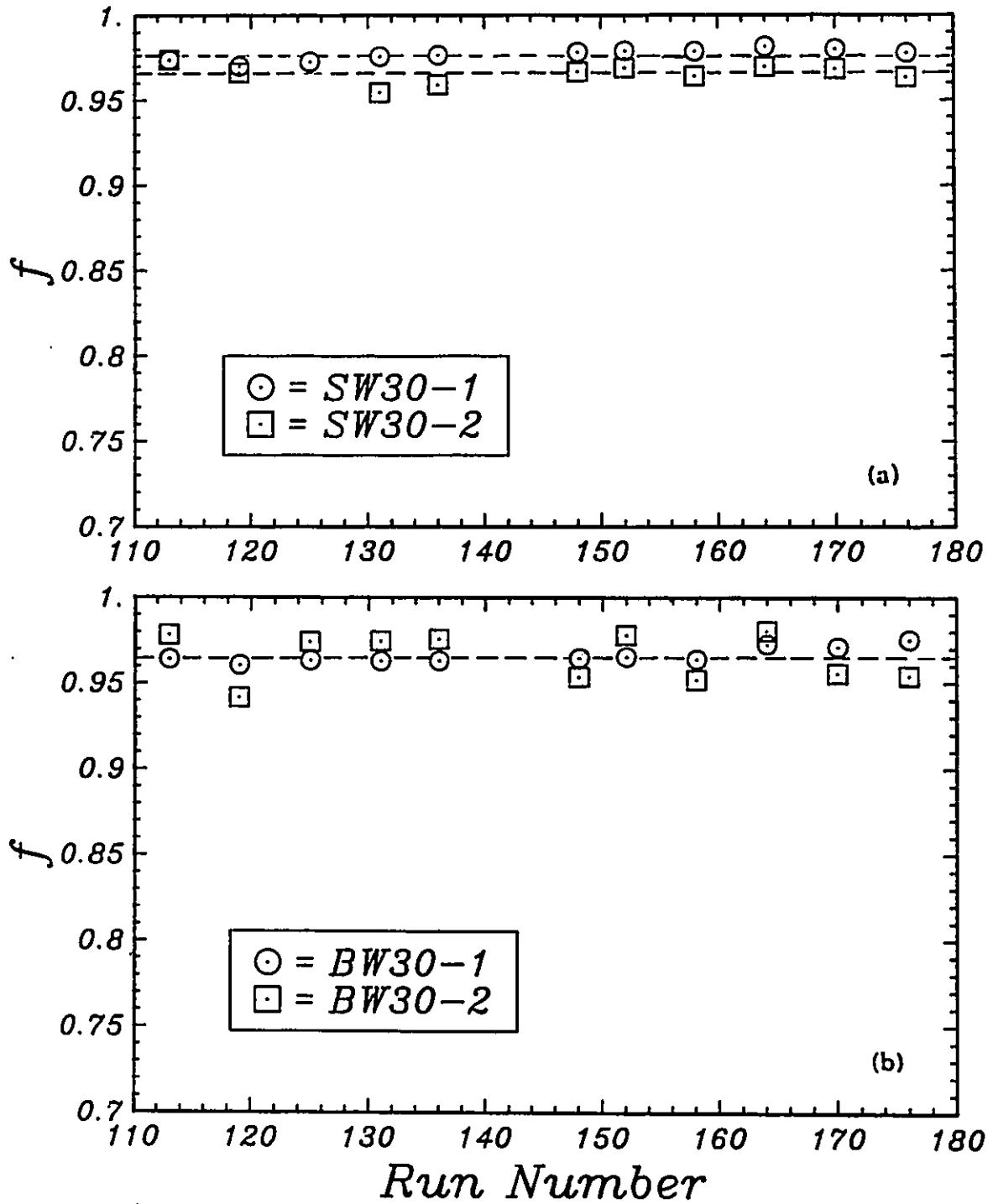
Figure 5.3: Standard experiments: (a) separation versus run number for the SW30 membranes (the dashed and the solid lines represent the average values of separation for the SW30-1 and SW30-2 membranes, respectively), (b) separation versus run number for the BW30 membranes (the dashed line represents the average value of separation for the two BW30 membranes).
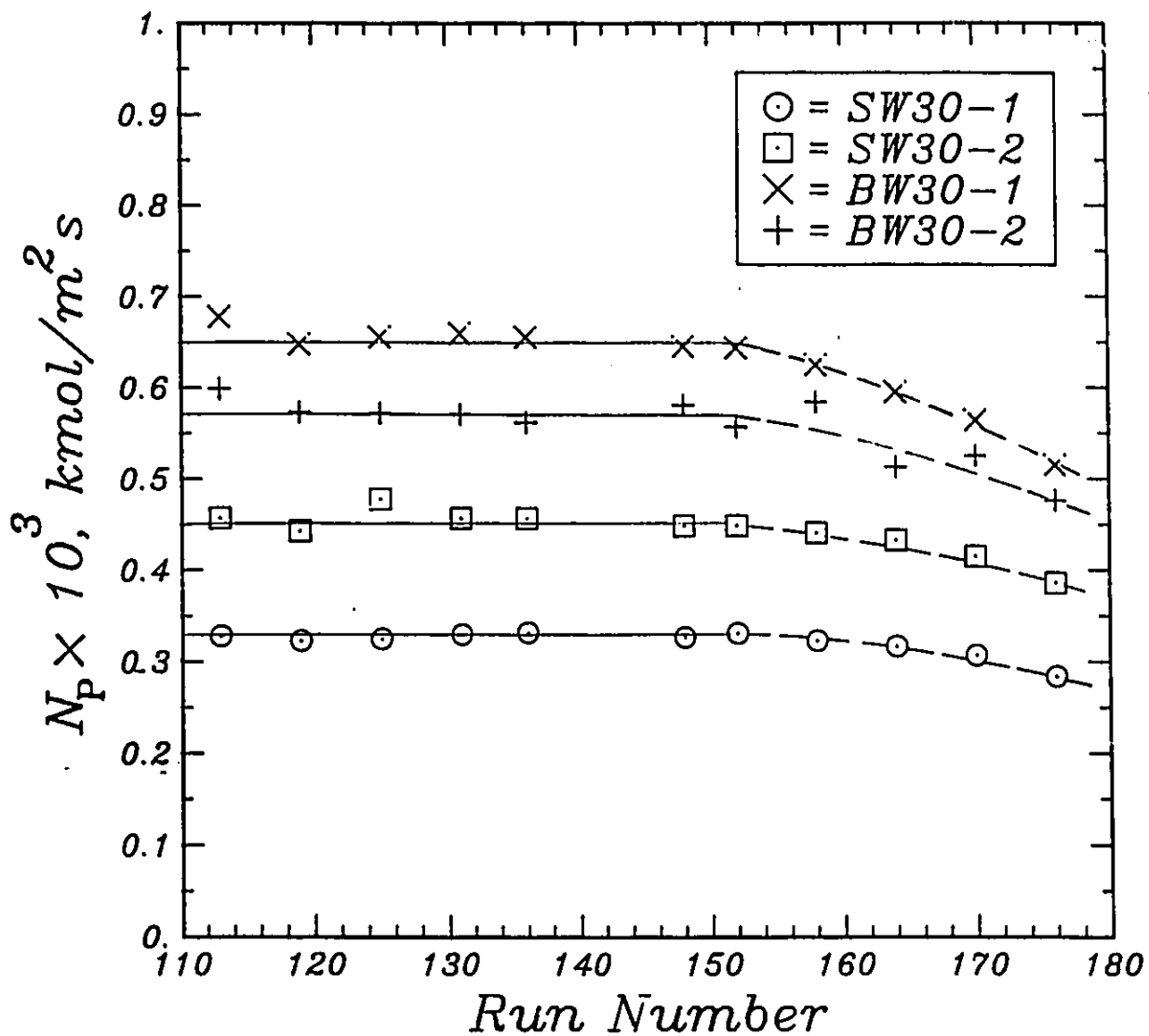
Figure 5.4:   Standard experiments: pure water flux versus run number for all the membranes. The solid line is the average flux measured up to run 152, and the dashed line is for the higher run numbers.

run performed at 40°C. This result indicates some progressive change in the membrane permeability occurs at 40°C and higher. Although different membrane materials were used these results are coincidently consistent with those observed by others (Merten et al., 1968; Kimura and Nomura, 1981). The BW30 membranes show a larger decrease in flux than the SW30 membranes, which is typical that higher flux membranes are more susceptible to changes in permeability. By comparison, the BW30 membranes have higher permeation fluxes (up to about 100% more) than the SW30 membranes, as expected. The cause of the change in permeability above 40°C is discussed later, in Section 5.1.1.4.

The small differences in flux and separation between the SW30-1 and SW30-2 can be expected for membrane samples cut from different places on the membrane sheet. Similar behaviour is observed for the two BW30 membranes. As expected, the higher flux membrane sample has a lower separation for both the SW30 and BW30 membranes.

5.1.1.4   Effects of pressure and temperature on pure water flux

In the absence of compaction, fouling, or other changes in membrane permeability, the pure water flux should increase linearly with pressure, as predicted by Eqn.(3.41); that is, A should be constant. A representative sample of the pure water data at various temperatures and over the low pressure and high pressure ranges are plotted in Figures 5.5 and 5.6. The points represent the experimental data. The fluxes appear linear, i.e., constant A, in the low pressure region and flux increases with temperature. In the higher pressure region, larger deviations from linearity are observed. These results imply that flux is only nonlinear in the higher pressure range.
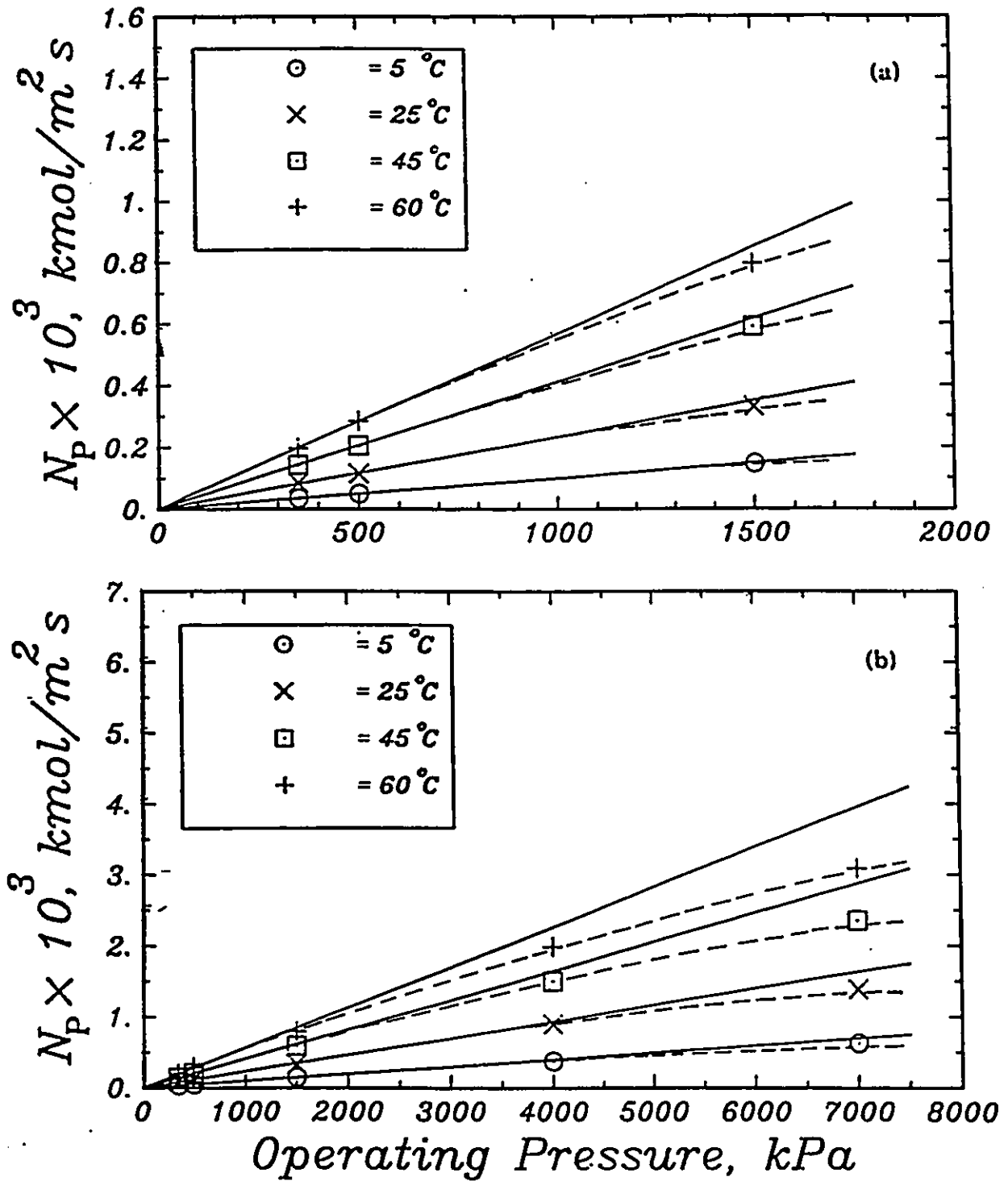
Figure 5.5:   Pure water flux versus operating pressure with temperature as a parameter for: (a) SW30-1 membrane, low- pressure range; and (b) SW30-1 membrane, full-pressure range. The straight lines are $N_P = A^° \Delta P$.
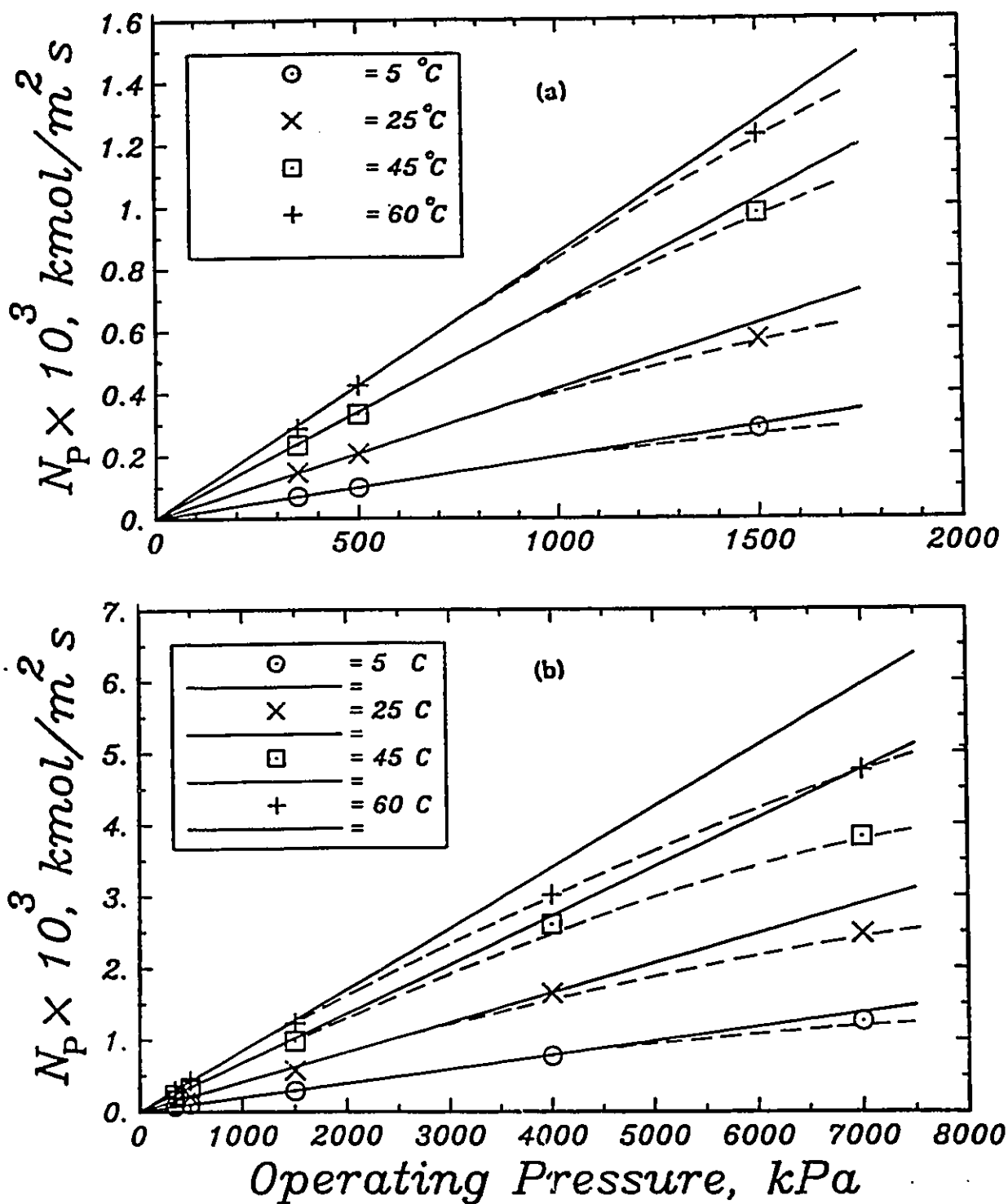
Figure 5.6: Pure water flux versus operating pressure with temperature as a parameter for: (a) BW30-2 membrane, low- pressure range; and (b) BW30-2 membrane, full-pressure range. The straight lines are $N_P = A^\circ \Delta P$.

However, when the data are replotted as A versus pressure for all temperatures, in Figure 5.7, apparently A decreases over the whole pressure range. The effect of pressure on A increases with increasing temperature. Figure 5.7 indicates that the permeability decreases linearly with pressure, as in Eqn.(3.87). The magnitude of the compaction effect is expressed by the parameter m. The variation of m with temperature is presented as ℓn m versus ℓn T for the SW30 and BW30 membranes, in Figure 5.8. There is a small difference in m for the SW30 membranes, while the two BW30 membranes can be represented by one curve. This information is consistent with the data in Figure 5.3 where two lines are required for the SW30 membranes, indicating some difference in behaviour for the two samples, and only one line is needed to represent the two BW30 membranes.

The above results can be interpreted in terms of membrane compaction. The thin-film composite membranes are made from three layers: a support fabric, a porous support membrane, and a thin surface layer. All three layers are potentially susceptible to compaction. However, the thin surface film creates the largest resistance to permeation and, therefore, probably this layer is undergoing compaction. In other words, the membrane surface structure is changed, under pressure, in a manner to decrease the membrane water permeability. The higher the pressure or temperature the larger the decrease in permeability. Similar behaviour has been observed for all four membranes and at all temperatures.

Equation (3.89) predicts that the pure water permeability coefficient, A^0, should increase with temperature according to an Arrhenius relationship. The A^0 values at various temperatures are plotted in the form of ℓn A^0 versus 1/T in Figure 5.9.a. Equation (3.89) predicts that one straight line could be drawn through all the data.
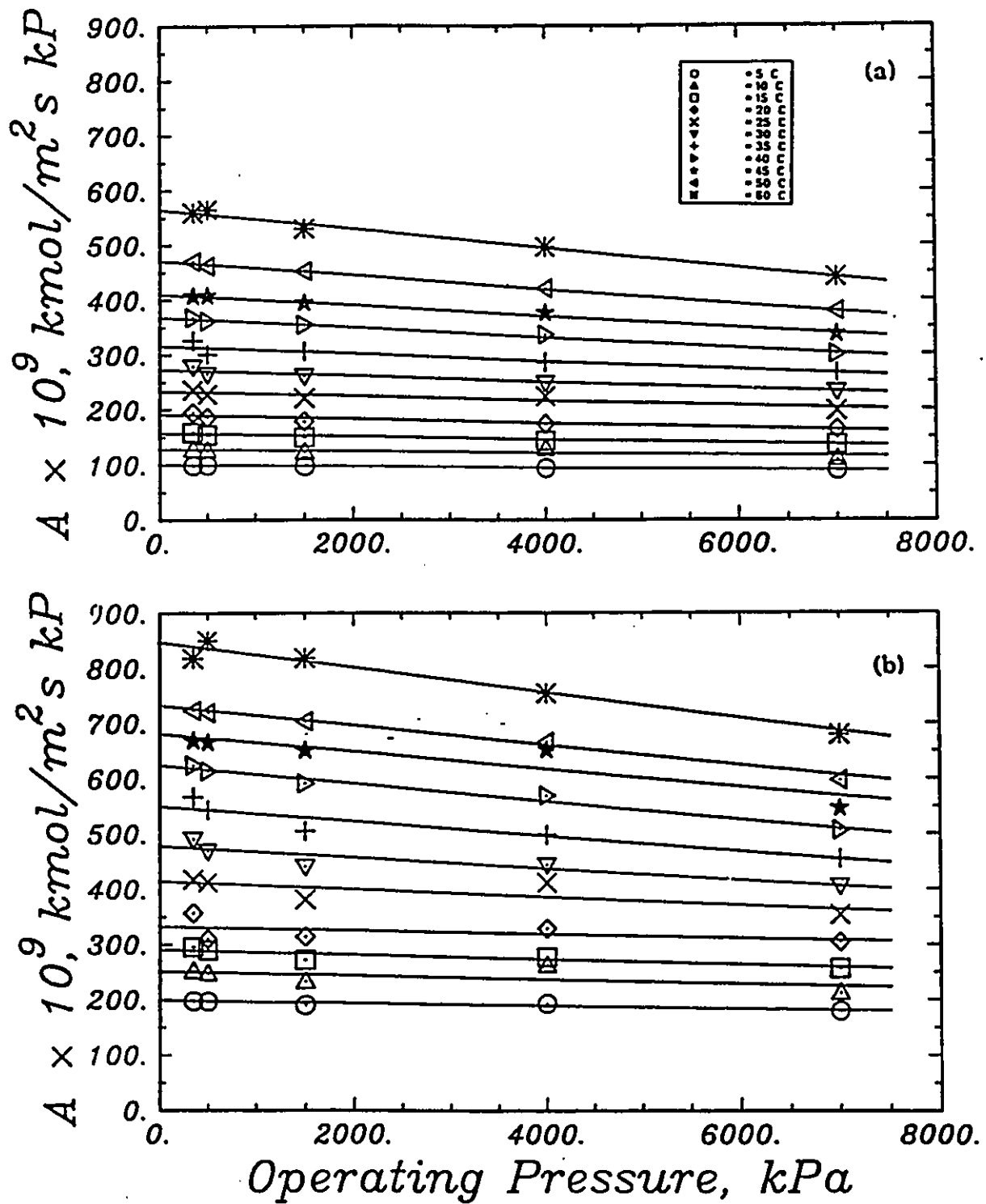
Figure 5.7: - Effect of pressure and temperature on compaction as represented by the decrease in pure water permeability coefficient, A. Back-extrapolation to zero pressure using linear least squares gives A⁰, the pure water permeabilityat zero pressure: (a) SW30-1, and (b) BW30-2 membranes.
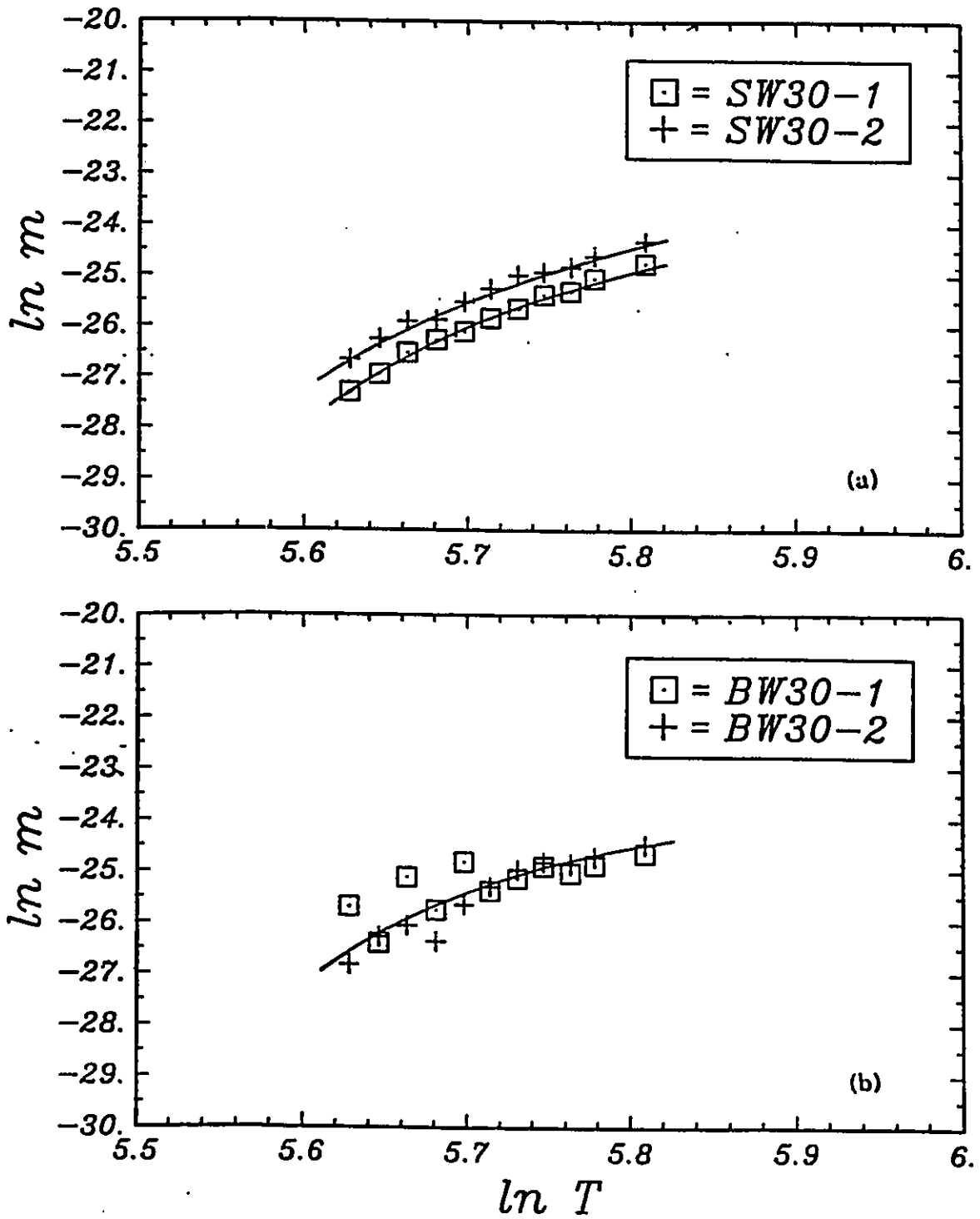
Figure 5.8:   Effect of temperature on the compaction coefficient, m: (a) SW30, and (b) BW30 membranes.
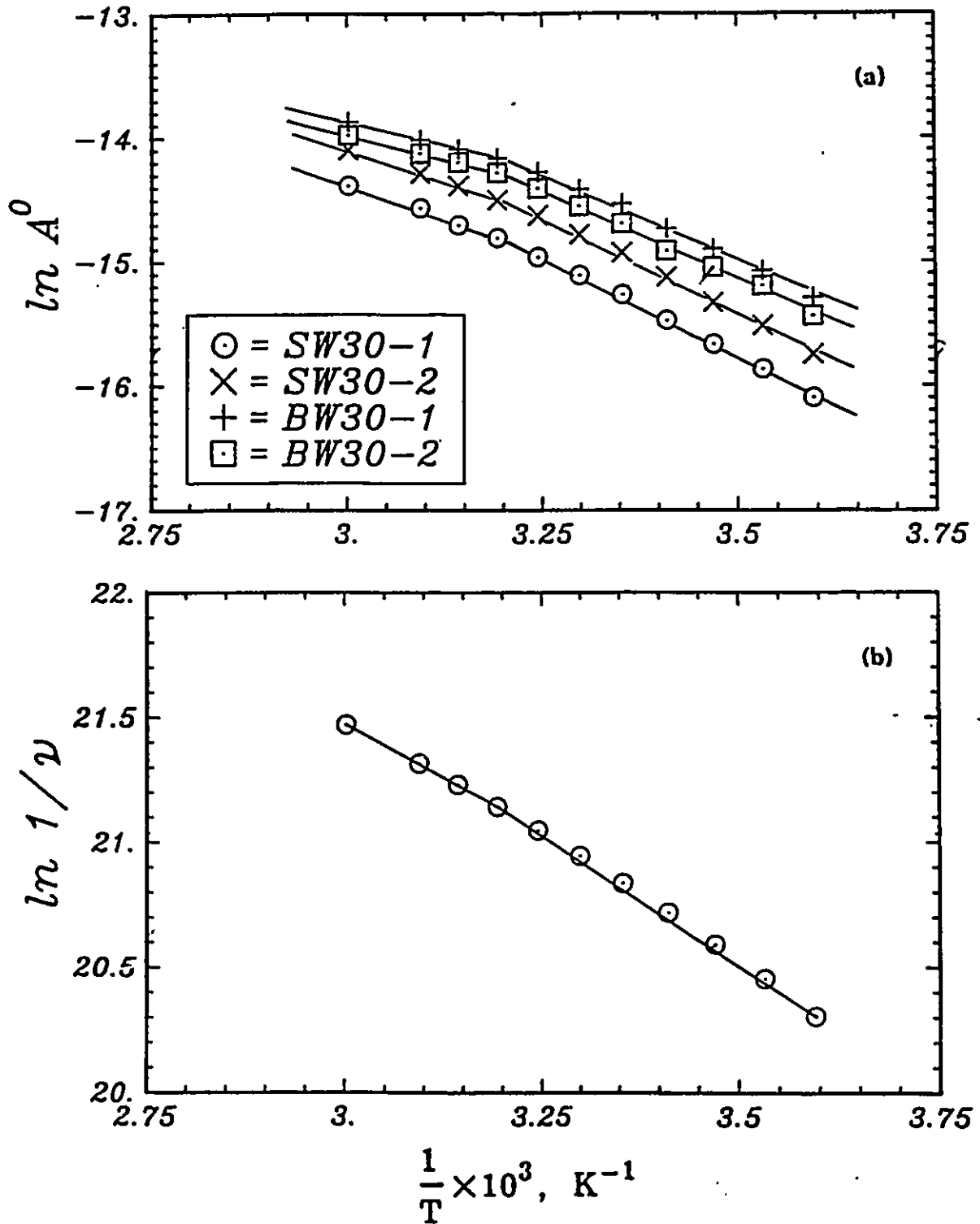
Figure 5.9:   Arrhenius plots: (a) ℓn A^0 versus 1/T for all the membranes, by
Eqn.(2.54); (b) ℓn (1/v) versus 1/T for water. The slopes of the lines
change at about 313 K.

From theory on transport in RO membranes it is expected that A^0 should vary with kinematic viscosity, v (Sourirajan, 1970). Therefore, in Figure 5.9.b, the dependence of logarithm of reciprocal of kinematic viscosity of water versus inverse temperature is plotted for comparison. Both A^0 and kinematic viscosity are approximately linear in the lower temperature region and in the higher temperature region with a change in slope at about 35 or 40°C. The apparent activation energies for both A^0 and inverse kinematic viscosity are tabulated in Table 5.1. Apparently the change in slope for A^0 is partially accounted for by the change in kinematic viscosity of water with temperature.

The apparent activation energies (listed in Table 5.1) are about 30% and 40% lower in the higher temperature range than in the lower temperature range for the SW30 and BW30 membranes, respectively. The lower activation energies at higher temperatures may be related to a shift in the mechanism of water transport. The values are about the same for the two different samples of the same membrane material, and the values for the SW30 membranes are about 10% and 40% larger than the values for the BW30 membranes in the lower and higher temperature range, respectively. The values obtained are qualitatively similar to those found by others. For example, Connell and Dickson (1988) studied the temperature effects on asymmetric cellulose acetate membranes and found that the pure water permeability coefficient changed with temperature according to an apparent activation energy of 22 000 kJ/kmol. These energies can be compared to the average activation energy for a Newtonian fluid, e.g. by Chen et al. (1983), which, based on the temperature dependency of inverse kinematic viscosity, is about 15 800 kJ/kmol for water. The values are about 17 300 and 14 240 kJ/kmol in the two temperature ranges for water (Table 5.1). Except for the BW30 membranes in the higher temperature range, the

Table 5.1

Apparent activation energies for the pure water permeability coefficient
(in Phase I) and for inverse kinematic viscosity

Membrane	5 - 40°C temperature range		40 - 60°C temperature range	
	Slope = $-E/R$, K	E, kJ/kmol	Slope = $-E/R$, K	E, kJ/kmol
SW30-1	$-3115.$	25 898.	$-2232.$	18 557.
SW30-2	$-2985.$	24 821.	$-2134.$	17 740.
BW30-1	$-2676.$	22 249.	$-1548.$	12 874.
BW30-2	$-2762.$	22 962.	$-1609.$	13 375.
1/v for water	$-2081.$	17 303.	$-1712.$	14 238.

activation energies were all larger than 15 800 kJ/kmol indicating that water transport was somewhat hindered. The apparent activation energies for the SW30 membranes should be larger than for the BW30 membranes due to the lower permeability for the SW30 membranes. This result is confirmed by the 10% and 40% larger activation energies for the SW30 membranes in the lower and higher temperature range, respectively.

In both the discussion on the variation in permeability with time, as presented in Figure 5.4, and the discussion above on apparent activation energies, there seems to be an additional effect on the permeability at higher temperatures. This effect could be caused by some separate change in the mechanism of transport in this temperature region or the effect could be the result of membrane fouling at higher temperatures. The experimental system was clean, using only distilled and deionized water and Analytical Reagent NaCℓ, and a 15 μm filter was put in line to trap any suspended materials, yet there may still have been some small amount of membrane fouling. The exact cause of this somewhat decreased permeability at higher temperatures is not known. The change is not due to compaction as compaction has already been accounted for as discussed in this section.

5.1.1.5   Effects of pressure and temperature on separation

The theoretical separation, f', which is calculated based on the boundary layer concentration (see Eqn.(2.6)) is plotted as a function of temperature and pressure in Figures 5.10 and 5.11 for the four membranes tested. For example, for the SW30-1 membrane the separation increases with pressure until a constant value of separation is reached. The increase in separation with pressure is expected for most reverse osmosis systems. This effect occurs because, increasing pressure, directly increases
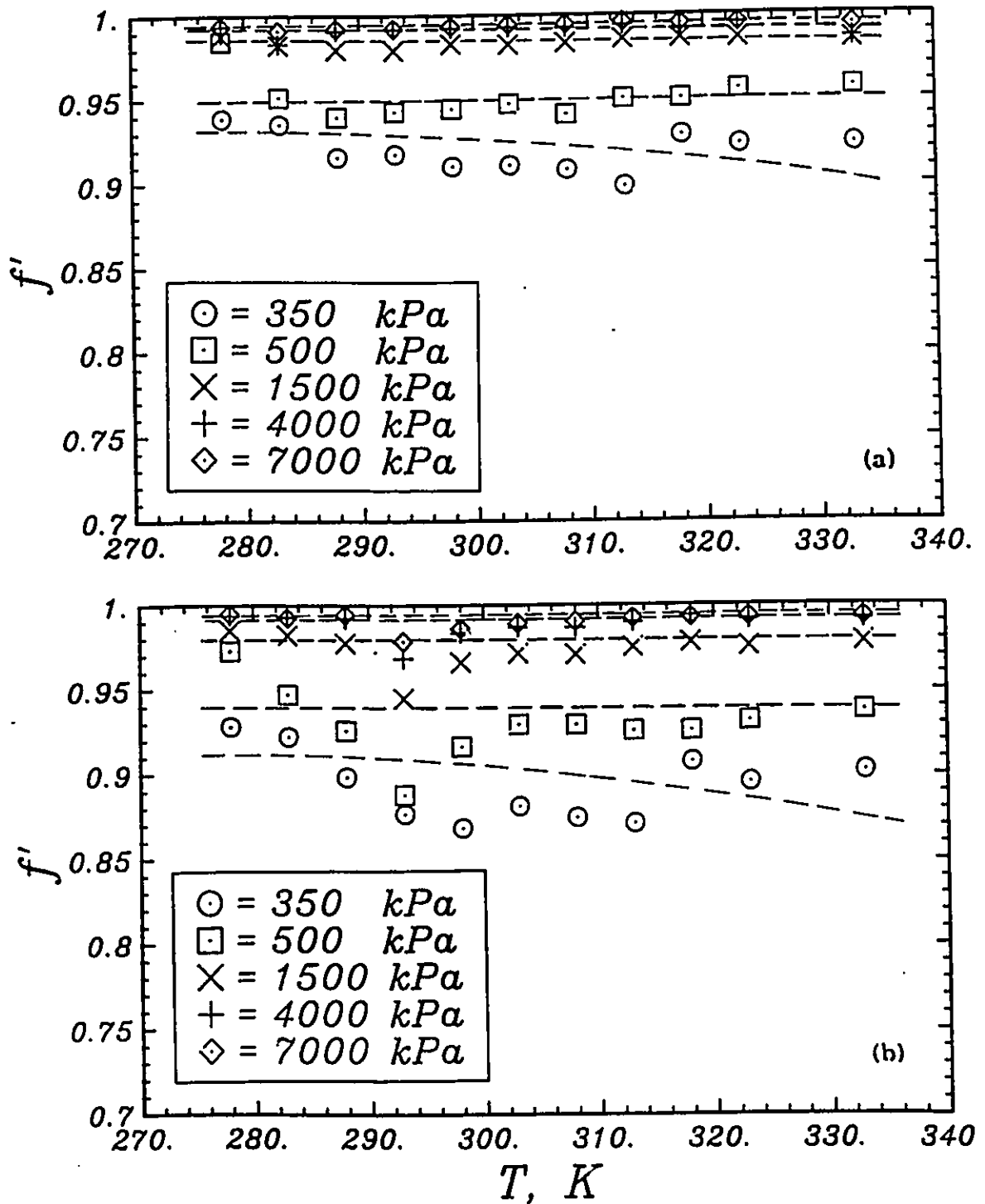
Figure 5.10: Theoretical separation versus temperature, with pressure as a parameter, for the (a) SW30-1, and (b) SW30-2 membranes.
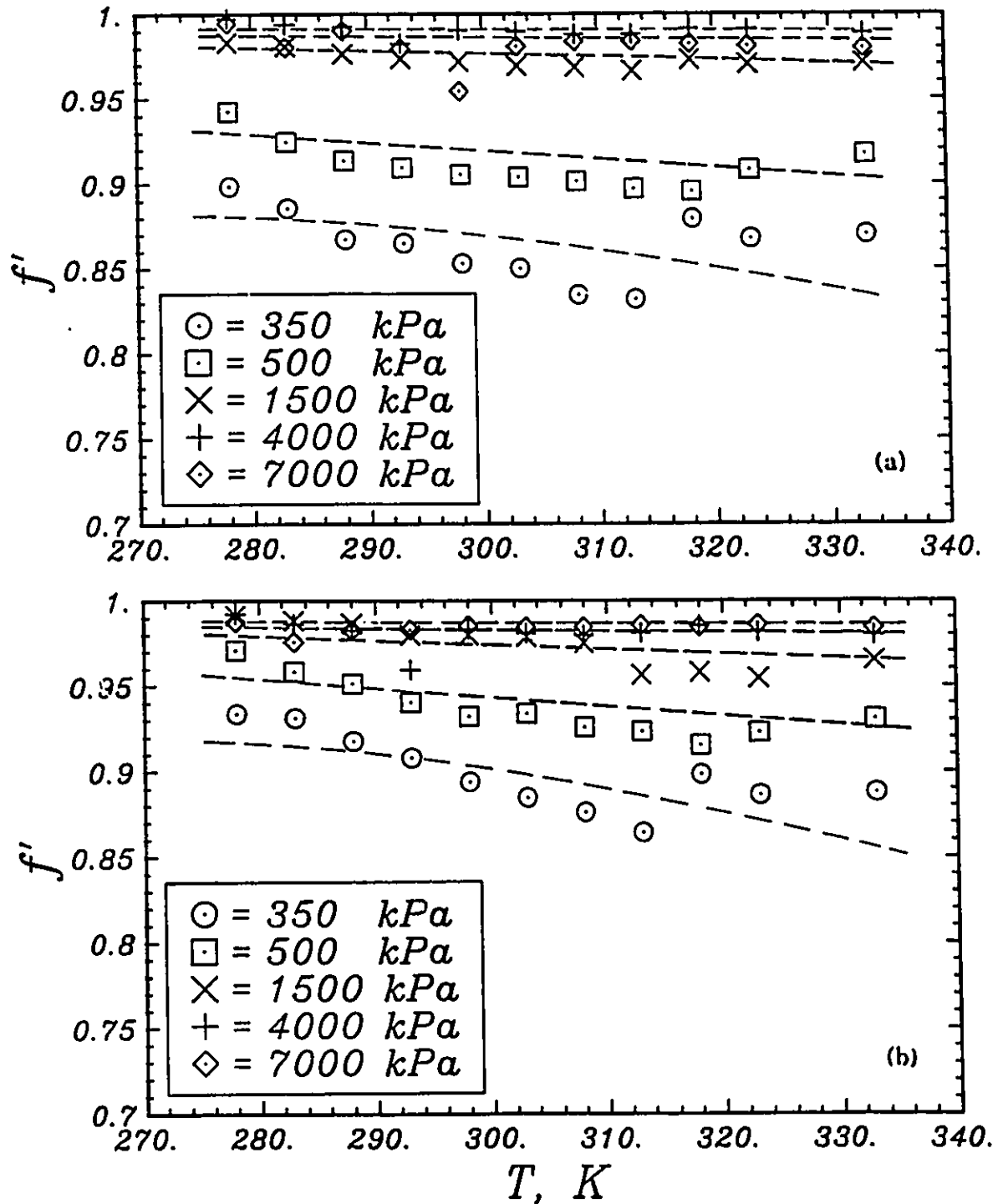
Figure 5.11: Theoretical separation versus temperature, with pressure as a parameter, for the (a) BW30-1, and (b) BW30-2 membranes.
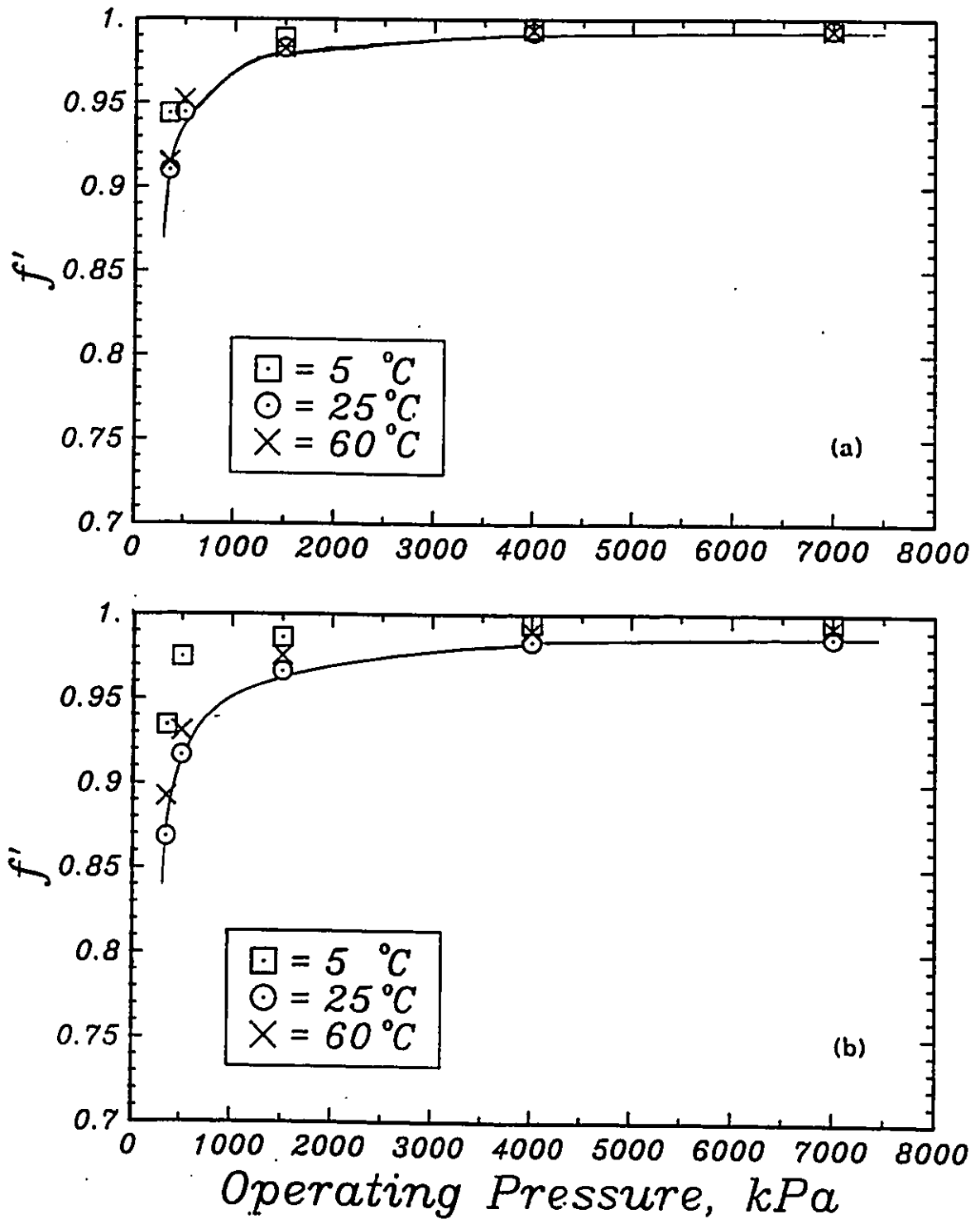
Figure 5.12:   Theoretical separation versus pressure, with temperature as a
parameter, for the (a) SW30-1, and (b) SW30- 2 membranes. Each
solid curve is the best-fit curve to each set of data at 25°C.
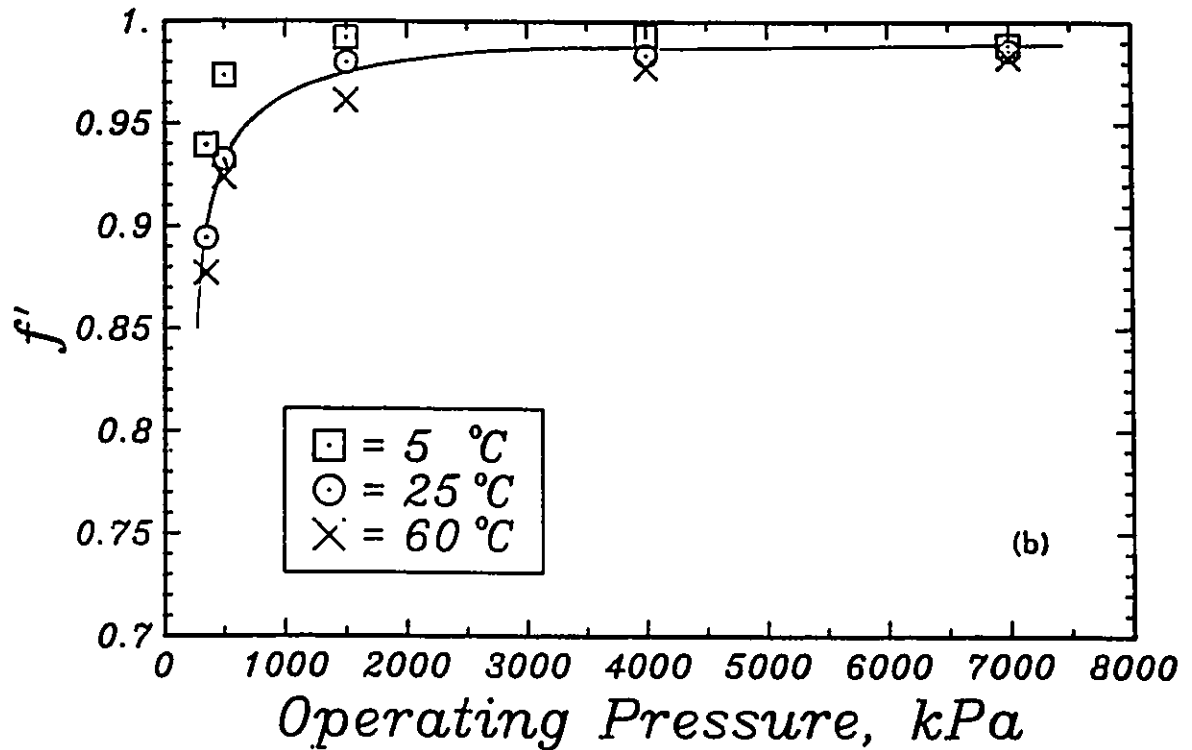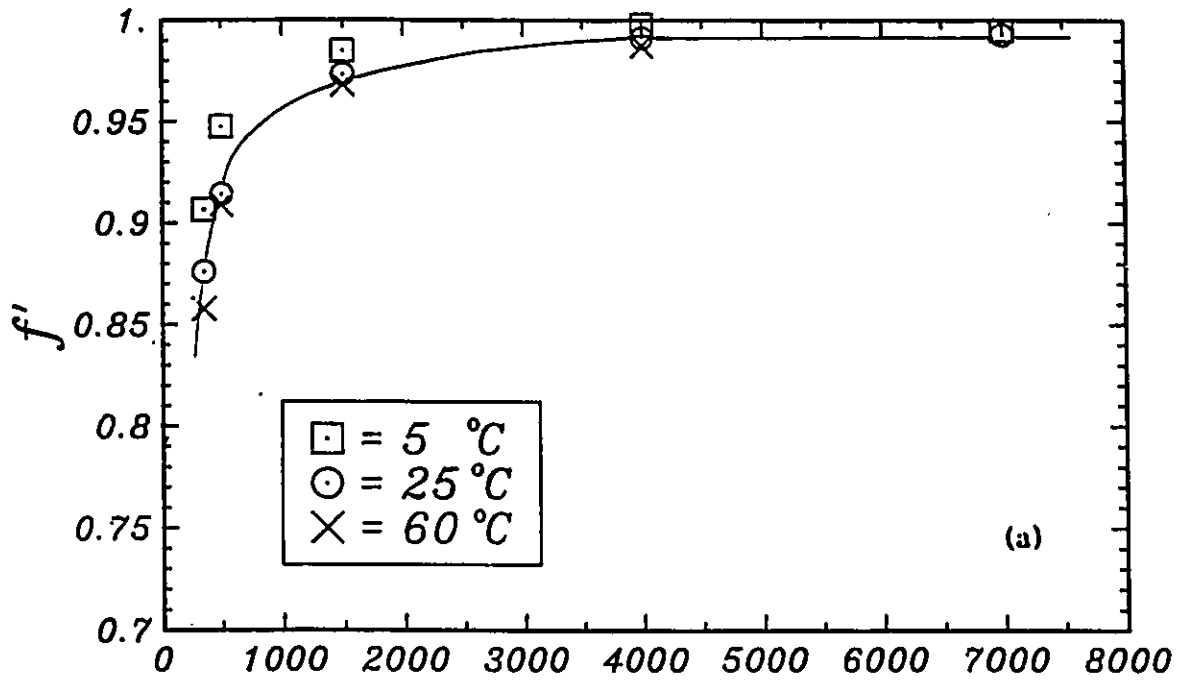
Figure 5.13:   Theoretical separation versus pressure, with temperature as a
parameter, for the (a) BW30-1, and (b) BW30- 2 membranes. Each
solid curve is the best-fit curve to each set of data at 25°C.

the flux of water while the concentration driving force for solute is almost unaffected. Hence more water in the permeate leads to higher separation. At higher pressures, the separation is approximately independent of the operating temperature. This result has been observed previously (Kimura and Nomura, 1981; Yang and Dickson, 1985). However, at the lower pressures, the separation appears to first decrease and then increase with increasing temperature. If this is true, the minimum separation is around 40°C. However, as is discussed in Section 5.3.3, the temperature-extended MD-SF-PF model predicts no such behaviour, and therefore the solid curves (in Figures 5.10 and 5.11) likely represent the experimental data; this matter is further discussed in Section 5.3.3.

Figures 5.10 and 5.11 illustrate similar results for the three remaining membrane samples. Again the separation increases with pressure to a maximum, as predicted by theory, and the separation is approximately independent of temperature at higher pressures.

Figures 5.12 and 5.13 are useful for illustrating the effect of pressure on separation explicitly. The separation increases with increasing pressure to a constant value at high pressures. The results are presented for 5, 25, and 60°C and the separation values are shown to be independent of temperature at high pressures. However, the independence of temperature implied by this plot ignores the variation with temperature that does exist for low pressures as shown in Figures 5.10 and 5.11.

5.1.1.6   Effects of pressure and temperature on solution flux

The solution flux is the flux of solute plus solvent measured when solute is present in the feed solution. The solution flux as a function of pressure is presented in Figures 5.14 and 5.15 for three temperatures. For all the membranes the flux was well
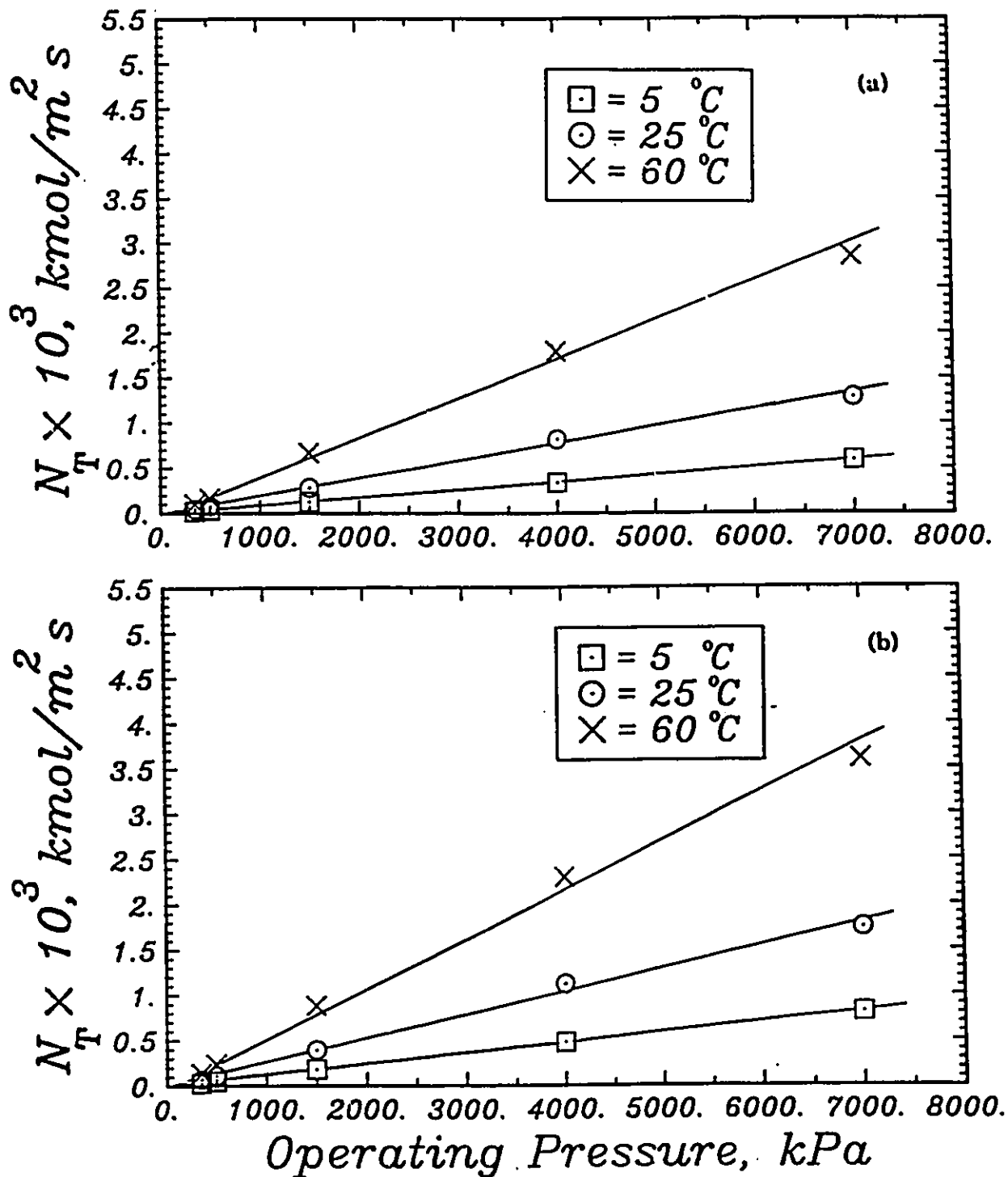
Figure 5.14:   Total permeation flux versus pressure, with temperature as a
parameter: (a) SW30-1, and (b) SW30-2 membranes.
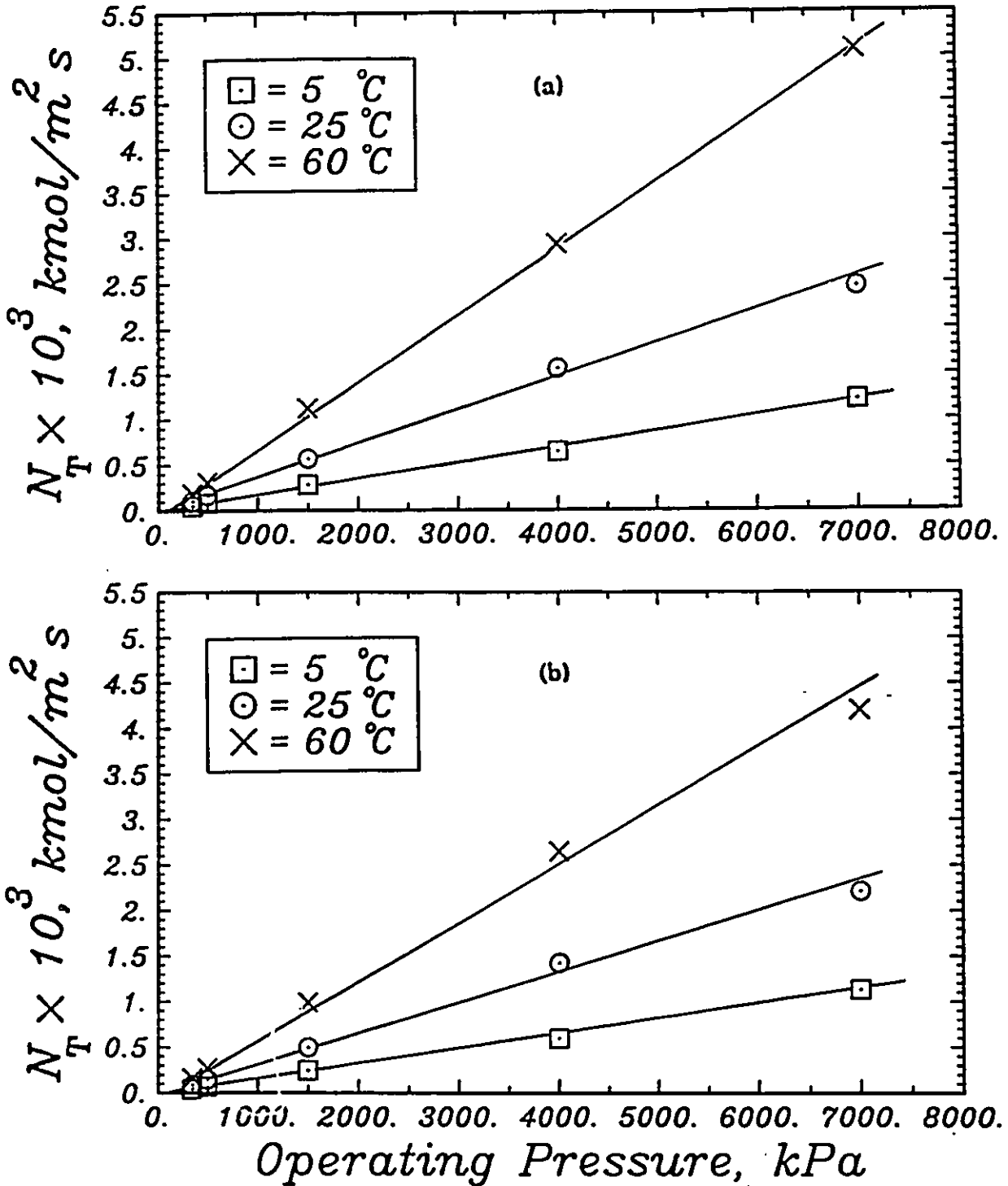
Figure 5.15:   Total permeation flux versus pressure, with temperature as a
parameter: (a) BW30-1, and (b) BW30-2 membranes.

represented by a straight line for each temperature. At the highest temperature there is a slight deviation from the straight line which may reflect some irreversible change to the membrane at higher temperatures.

5.1.1.7   Experiments at higher concentrations

These are experiments at the higher concentrations of 5000, 10 000, and 15 000 ppm NaCℓ and at 25°C temperature and 1500 kPa pressure, as documented as run numbers 1001 to 1003 in **Appendix C.**

The experimental results are shown by data points in Figures 5.16 and 5.17 in the form of theoretical separation and flux versus feed concentration, for SW30-1 and BW30-1 membranes, respectively. As expected, the solution flux and separation decrease with increasing feed concentration for all of the membranes. As the feed concentration is increased the theoretical separation decreases. This phenomenon happens since increasing the feed concentration decreases the solvent (water) permeation flux due to an increase in the feed osmotic pressure (see Eqn.(2.25)) and increases the driving force for solute transport through the membrane (see Eqn.(2.26)), so that a relatively larger fraction of solute is transported through the membrane and, therefore, the theoretical separation decreases.

The MD-SF-PF model predictions for the above data are presented in Section 5.3.2.

5.1.2   Phase II (Other 1-1 electrolytes)

The raw data for all the experiments have been analyzed by the computer code explained in Section 5.1.1.1, and the results are documented in **Appendix D,** for the electrolyte solutions: KCℓ-water, LiCℓ-water, and LiNO$_3$-water.
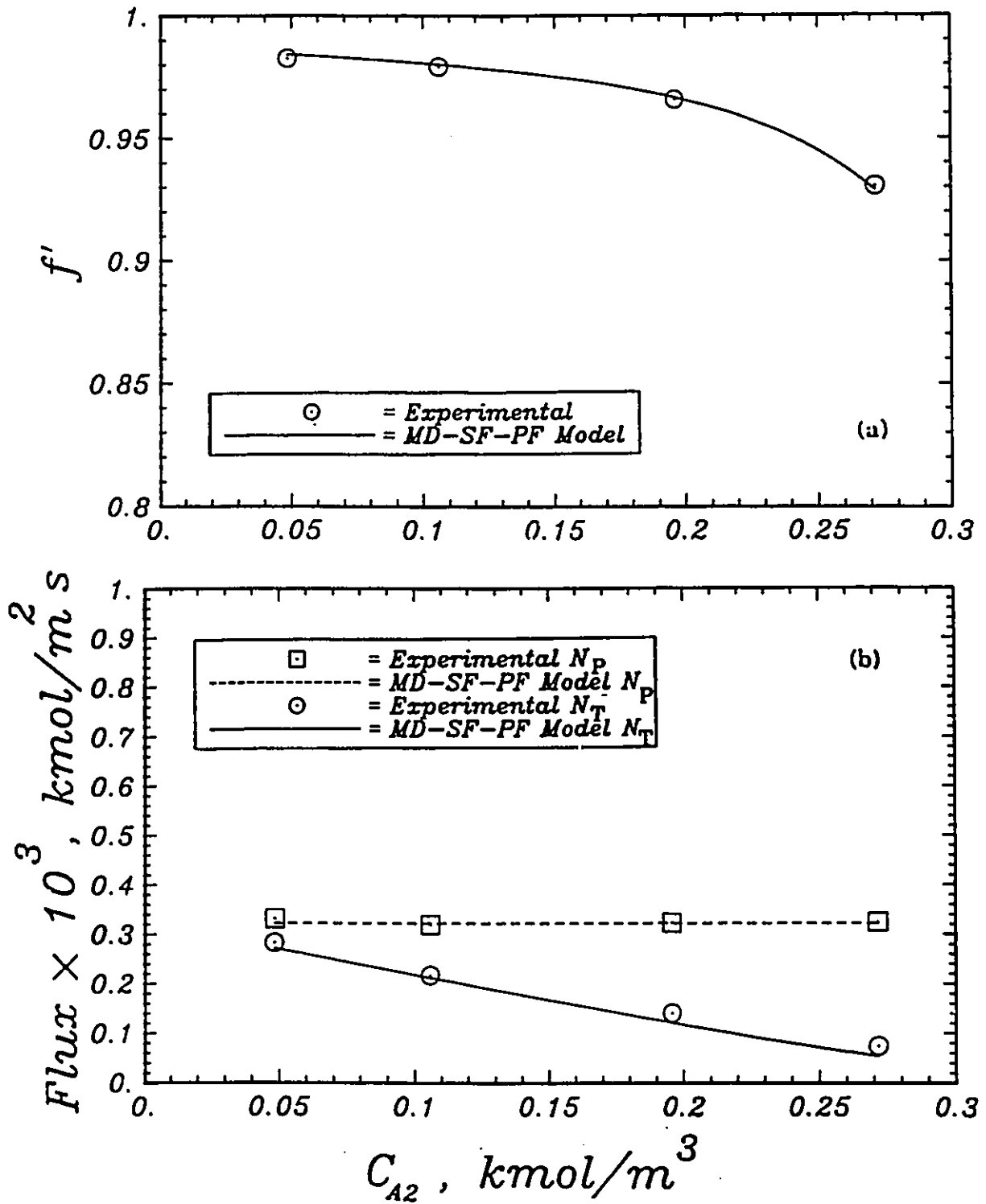
Figure 5.16:   Separation and permeat:.n fluxes versus feed concentration for the
SW30-1 membrane: a comparison between the experimental data
and the predictions of the MD-SF-PF model.
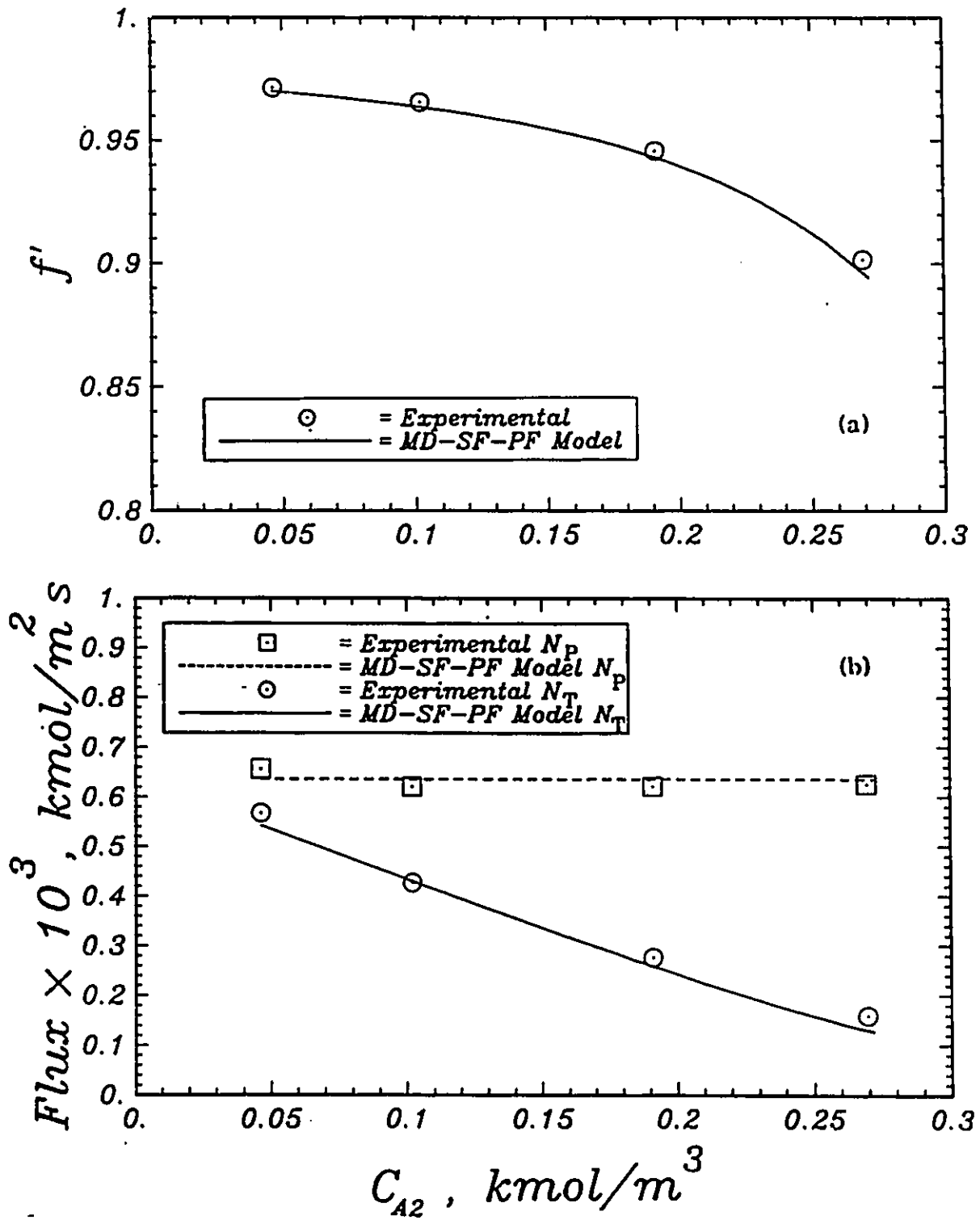
Figure 5.17: Separation and permeation fluxes versus feed concentration for the BW30-1 membrane: a comparison between the experimental data and the predictions of the MD- SF-PF model.

The results are plotted in the form of theoretical separation, f', and solution flux, N_T in Figures 5.18 to 5.23 for the $KC\ell$, $LiC\ell$, and $LiNO_3$ solutes, respectively (Mehdizadeh and Dickson, 1989g). Only one membrane of each group (that is, SW30-1 and BW30-1 membranes) are presented; the performance for the other membranes are similar. The MD-SF-PF model predictions, shown in Figures 5.18 to 5.23, are discussed in Section 5.3.2.

Figure 5.18.a illustrates the separation of $KC\ell$ as a function of operating pressure, for the SW30-1 membrane. As pressure is increased, separation increases and reaches a plateau, which is characteristic of systems in which strong solvent-membrane affinity exists. Figure 5.18.b illustrates the total permeation flux as a function of the operating pressure for the SW30-1 membrane. The flux increases linearly as a function of pressure. Figure 5.19 illustrates the same trends for the BW30-1 membrane. For the BW30 membrane, the separations are lower and the fluxes are higher than those for the SW30 membrane. The relative behaviour for the two membranes are as expected for seawater (SW30) and brackish water (BW30) membranes.

Figures 5.20 to 5.23 present similar data for the systems $LiC\ell$-water and $LiNO_3$-water, respectively. In all of these systems, the separation values are higher, and the flux values are lower, for the SW30 membrane than those for the BW30 membrane.

Typical values of pure water flux, N_P, for the SW30-1 and BW30-1 membranes were about 0.30 and 0.55×10^{-3} kmol/m^2 s at 1500 kPa pressure and 25°C.

The pH values for the feed and permeate streams, for all the solute systems, were in the range of 7.0 to 7.1, and, therefore, no pH adjustments were done.
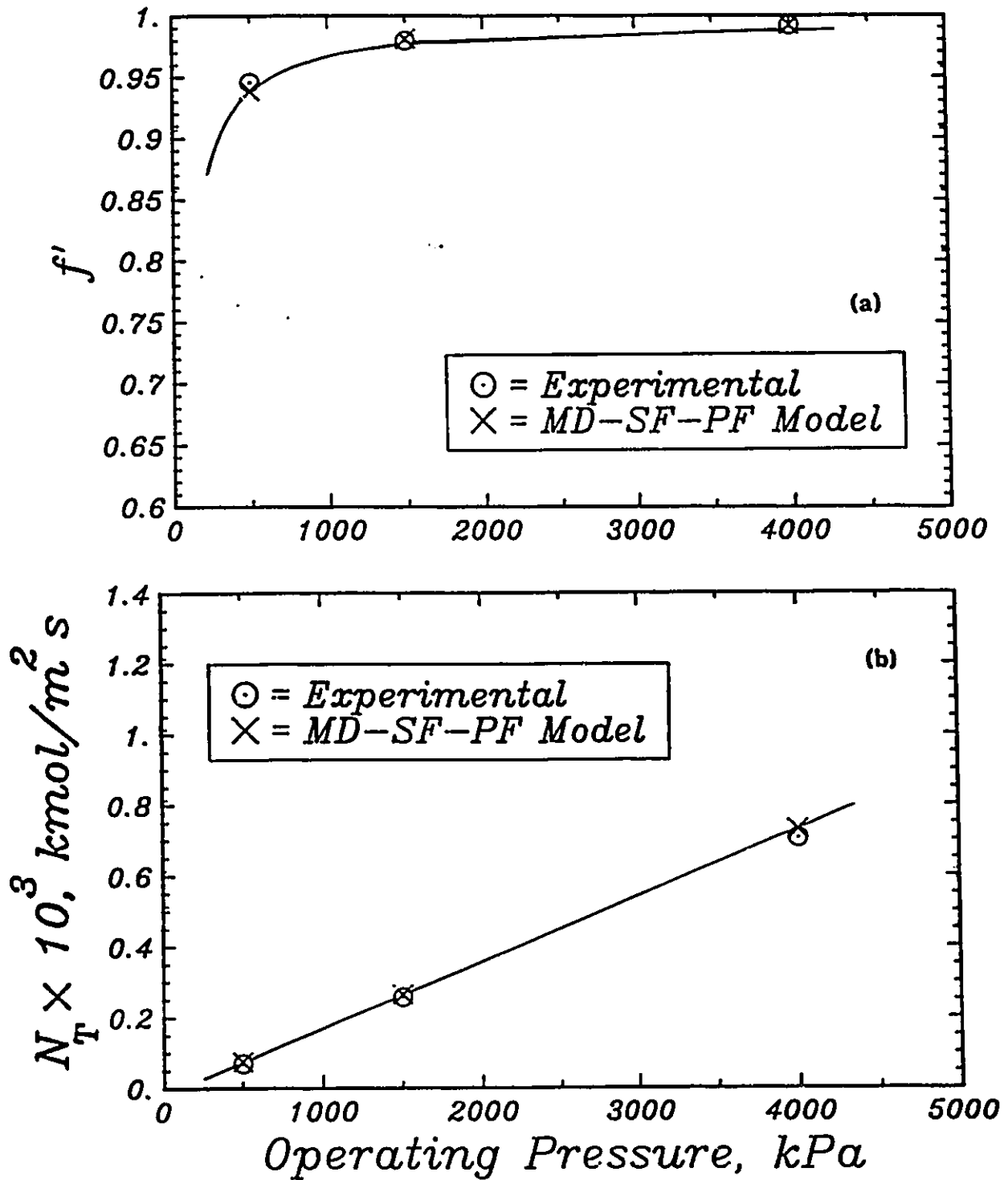
Figure 5.18: Experimental values and MD-SF-PF model predictions of membrane performance for the solute KCℓ: (a) separation versus operating pressure for SW30-1 membrane, and (b) total solution permeation flux versus operating pressure for SW30-1 membrane.
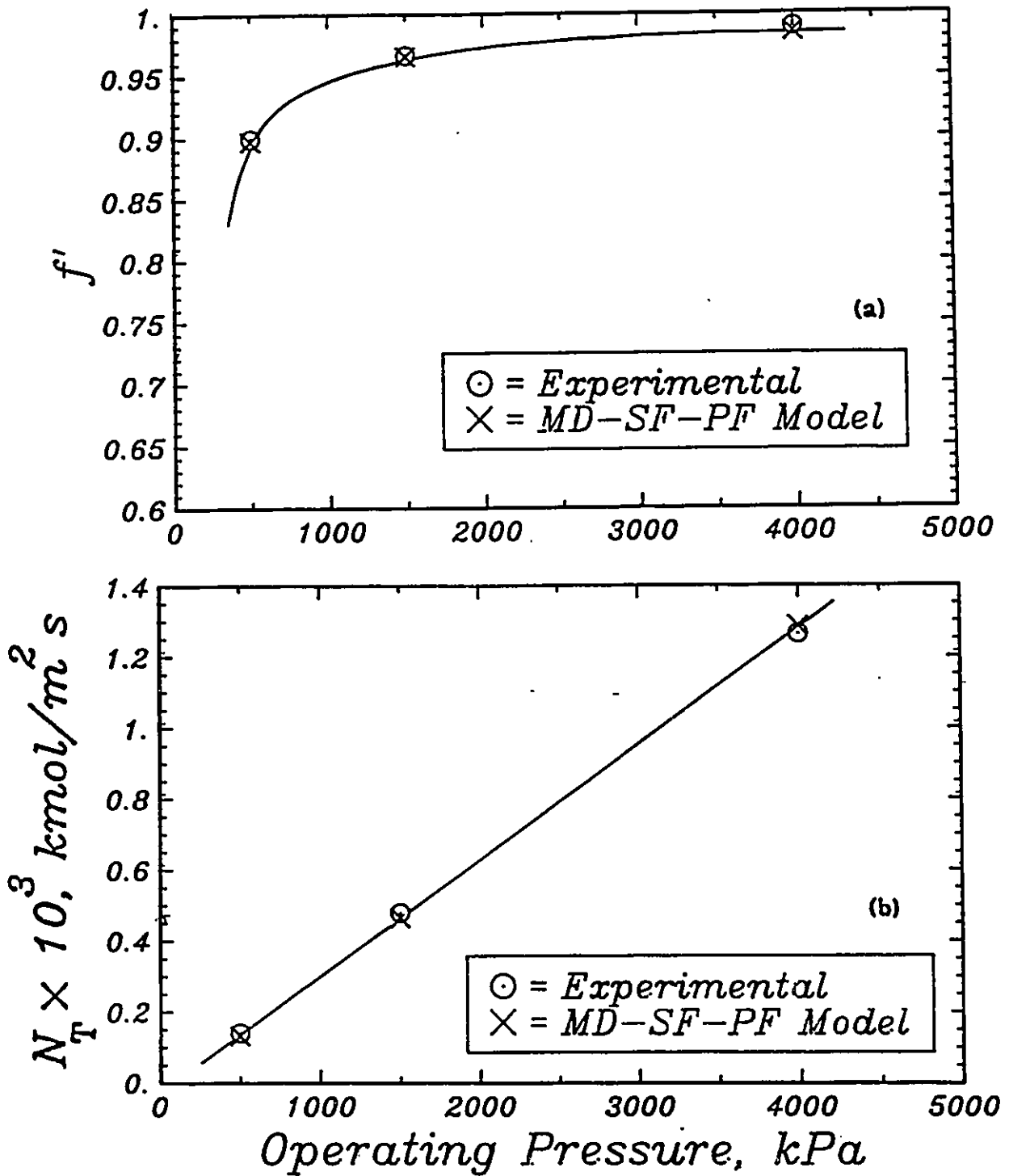
Figure 5.19: Experimental values and MD-SF-PF model predictions of membrane performance for the solute $KC\ell$: (a) separation versus operating pressure for BW30-1 membrane, and (b) total solution permeation flux versus operating pressure for BW30-1 membrane.
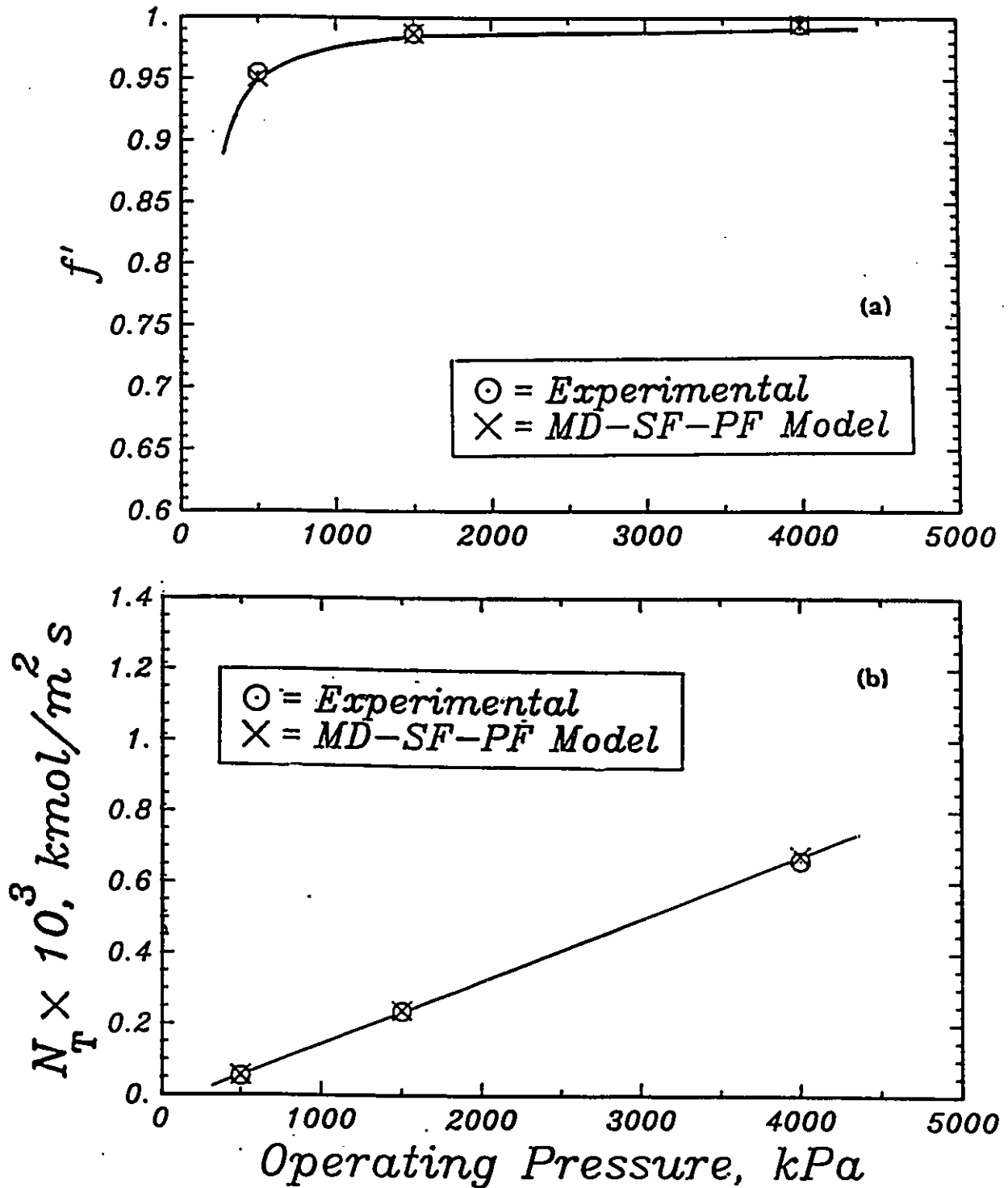
Figure 5.20: Experimental values and MD-SF-PF model predictions of membrane performance for the solute LiCℓ: (a) separation versus operating pressure for SW30-1 membrane, and (b) total solution permeation flux versus operating pressure for SW30-1 membrane.
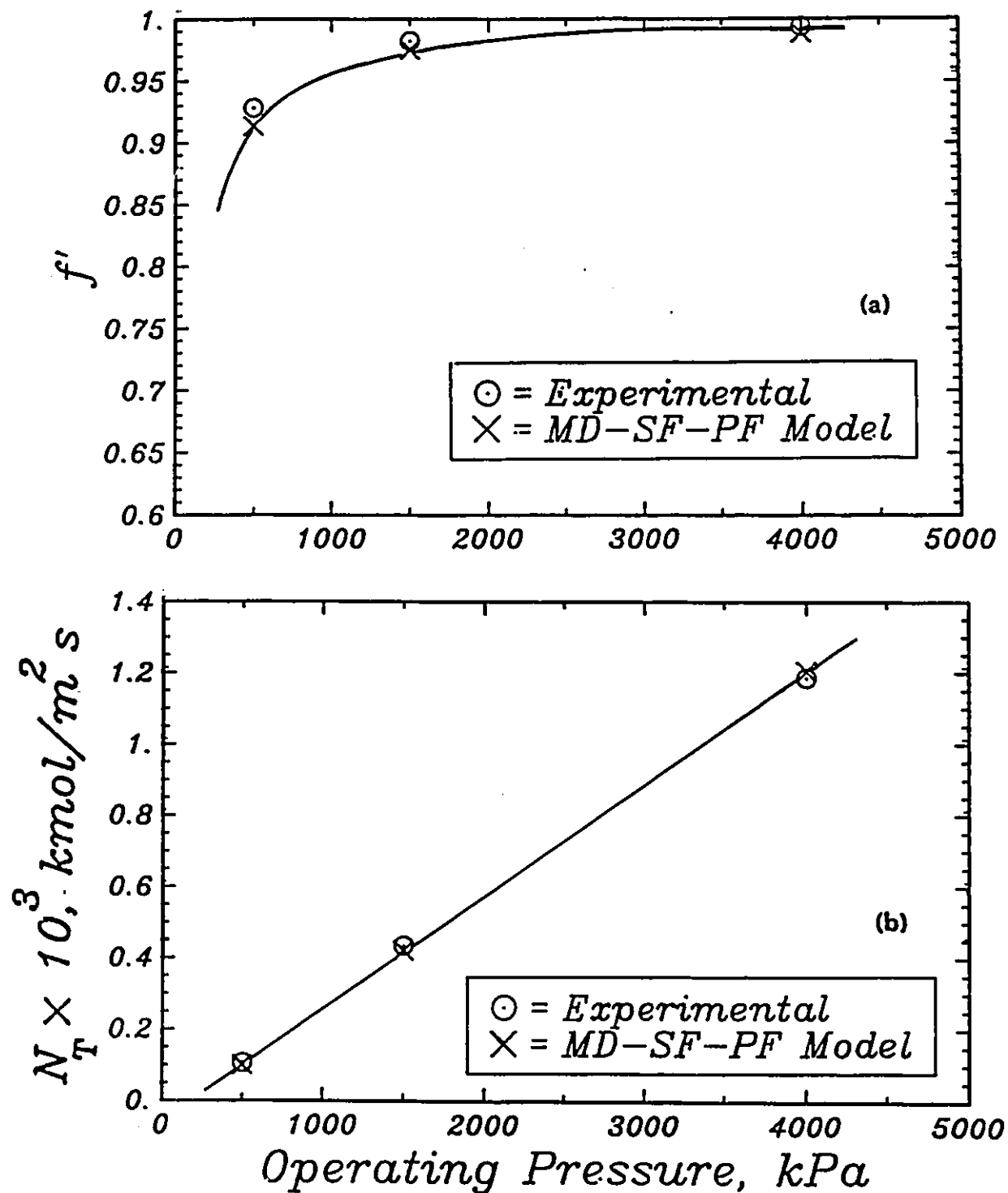
Figure 5.21:   Experimental values and MD-SF-PF model predictions of membrane performance for the solute LiCℓ: (a) separation versus operating pressure for BW30-1 membrane, and (b) total solution permeation flux versus operating pressure for BW30-1 membrane.
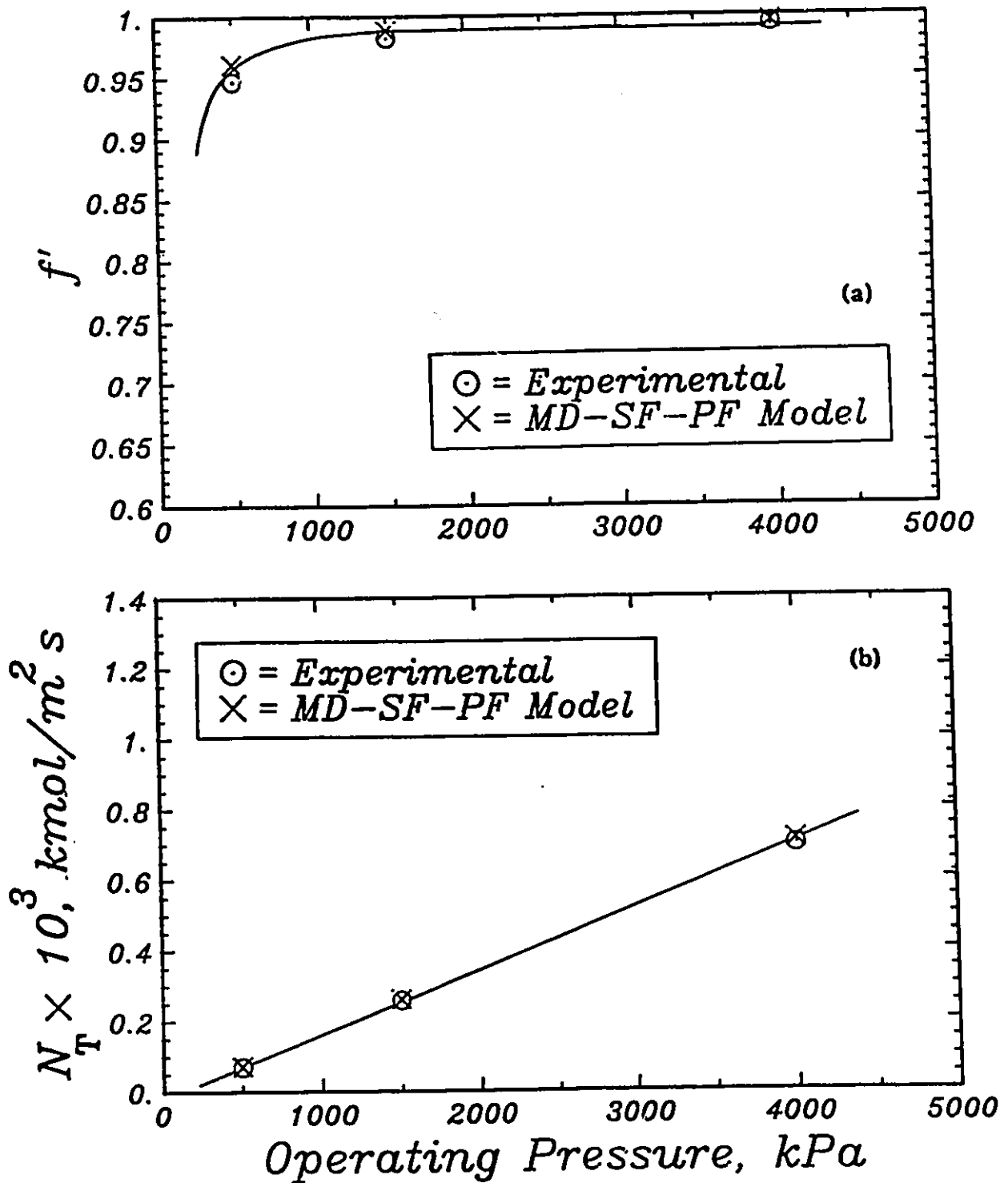
Figure 5.22: Experimental values and MD-SF-PF model predictions of membrane performance for the solute LiNO$_3$: (a) separation versus operating pressure for SW30-1 membrane, and (b) total solution permeation flux versus operating pressure for SW30-1 membrane.
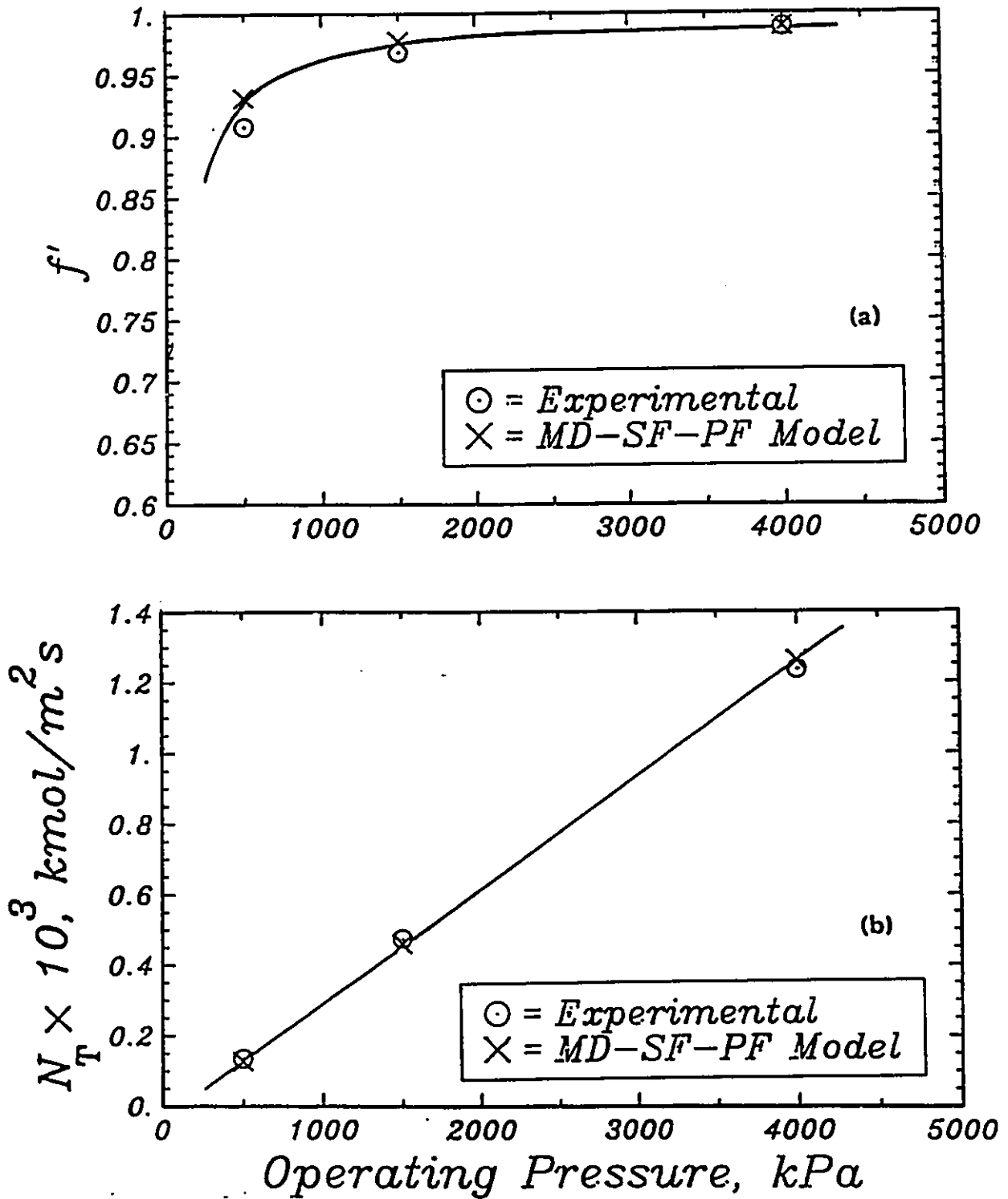
Figure 5.23:   Experimental values and MD-SF-PF model predictions of
membrane performance for the solute LiNO$_3$: (a) separation versus
operating pressure for BW30-1 membrane, and (b) total solution
permeation flux versus operating pressure for BW30-1 membrane.

5.1.3   Phase III (Sea water concentrations)

In this section, the experimental results for Phase III (sea water concentrations) are presented and discussed (Mehdizadeh and Dickson, 1989h). The discussion parallels and is compared with the discussion for Phase I experimental plan in Section 5.1.1.

5.1.3.1   Analysis of raw data

The raw data for all the 30 experiments are processed by the procedure described in Section 5.1.1.1. The results are tabulated in **Appendix E**.

The values of feed and permeate pH, measured in some experiments, were all in the range 6.5 to 6.7, which were as expected. Therefore, no attempt was made to adjust for the pH.

5.1.3.2   Mass transfer coefficients

The mass transfer coefficients are known from the experiments in Phase I and the discussion in Section 5.1.1.2. The values are 15.35×10^{-6}, 22.49×10^{-6}, 32.84×10^{-6}, and 27.65×10^{-6} m/s for the SW30-1, SW30-2, BW30-1, and BW30-2 membranes, respectively. These values are then used as the reference values in Eqn.(2.55) to determine the coefficients at other temperatures.

The values for solute diffusivities, and solution densities, viscosities, and osmotic pressures can be found in the literature (Stoughton and Lietzke, 1965; Korosi and Fabuss, 1968; Sourirajan, 1970; Weast, 1975; Reid et al., 1977).

5.1.3.3   Standard experiments

The results obtained for the standard experiments at different times are presented in Figures 5.24 and 5.25 by run numbers 301 to 330 for Phase III. Run number represents the order in which experiments were performed, as described in Section 5.1.1.3. The results obtained for Phase I standard experiments (i.e., run numbers 111 to 179) are also included in Figures 5.24 and 5.25 for comparison. Figure 5.24 presents the variation of separation with time for the SW30 and BW30 membranes, respectively. The dashed lines in Figures 5.24 and 5.25 represent the period of time during which no experiments were run. The average values of separation in the new set of experiments (i.e., run numbers 301 to 330) are about 98.5% and 98.0% for the SW30-1 and SW30-2 membranes, respectively, and about 97.5% and 97.0% for the BW30-1 and BW30-2 membranes, respectively. Compared with the results in Phase I (i.e., run numbers 111 to 179), which give the separation values of 97.7% and 96.7% for the SW30-1 and SW30-2 membranes and an average 96.4% for the BW30 membranes (see Section 5.1.1.3), the separation values for the standard experiments in Phase III are a little higher (about 1%). This means that the FT30 membranes have not lost their solute rejection character during the above period of time. Also, the BW30-2 membrane, which had an oscillating behaviour for separation in Phase I (see Section 5.1.1.3) did not act in this manner, in Phase III, as presented by the lower flat line in Figure 5.24.b.

Figure 5.25 presents the pure water flux versus time. Similar to Figure 5.24, the experimental results in Phase I (i.e., run numbers 111 to 179) are also included for comparison. The dashed lines represent the period of time during which no experiment was run. The reason for the flux decline with respect to time, in Figure 5.25, is not known with certainty; however, as discussed in Section 5.1.1.4,
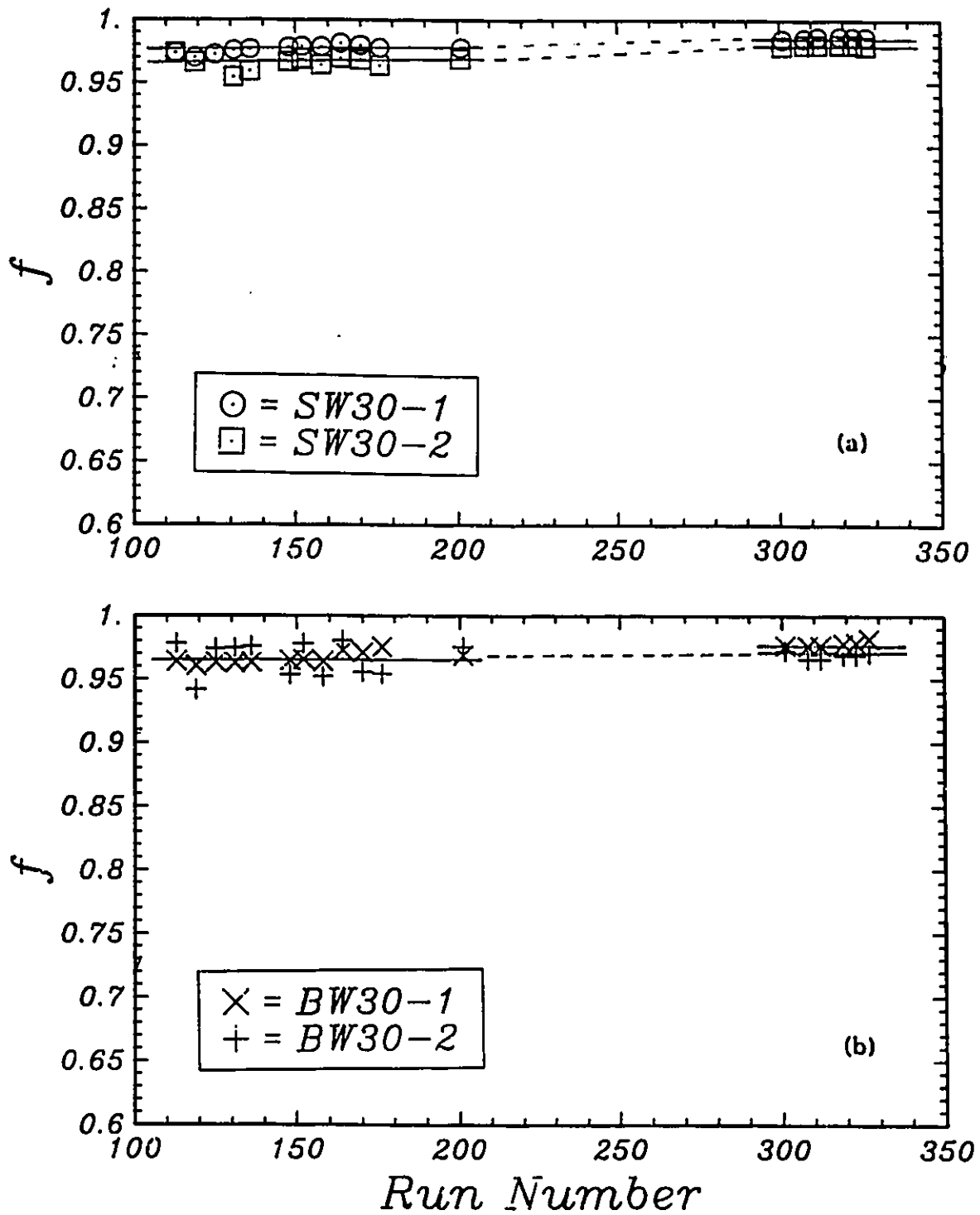
Figure 5.24:   Standard experiments: (a) separation versus run number for SW30 membranes, and (b) separation versus run number for BW30 membranes. The lines represent the experimental trends.
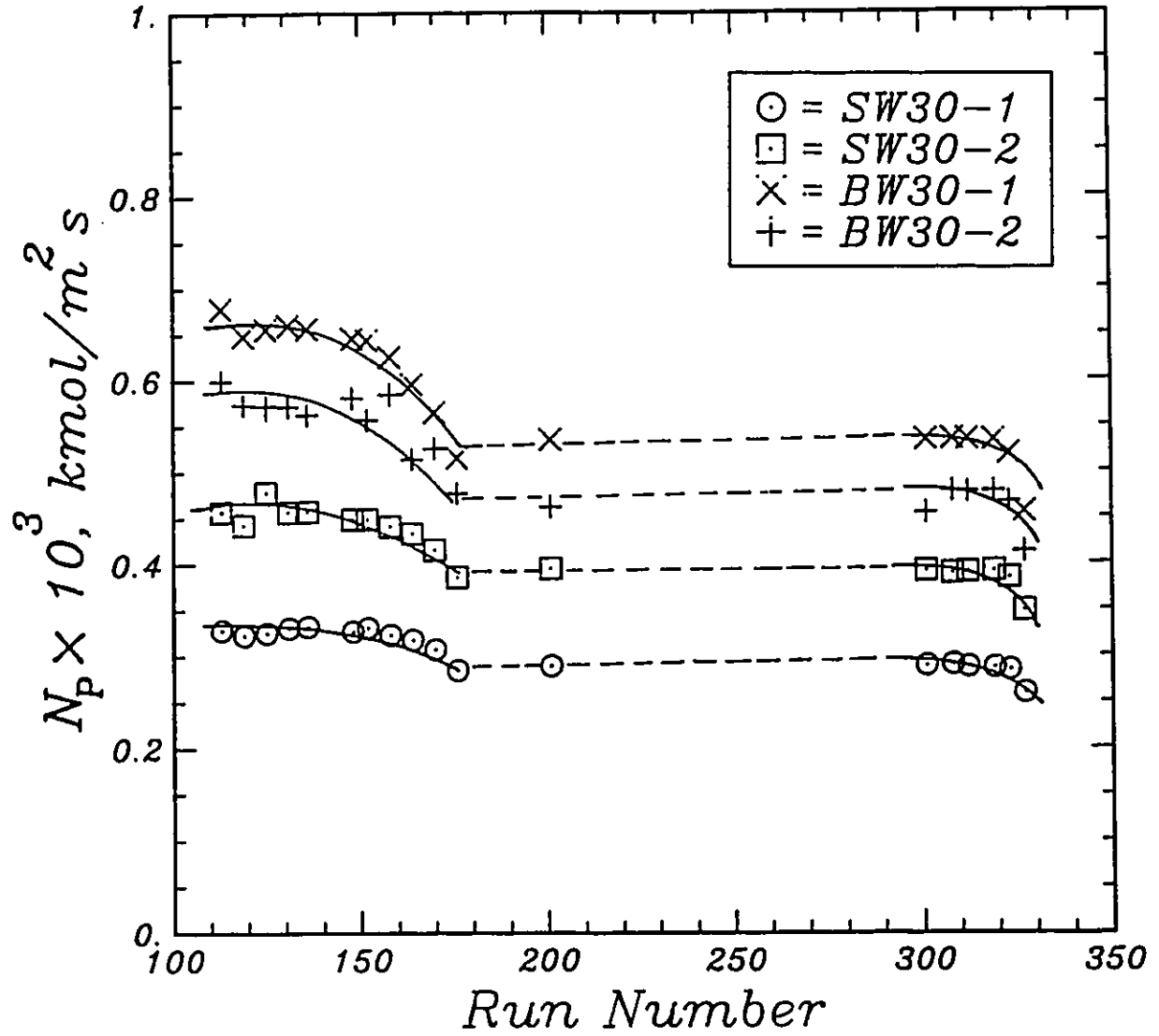
Figure 5.25: Standard experiments: pure water flux versus run number for all the membranes. The lines represent the experimental trends.

since the flux decline starts from the first standard experiment after 40°C temperature the phenomenon might be the result of membrane fouling at higher temperatures due to the presence of trace contaminants in sodium chloride or it could be due to some separate change in the structure of the membranes.

The BW30 membranes, which have higher permeation fluxes, show a larger decrease in flux than the SW30 membranes. As compared with the results for Phase I (i.e., run numbers 111 to 179), the early experimental fluxes in Phase III matched the last values of the fluxes in Phase I. The relative differences in fluxes between the four membranes have remained constant over the time of testing. As expected, the higher flux membranes have the lower separations.

5.1.3.4   Effects of pressure and temperature on pure water flux

As discussed in Section 5.1.1.4, the pure water flux should increase linearly with pressure if no compaction and fouling exist in the system; in such a case the pure water permeability coefficient, A, should be independent of pressure. It was found, in Section 5.1.1.4, that more information could be obtained about the dependency of A on pressure by plotting A versus pressure (such as in Figure 5.7) rather than plotting the pure water flux versus pressure (such as in Figures 5.5 and 5.6). For the pure water experiments in Phase III, the A values are plotted versus pressure (in Figure 5.26). The trend in Figure 5.26, as shown by the best-fit straight lines, reveal that the pure water permeability coefficient, A, decreases over the whole pressure range and the change can be considered as linear. The value of A at zero pressure, A^0, and the compaction parameter, m (defined in Eqn.(3.87)), are determined at any fixed temperature, as in Section 5.1.1.4.
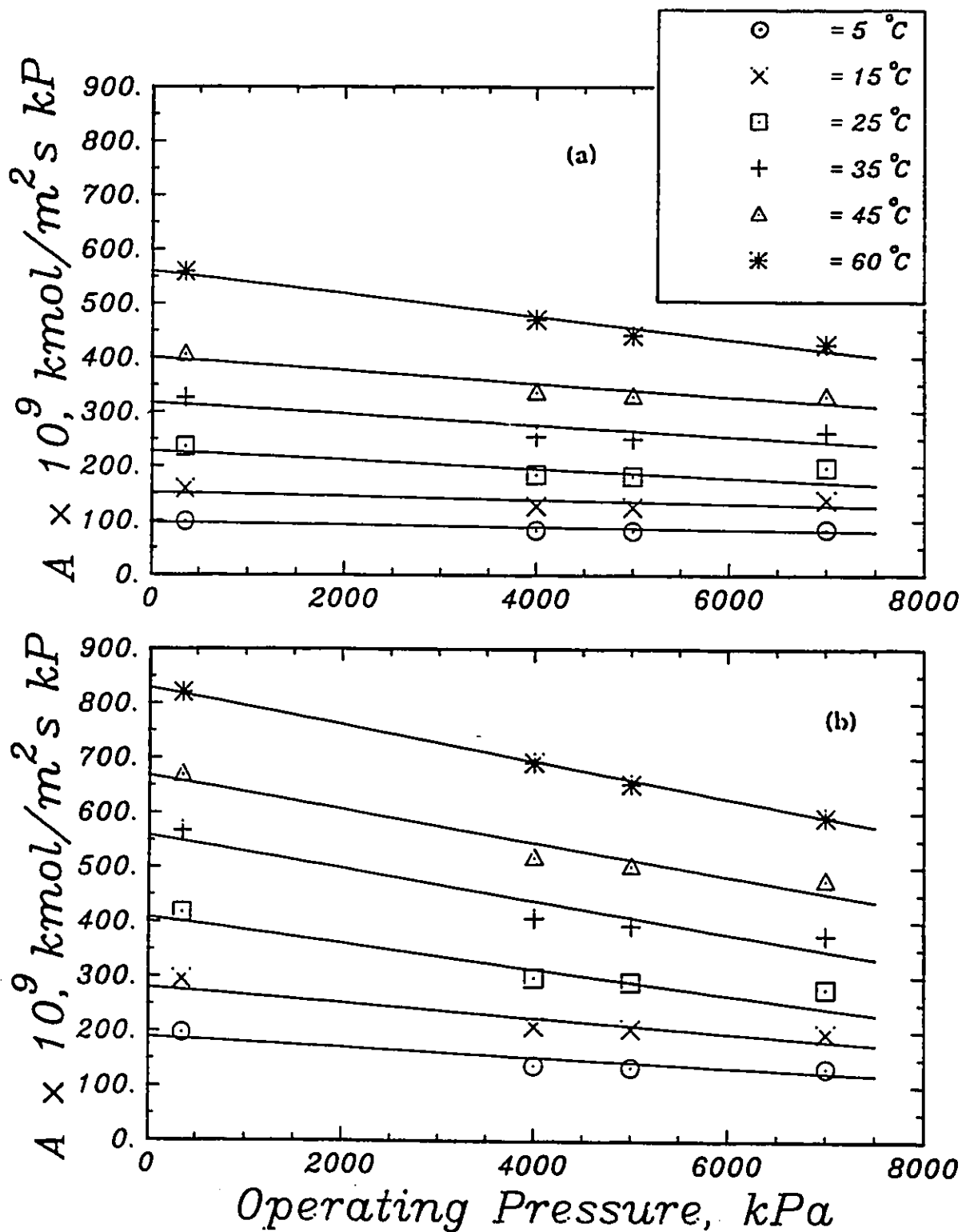
Figure 5.26: Pure water permeability coefficient as a function of operating pressure and temperature: (a) SW30-1 membrane, and (b) BW30-2 membrane. The straight lines are the best-fit lines by least squares for each set of data.

Similar to the pure water experiments in Phase I (see Section 5.1.1.4), the A^0 values are plotted as a function of temperature in Figure 5.27.a for the SW30-1 and BW30-2 membranes, respectively. The compaction-free pure water permeability coefficient (A^0) for each membrane follows the Arrhenius-type behaviour in two temperature intervals: 5-35°C and 35-60°C; similar behaviour was found for the pure water experiments in Phase I, as shown in Figure 5.9.a. The change in slope appears to occur in the same region, 35°C to 40°C, in both Phase I and Phase III experiments. The similarity of the data in Figures 5.27.a and 5.9.a indicates the reproducibility of the pure water experimental data. Again, this change in slope may represent a change in membrane transport of water at about 35-40°C.

Similar to Figure 5.8 for the pure water experiments in Phase I, the compaction coefficients, m, are plotted versus temperature on a log-log scale in Figure 5.27.b. That the compaction curves in Figure 5.27.b follow similar trends (and fall into the same range of changes) as those in Phase I (Figure 5.8) represents, again, the reproducibility of the pure water experimental data.

To complete the analogy between the pure water experimental data in Phases I and III, Equation (3.89) is employed to determine the magnitudes of the apparent activation energies of water transport for each membrane. The energies are tabulated in Table 5.2. These energies are about 30% and 45% lower in the higher temperature range than in the lower temperature range for the SW30 and BW30 membranes, respectively; these values are close (about 10% difference) to the 30% and 40% values in Phase I. The lower activation energies at higher temperatures may be related to a shift in the mechanism of water transport. The values are about the same (about 1% difference) for the other samples of the same membrane material. The apparent activation energy values for the SW30 membrane are about 10% an 35%
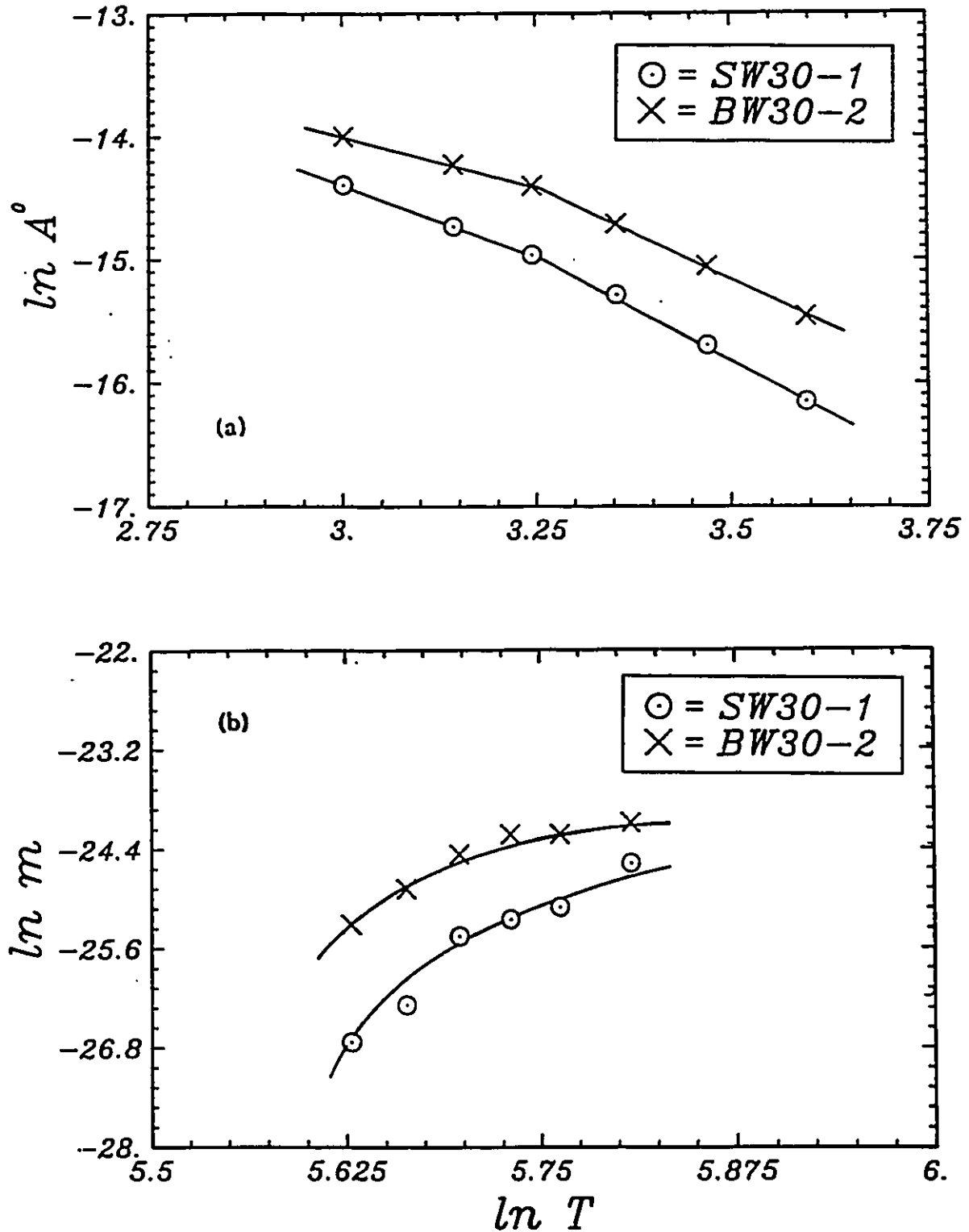
Figure 5.27: Characteristics of pure water permeability coefficient for the SW301- and BW30-2 membranes: (a) Arrhenius plot of compaction-free pure water permeability coefficient as a function of temperature (the slopes of the straight lines change at about 35°C), (b) compaction coefficient as a function of temperature.

Table 5.2

Apparent activation energies for the pure water permeability coefficient
(in Phase III) and for inverse kinematic viscosity

Membrane	5 - 35°C temperature range		35 - 60°C temperature range	
	Slope = −E/R, K	E, kJ/kmol	Slope = −E/R, K	E, kJ/kmol
SW30-1	−3403.	28 295.	−2333.	19 400.
SW30-2	−3047.	25 337.	−1627.	13 530.
1/ν for water	−2081.	17 303.	−1712.	14 238.

larger than the values for the BW30 membranes in the lower and higher temperature range, respectively (which are very close to the corresponding 10% and 40% found in Phase I experiments). The proximity of the new values to the old values indicates that the membranes in Phase III have the same characteristics as in the last experiments in Phase I and, therefore, could still be used for Phase III experiments.

Up to now, the reproducibility of the pure water experimental results have been discussed. Now, attention is given to the results for the salt solutions at the operating conditions of Phase III, and the results are discussed in terms of pressure and temperature effects on membrane separation and permeation flux.

5.1.3.5   Effects of pressure and temperature on separation

Similar to the results in Phase I (see Section 5.1.1.5, Figures 5.10 and 5.11), the theoretical separation, f', is plotted as a function of temperature, with pressure as a parameter, in Figures 5.28 and 5.29 for all the FT30 membranes. The following trends are observed in the data in Figures 5.28 and 5.29.

In general, at a fixed pressure, as the temperature is increased the separation decreases at the lower pressures (i.e., 4000 and 5000 kPa) but the separation does not change remarkably at the highest pressure (i.e., 7000 kPa). Previously, as observed in the data of Phase I (i.e., the experiments at brackish water concentration level), the separation was independent of temperature at the highest pressures (see Section 5.1.1.5). The fact that separation is independent of temperature at the highest operating pressures is common in both the sea water concentration experiments (Phase III) and the brackish water concentration experiments (Phase I). The change in separation with temperature at the lower pressures, in Figures 5.28 and
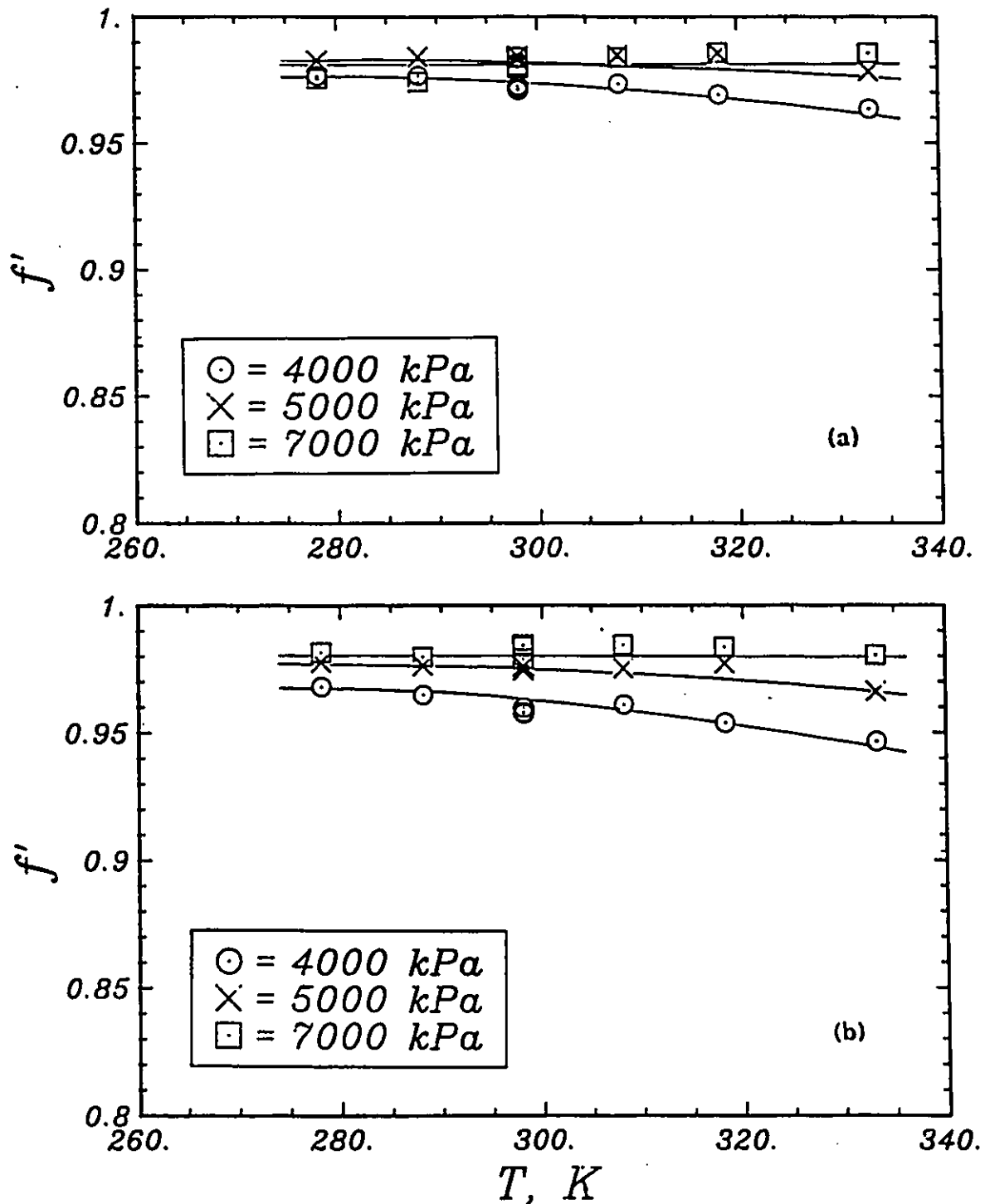
Figure 5.28:   Theoretical separation versus temperature, with operating
pressure as a parameter: (a) SW30-1, and (b) SW30- 2 membranes.
The lines represent the experimental trends.
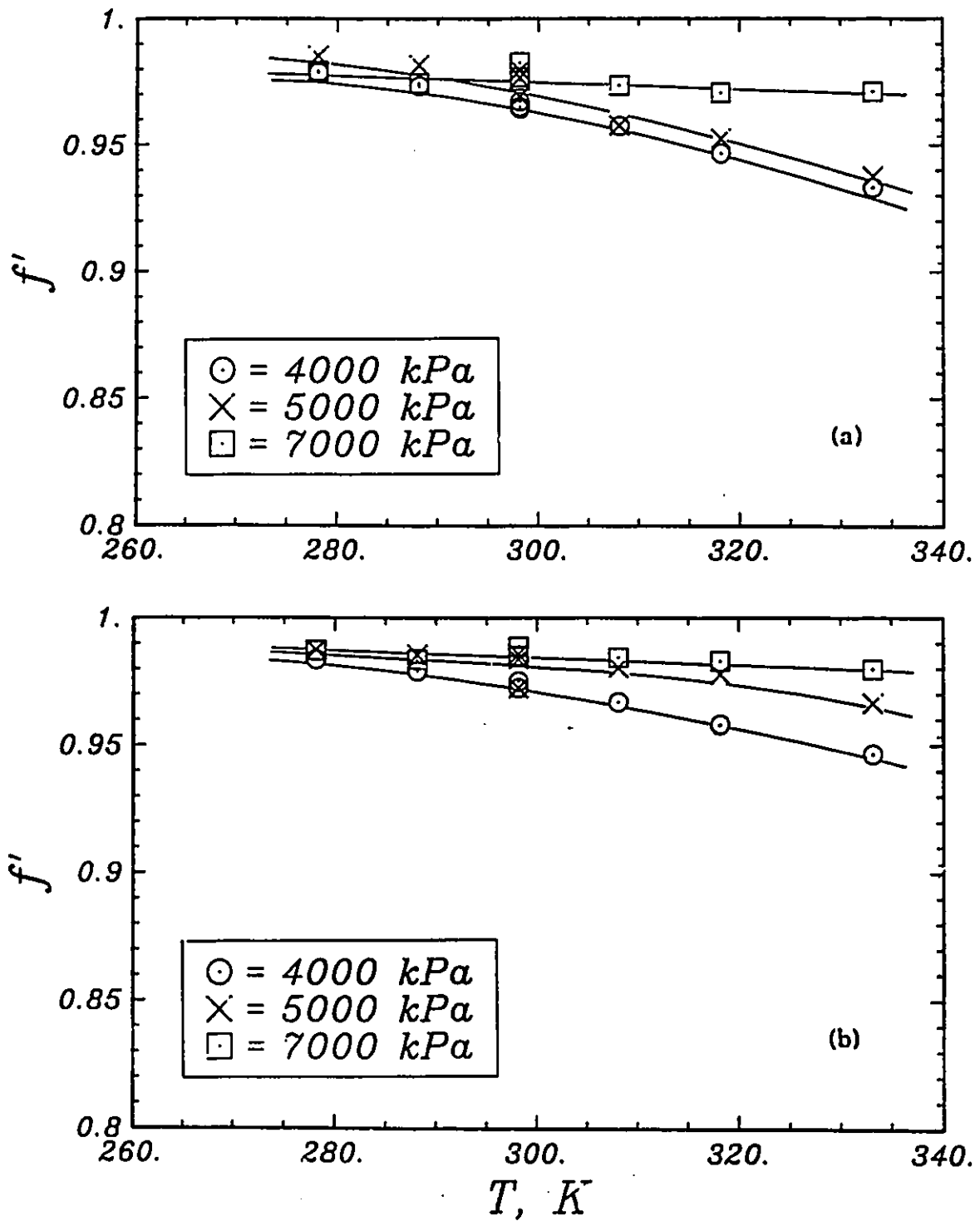
Figure 5.29:   Theoretical separation versus temperature, with operating
pressure as a parameter: (a) BW30-1, and (b) BW30-2 membranes.
The lines represent the experimental trends.
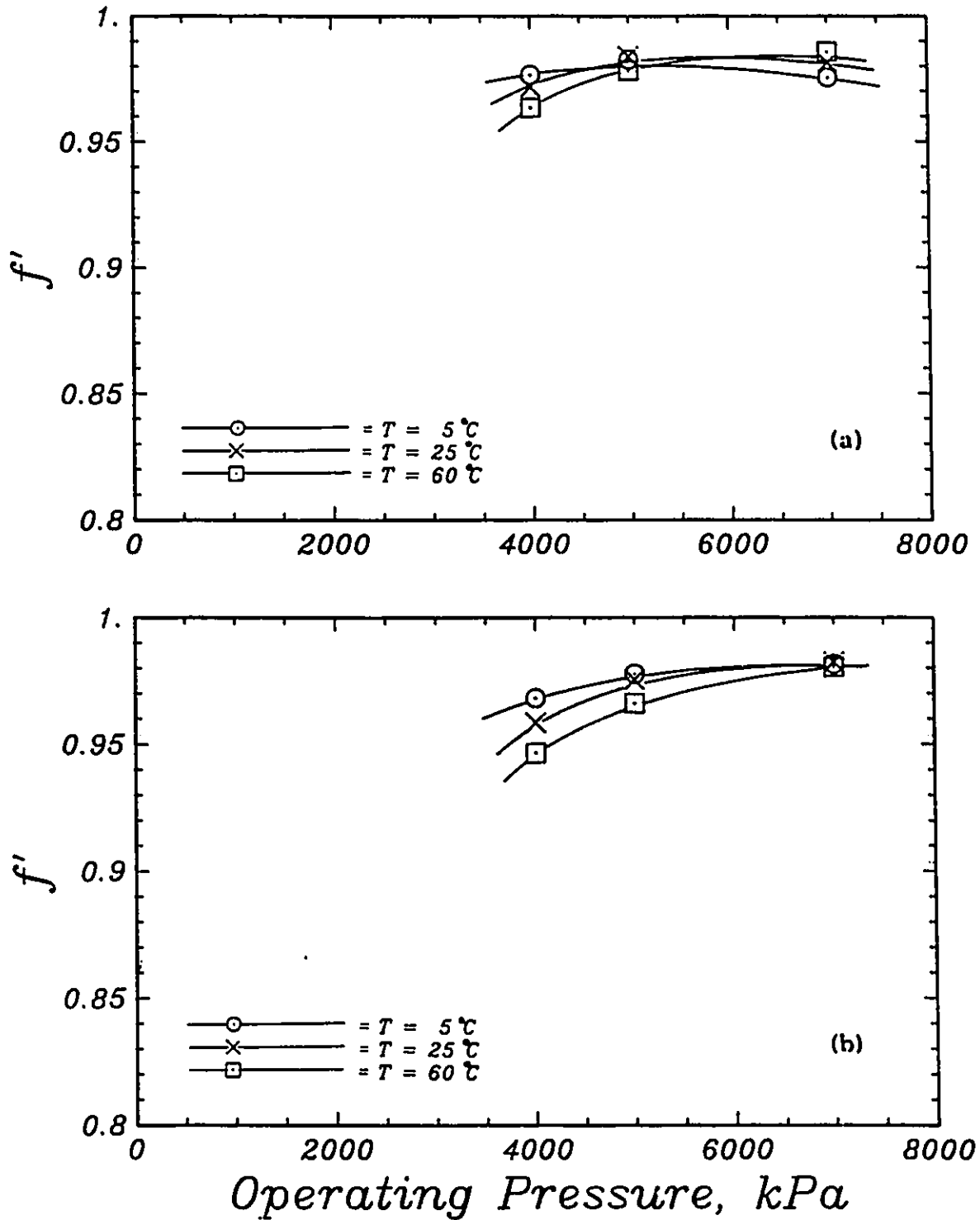
Figure 5.30: Theoretical separation versus operating pressure, with temperature as a parameter: (a) SW30-1, and (b) SW30-2 membranes. The lines represent the experimental trends.
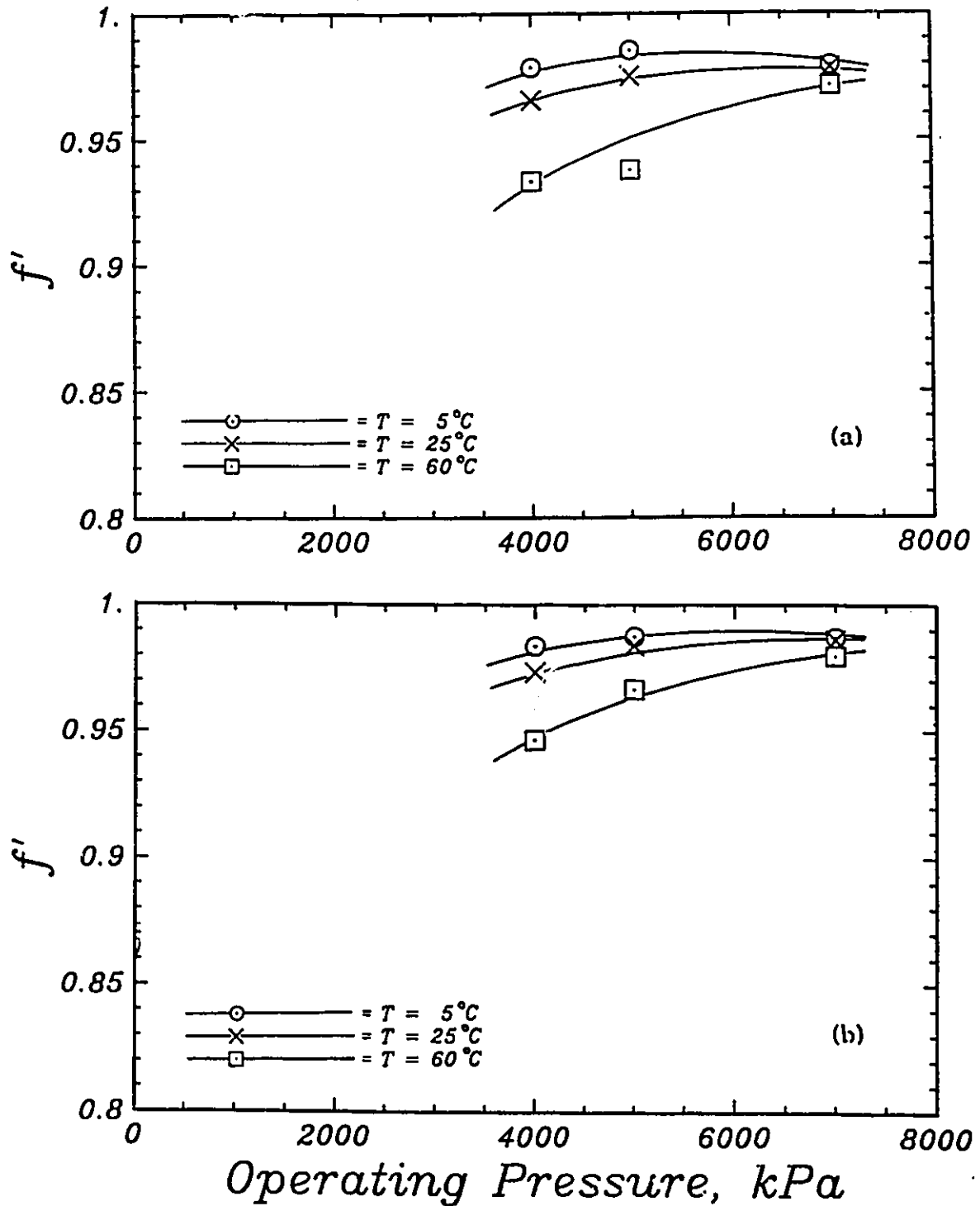
Figure 5.31:   Theoretical separation versus operating pressure, with
temperature as a parameter: (a) BW30-1, and (b) BW30-2
membranes. The lines represent the experimental trends.

5.29, is stronger for the BW30 membranes than for the SW30 membranes; this trend was also observed in Phase I (see Section 5.1.1.5).

At a fixed temperature, in general, as the pressure is increased the separation increases, in Figures 5.28 and 5.29; this trend can be better seen in Figures 5.30 and 5.31 where the separation is plotted versus pressure, with temperature as a parameter. The results are presented only for 5, 25, and 60°C temperatures. The reason for the increase in separation with an increase in pressure has been explained in Section 5.1.1.5. The separation increases with pressure to a constant value at the highest pressure of 7000 kPa. However, as can be seen in Figures 5.28 and 5.29, for some of the membranes (i.e., the SW30- 1 and BW30-1) at some temperatures (5 and 25°C for the SW30-1 and 5°C for the BW30-1), the separation decreases with pressure at pressures higher than 5000 kPa. This phenomenon might be either due to some experimental error or could be the result of larger concentration polarization in these systems at the highest pressure of 7000 kPa; that is, as pressure is increased beyond 5000 kPa the boundary-layer feed concentration, C_{A2}, is increased such that osmotic pressure becomes the dominant factor leading to an increased solute driving force. However, since this phenomenon did not happen for the SW30-2 and BW30-2 membranes (see Figures 5.30 and 5.31) the phenomenon might be due to experimental error.

5.1.3.6   Effects of pressure and temperature on solution flux

The solution flux for each membrane varies with the system pressure and temperature according to Figures 5.32 and 5.33. Only the temperatures of 5, 25, and 60°C are shown. For all the FT30 membranes, the total permeation flux changes linearly with pressure, and the straight lines shown are the best-fit straight lines
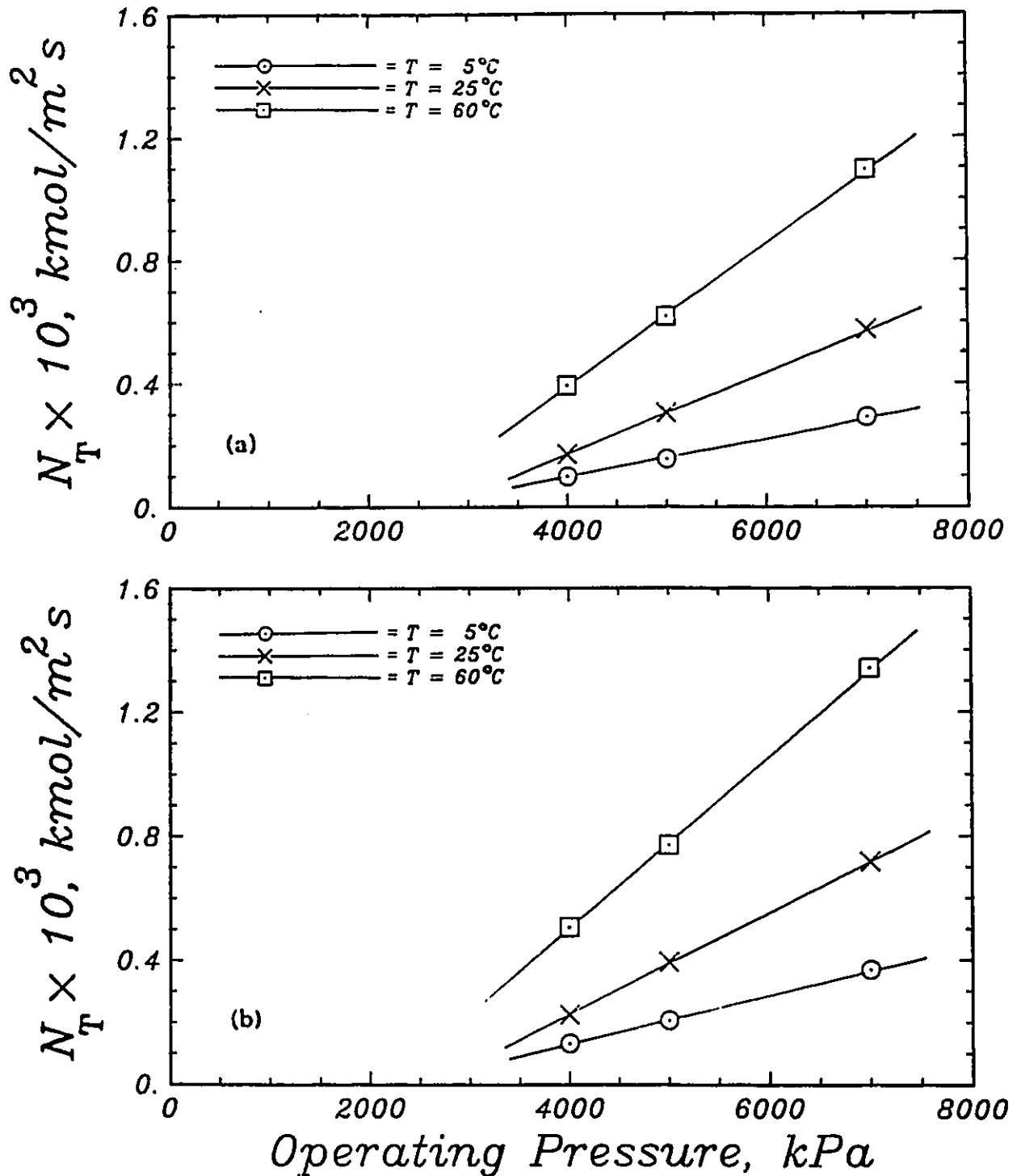
Figure 5.32:   Solution flux as a function of operating pressure and temperature
as a parameter: (a) SW30-1, and (b) SW30-2 membranes. The
straight lines represent the experimental trends.
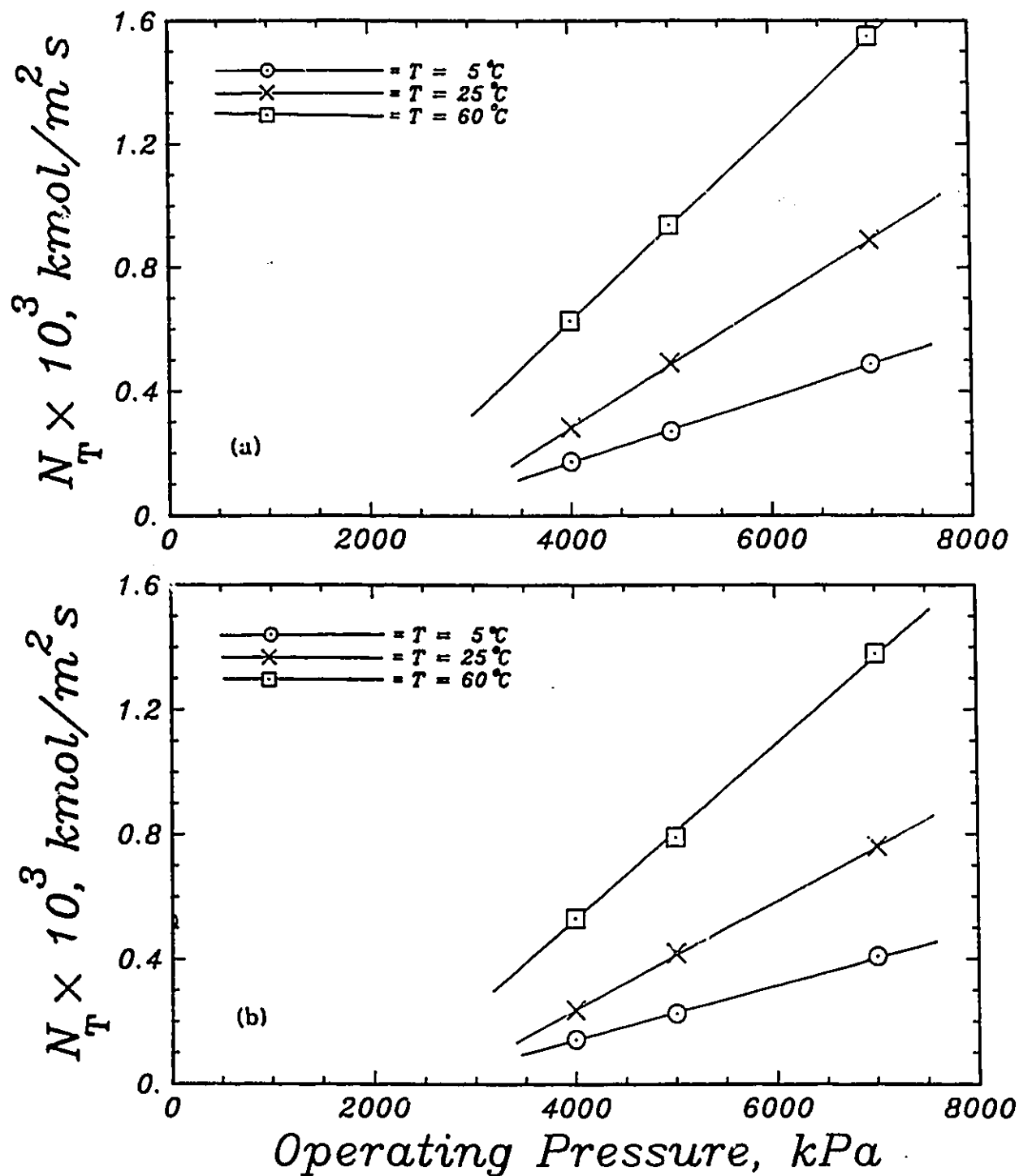
Figure 5.33:   Solution flux as a function of operating pressure and temperature
as a parameter: (a) BW30-1, and (b) BW30-2 membranes. The
straight lines represent the experimental trends.

through the data points. The results for the sea water concentration level (Phase III) shown in Figures 5.32 and 5.33 are similar to those for the brackish water concentration experiments (Phase I) shown in Figures 5.14 and 5.15; the differences between Figures 5.32, 5.33, 5.14, and 5.15 are: i) the data in Figures 5.32 and 5.33 fall into a narrower range of flux values due to the high osmotic pressures for the sea water, and ii) the deviations from linearity in Figures 5.32 and 5.33 are less than those in Figures 5.14 and 5.15.

According to Figures 5.32 and 5.33, temperature can remarkably increase the solution flux.

5.2 Solution of the Model Equations

The procedure to solve for each model, which has been developed during the present research, is discussed in this section. The discussion is followed by parameter estimation and optimization procedures. Finally, the results of using the orthogonal collocation numerical technique are presented.

5.2.1 Solution to the MD-SF-PF and SF-PF models

In order to use the MD-SF-PF model, outlined in Section 3.2.4, a scheme is required to solve the model equations. The appropriate equations that need to be solved, for the MD-SF-PF model, are Eqns.(3.24), (3.35), (3.40), (3.44), and (2.31). The unknown parameters in the model are: θ_1, R_W, and τ/ε, provided that Eqn.(3.44) is employed as the equation of potential function with $\theta_2 = 1/2$. It should be recalled, from Section 3.1.6, that the value of θ_2, in Eqn.(3.44), can be set at 1/2, at least for the FT30 aromatic polyamide membranes. For simulation purposes the three parameters (i.e., R_W, θ_1, and τ/ε) are assumed to be known. In general, however, the unknown

parameters can be determined by fitting experimental data to the model using a nonlinear parameter estimation routine, as discussed later, in this section.

The following procedure is recommended to solve the MD-SF-PF model:

i.   Make an initial guess for the permeate concentration, C_{A3}.

ii.   Solve Eqn.(3.24), with the boundary conditions Eqns.(2.34) and (2.35) for the velocity profile, $\alpha(\rho)$.

iii.   Calculate C_{A3} from Eqn.(3.35).

iv.   If C_{A3} from steps i and iii agree (within a tolerance) the model has converged. If not, then, repeat steps i to iv. The C_{A3} calculated in step iii is a good next guess.

v.   Use Eqns.(2.6) and (3.40) to calculate the separation and flux, respectively, for the membrane.

In order to solve the SF-PF model the following procedure has been adopted:

i.   Solve Eqn.(2.33), using Eqns.(2.34), (2.35), (2.40), and (2.45) or (2.46) to obtain $\alpha(\rho)$.

ii.   Obtain $C_{A3}(\rho)$ using Eqn.(2.40).

iii.   Calculate C_{A3} using Eqn.(2.42).

iv.   Calculate the separation using Eqn.(2.6).

Computer programs have been developed to solve the MD-SF-PF and the SF-PF models. "Orthogonal collocation" method of weighted residuals, discussed in Sections 2.6 and 3.6, is used to solve the differential equation for the velocity profile (Eqn.(3.24) for the MD-SF-PF model, and Eqn.(2.33) for the SF-PF model). Shifted Legendre polynomials are used as the orthogonal polynomials and the Lagrange interpolation polynomial for the case of interpolations. The boundary conditions were imposed explicitly (mixed collocation).

Overall the above solution algorithm has been found to be fast, efficient, and accurate.

5.2.2   Solution to the Extended MD-SF-PF model

The procedure is similar to that for the MD-SF-PF model, discussed in Section 5.2.1. Only, in this case, the equations to be solved are: Eqns.(3.75), (3.80), (3.82) for non-electrolytes or (3.44) for electrolytes, (3.79), and (3.83), with the help of Eqns.(2.34), (2.35), (3.70), and (3.71).

5.2.3   Solution to the MD-FPM and FPM relationships

In order to use the MD-FPM model, as outlined in Section 3.4, the equations describing the fluid permeation flux and separation are coupled and, therefore, a trial and error technique is required to find the solution. The appropriate equations that need to be solved for the MD-FPM-3 relationship are Eqns.(3.131), and (3.133) to (3.136); Eqn.(3.132) can be used instead of Eqn.(3.131) if Eqn.(3.110) holds. The Faxen equation, Eqn.(2.31), is used to predict the friction factor in the case of solute exclusion from the membrane.

That partition coefficient, K, and friction function, b, are functions of membrane pore size (e.g., Mehdizadeh and Dickson, 1989a) is well known. The partition coefficient decreases with increasing pore size as the less of the pore space is excluded from the solute and the potential function between the solute and the pore wall decreases with increasing distance. Therefore, some relationship between K and R_W is needed. On the other hand, the relationship between radial partition coefficient, $K(\rho)$, and membrane surface potential, $\phi(\rho)$, can be related by the Boltzmann theorem, Eqn.(3.10), so that the radially-averaged K values are given by Eqns.(3.59) and (3.60);

for the MD-FPM-3 relationship, K_2 and K_3 are equal. Therefore, to solve for exact solution in the MD-FPM relationships, a relationship is needed for the potential function; the equation proposed in the MD-SF-PF model, Eqn.(3.44), may be used for this purpose. The relationship between b and pore size can be approximated by the Faxen equation.

To solve the MD-FPM-3 relationship, knowing the parameters of the model (R_W, τ/ε, and K or θ_1), the following procedure is recommended:

i) Make an initial guess for C_{A3}.

ii) Solve Eqn.(3.131) to find α. An iterative technique is required to solve this equation. If Eqn.(3.110) holds, Eqn.(3.132) can be used, instead, explicitly.

iii) Solve Eqn.(3.136) to find the separation, f'. If the C_{A3} value obtained from this f' value is about the guessed C_{A3} proceed to the next step; otherwise, make another guess for C_{A3} and go back to step (ii).

iv) Solve Eqn.(3.133), using Eqn.(3.134), to find the total permeation flux, N_T.

In the above procedure, the Faxen equation, Eqn.(2.31), has been assumed to predict the b factor. If the parameter θ_1 is used, rather than the K factor, then Eqns.(3.44) and (3.10) are used to determine the K factor, by integrating over the pore surface area, as in Eqn.(3.59).

A similar procedure can be used to solve the MD-FPM-4 relationship. In this case, the equations to be solved are Eqns.(3.109), (3.117), (3.120), and (3.122). Equation (3.111) can be used instead of Eqn.(3.109) if Eqn.(3.110) holds.

For the case of FPM relationships, Eqns.(3.104), (3.128) and (3.129) are used, and for the FPM-4 relationship, Eqns.(3.104) and (3.128) are used to solve the models.

5.2.4   Optimization and parameter estimation

In order to determine model parameters, a comparison of model calculations and experimental data are used as a basis to optimize an appropriate objective function. The optimization routine, used in the present research, is the nonlinear optimizer UWHAUS, which is an iterative technique based on Marquardt's method (Marquardt, 1963); this method combines the Gauss (Taylor series) method and the method of steepest descent.

The unknown parameters for each model are adjusted to minimize the sum of square errors between the model and the experimental f' values. That is, the objective function to be minimized has been selected to be:

$$F = \sum_i \left(f'_{model} - f'_{exp'l} \right)^2_i \tag{5.2}$$

However, a better objective function to be minimized is:

$$G = W_f \sum_i \left(f'_{model} - f'_{exp'l} \right)^2_i + W_N \sum_i \left(N_{T,model} - N_{T,exp'l} \right)^2_i \tag{5.3}$$

where W_f and W_N are weighting factors, for the variances of f' and N_T, respectively. There are two difficulties associated with using Eqn.(5.3). Firstly, information on the variance in f' and N_T is needed. Secondly, another adjustable parameter, τ/ε, is needed (to determine the flux, N_T) that must be estimated simultaneously with the other parameters. In the present research, Eqn.(5.2) has been minimized, to avoid the above two problems. As is shown in the next sections, even though the error function is minimized in separation only, the model does an excellent job of predicting the flux as well; in this way, the value of τ/ε is determined from pure solvent (water) experiments, and, therefore, the parameters for each model are: R_W, θ_1, and θ_2 for MD-SF-PF model (θ_2 is found to be 1/2, later in this section); and R_W, and A for SF-PF model.

To estimate the parameters, the experimental data of Phase I (Section 4.1) at 2000 ppm concentration, 25°C temperature, and different pressures (350-7000 kPa) have been employed to fit each model. The results are shown in Figure 5.34. Initially, the data were fit for each membrane separately and the values of the potential parameters for each group of membranes (i.e., SW30 or BW30) were close (within 1%) to each other, for each model. A constant value for the potential parameters for the SW30 (or for the BW30) membranes is reasonable since the membrane samples are identical in chemical nature. Therefore, it was hypothesized that the only difference between the SW30-1 and SW30-2 membranes (and between the BW30-1 and BW30-2 membranes) was the pore size. Therefore, the data were pooled for the two SW30 membranes and the model parameters were $R_{w,1}$, $R_{w,2}$, θ_1, and θ_2 for MD-SF-PF model and $R_{w,1}$, $R_{w,2}$, and A for SF-PF model, where subscripts 1 and 2 refer to the SW30-1 and SW30-2 (and the BW30-1 and BW30-2) membranes, respectively.

The results of the parameter estimation for the MD-SF-PF and the SF-PF models are shown in Tables 5.3 and 5.4, respectively. The 95% confidence interval for each estimated parameter has also been presented. At this concentration (2000 ppm NaCl in water), the effect of pressure on theoretical separation f′, is well represented by both models as illustrated in Figure 5.34.

The parameters, determined within the narrow ranges of the confidence intervals, indicate that the SW30 membranes have a smaller pore size than the BW30 membranes and the potential parameter(s) for the BW30 membranes are a little higher (about 15%) than those for the SW30 membranes. The estimated values for the average pore radius, R_w, are about 1.0 and 1.2 nm for the SW30 and BW30 membranes, respectively. The estimated values for the potential parameter, θ_1, are about 5.4 and 6.2 nm for the SW30 and BW30 membrane, respectively. Considering
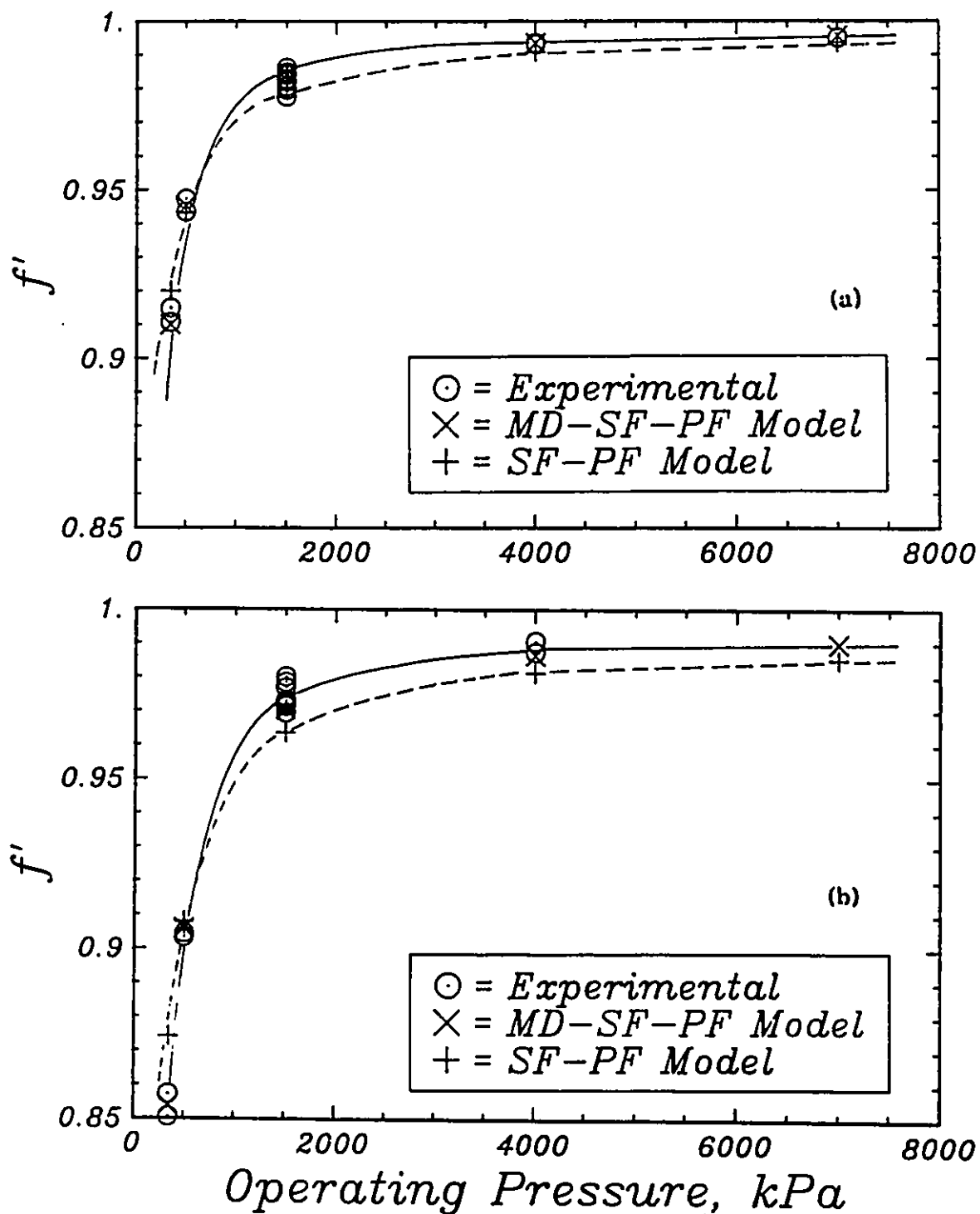
Figure 5.34: Experimental results and predictions by the MD-SF-PF and the SF-PF models at 2000 ppm feed concentration of NaCℓ in water and 25°C: (a) SW30-1, and (b) BW30-1 membranes.

Table 5.3

Estimated parameters and statistics for all the membranes using MD-SF-PF model*

	SW30 Membranes	BW30 Membranes
$R_{w,1} \times 10^{10}$, m	$8.97 < 9.39 < 9.82$	$12.88 < 13.07 < 13.26$
$R_{w,2} \times 10^{10}$, m	$10.14 < 10.38 < 10.63$	$11.27 < 11.89 < 12.50$
$\theta_1 \times 10^{10}$, m	$52.45 < 53.73 < 55.01$	$60.33 < 61.57 < 62.81$
θ_2	$0.4873 < 0.4901 < 0.4929$	$0.4889 < 0.4921 < 0.4953$
SSQ	0.004849	0.003732
Var (Res.)	0.0001426	0.0001096
dof	34	34

* 95% confidence intervals are shown.

Table 5.4

Estimated parameters and statistics for all the membranes using SF-PF model*

	SW30 Membranes	BW30 Membranes
$R_{w,1} \times 10^{10}$, m	$9.06 < 9.46 < 9.87$	$13.19 < 13.21 < 13.23$
$R_{w,2} \times 10^{10}$,m	$11.23 < 11.83 < 12.43$	$11.62 < 11.63 < 11.64$
$A \times 10^{10}$,m	$26.99 < 28.73 < 30.47$	$30.50 < 30.55 < 30.60$
SSQ	0.004274	0.004697
Var (Res.)	0.0001221	0.0001342
dof	35	35

* 95% confidence intervals are shown.

the value of the potential function at the pore centerline, θ_1/R_W (see Eqn.(3.44)), the values are about 5.4 (i.e., 5.4/1.0 = 5.4) for the SW30 membranes and about 5.1 (i.e., 6.2/1.2 = 5.1) for the BW30 membranes, which implies a stronger potential field (about 6%) for the SW30 membranes as compared with the BW30 membranes. These results are consistent with the reality that the SW30 membranes are the high-rejection membranes. The variance of residual values for the MD-SF-PF model are higher (about 20%) than those for the SF-PF model because the number of degrees of freedom for the MD-SF-PF model is one degree smaller than that for the SF-PF model (since the MD-SF-PF model has one parameter more than the SF-PF model). According to the estimated parameters by the MD-SF-PF model, in Table 5.3, all of the SW30 membranes have smaller pore size than the BW30 membranes which makes sense. However, according to the SF-PF model, Table 5.4 indicates that the BW30-2 membrane has a smaller pore size than the SW30-2 membrane, which is not expected in reality.

Examining the data in Table 5.3 suggests that the θ_2 parameter, for all the membranes, can be reasonably approximated by the value 1/2. Deviations from 1/2 has negligible errors in the value of the potential. Therefore, the MD-SF-PF model can be regarded as a three-parameter model: R_W, θ_1, and τ/ε.

5.2.5 Results from orthogonal collocation

The principles of orthogonal collocation, discussed in Section 2.6, have been applied to the MD- SF-PF model in Section 3.5, and the differential equation of velocity profile in MD-SF-PF model, given by Eqn.(3.24), was converted to a set of ordinary differential equations (ODE) in Eqn.(3.141).

In order to solve the set of ODE's in Eqn.(3.141), one has to use a numerical technique to integrate these equations with respect to time. The numerical integration package, LSODE (Hindmarsh, 1983), has been used for this integration.

The main objective is to compute the $A_{i,j}$ and $B_{i,j}$ coefficients, defined in Eqns.(2.73) and (2.74), so that the coefficients in Eqns.(3.143) to (3.145) could be computed. For a chosen number of interior collocation points, N, the zeros of $P_N^{(0,0)}(\rho)$ and the matrices $A=\{A_{i,j}\}$ and $B=\{B_{i,j}\}$ are found by the subroutines JCOBI and DFOPR in **Appendix F** (from: Villadsen and Michelsen, 1978), respectively. The velocity function value at the pore centerline, a_1, (i.e., at $\rho=0$) is determined from Eqn.(3.140) and the velocity at the wall, a_{N+2}, (i.e., at $\rho=1$) is zero due to the non-slip boundary condition. The velocity function values at desired intermediate points (e.g., at $\rho = 0.1, 0.2, ..., 0.9$) are calculated using the Lagrange interpolation polynomial, Eqn.(2.70), by subroutine INTRP in **Appendix F** (from: Villadsen and Michelsen, 1978).

Before looking at the results of the numerical calculations, consider the form of Eqn.(3.24) and the two special case solutions, Eqns.(3.28) and (3.29). Since these analytical solutions are much easier to use, compared to the CPU time required to solve Eqn.(3.24), it is tempting to use these approximate solutions. For example, this simpler approach is suggested in the literature for the similar equation in the SF-PF model, Eqn.(2.33), (Bhattacharyya et al., 1986). In this section the validity of this approximation is examined.

First, the numerical technique developed above is tested for the special case of Poiseuille flow (i.e., $b=1$ and $\phi=0$). This test has been done for an aqueous sodium chloride feed solution and the following operating conditions: $\Delta P=7000$ kPa, $T=25°C$, $R_W=10\times10^{-10}$ m, and $C_{A2}=0.048$ kmol/m^3. For sodium chloride aqueous solution:

$D_{AB} = 1.566 \times 10^{-9}$ m²/s, $\eta = 0.8965 \times 10^{-6}$ kPa s, and $R_A = 1.55 \times 10^{-10}$ m. The results are shown in Figure 5.35.a and 5.35.b for the case of 3 and 5 interior collocation points (i.e., $N = 3$ and 5), respectively. As illustrated in Figure 5.35.a, the numerical solution passes through the exact solution (Poiseuille equation, given by Eqn.(3.28)), for this small number of collocation points. The CPU time for this computation is 0.28 s on VAX 8600. The same computation using $N = 5$ shows the same accuracy but has a larger CPU time of 0.49 s on the VAX.

Next, the velocity profiles for real reverse osmosis conditions have been determined. Figure 5.36 illustrates the actual velocity profile (solid curve) and the special case of complete solute rejection, Eqn.(3.29), under the operating conditions of: $\Delta P = 7000$ kPa, $C_{A2} = 35\,000$ ppm NaCℓ in water, $T = 25°C$, $R_W = 10 \times 10^{-10}$ m, $\theta_1 = 53.73 \times 10^{-10}$ m, and $\theta_2 = 0.4901$, using $N = 2$. The real solution is close to the special case of Eqn.(3.29), which means that almost all of the solute molecules are rejected from the membrane. Increasing the number of collocation points from 2, to 5, and to 8, did not appreciably affect the accuracy of the solution, but of course the CPU time (on VAX 8600) increased from 1.11, to 2.76, and to 5.43 s, respectively. Therefore, it is a wise choice, for similar cases, to use the minimum number of the collocation points (e.g., $N = 2$) or to use the analytical solution of Eqn.(3.29). Figure 5.36 implies that the average value of α, under the above conditions is about 0.3, which means that the fluid is transported by both diffusion and convection.

Now, if the applied pressure is reduced to 1500 kPa and for $C_{A2} = 15\,000$ ppm NaCℓ in water, the velocity profile is shown, for $N = 3$, in Figure 5.37 (solid curve) together with the profile (dashed curve) expected from Eqn.(3.29). The CPU time is 1.49 s on the VAX. These are real experimental conditions (Mehdizadeh and Dickson, 1989f) for a membrane that has about 93% NaCℓ-water separation. In
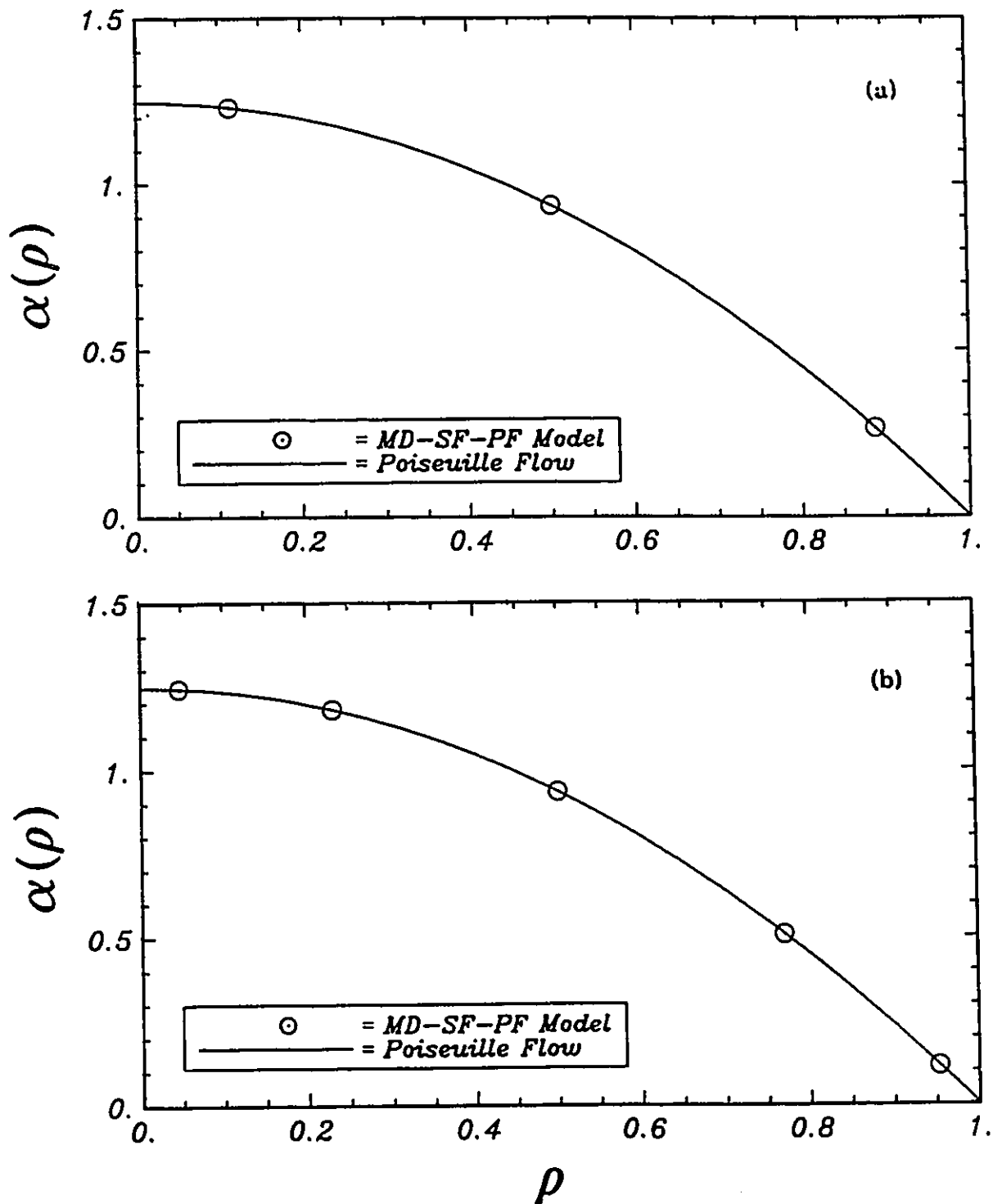
Figure 5.35:   Velocity profile inside a pore by MD-SF-PF model when $\Phi = 0$ and $b = 1$ as compared with Poiseuille flow velocity profile; conditions are $\Delta P = 7000$ kPa and $R_W = 10 \times 10^{-10}$ m: (a) $N = 3$, and (b) $N = 5$.
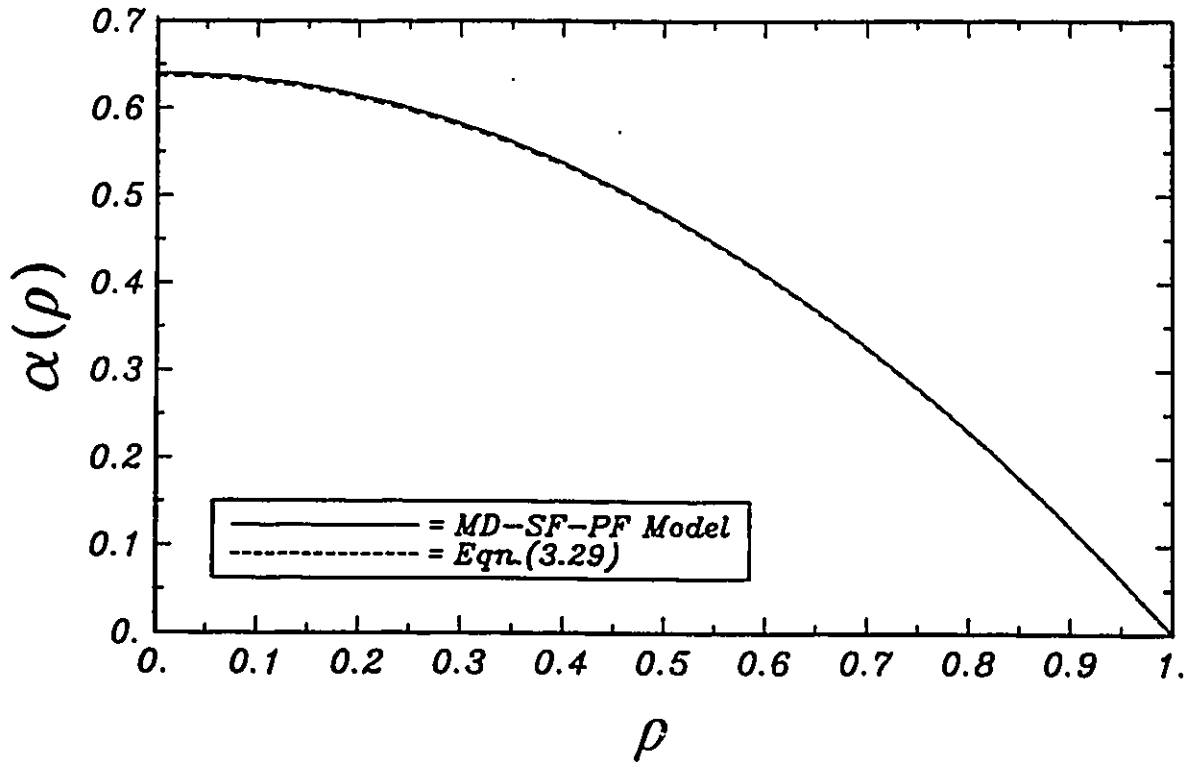
Figure 5.36:   Velocity profile inside a pore by MD-SF-PF model as compared with Eqn.(3.29), when $N=2$. The conditions are: $\Delta P = 7000$ kPa, $C_{A2} = 35\ 000$ ppm, $T = 25°C$, $\theta_1 = 53.73 \times 10^{-10}$ m, and $R_W = 9.39 \times 10^{-10}$ m.
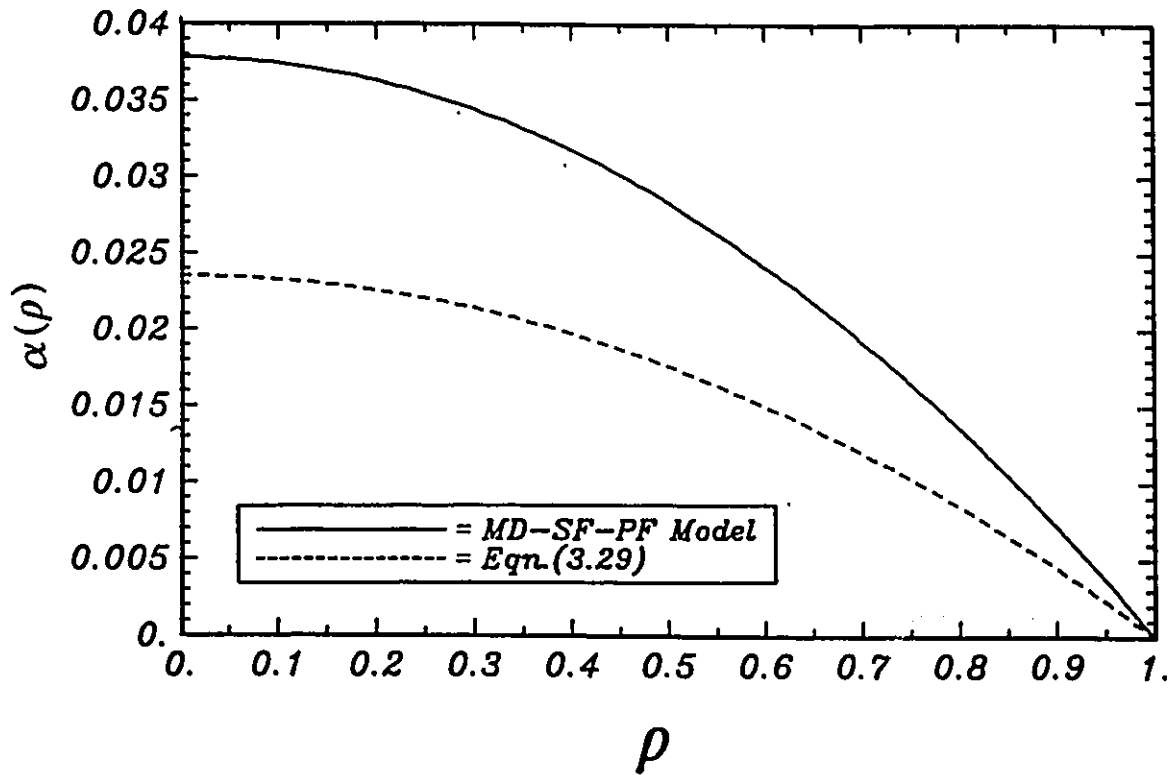
Figure 5.37:   Velocity profile inside a pore by MD-SF-PF model as compared with Eqn.(3.29), when $N=3$. The conditions are: $\Delta P = 1500$ kPa, $C_{A2} = 15\ 000$ ppm, $T = 25°C$, $\theta_1 = 53.73 \times 10^{-10}$ m, and $R_W = 9.39 \times 10^{-10}$ m.

this case, using the approximation of Eqn.(3.29) would result in a large error in the velocity profile. This deviation is the result of the importance of the third and fourth terms in the solution of Eqn.(3.24).

Since $\alpha(\rho)$ may be considered as the pore radial Peclet number, representing the ratio of convective to diffusive fluxes, values of α near 1.0 indicate that convection and diffusion are of equal importance. Therefore, under the above conditions, in Figure 5.37, the fluid is mainly transported by diffusion through the membrane since the average α value is about 0.02. Comparing Figure 5.36 to Figure 5.37, the convection and diffusion are about the same order of magnitude near the pore centerline in Figure 5.36. When the pressure is reduced, as in Figure 5.37, the convection is small compared to the diffusion term. Therefore the difference between the numerical solution and the algebraic approximation is more significant when the transport is controlled by diffusion.

The CPU times for both of the examples, above, are quite small (around one second). Therefore, this numerical routine is efficient and can be linked with a numerical optimization routine and parameter estimations can be obtained in realistically short times (Mehdizadeh and Dickson, 1989f); around one minute of CPU is typical. Note, that with the Runge-Kutta method, previous workers often let their computers run overnight to do one parameter estimation run (e.g., Dickson, 1985).

5.3 Simulations and Predictions for the MD-SF-PF and SF-PF Models

Simulation results are presented for the MD-SF-PF and SF-PF models. Next, true predictions by the MD-SF-PF model under the experimental conditions of Phases I, II, and III (see Sections 4.1, 4.2, and 4.3 for the experimental conditions) are

presented. Some predictions by the SF-PF model are also presented and compared with those by the MD-SF-PF model.

5.3.1   Simulation results

In order to see how the MD-SF-PF model behaves under different conditions, simulation studies have been done, and compared to those for the SF-PF model, where possible. The studies have been done in the forms of the effects of operating pressure and feed concentration on membrane separation and flux. Concentration profiles are also shown for inside the pores.

5.3.1.1   Separation and flux ratio vs. pressure and feed concentration

The MD-SF-PF model (developed in Section 3.1) has been evaluated under a variety of simulation conditions (Mehdizadeh and Dickson, 1989b). The following values or ranges of values for the model parameters were chosen to illustrate the predictive behaviour of this model at 25°C: $\theta_1 = 54.434 \times 10^{-10}$ m, $\theta_2 = 0.491$, and $R_W = 8 \times 10^{-10}$ to 20×10^{-10} m. In order to calculate the flux ratio, N_T/N_P, it is not necessary to specify the τ/ε parameter; this parameter is only required to calculate the absolute fluxes, N_T and N_P.

Using the method of solution outlined in Section 5.2.1, the membrane performance has been simulated in terms of separation, f', and the flux ratio, N_T/N_P. These results are presented in Figures 5.38 and 5.39. Figure 5.38.a illustrates the effect of pressure on separation. As pressure is increased the separation increases; this phenomenon happens because increasing the pressure increases the water flux (see Eqn.(2.25)) but has almost no effect on the solute flux (see Eqn.(2.26)) so that the relative permeation of solvent increases. The separation is lowest for the largest pores
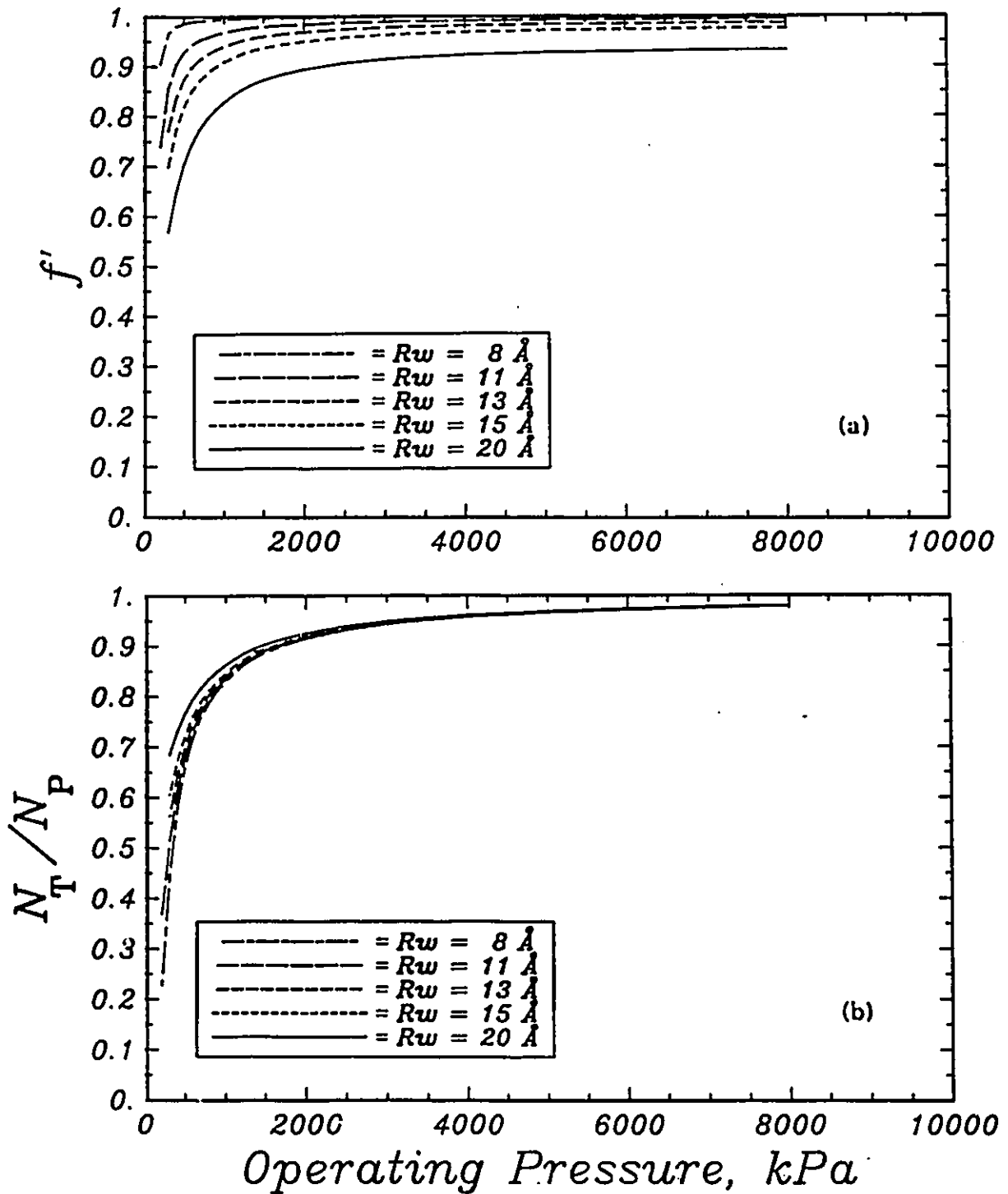
Figure 5.38:   The effect of operating pressure on: (a) separation; and (b) flux
ratio; with pore size as a parameter, in the MD-SF-PF model.
Conditions are: $\theta_1 = 54.43 \times 10^{-10}$ m, $\theta_2 = 0.491$, T = 25°C, and
$C_{A2} = 0.0344$ kmol/m³.
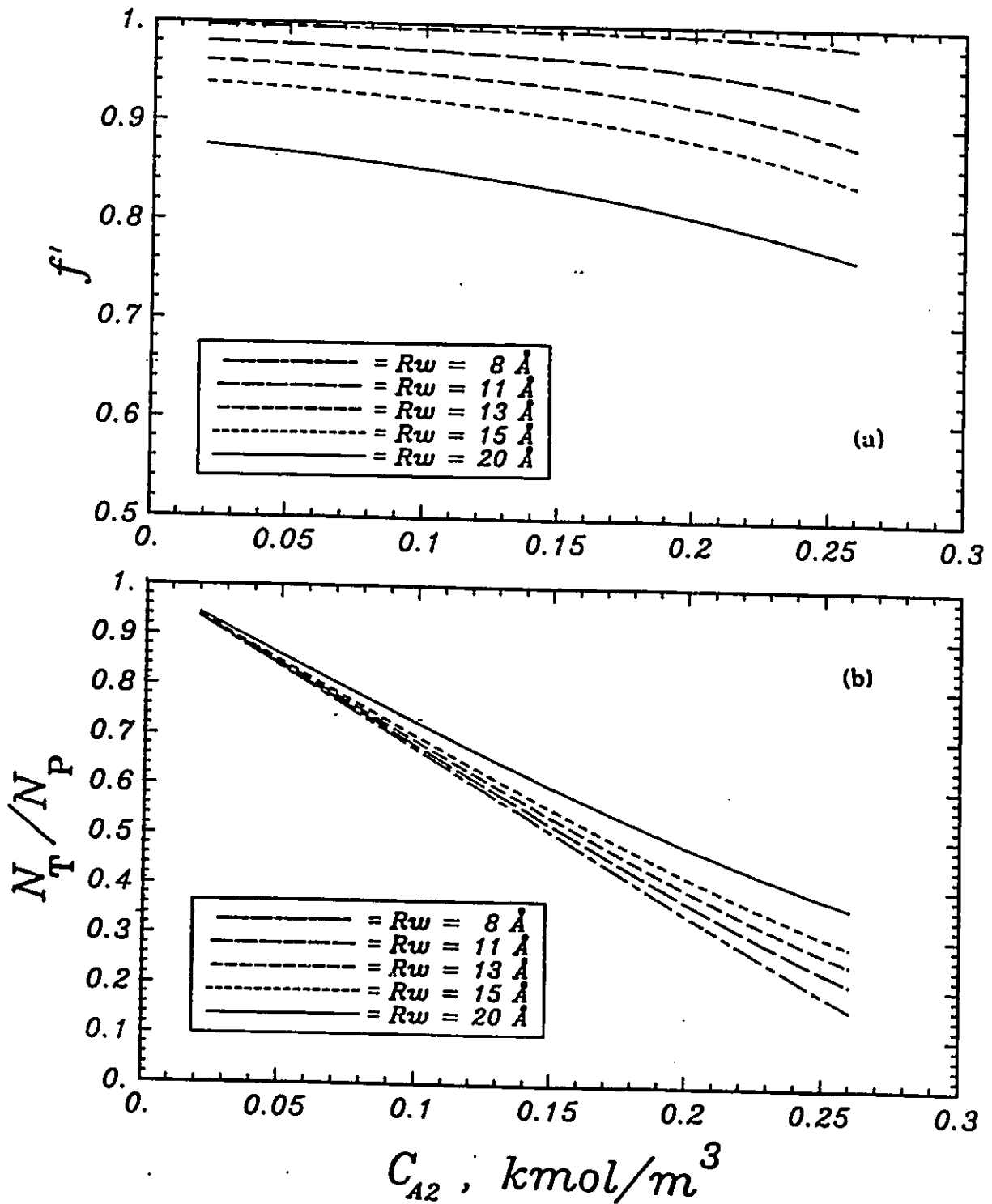
Figure 5.39: The effect of feed concentration on: (a) separation; and (b) flux ratio; with pore size as a parameter, in the MD-SF-PF model. Conditions are: $\theta_1 = 54.43 \times 10^{-10}$ m, $\theta_2 = 0.491$, T = 25°C, and $\Delta P = 1500$ kPa.

and highest for the smallest pores. Figure 5.38.b illustrates the effect of pressure on the flux ratio, N_T/N_P; as pressure is increased the flux ratio increases. The flux ratio is almost independent of the pore size in the range investigated, with the smallest pores having the largest flux ratio.

Figures 5.39.a and 5.39.b illustrate the effect of feed concentration on the separation and flux ratio, respectively. The separation and flux ratio both decrease with increasing concentration due to the osmotic pressure effect. The effect of concentration on separation is more dramatic for the lower separation membranes than for the higher separation membranes. The flux ratio increases with increasing pore size.

All of the results illustrated in Figures 5.38 and 5.39 and discussed above are quite consistent with the results observed experimentally for reverse osmosis membranes (Sourirajan, 1970). Therefore the model, in the MD-SF-PF form, looks promising for describing reverse osmosis membrane behaviour. The results of fitting experimental data to the model and using the model to predict results are presented in subsequent sections.

5.3.1.2 Concentration profiles

The concentration profile in the pore is given by Eqn.(3.20) for the MD-SF-PF model and by Eqn.(3.23) for the SF-PF model. Figure 5.40.a illustrates the concentration profile, in the MD-SF-PF model, for the conditions: $\theta_1 = 5.0 \times 10^{-10}$ m, $\theta_2 = 2.0$, $R_W = 7.0 \times 10^{-10}$ m, $\Delta P = 7000$ kPa, $C_{A2} = 1.0$ kmol/m^3, and T = 25°C. The curves in Figure 5.40.a indicate that, at any given radial position, the concentration decreases in a uniform manner from the inlet to the outlet condition. The concentration drops to zero for $\rho > 0.778$, because of the finite radius of the solute molecule; which is assumed to be 1.55×10^{-10} m for sodium chloride in water at 25°C.
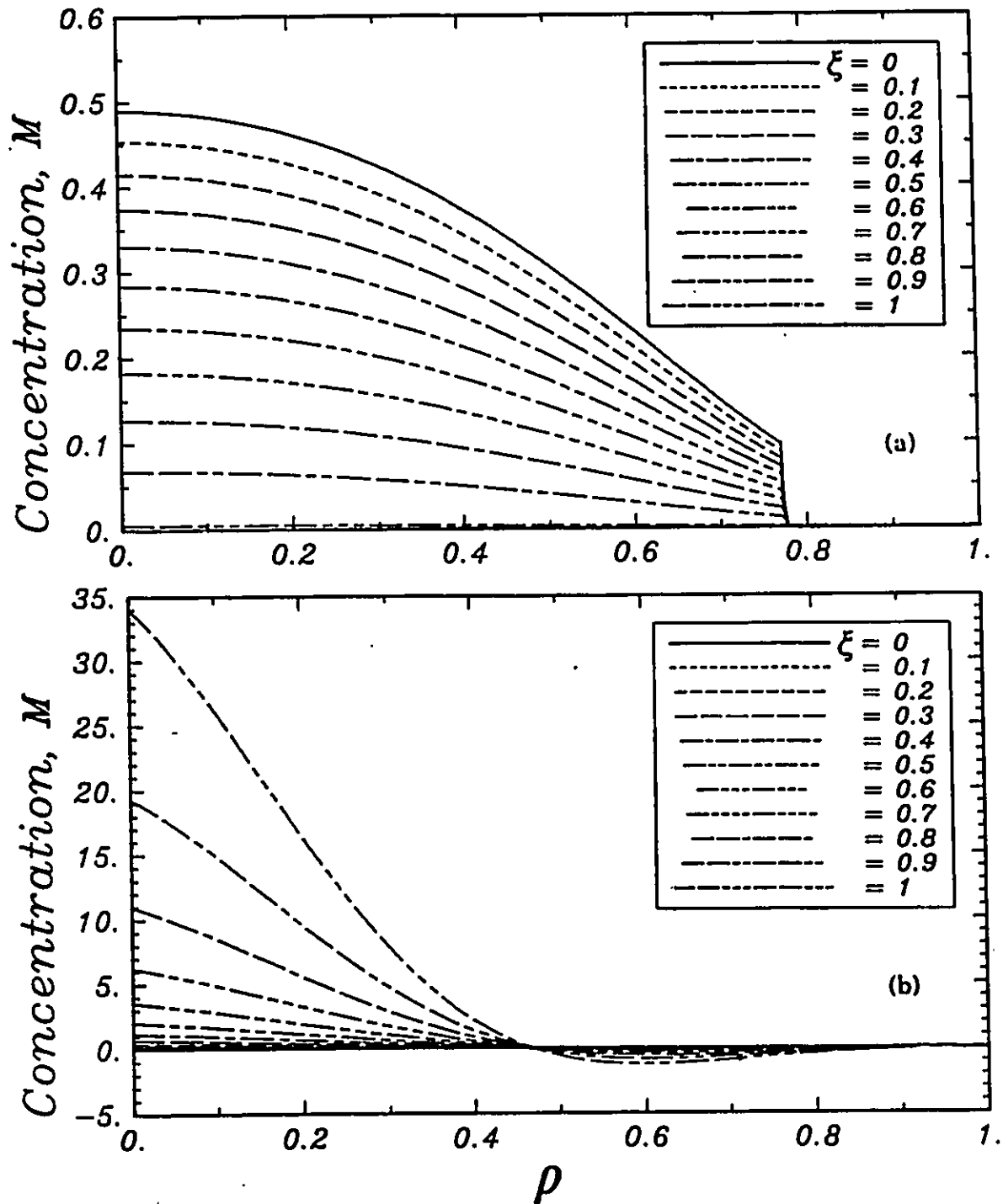
Figure 5.40: Simulation of concentration profile as a function of dimensionless radial, ρ, and axial, ξ, positions by: (a) MD-SF-PF model (conditions: $R_W = 7 \times 10^{-10}$ m, $\Delta P = 7000$ kPa, $C_{A2} = 1.0$ kmol/m^3, $\theta_1 = 5. \times 10^{-10}$ m, $\theta_2 = 2.0$, and $T = 25^\circ C$); (b) SF-PF model (conditions: $R_W = 18.2 \times 10^{-10}$ m, $\Delta P = 9646$ kPa, $C_{A2} = 0.576$ kmol/m^3, $A = 21 \times 10^{-10}$ m, and $T = 25^\circ C$).

The value for solute molecular radius has been estimated using Stokes-Einstein equation (Cussler, 1984):

$$R_A = \frac{k_0 T}{6 \pi \eta D_{AB}}$$ (5.4)

The solute is rejected from the pore wall so that the concentration is highest at the centre of the pore.

A concentration profile for the SF-PF model is presented in Figure 5.40.b. Because the form of the potential function is not the same, a direct comparison of the two models is not possible. Instead, the concentration profile is shown for an actual case presented in Matsuura and Sourirajan's paper (see Table I in: Matsuura and Sourirajan, 1981). The conditions are: $A = 21.0 \times 10^{-10}$ m, $R_W = 18.2 \times 10^{-10}$ m, $\Delta P = 9646$ kPa, $C_{A2} = 0.576$ kmol/m^3, and $C_{A3} = 0.0575$ kmol/m^3. Note, in Figure 5.40.b, that the concentration is actually calculated as negative for some of the positions within the pore. Obviously, this situation is impossible. This result is a reflection of the incorrect form of the material balance used in the derivation of the SF-PF model, as discussed in Section 3.1.3.

5.3.2   Predictions by the MD-SF-PF and SF-PF models

The parameters estimated for each model (see Tables 5.3 and 5.4 in Section 5.2.4), for each of the FT30 membranes, were used to predict each membrane performance as a function of concentration, for the SF-PF and MD-SF-PF models. The lines drawn in Figures 5.16 to 5.17 and in Figures 5.41 to 5.42 are the predictions by the MD-SF-PF and SF-PF models, respectively, which can be compared to the experimental data in Phase I at concentrations higher than 2000 ppm NaCℓ, as discussed below.
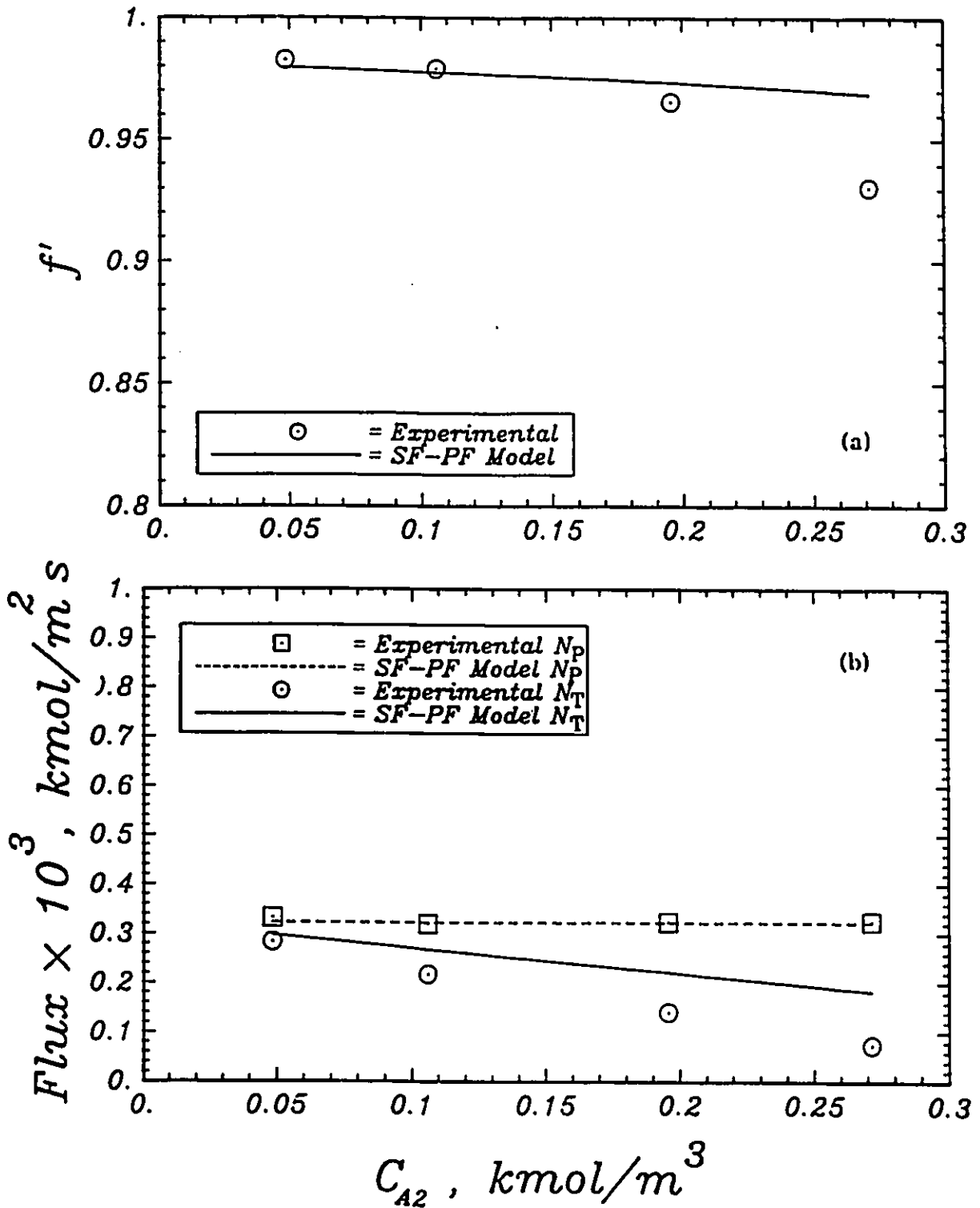
Figure 5.41: Separation and permeation fluxes versus feed concentration for the SW30-1 membrane: a comparison between the experimental data and the predictions of the SF-PF model.
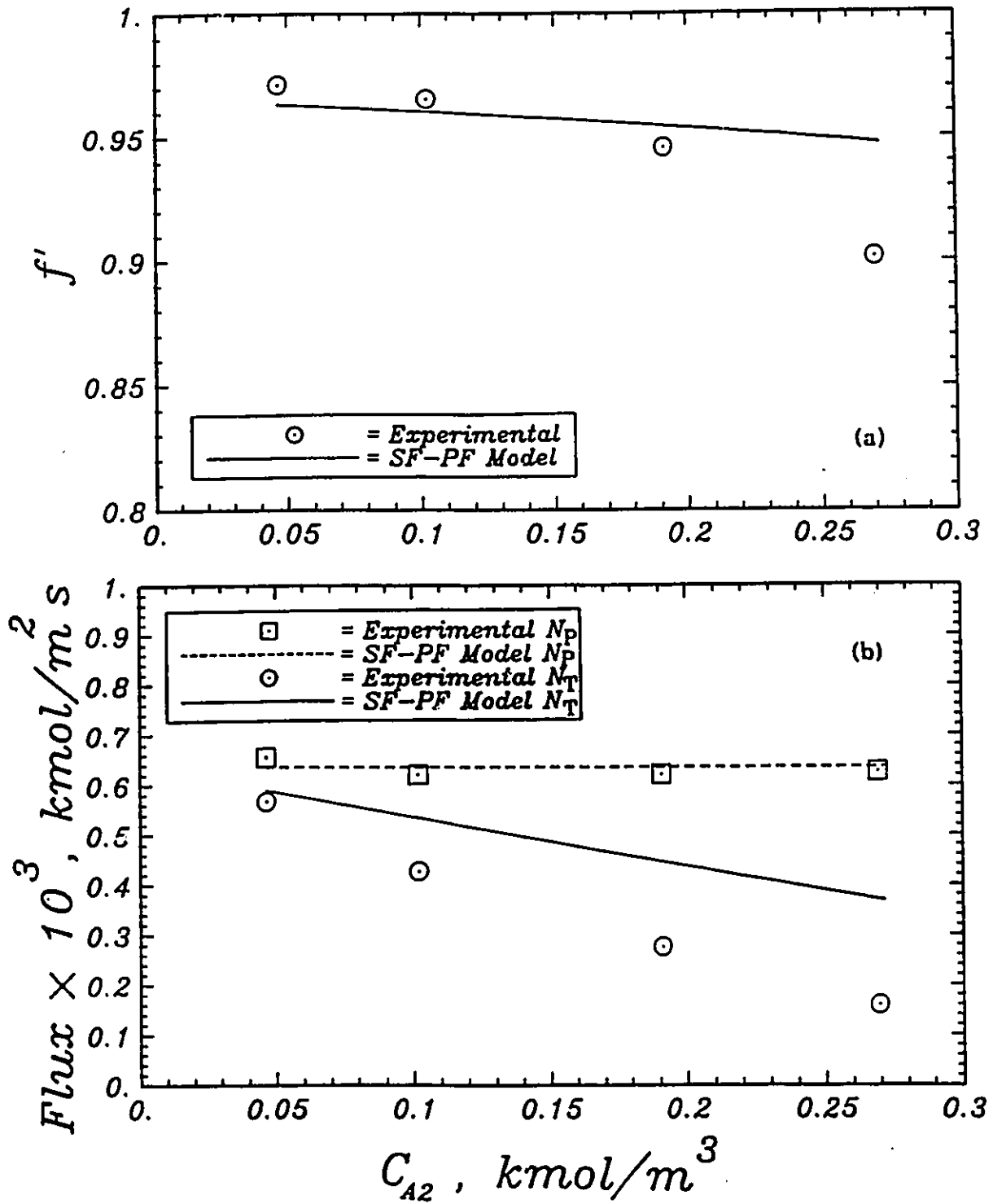
Figure 5.42:   Separation and permeation fluxes versus feed concentration for the
BW30-1 membrane: a comparison between the experimental data
and the predictions of the SF-PF model.

As mentioned in Section 5.3.1, an additional parameter (τ/ε) is needed to obtain the absolute values of the solution flux, N_T. An estimate of τ/ε has been determined by averaging the τ/ε values obtained from the pure water flux values, N_P, in Eqn.(3.88). The average values determined for each membrane by each model has been summarized in Table 5.5.

Figure 5.16 compares the experimental data (Phase I, higher concentrations) with the MD-SF-PF model predictions, for the SW30-1 membrane, in the form of theoretical separation, f', versus feed concentration. Note that the MD-SF-PF model has done a good job of predicting solution flux and separation <u>as functions of concentration</u> for this membrane. Figure 5.17 illustrates the prediction results by the MD-SF-PF model for the BW30-1 membrane.

Figures 5.41 and 5.42 present the prediction results by the SF-PF model (which parallels Figures 5.16 and 5.17 for MD-SF-PF model) for the SW30-1 and BW30-1 membranes, respectively. In Figures 5.41 and 5.42, the SF-PF model is not able to predict the experimental data for this system. As the feed concentration is increased the discrepancy between the SF-PF model and the real data becomes larger. The reasons causing this failure have been discussed in Section 3.1; most of the discrepancy is from neglecting the osmotic effects for the electrolyte. This explanation is confirmed by the following computer testing. If the osmotic effects are corrected in the SF-PF model, then the obtained model has the following estimated parameters: $R_W = 10.79 \times 10^{-10}$ m, and $A = 32.56 \times 10^{-10}$ m, for the SW30-1 membrane. The corrected model (SF-PF-OSM model), then, predicts the data as illustrated in Figure 5.43, which is a much better prediction than in Figure 5.41. Figure 5.43.a illustrates that the SF-PF model, when corrected for osmotic effects, is still under-predicting the separation. The remaining difference is due to other problems in the

Table 5.5

Values of τ/ε for all the membranes obtained for each of the MD-SF-PF
and SF-PF models

	SF-PF Model	MD-SF-PF Model
SW30-1	0.3213×10^{-4},m	0.3166×10^{-4},m
SW30-2	0.3656×10^{-4},m	0.2820×10^{-4},m
BW30-1	0.3176×10^{-4},m	0.3110×10^{-4},m
BW30-2	0.2777×10^{-4},m	0.2903×10^{-4},m
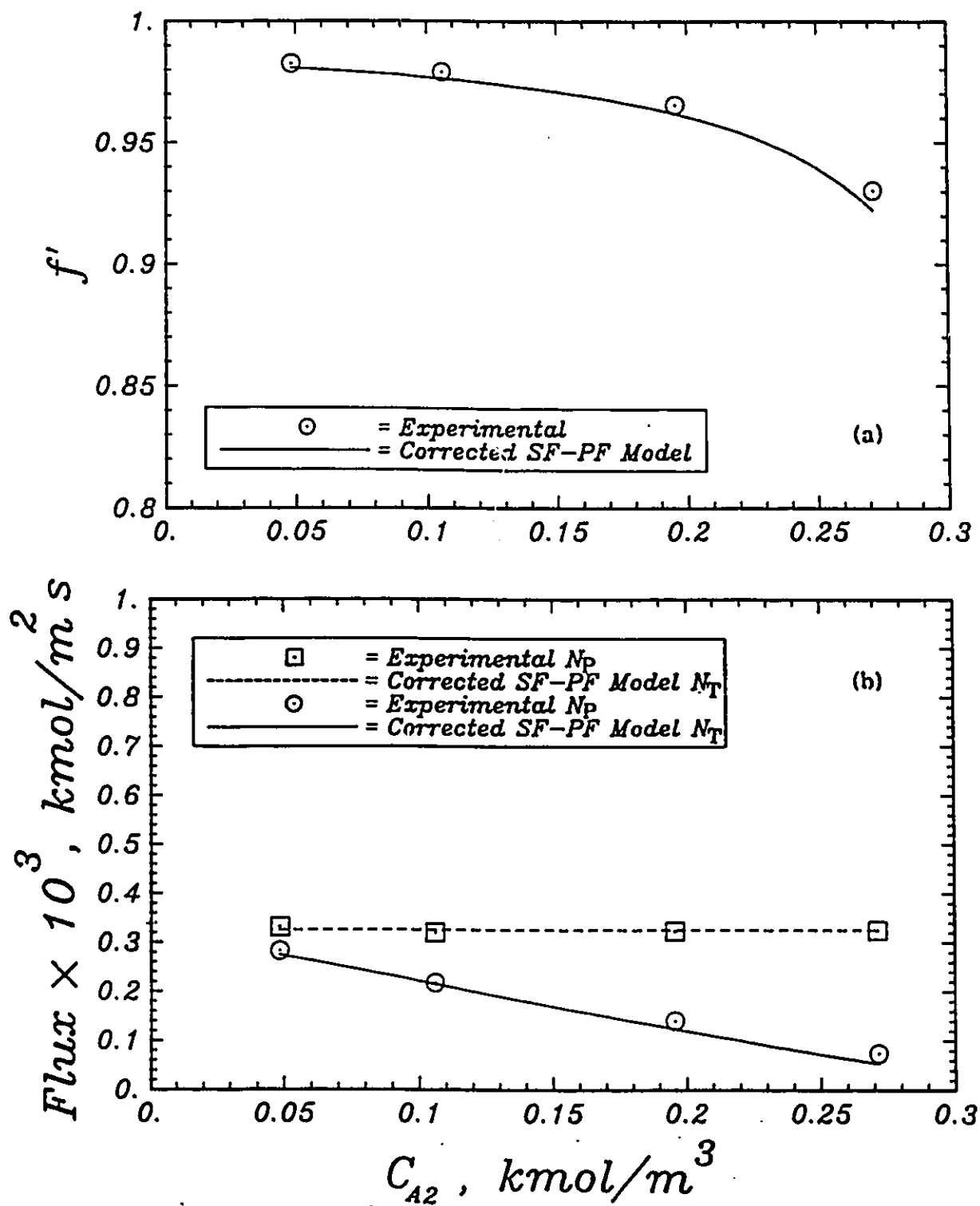
Figure 5.43: Separation and permeation fluxes versus feed concentration for the SW30-1 membrane: a comparison between the experimental data and the predictions of the SF-PF- OSM model.

SF-PF model, such as the incorrect form of material balance (see Section 3.1). Comparing Figures 5.43 and 5.16 reveals that the SF-PF model, if corrected for osmotic effects, can be close to the MD-SF-PF model. In this case, most of the solute flux is contributed by convection rather than diffusion inside the pores (since, the SF-PF model assumes that solute flux is mostly convective through the pore, as discussed in Section 3.1). If the opposite case happens (i.e., solute diffusion > solute convection) there can be large differences between the SF-PF and MD-SF-PF model, with the latter one behaving in a proper manner. Therefore, the two models (i.e., SF-PF and MD-SF-PF) can approach each other when all of the following conditions are satisfied:

i)   for the case of non-dissociating solutes (e.g., most organics) so that the osmotic effects are the same in the two models,

ii)   when the solute is transported mainly by convection (and not diffusion) through the pore,

iii)   and if the pore size is large so that the potential functions of the two models become similar.

The average value for α have been determined for some experimental conditions in Phase I, and some results are presented as follows. The average value for α is about 0.01 for the standard experiment (i.e., 2000 ppm NaCℓ, 1500 kPa pressure, and 25°C temperature) which implies that the fluid is mainly transported by diffusion rather than by convection (see Section 5.2.5 for the discussion on Peclet number). The average α value is about 1.0 at 7000 kPa pressure and 25°C temperature for the 2000 ppm NaCℓ solution, which implies that when the pressure is increased to 7000 kPa convection becomes as important as diffusion. For the solute transport through membrane, a numerical study of the equation of solute flux in a pore, Eqn.(3.11) or Eqn.(3.14), reveals that the solute transport is mainly by convection, even at the

lowest operating pressure in Phase I (i.e., 350 kPa), since the convection term (i.e., the second term in Eqn.(3.11)) always dominates the diffusion term (i.e., the first term in Eqn.(3.11)); a typical example is that the value for the convection term is about 10 times the value for the diffusion term at the low operating pressure of 500 kPa. The above numerical examples reveal that, at the brackish-water level of concentration and at the room temperature, solvent transport is usually controlled by diffusion (except at high operating pressures where convection becomes as important as diffusion) and the solute transport is mainly controlled by fluid convection (i.e., solute diffusion plays a minor role).

5.3.3   Predicting temperature effects under Phase I conditions

The temperature-extended version of the MD-SF-PF model has been discussed in Section 3.3.1. In this section, this temperature-extended model is used together with the parameters for the MD-SF-PF model, estimated at 25°C (see Section 5.2.4), to predict the performance of each of the FT30 aromatic polyamide membranes, with respect to temperature and pressure, under the experimental conditions of Phase I.

The numerical values of the free diffusivity in water have been determined from Nernst-Haskell equation (Ch. 11 in: Reid et al., 1977). The temperature dependencies of the density and viscosity of water, and the diffusivity of dilute NaCℓ in water are shown in Figures 5.44 and 5.45, respectively. The following section discusses the comparison of the model predictions with the experimental data.

The model parameters used in the analysis, for each membrane, are those determined at 25°C temperature and 2000 ppm feed concentration, as shown in Table 5.3. These parameter values have been used together with the above
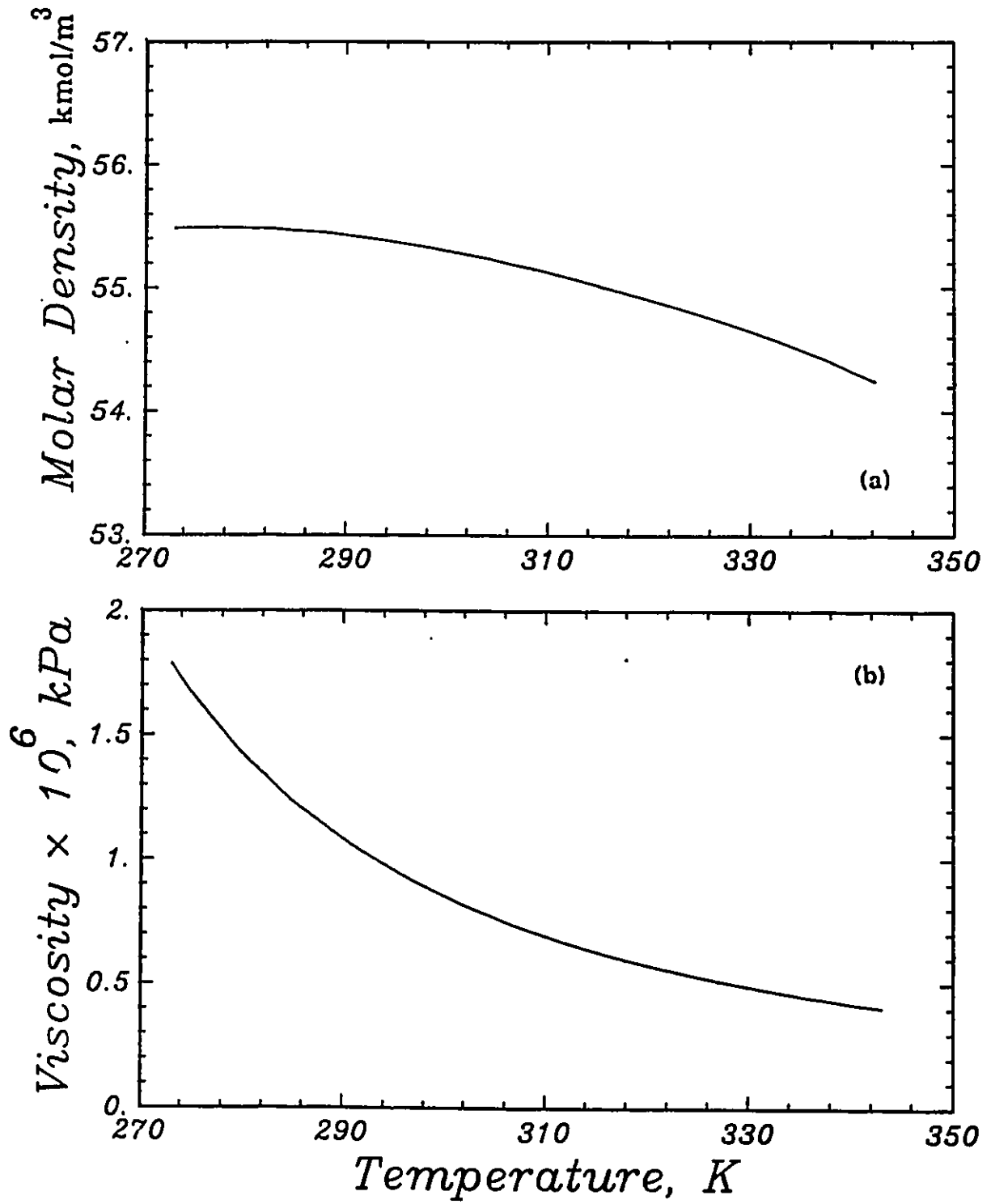
Figure 5.44:   Physical properties of water as functions of temperature: (a) molar
density versus temperature, and (b) viscosity versus temperature.
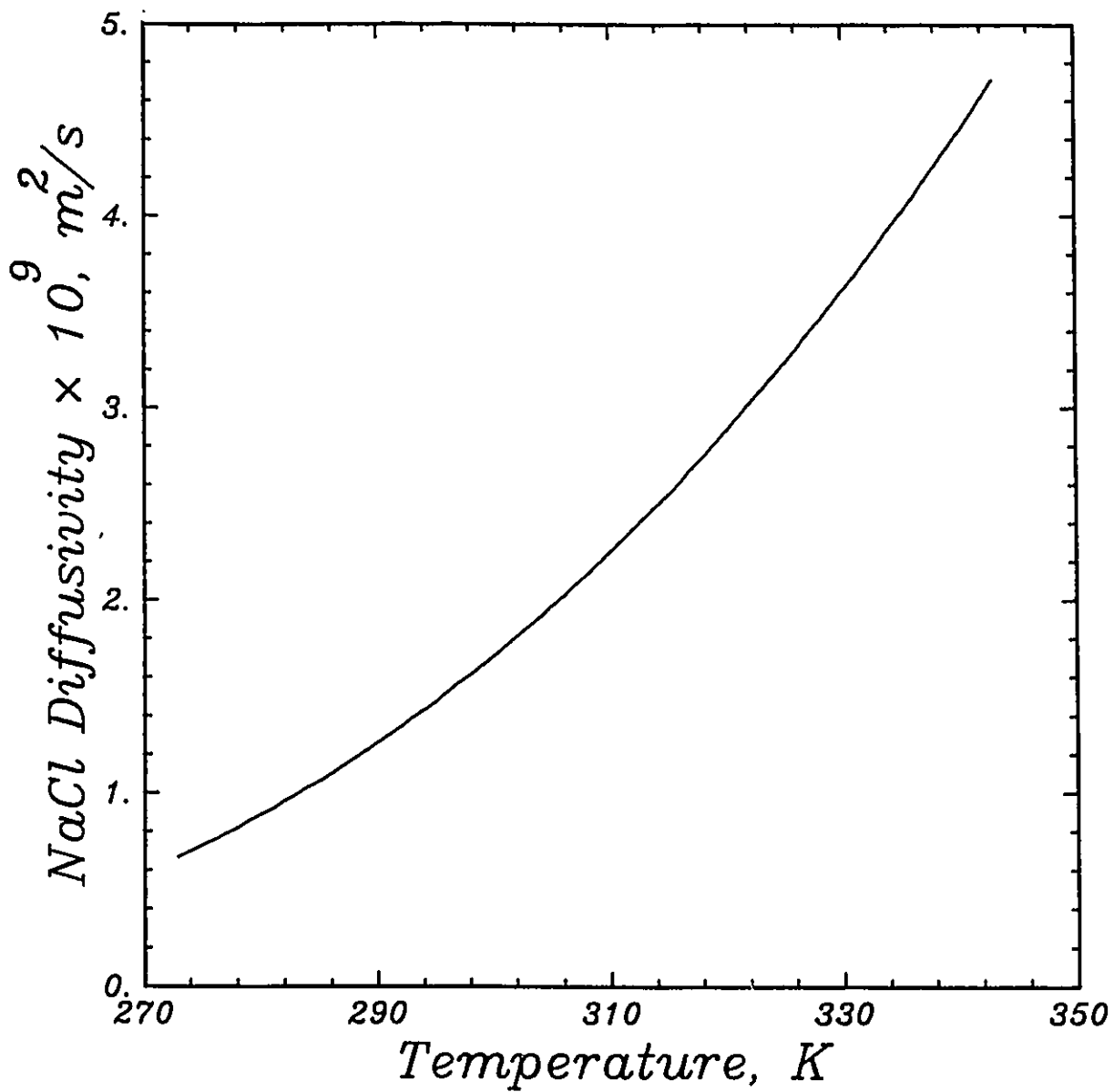
Figure 5.45:   Diffusivity of sodium chloride in water versus temperature.

temperature dependencies of the physical properties in the MD-SF-PF model to predict each membrane performance at other temperatures and pressures. The results are shown in the forms of separation, f', and flux ratio, N_T/N_P, versus temperature, for all the four membranes, in Figures 5.46 to 5.49 (Mehdizadeh and Dickson, 1989d).

In Figure 5.46, a comparison between the predictions of the temperature-extended model and the experimental data, for the SW30-1 membrane, is presented. The model predictions, based on the model parameters determined at 25°C, are good. A quick perusal over the results for all four membranes, in Figures 5.46 to 5.49, illustrates that generally the model is well representing the experimental data. Both the influence of the operating pressure and temperature are well modeled even though no adjustable parameters are used. The following features of the data are well represented by the model. The effect of pressure has a large influence on both separation and flux ratio and this trend is well represented by the model. At high pressures for the SW30 membranes, the separation is nearly temperature independent. For the lower- separation BW30 membranes at higher pressures, there is a small temperature dependence. For lower pressures, for all the membranes, the effect of temperature on separation is more significant and the model follows this trend.

Generally, increasing pressure increases the flux ratio for all the membranes. An increase in pressure reduces the relative effect of osmotic pressure on the effective pressure driving force so that the solution flux approaches the flux obtained for pure water. The temperature dependency of the flux ratio is small and similar for all pressures and membranes. These trends are well represented by the model.
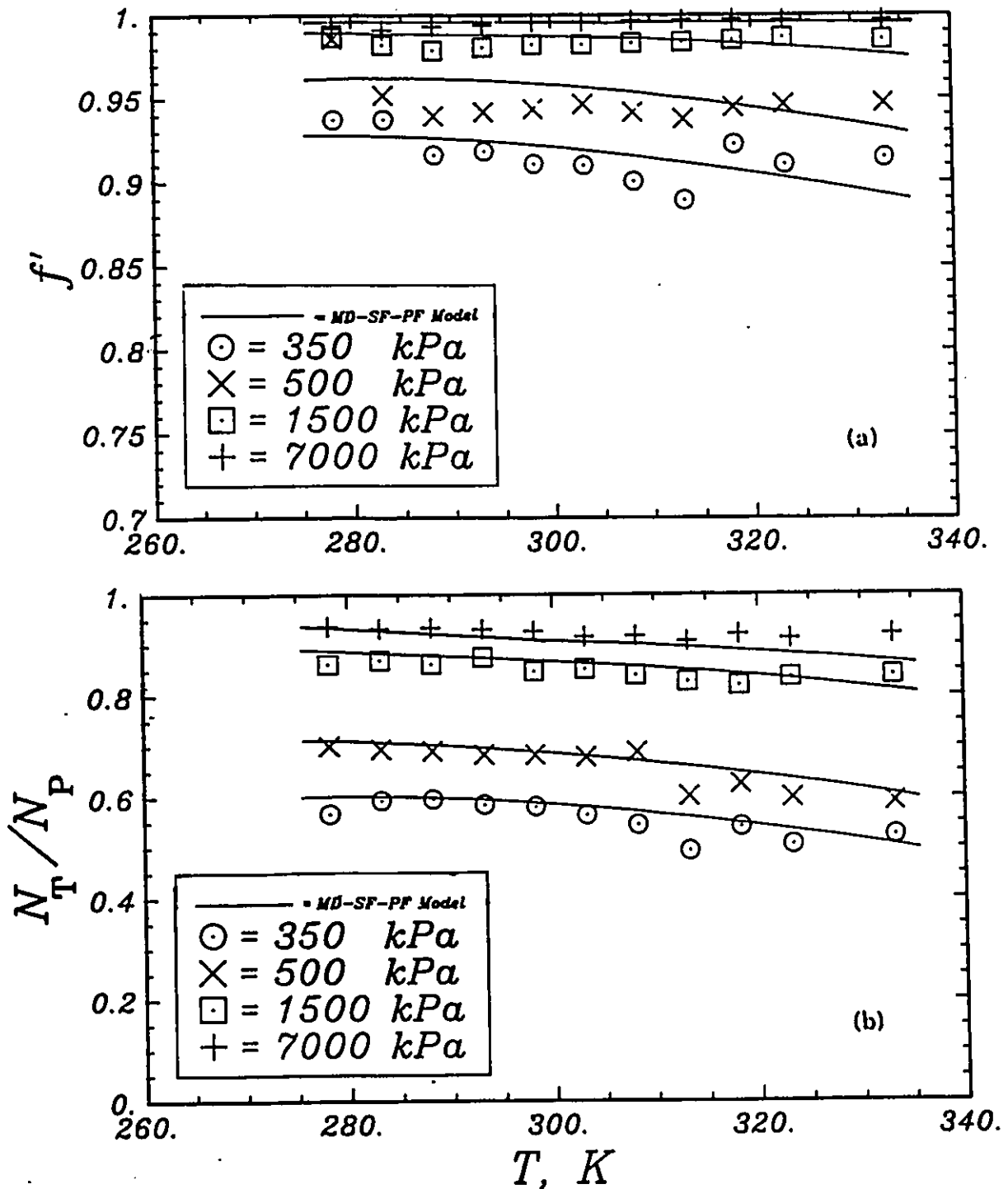
Figure 5.46:   Experimental data versus the temperature-extended MD-SF-PF model for SW30-1 membrane: (a) separation versus temperature, (b) flux ratio versus temperature.
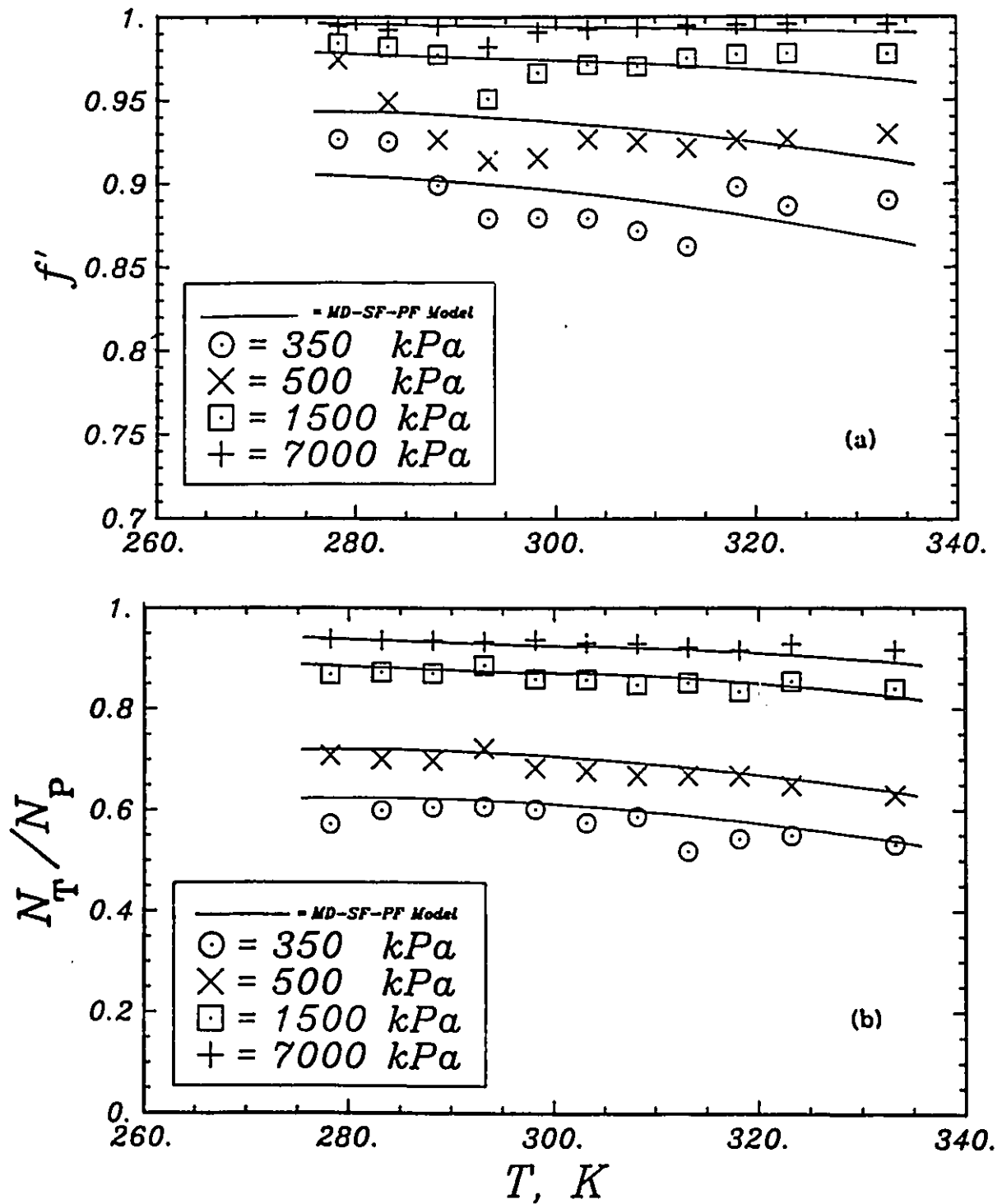
Figure 5.47: Experimental data versus the temperature-extended MD-SF-PF model for SW30-2 membrane: (a) separation versus temperature, (b) flux ratio versus temperature.
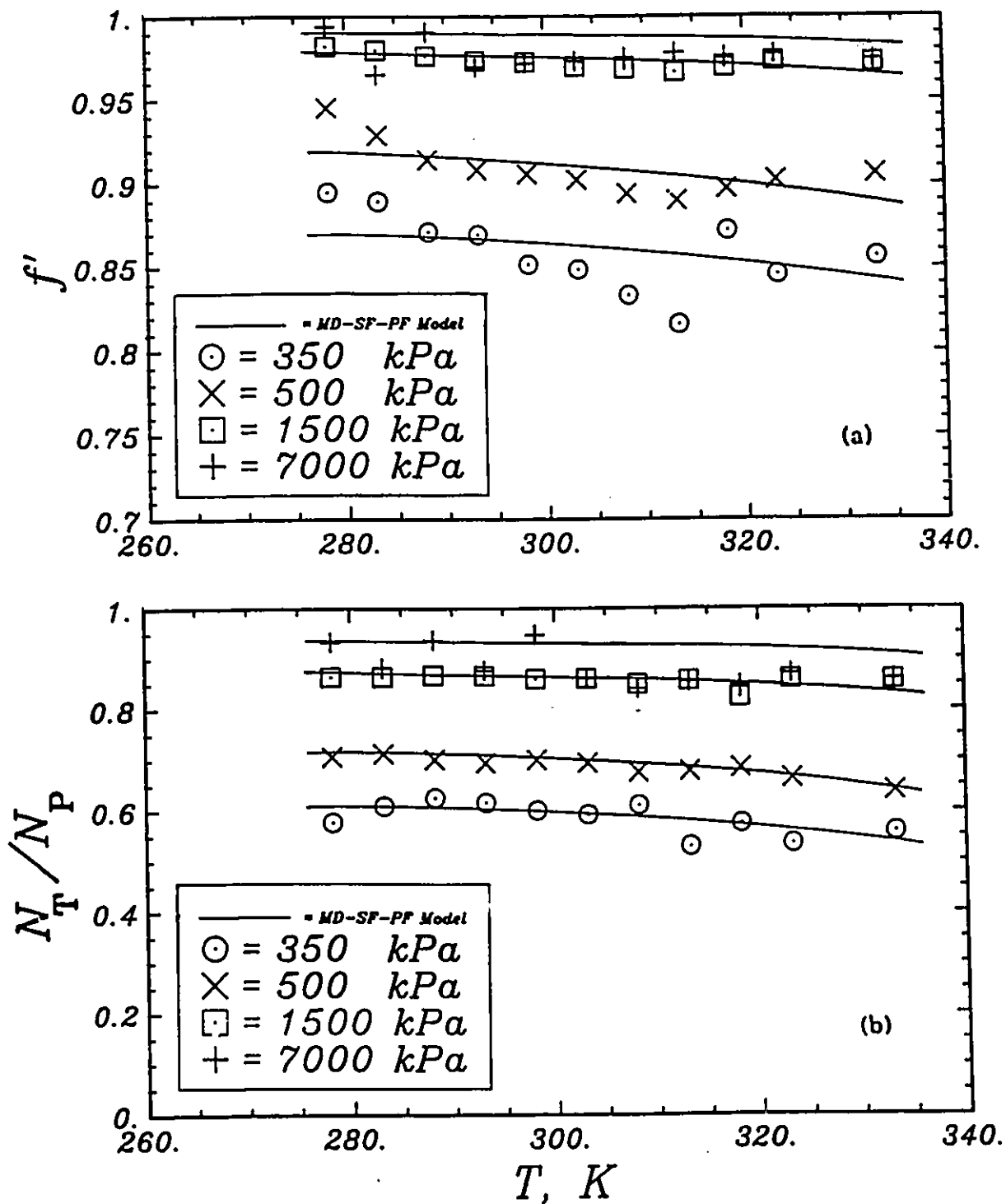
Figure 5.48:   Experimental data versus the temperature-extended MD-SF-PF
model for BW30-1 membrane: (a) separation versus temperature,
and (b) flux ratio versus temperature.
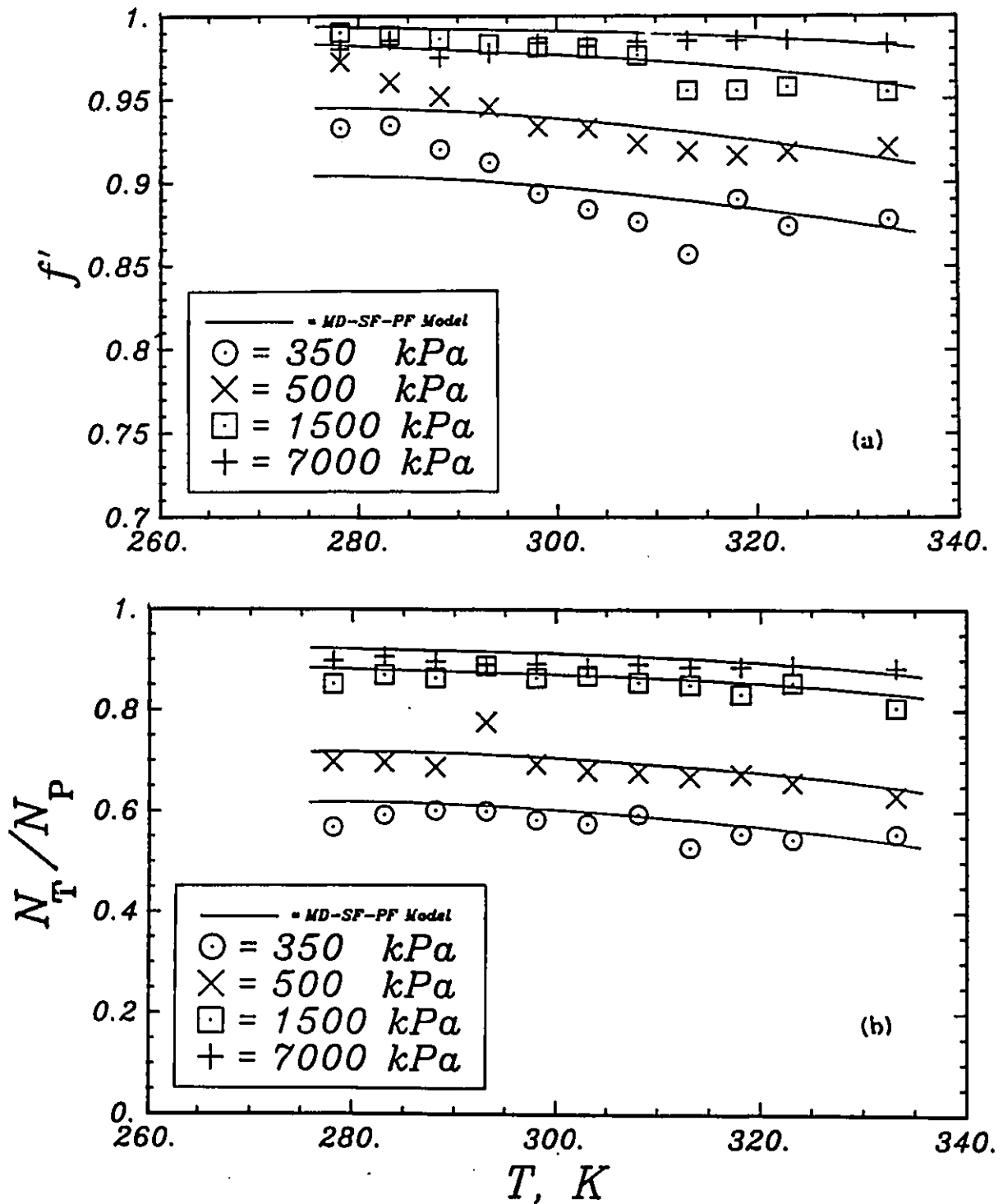
Figure 5.49: Experimental data versus the temperature-extended MD-SF-PF model for BW30-2 membrane: (a) separation versus temperature, and (b) flux ratio versus temperature.

Some discrepancy may be seen between the theoretical and the experimental data as discussed below. The experimental separation data, for all membranes, at the lower pressures (i.e., 350 and 500 kPa), are more scattered than the data at other pressures. The experimental data on the variation of separation with temperature indicates a possible minimum in separation with increasing temperature at lower pressures. However, the extended model predicts that separation decreases smoothly with increasing temperature. Possibly there is larger experimental error at the lower pressures that masks the real trend predicted by the model. Another possibility is that the experimental data represent the correct trend and there is some unknown change in the mechanism of transport and/or the membrane structure (around 35 or 40°C) which is not included in the model.

The largest deviation between the model predictions and the experimental data is found for the SW30-1 membrane at the most extreme conditions (i.e., at 7000 kPa pressure and the higher temperatures). Better agreement is found for the other membranes over all the temperature and pressure ranges. The discrepancy between the model and the experimental data for the SW30-1 membrane at the most extreme conditions suggests a limit of the model at the highest temperature and pressure for the highest separation membrane.

In addition to the above data, experiments were also performed at 4000 kPa pressure as reported in Section 5.1 (Mehdizadeh et al., 1989). These data were quite close to the data at 7000 kPa and were fit by the model well; these data have been omitted from the Figures for clarity. The flux ratio for the BW30-1 membrane at 4000 kPa were closer to the model indicating that the scatter illustrated for 7000 kPa were probably due to experimental error. Again, the above comparison may indicate a

limit in the model at the highest temperatures for the BW30-1 membrane (Mehdizadeh and Dickson, 1989d).

As discussed in Section 3.3.1, higher temperature should cause a larger potential field inside the membrane pores and this leads to higher solute separation (for electrolytes). Therefore, an increase in separation with increasing temperature is expected. However, there are other effects due to the temperature dependence of physicochemical properties of the system which oppose the trend of the potential function. Thus, the increase in solute diffusivity and solution viscosity (see Figures 5.44 and 5.45) with temperature causes overall a decrease in separation.

The discrepancy between the theory and the experimental data, which exist in few cases, may be due to various factors. The membrane physical characteristics may change with increasing temperature which have not been taken into account in the model. For instance, size and/or length of the pores may change with temperature. Since the membranes are being evaluated at temperatures much lower than the glass transition temperature for the polymer these effects should be small. Also, the chemical nature of the membranes could change with an increase in temperature; this change should appear as a change in the parameter θ_1. But the data are well fit by a constant θ_1 for each type of membrane. Finally, the deviations can be due to experimental error and the limits of the model, which seems to be the most likely case. The following section discusses the modeling of compaction effect and the solution flux.

Compaction has a significant effect on membrane performance (see Section 3.3.1) and, therefore, it is surprising that compaction does not affect the separation and flux ratios discussed and modeled above. The fact that the compaction can have no effect on the separation and flux ratio can be explained as follows. Apparently, the compaction only affects the absolute values of fluxes (N_T and N_P) and does not affect

the flux ratio, N_T/N_P. This result can be expected since compaction can effect the pure solvent flux and solution flux, obtained at the same temperature and pressure, equally, so that, when the ratio is calculated, the two effects cancel out. For the separation, it is likely that compaction has no effect on the potential field of the membrane, which is a property of the solute-solvent-membrane system; the potential field controls the separation and partitioning effects. This result is true when θ_1 and R_W, in Eqn.(3.44) are independent of temperature; hence, compaction has no direct effect on separation (Mehdizadeh and Dickson, 1989d).

In order to determine the absolute values of the fluxes, N_T and N_P, the values of τ/ϵ at different temperatures are needed, as discussed in Section 3.3.1. This parameter can be modeled by Eqns.(3.86) to (3.89). An alternative is to use Eqn.(3.90), where τ/ϵ is modeled empirically by an Arrhenius equation to give an apparent activation energy, E_t.

As discussed in Section 3.3.1, a better approach would be to model the physical properties of the polymeric membrane from a material science point of view. However, this endeavour is left for future research, and the empirical Eqn.(3.90) is employed to model the compaction effect.

In order to model the compaction effect, one may plot the $[(\tau/\epsilon)/R_W{}^2]$ parameter (from Eqn.(3.86) and experimental N_P values) versus reciprocal temperature on a semi-log scale. Then, assuming that the pore size, R_W, is temperature independent, all the temperature effect is contained in the τ/ϵ parameter. The apparent activation energy, E_t, can be obtained by measuring the slopes of such straight lines. The results are shown in Figure 5.50 with the values of the apparent activation energies (for all the membranes) in Table 5.6. Figure 5.50 suggests that the Arrhenius relationship can be obtained in the two temperature ranges of 5-35 and 35-
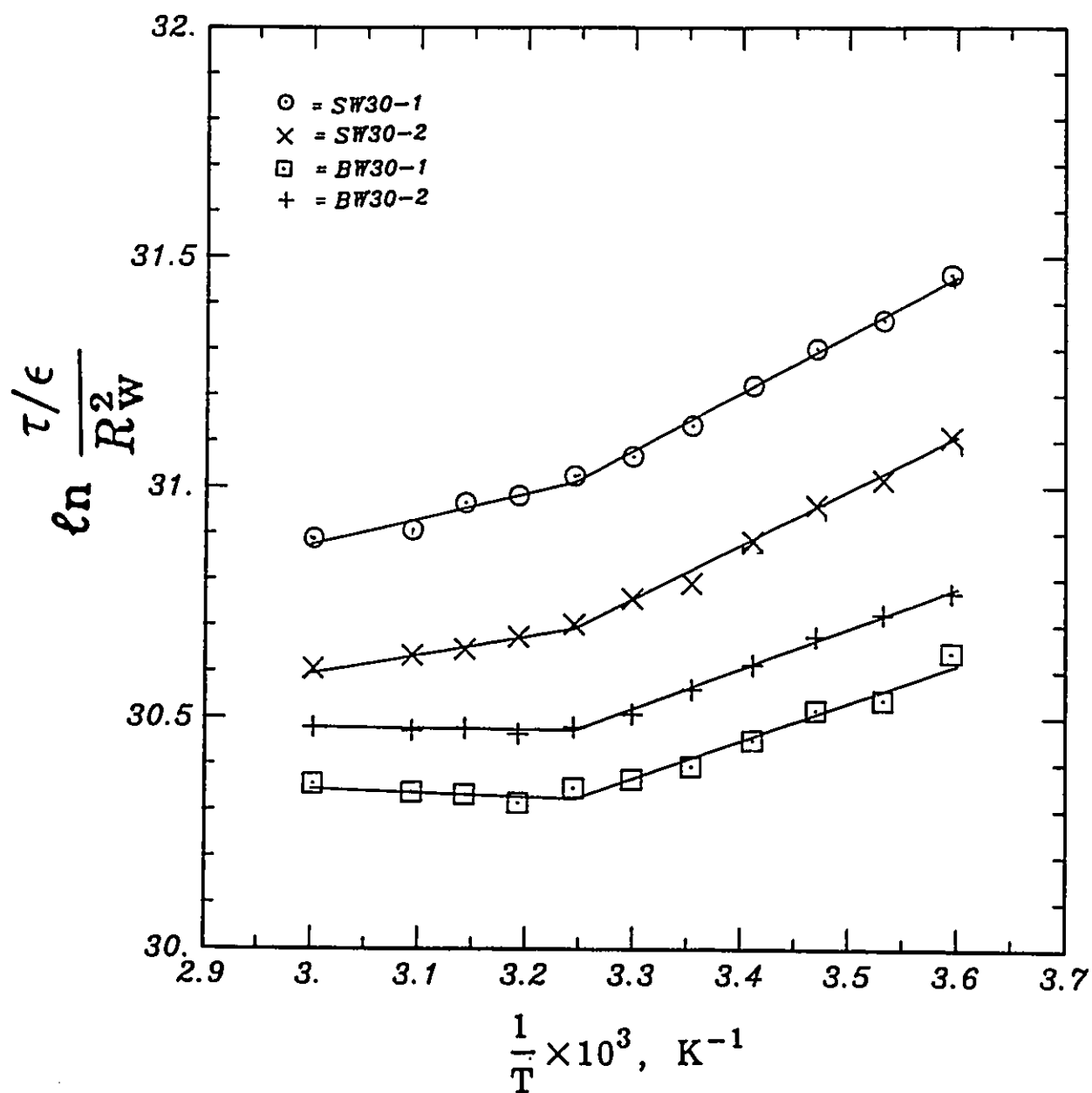
Figure 5.50:   Temperature dependency of τ/ε for all the FT30 membranes: (a) SW30-1, (b) SW30-2, (c) BW30-1, and (d) BW30-2. The straight lines are the best-fit lines in the two temperature ranges of 5-35°C and 35- 60°C.

Table 5.6

Apparent activation energies for the τ/ε factor for all the membranes

Membrane	5 - 35°C temperature range		35 - 60°C temperature range	
	$-E_t/R$, K	E_t, kJ/kmol	$-E_t/R$, K	E_t, kJ/kmol
SW30-1	1274.	$-10\,592.$	575.	$-4781.$
SW30-2	1172.	-9744	392.	-3257
BW30-1	829.	$-6891.$	0.	0.
BW30-2	869.	$-7226.$	0.	0.

60°C. Previously, it was found that the Arrhenius plots of A^0 versus $1/T$ were possible with an intersection temperature of about 35 to 40°C, and the change in the trend, about this temperature, was presumed to be due to some change in the mechanism of water transport in the membranes (see Section 5.1.1.4). The similar change in slope in Figure 5.50 (at 35°C) may be due to some irreversible change in the physical structure of the membranes. In Figure 5.50, the best-fit straight lines are determined by regression for each membrane and the values of the slopes of these lines are given in Table 5.6. The straight lines for each pair of the SW30HR and the BW30 membranes are almost parallel. The straight lines for the BW30 membranes in the higher temperature range (i.e., 35-60°C) had slightly negative slopes, which were not significantly different from zero, and, therefore, were set to zero. The apparent activation energy E_t represents the minimum energy the membrane should acquire until the τ/ε parameter can change with temperature.

The energies, presented in Table 5.6, are negative meaning that the effective length of the pore, τ, tends to decrease with increasing temperature; that is as the temperature is increased, the polymeric structure of the membrane plasticises in a manner in which the effective length of the pore decreases. The activation energy, E_t, is larger in absolute value for the SW30 membranes than for the BW30 membranes, in both the low and high temperature ranges (Table 5.6); that is the plasticisation occurs more readily for the BW30 membranes. For each membrane, the energy is less for the higher temperature range than for the lower temperature range; therefore, each membrane needs less energy, at higher temperatures, to change the τ/ε parameter as compared with the lower temperatures. The data for the higher temperature range of the BW30 membranes (almost zero energy) indicates that very little energy is needed to make changes in the effective length of the membrane pores at higher temperatures
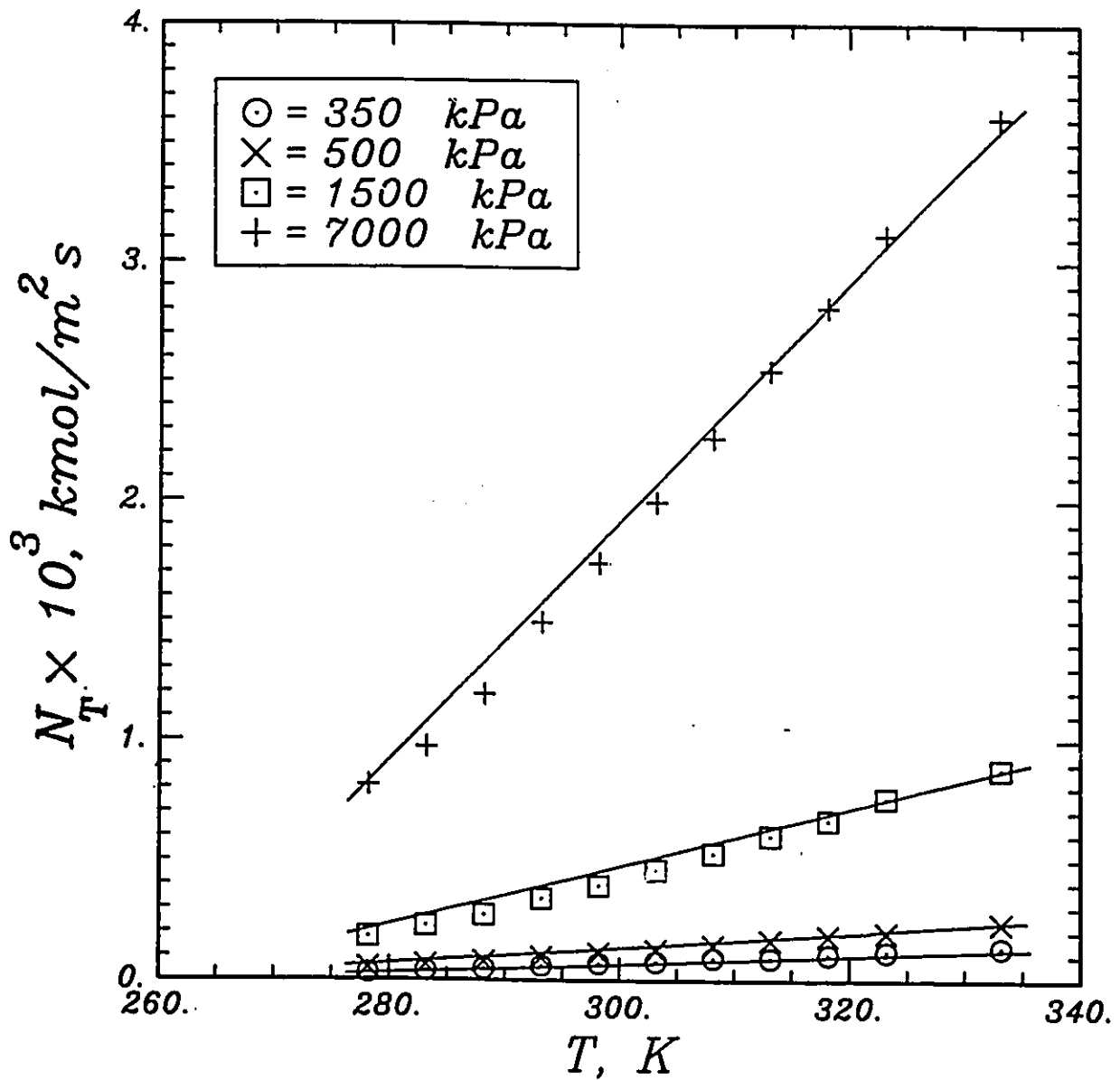
Figure 5.51:   Total solution flux as a function of temperature and pressure for the SW30-2 membrane.   The points represent the experimental data and the solid lines represent the predictions of the temperature-extended MD-SF-PF model.

(Mehdizadeh and Dickson, 1989d). These membranes (i.e., the BW30-1 and BW30-2) have previously shown another strange behaviour in the higher temperature range for the activation energies of the compaction-free permeability coefficient of solvent in a way that the activation energies were lower than those for the transport of free water (see Section 5.1.1.4); the effect was attributed to a possible change in the transport mechanism of water in these membranes. The following section discusses the prediction of absolute flux at different temperatures.

As discussed in Section 3.3.1, once the compaction effect is modeled, the total permeation flux, N_T, can be determined from Eqn.(3.40). For example, this calculation has been done for the SW30-2 membrane as shown in Figure 5.51. The agreement between the model predictions and the experimental data is good. Generally, at each pressure, the flux increases with increasing temperature and the effect is larger at higher pressures than at lower pressures. Similar agreement is predicted for the other membranes as well.

5.3.4   Predictions for other electrolytes (Phase II)

One goal of RO transport models is to predict the performance of one membrane system from information on the membrane performance for a reference case. In this section, the MD-SF-PF model (developed in Section 3.1) is used together with the model parameters determined for NaCℓ-water system (see Section 5.2.4 and Table 5.3) to predict membrane performance for three new solute systems: KCℓ-water, LiCℓ-water, and LiNO$_3$-water, for each of the FT30 aromatic polyamide membranes.

To predict for the other three salts requires information on the potential functions for the salts as well as the differences in physical properties: diffusivity, osmotic pressure, viscosity, and density. As a first approximation, the membrane

potential function, determined from the NaCℓ experiments, has been assumed to be independent of solute and concentration for the other 1-1 electrolytes. This function was used to determine the membrane performance for each new system. The prediction results by the MD-SF-PF model are shown in the Figures 5.18 to 5.23. The data for NaCℓ-water system were illustrated in Figure 5.34.

In general, the agreement between the model and the experimental results is good. The best agreements are for the KCℓ-water and LiCℓ-water systems which have the same anions as the NaCℓ. Considering that these FT30 membranes are partially negatively charged (Cadotte, 1985; Bhattacharyya, 1986), one would expect that the separation should change significantly when the coion (i.e., anion in this case) changes from solute to solute; that is LiNO$_3$ should have the largest difference in separation values from the NaCℓ, KCℓ, or LiCℓ systems. This trend is justified by the MD-SF-PF model since comparing the separation values predicted by the MD-SF-PF model for each membrane at different systems (i.e., different solutes), and at any system pressure, with each other reveals that the separation varies in the order of KCℓ < NaCℓ < LiCℓ < LiNO$_3$, and the total permeation flux, N$_T$, varies in the reverse order (i.e., KCℓ > NaCℓ > LiCℓ > LiNO$_3$) as expected (Mehdizadeh and Dickson, 1989g).

However, the experimental data (see Section 5.1.2) indicate the separation varies in the order of KCℓ < NaCℓ < LiNO$_3$ < LiCℓ. Some experimental errors may exist which causes the difference between the experimental trend and the model; repetitive experiments may improve the agreement between the model and the data. In general, it is expected that the potential function, in Eqn.(3.44), should be different for different solutes. Therefore, that the same potential function can describe the results for the four 1-1 electrolytes implies that the strength of the potential field, for

the four cases, might be about the same value. For other solutes, different potential functions are expected.

If the potential function for a new solute system can be estimated by some theory or experimental measurement of some pertinent characteristic of the new system the MD-SF-PF model can be employed to predict the membrane performance for the new solute system. This usage of the model for predictions is an important power of the model which can eliminate, at least partially, the expenses of experimentation.

5.3.5   Predicting temperature effects under Phase III conditions

The experimental conditions and the experimental results for Phase III were presented in Sections 4.3.1 and 5.1.3, respectively. The main difference between the Phases III and I is the condition of feed concentration, which is 35 000 ppm (sea water) in Phase III and 2000 ppm (brackish water) in Phase I.

In this section, the results of modeling the performance of the four FT30 membranes under the experimental conditions of Phase III, using the temperature-extended MD-SF-PF model, are presented and compared to the experimental results.

Similar to the modeling of temperature effects under the conditions of Phase I, discussed in Section 5.3.3, the model parameters used are those obtained at 25°C temperature and 2000 ppm concentration of NaCℓ aqueous solutions at different pressures (see Table 5.3). Using these model parameters, incorporating the temperature dependencies of the physical parameters of the electrolyte, such as osmotic pressure, diffusivity, and viscosity (discussed in Section 3.3.1), and assuming R_W and θ_1 to be temperature independent (as in Section 5.3.3), the temperature-

extended MD-SF-PF model has been employed to determine the predicted performance for each of the FT30 membranes. The results are shown in Figures 5.52 to 5.55.

Figure 5.52 presents a comparison between the experimental and the predicted values of separation, f', and flux ratio, N_T/N_P, as functions of temperature, for the SW30-1 membrane. The model predicts that as the temperature is increased the separation and flux ratio decrease, and as the pressure is increased the separation and flux ratio increase. The model is doing an excellent job of prediction. Similar trends are predicted for the SW30-2 membranes, as shown in Figure 5.53.

Figures 5.54 and 5.55 present the model predictions for the BW30-1 and BW30-2 membranes, respectively. Again, the agreement between the theory and the experimental data is excellent, and the model is predicting the correct trends for the change in performance as a function of operating temperature and pressure. Even though the flux ratio changes little with increasing temperature, the absolute fluxes are strongly temperature dependent (as shown in Figure 5.51).

The above results imply that the assumptions that the membrane pore size and the potential parameter do not change appreciably with temperature are very reasonable. The validity of these two assumptions was discussed in Section 5.3.3. Note that absolute fluxes are determined from the Arrhenius-type model for the compaction effect, as discussed in Section 5.3.3.

The ability of the temperature-extended MD-SF-PF model to predict each FT30 membrane performance under the wide ranges of operating temperature, pressure, and feed concentration makes the model very promising to describe and predict the performance of thin-film composite RO membranes.
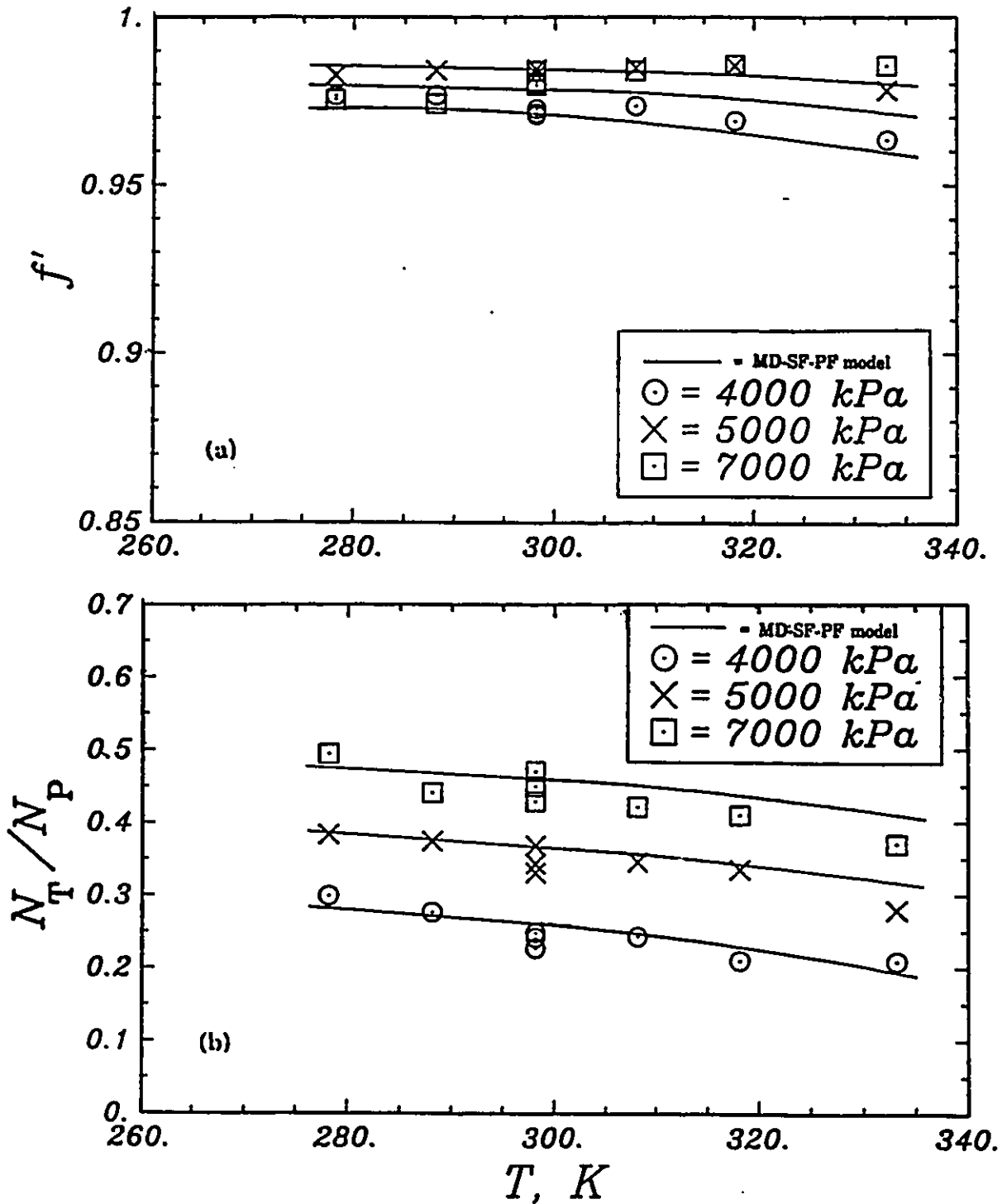
Figure 5.52: Experimental data (Phase III) versus the temperature-extended MD-SF-PF model for SW30-1 membrane: (a) separation versus temperature, (b) flux ratio versus temperature.
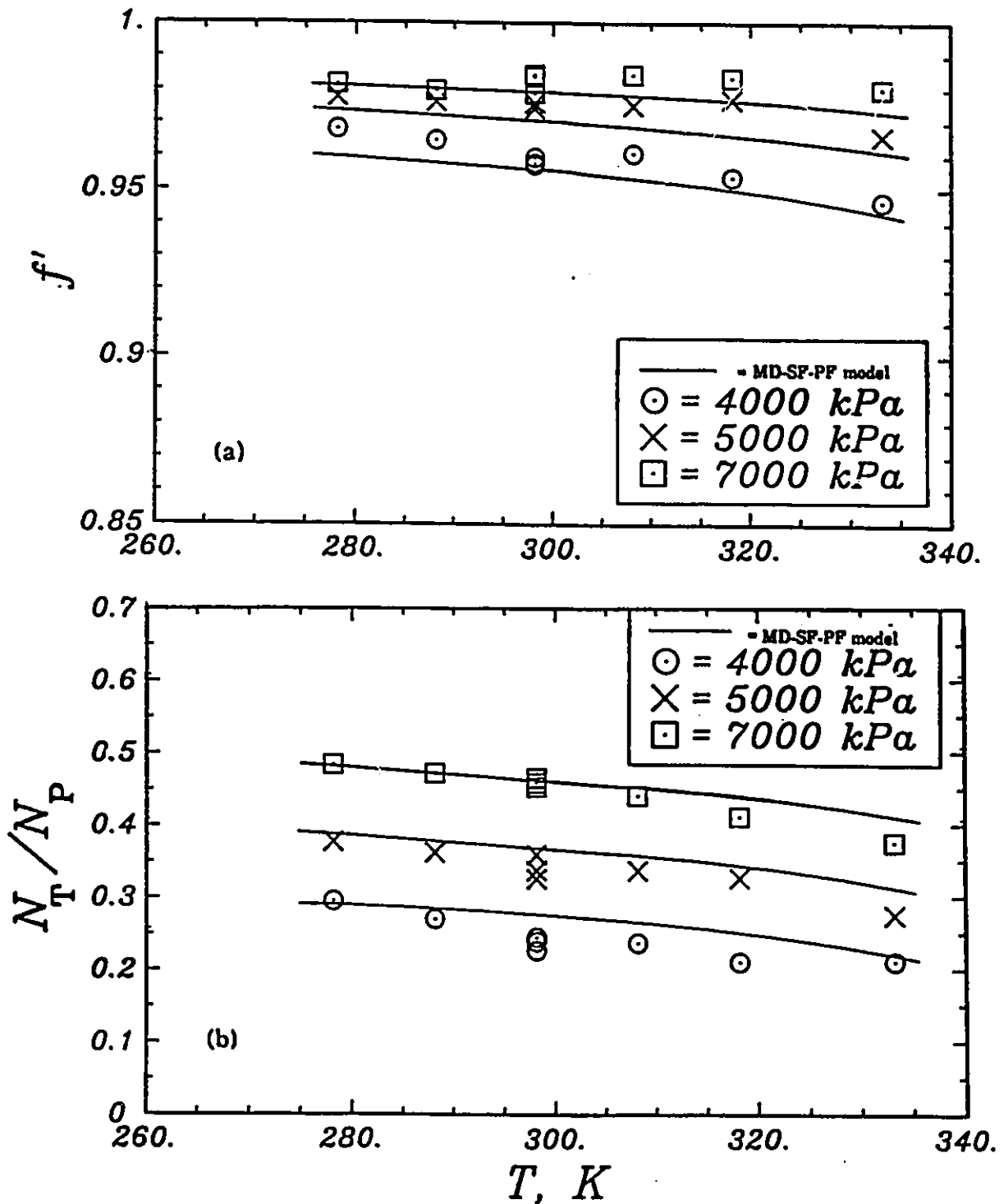
Figure 5.53:   Experimental data (Phase III) versus the temperature-extended
MD-SF-PF model for SW30-2 membrane: (a) separation versus
temperature, (b) flux ratio versus temperature.
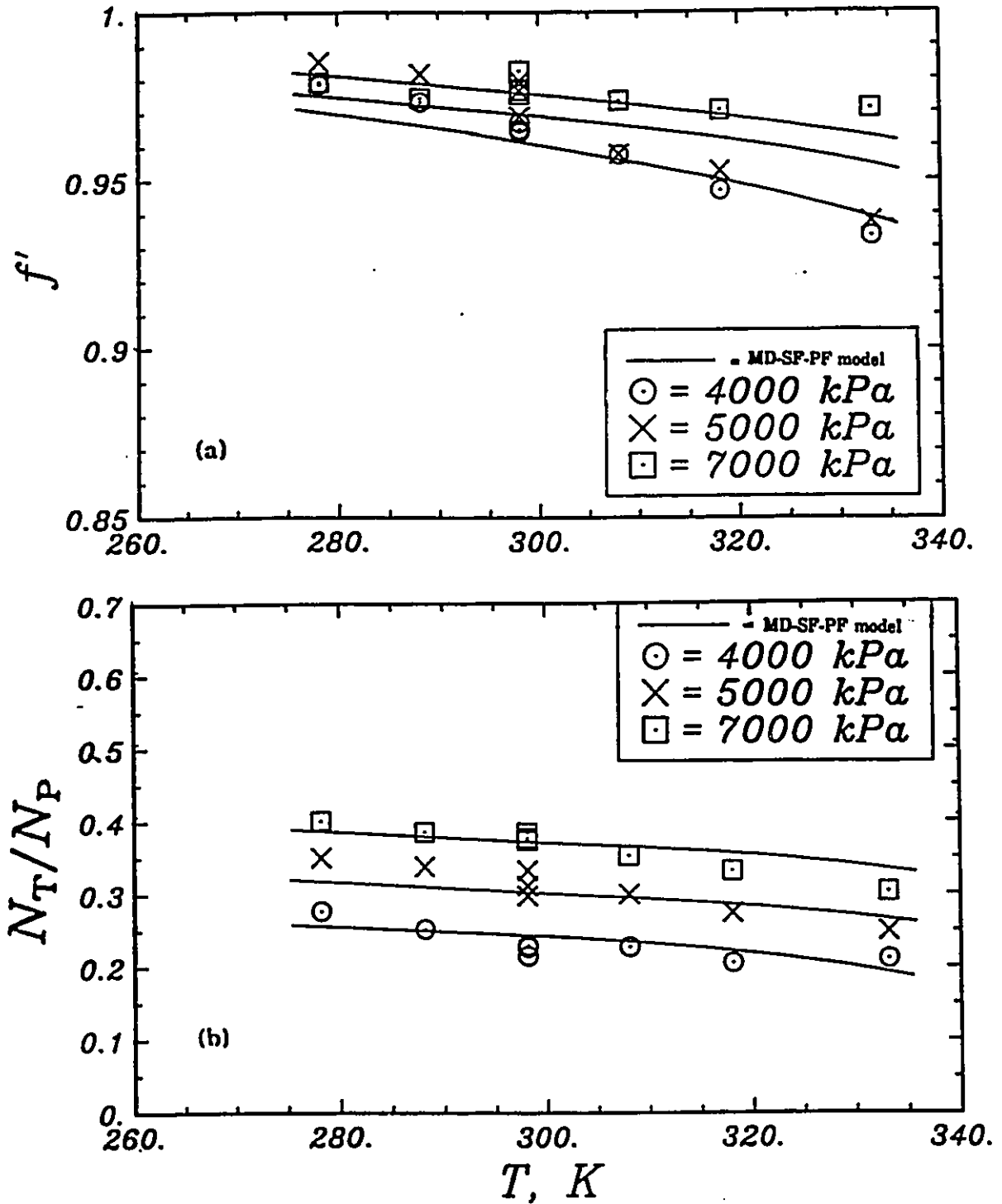
Figure 5.54: Experimental data (Phase III) versus the temperature-extended MD-SF-PF model for BW30-1 membrane: (a) separation versus temperature, (b) flux ratio versus temperature.
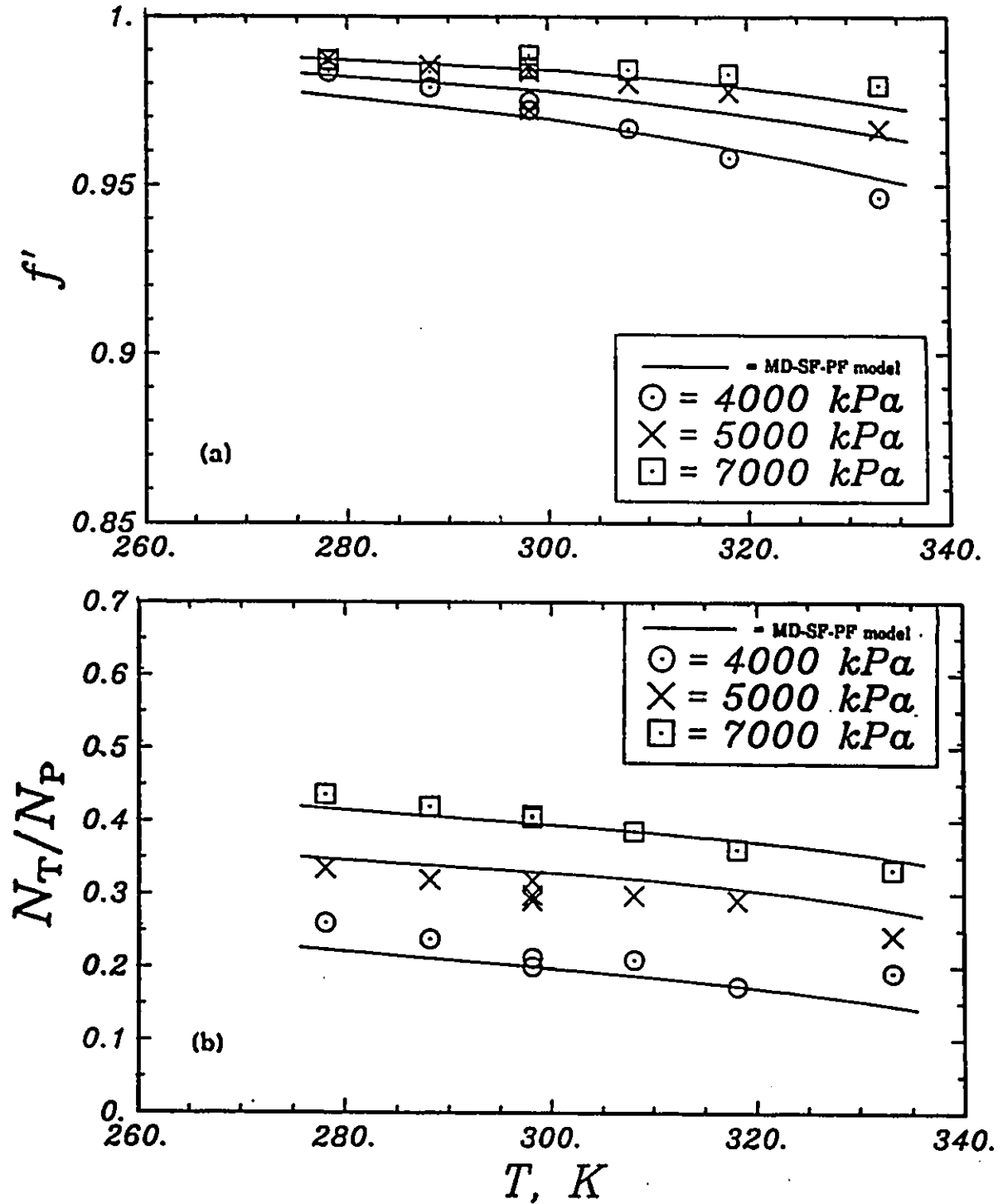
Figure 5.55: Experimental data (Phase III) versus the temperature-extended MD-SF-PF model for BW30-2 membrane: (a) separation versus temperature, (b) flux ratio versus temperature.

5.4   Simulations and Predictions for the Extended MD-SF-PF Model

In this section, the results of simulations and model predictions for the Extended MD-SF-PF model (developed in Section 3.2) are presented. The experimental data, which have been compared with the model predictions, are from aqueous solutions of toluene (Connell, 1986), cumene (Dickson, 1985), and p-chlorophenol (Dickson et al., 1976). The values for the partial molar volumes (v_A) used in the model are 0.106 and 0.140 m^3/kmol for toluene and cumene, respectively, (Dickson, 1985); and 0.112 m^3/kmol was estimated for p-chlorophenol using pure solute density data, as suggested by Reid et al. (1977). The numerical method used to solve the nonlinear differential equation of the model, Eqn.(3.75), is the orthogonal collocation method of weighted residuals, discussed in Sections 2.6, 3.6, and 5.2.5.

5.4.1   Simulation results

To see how the model works under simulated conditions, the following operating conditions have been employed: $\Delta P = 1000$ to 8000 kPa, $T = 25°C$, $C_{A2} = 0.002925$ kmol/m^3 toluene in water, and a membrane with the following typical characteristics has been assumed: $R_W = 24. \times 10^{-10}$ m, $\theta_1 = -54. \times 10^{-10}$ m, $E = 40. \times 10^{-10}$ m, $\gamma = 0.315$, and $\tau/\varepsilon = 0.6686 \times 10^{-3}$ m. The membrane performance as described by the model is shown in Figure 5.56 in which the membrane separation, f', has been plotted versus the total permeation (volumetric) flux, J_v. As the system pressure is increased the separation decreases while the flux increases; this phenomenon is typical for solute-membrane affinity systems (discussed in Section 2.3.3).

Considering only one point on the curve of Figure 5.56, e.g., at $\Delta P = 8000$ kPa (corresponding to $f' = -0.26$ in Figure 5.56), the concentration profile
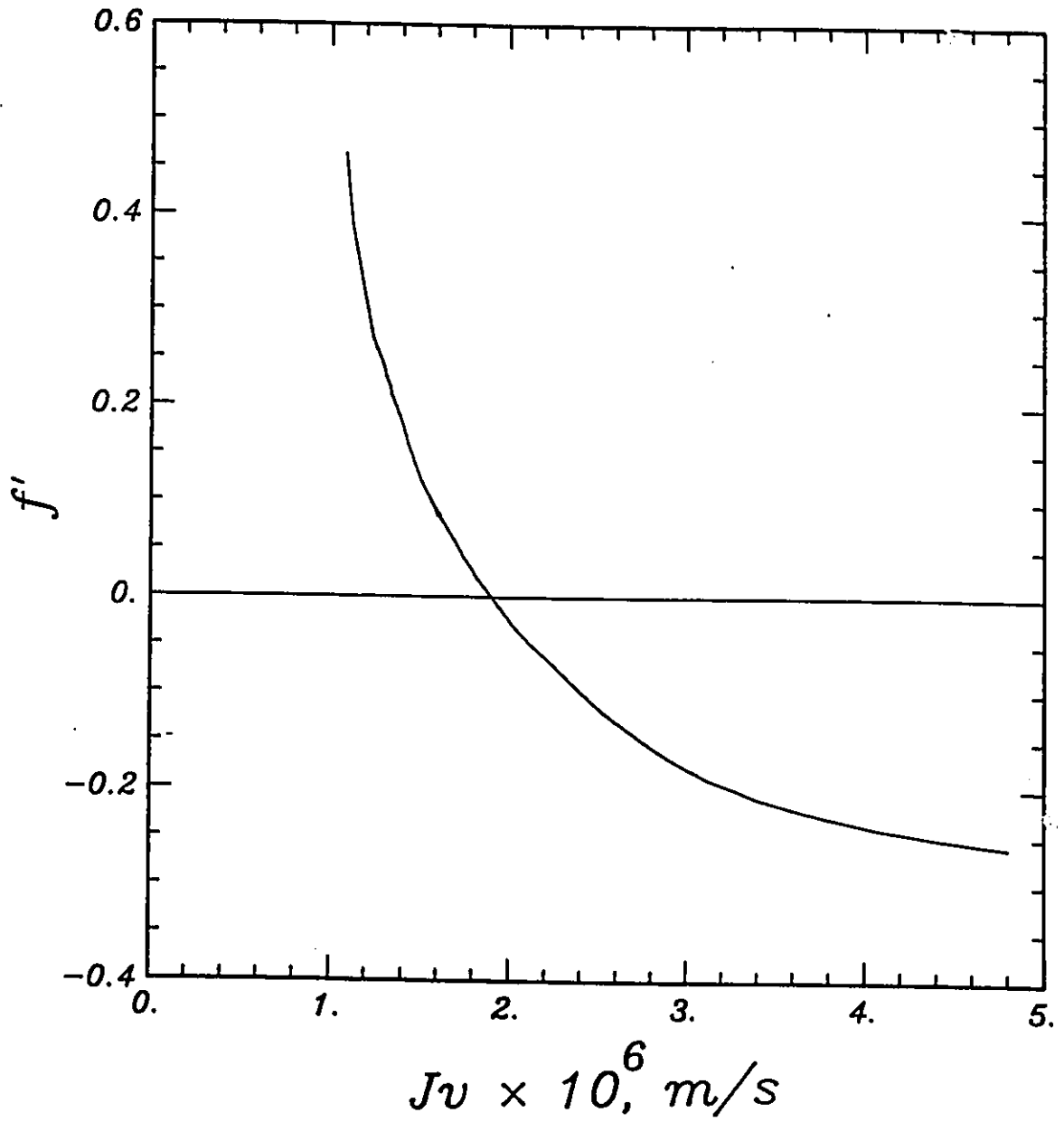
Figure 5.56: Separation versus permeation flux for toluene-water system as simulated by the Extended MD-SF-PF model at the feed concentration of $C_{A2} = 0.002925$ kmol/m^3. The membrane characteristics are: $R_W = 24 \times 10^{-10}$ m, $\theta_1 = -54 \times 10^{-10}$ m, $E = 40 \times 10^{-10}$ m, $\gamma = 0.315$, and $\tau/\varepsilon = 0.6686 \times 10^{-3}$ m.

inside the pore is shown in Figure 5.57, together with the potential function, as a function of radial and axial positions. Both the profiles, in Figure 5.57, have zero slopes at the pore centerline and have maximum slopes near the pore wall. The potential (negatives indicating the solute is attracted to the membrane) increases, in absolute value, from the inlet to the outlet of the pore; the concentration also increases in the same direction. Higher values of potential at the pore exit means higher values for the partition coefficient at the membrane exit compared with that at the pore entrance; that is the partitioning effect is stronger at the pore exit.

In order to see how the Extended MD-SF-PF model behaves when feed concentration changes, simulation studies have been done for the system toluene-water with the following parameters for the membrane system: $R_W = 20 \times 10^{-10}$ m, $\theta_1 = -36 \times 10^{-10}$ m, $\gamma = 0.286$, $E = 40 \times 10^{-10}$ m, and $\tau/\varepsilon = 0.4533 \times 10^{-3}$ m. The operating conditions are: $C_{A2} = 0.0006$ to 0.0060 kmol/m^3, $\Delta P = 2000$ to 8000 kPa; the system temperature remains constant at 25°C. The model behaviour is depicted in Figure 5.58. For any feed concentration, the separation decreases as the pressure is increased, and as the feed concentration is increased the separation increases due to the weakening of the (negative) attraction potential field (see Eqn.(3.82)). The increase in separation, as the feed concentration is increased, can be seen in the literature (e.g., Dickson et al., 1976; Dickson, 1985; Connell and Dickson, 1988). The flux decline with increase in feed concentration is due to the concentration dependency of potential function. The concentration dependent potential function means that the strength of the potential field, inside the membrane pores, depends on the number of solute molecules per unit volume of the pore, and the higher the concentration the weaker is the potential function (i.e., the larger is the absolute value of the negative potential). That is, if the potential function can be represented by Hamaker constant,
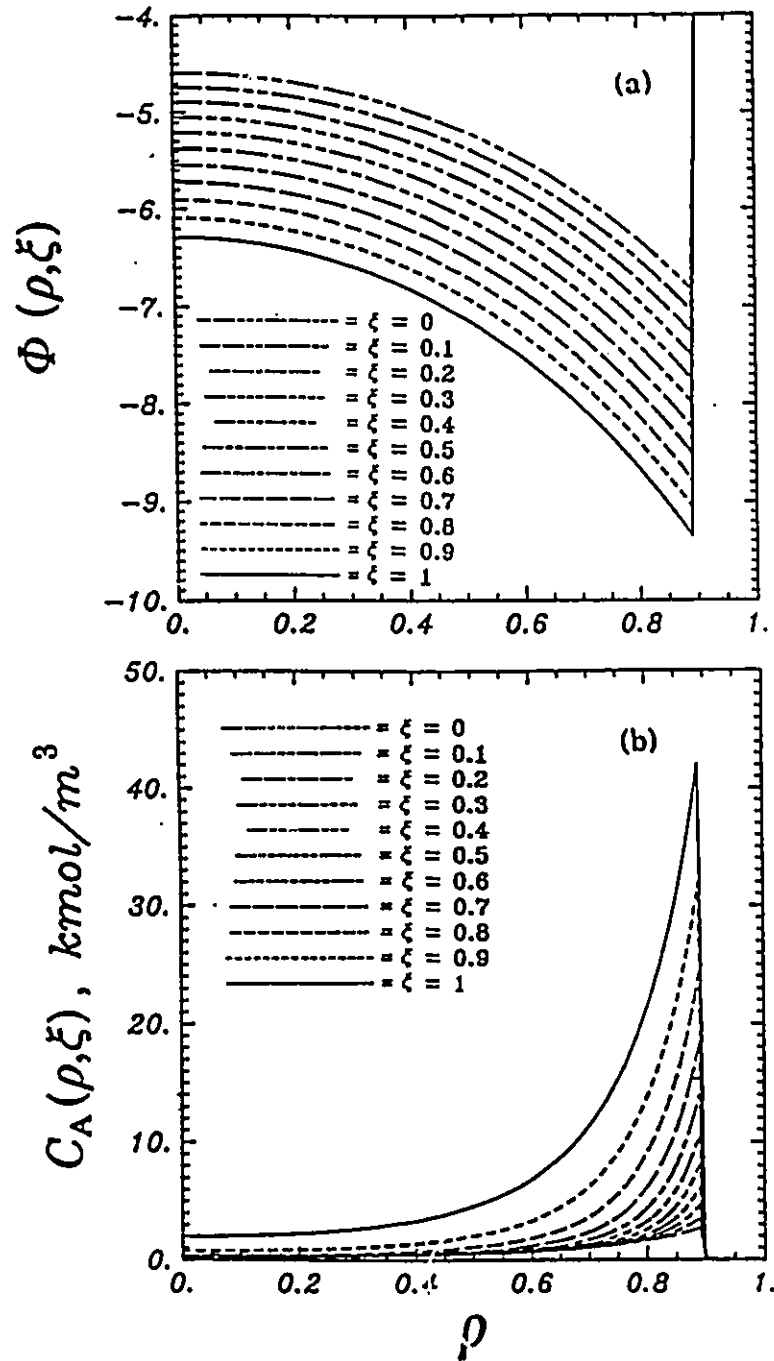
Figure 5.57:   Simulation results, by the Extended MD-SF-PF model, for toluene-water system at $\Delta P = 8000$ kPa and $C_{A2} = 0.002925$ kmol/m³ (membrane characteristics are given in Figure 5.43): (a) potential function as a function of radial and axial positions inside the pore, (b) solute concentration as a function of radial and axial positions inside the pore.
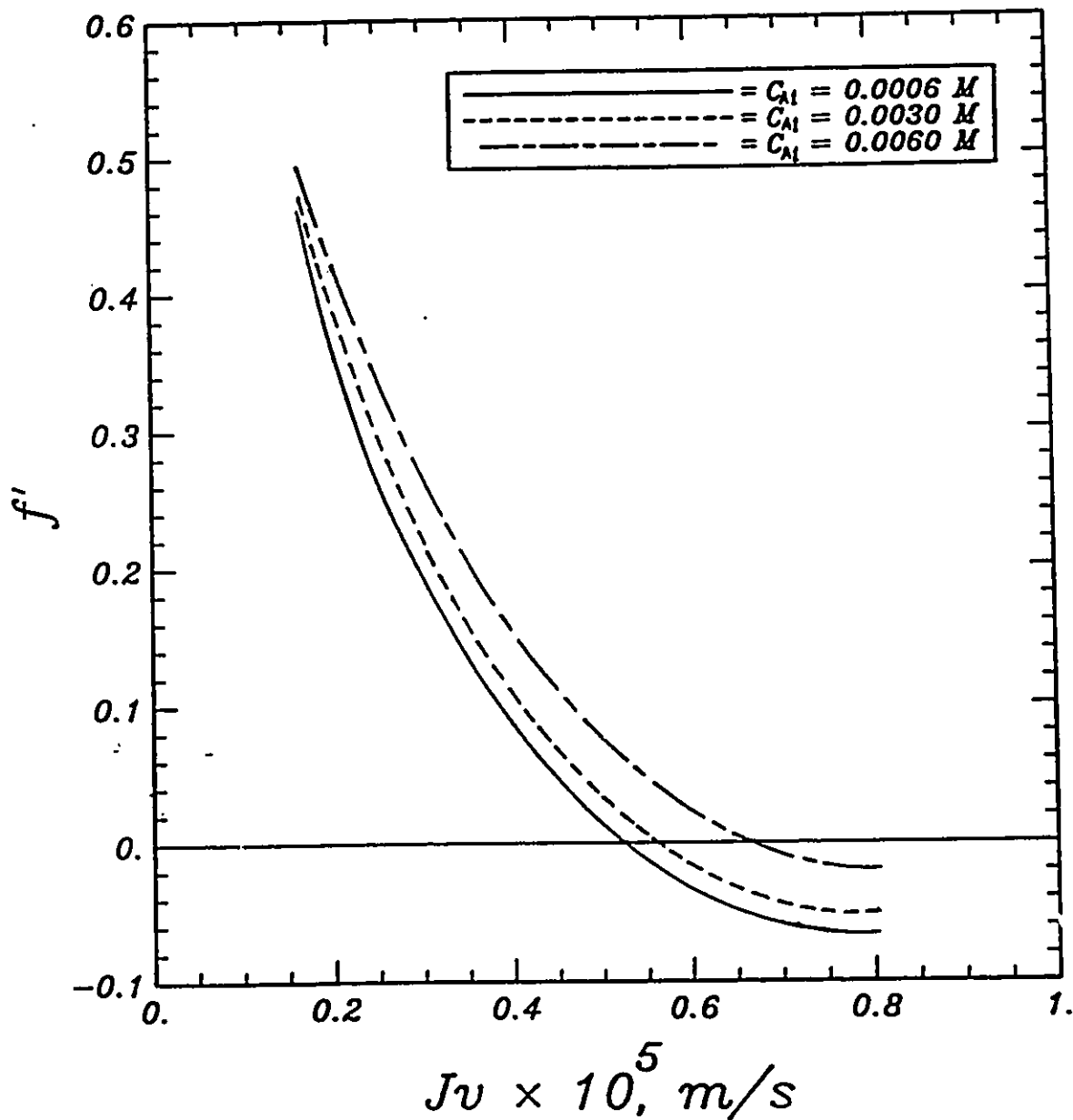
Figure 5.58:   Theoretical separation versus permeation flux, with feed concentration as a parameter, as simulated by the Extended MD-SF-PF model for toluene-water solution. The membrane characteristics are: $R_W = 20 \times 10^{-10}$ m, $\theta_j = -36 \times 10^{-10}$ m, $\gamma = 0.286$, $E = 40 \times 10^{-10}$ m, and $r/\varepsilon = 0.4533 \times 10^{-3}$ m.

for the case of nondissociable organics, the Hamaker constant changes as the solute concentration is changed.

5.4.2   Model description of real systems

As mentioned earlier in this section, the three systems which have been employed to test the Extended MD-SF-PF model are dilute aqueous solutions of toluene (Connell and Dickson, 1988), cumene (Dickson, 1985), and p-chlorophenol (Dickson et al., 1976). The type of membrane used in all these cases was cellulose acetate. The extended MD-SF-PF model was fitted to the experimental data, according to Eqn.(5.2), to determine the parameters of the model for each system. The results are as follows.

For the toluene-water-cellulose acetate system, the model fit to the data is illustrated in Figure 5.59. Note that both the separation and the flux values are predicted by the model. The model fits the data well; as the permeation flux is increased (by increasing the system pressure) the separation decreases. The separation decreases with an increase in pressure because, at higher pressures, the mobility of the solute molecules is increased in the membrane pores due to the higher convective forces, against the membrane-solute attraction force. The feed concentrations in this case are in the range of 0.0004 to 0.004 kmol/m^3, and the operating pressures are in the range of 1000 to 7000 kPa. The temperature in all these systems remains at 25°C.

The Extended MD-SF-PF model parameters, determined for the toluene-water system, are tabulated in Table 5.7. The estimated average pore radius is at the end limit of the pore size range for reverse osmosis membranes. The confidence intervals are very wide, and narrower intervals could not be reached due to the small
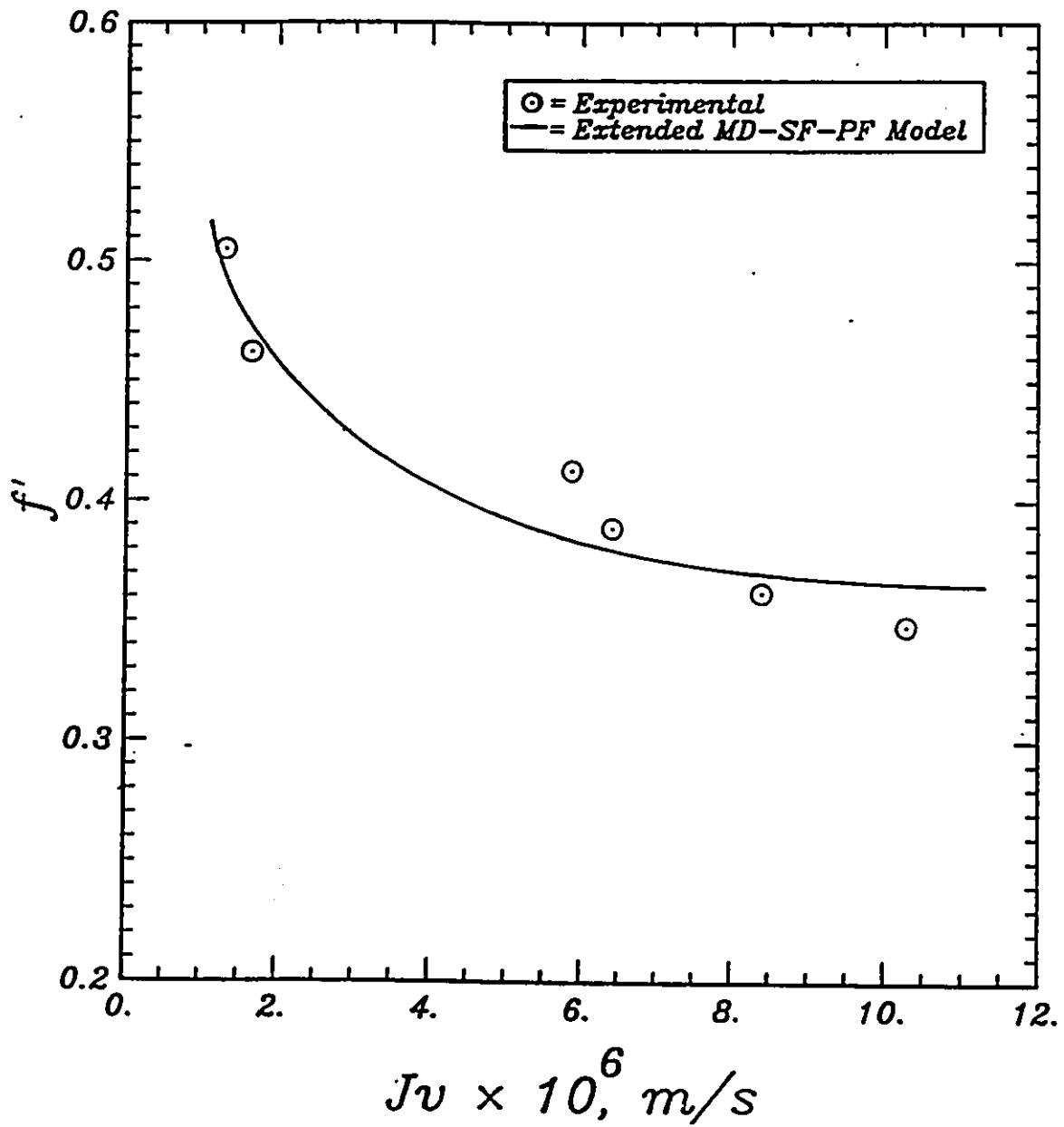
Figure 5.59:   Experimental data versus the extended MD-SF-PF model predictions for the toluene-water-cellulose acetate system at 25°C; the experimental data are from Connell (1986).

Table 5.7

Estimated parameters and statistics for the toluene-water system
using the Extended MD-SF-PF model*

$$-7.29 < R_W \times 10^{10} = 23.16 < 53.61$$

$$-125.60 < \theta_1 \times 10^{10} = -32.33 < 60.95$$

$$-78.76 < E \times 10^{10} = 40.07 < 158.90$$

$$-1.01 < \gamma = 0.2860 < 1.58$$

$$SSQ = 0.001604$$

$$Var(Res.) = 0.0008019$$

$$dof = 2$$

* 95% confidence intervals are shown.

number of the experimental data points (i.e., degrees of freedom = 2). Therefore, the model parameters, shown in Table 5.7, are not accurate and more experimental data are required to get better parameter estimates. However, the model fit to the data is good, which means that the model can describe the observed data. The value of τ/ε, needed to calculate the flux, has been calculated from pure water experiments as $\tau/\varepsilon = 0.4533 \times 10^{-3}$ m. Each experimental data point, in Figure 5.59, has some experimental error, and the error can be large especially in the case of volatile organic solutes. The real model description of the data has some small fluctuations about the curve of Figure 5.59, and the curve has been drawn through the real points of the model behaviour since the deviations from the curve are small. The small deviations from the curve are the result of dependency of the potential function on concentration, as the experimental points in Figure 5.59 are at different feed concentrations.

For the cumene-water-cellulose acetate system, the results are shown in Figure 5.60. The feed concentrations are in the range of 0.00006 to 0.0002 kmol/m³, and the operating pressures are in the range of 690 to 6900 kPa. The system temperature remains at 25°C. The model parameters determined from the data fitting are shown in Table 5.8. The wide confidence intervals are again a result of the small number of experimental data points available (i.e., degrees of freedom = 4). The model, as represented by the curve in Figure 5.60, is trying to best represent the experimental data which have a large scattering. For the cumene-water system, as for the toluene-water system, the real model description of the data has some small deviations above and below the curve in Figure 5.60. These small deviations from the curve, which are a result of the concentration dependency of the potential function in the model, are not shown in Figure 5.60; the curve in Figure 5.60 is the best curve through the points of the model behaviour. The model, in Figure 5.60, can well
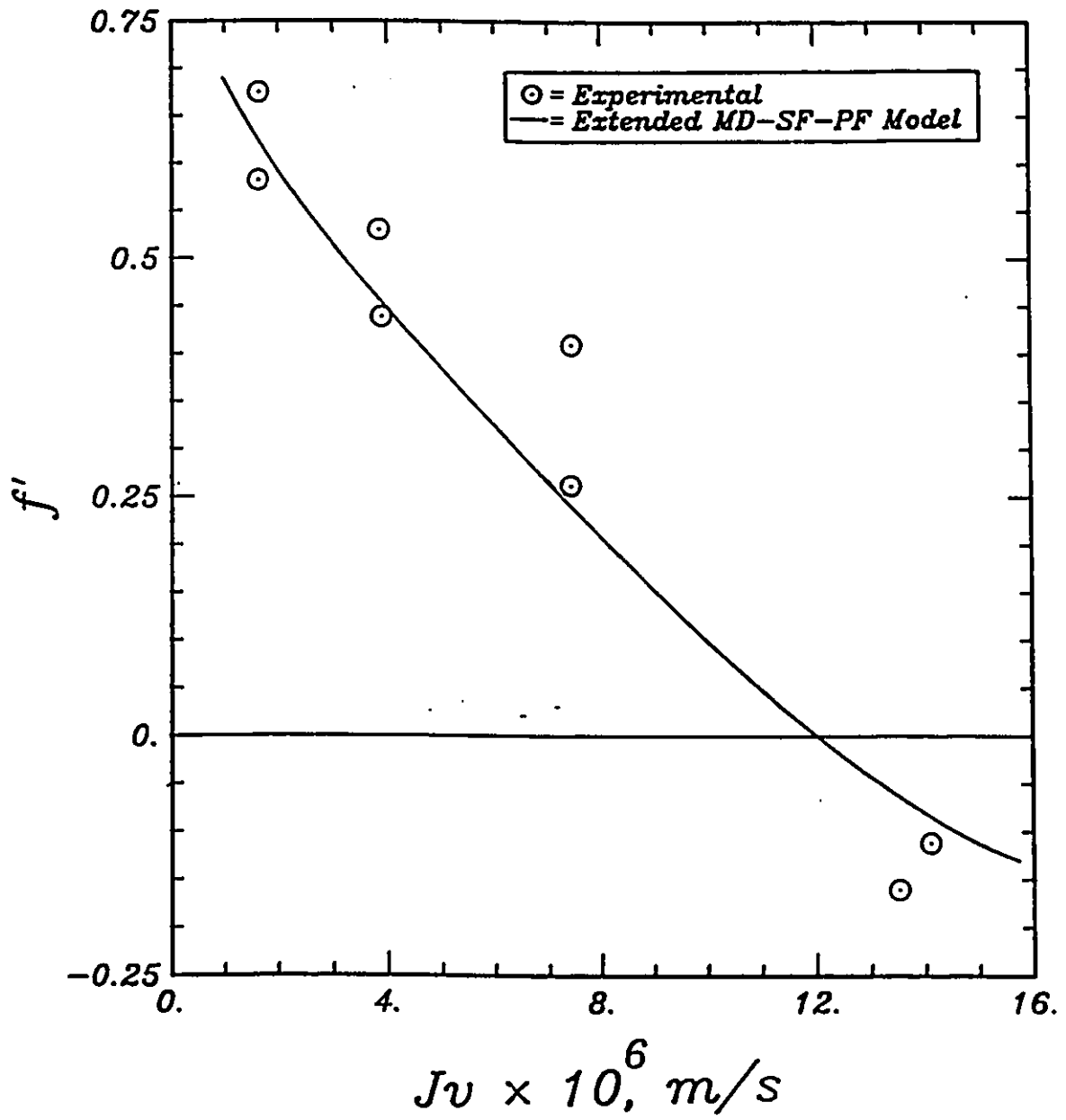
Figure 5.60: Experimental data versus the extended MD-SF-PF modelpredictions for the cumene-water-cellulose acetate system at 25°C; the experimental data are from Dickson (1985).

Table 5.8

Estimated parameters and statistics for the cumene-water system
using the Extended MD-SF-PF model[*]

$$5\ 11.98 < 18.86$$

$$-71.66 < \theta_1 \times 10^{10} = -36.23 < -0.79$$

$$-12.46 < E \times 10^{10} = 41.79 < 96.04$$

$$-0.1280 < \gamma = 0.1809 < 0.4897$$

$$SSQ = 0.0230$$

$$Var(Res.) = 0.005750$$

$$dof = 4$$

[*] 95% confidence intervals are shown.

describe the performance of the membrane when the separation decreases from positive to negative values (with negative separation meaning that the permeate concentration is larger than the feed concentration). In this case, the separation attains values as low as −15%. The value of t/ε, which is needed to calculate the flux, has been calculated from pure water experimental data as 0.8755×10^{-4} m.

The model description of data for the case of p-chlorophenol-water-cellulose acetate system is shown in Figure 5.61. The feed concentrations are in the range of 0.0001 to 0.904 kmol/m^3, and the operating pressures are in the range of 690 to 10 350 kPa (100 to 1500 psi). The system temperature remains at 25°C. The model parameters determined from the data fitting are presented in Table 5.9. Again, the wide confidence intervals for the parameters are due to the small number of the experimental data points (i.e., degrees of freedom = 6). The model, represented by the curve in Figure 5.61, is the best curve through the real model behaviour which has small deviations from the curve, because of the dependency of the potential function upon concentration (and because the experimental data points are at different feed concentrations). The model description of the experimental data is successful as the separation decreases from about 10% down to about −100% (at −100% separation, the permeate concentration is twice the feed concentration). The large negative separations, such as −100%, imply that the solute molecules have faced a very strong (adsorption) potential field inside the membrane pores. The value of t/ε has been determined from pure water experimental data as 0.3519×10^{-3} m.

The values for E (representing the frictional drag in Eqn.(3.83)) and R_W, in all the cases discussed above, are such that the friction function, $b(\rho)$, attains values which are much larger than values predicted by the Faxen equation. Therefore, the result of the Extended MD-SF-PF model implies that, once the organic solute
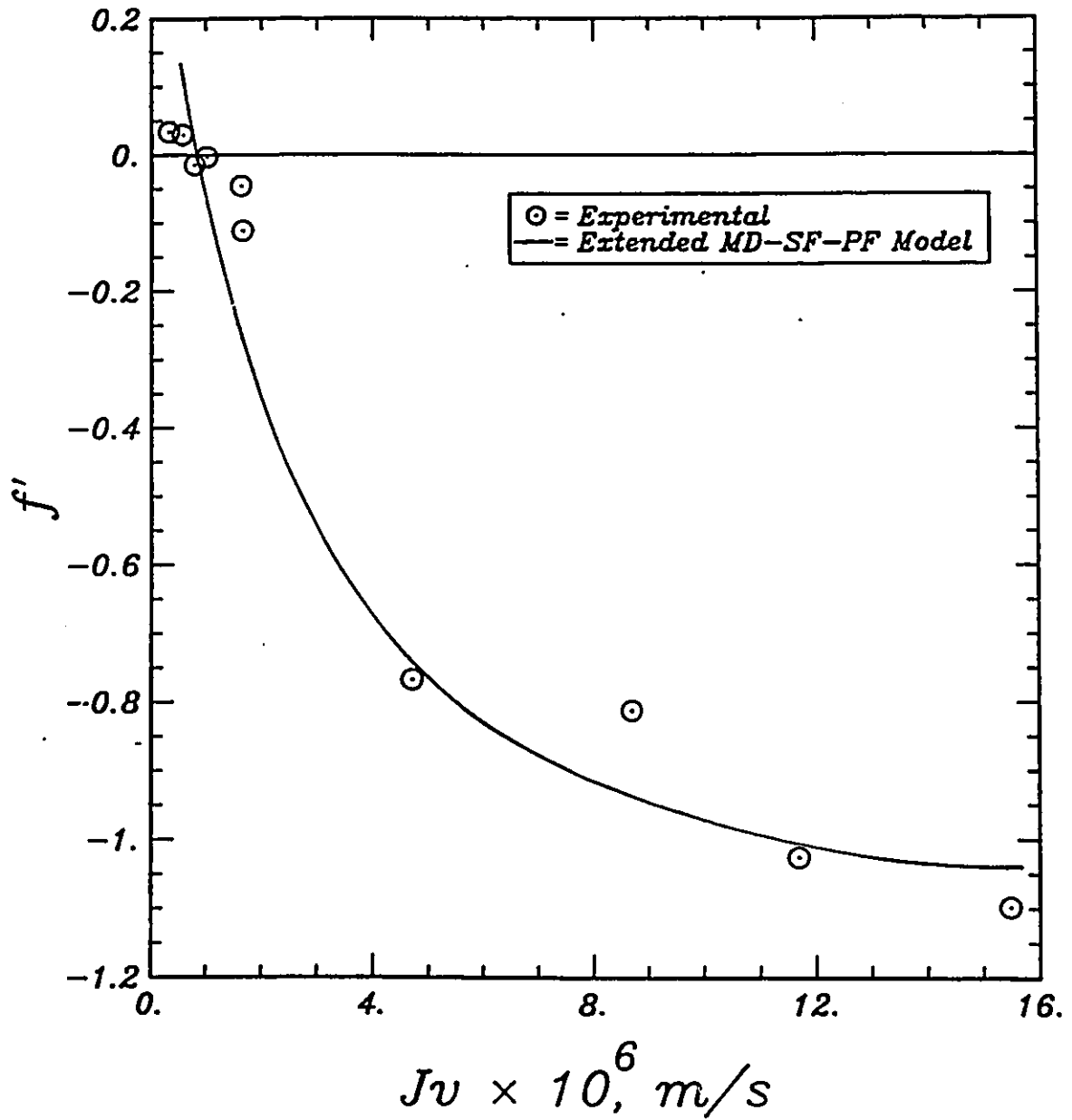
Figure 5.61: Experimental data versus the extended MD-SF-PF model predictions for the p-chlorophenol-water-cellulose acetate system at 25°C; the experimental data are from Dickson et al. (1976).

Table 5.9

Estimated parameters and statistics for the p-chlorophenol-water system using the
Extended MD-SF-PF model*

$$8.91 < R_W \times 10^{10} = 17.38 < 25.85$$

$$-72.43 < \theta_l \times 10^{10} = -40.13 < 7.82$$

$$-8.25 < E \times 10^{10} = 42.28 < 92.80$$

$$-0.0290 < \gamma = 0.0407 < 0.1110$$

$$SSQ = 0.05952$$

$$Var(Res.) = 0.009920$$

$$dof = 6$$

* 95% confidence intervals are shown.

molecules are sorbed by the membrane, the frictional drag on the solute molecules is high so that the molecules move slowly through the membrane pores.

Overall, the Extended MD-SF-PF model has been able to describe the experimental data for the three systems of toluene-water (f' = 50% to 37%), cumene-water (f' = 65% to -15%), and p-chlorophenol (f' = 10% to -100%), with cellulose acetate membranes. The separation values for the above three volatile organic solutes is in the order of toluene > cumene > p-chlorophenol (i.e., p-chlorophenol yields the poorest separation values). The p-chlorophenol and other phenol derivatives are of practical interest in wastewater treatment; therefore, the negative separation for p-chlorophenol implies that poor separations of the solute would be obtained if the solute is present in a wastewater and cellulose acetate is used as the membrane material. The reason for the negative separation of p-chlorophenol (i.e., preferential sorption of the solute) might be as follows. The membrane material (i.e., cellulose acetate) has a net proton acceptor character since it is slightly negatively charged. Since p-chlorophenol has a higher acidity than water (Matsuura and Sourirajan, 1971), p-chlorophenol should be more attracted to the membrane surface than water. Therefore, p-chlorophenol is preferentially sorbed at the membrane-solution interface. On the other hand, p-chlorophenol has less mobility than that of water, and the solute mobility tends to increase with increase in operating pressure (Dickson et al., 1979). The increased mobility of the solute molecules with pressure is due to the increased shear effect on the solute molecules by the increased fluid velocity. The facts that p-chlorophenol is preferentially sorbed to the membrane and the solute mobility, in the membrane, increases with pressure are well predicted by the Extended MD-SF-PF model. A schematic profile of concentration variation for the p-chlorophenol-water system was shown in Figure 2.4.

For the toluene-water system, the solute molecules are still attracted to the membrane by the attractive potential forces; however, positive separations are obtained due to the smaller mobility of the solute molecules, as compared with the p-chlorophenol molecules. The overall concentration profile for such systems was shown in Figure 2.3.

Comparison of the parameters, for the three solutes in Tables 5.7 to 5.9, is tempting but dangerous due to the large confidence intervals. Note that θ_1 is always negative for the nondissociable organic solutes indicating solute-membrane affinity, and E is always positive indicating frictional hinderance on the solute molecules.

5.5 Simulations for the MD-FPM and FPM Relationships

The Modified Finely Porous Model (MD-FPM) was formulated in Section 3.4. due to the existence of some serious mistakes in the Finely Porous Model (FPM). In order to see how the MD-FPM relationship behaves differently from the FPM relationship, the three-parameter version of the two models (i.e., MD-FPM-3 and FPM-3) have been evaluated under a variety of simulated conditions. These results are discussed below.

5.5.1 Separation and flux ratio

The effect of K/b factor, which is a measure of membrane separation ability (i.e., the smaller the value of K/b the higher the separation), on membrane separation is illustrated in Figure 5.62 for both the FPM-3 and MD-FPM-3 relationships. The operating conditions are: $C_{A2} = 0.04840$ and 0.27151 kmol/m^3 of NaCℓ in water in Figures 5.62.a and 5.62.b, respectively, $\Delta P = 1500$ kPa, and T $= 25°$C; the membrane has a pore radius of 9.39×10^{-10} m. For both models, separation increases with
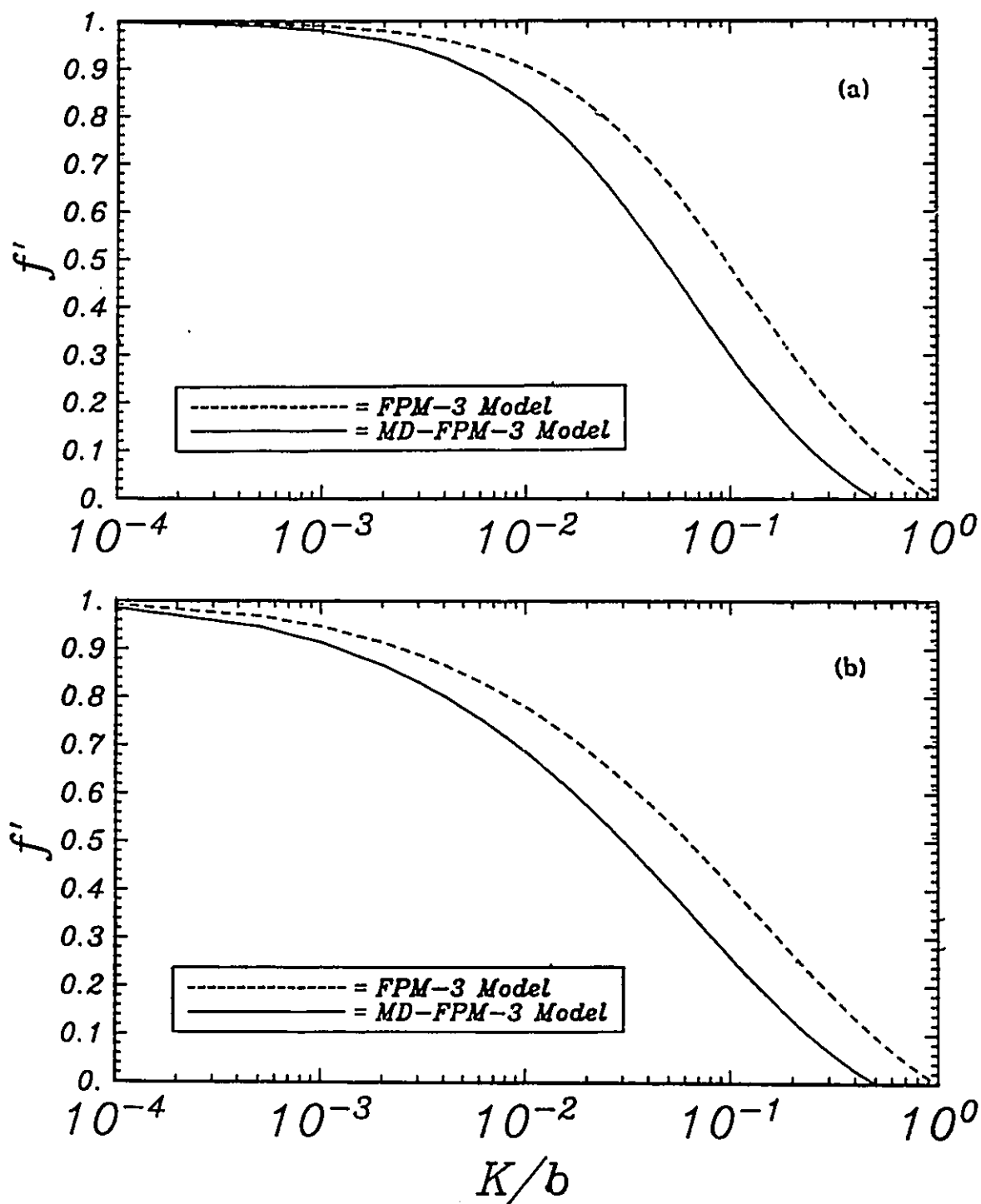
Figure 5.62: Effect of K/b ratio on membrane separation for NaCℓ-H₂O system as predicted by the MD-FPM model (solid line) and FPM model (dashed line): (a) $C_{A2}=0.04840$ kmol/m³, (b) $C_{A2}=0.27151$ kmol/m³. Other conditions are: $\Delta P=1500$ kPa, T=25°C, and $R_W=9.39\times10^{-10}$ m.

decreasing K/b (increasing potential according to Eqn.(3.10). Calculations are only done for K/b in the range 1.0 to 1.0×10^{-4} as normally K/b values for NaCℓ solute would fall in this range. These results are consistent with the limiting cases discussed in Section 3.4.3. It should be noted that, since K and b are both functions of pore size, then the results in Figure 5.62 (at a fixed pore size) imply a fixed b value (for the fixed solute NaCℓ) and a change in membrane potential as K/b changes (see Eqn.(3.10)). What is clear is the two models predict different separation values for the same value of K/b parameter; the FPM-3 model overpredicts separation values by up to 90%. Over the whole range, the separation is always predicted to be lower by the MD-FPM relationship than by the FPM relationship. This difference is caused by the correct inclusion of solute osmotic pressure and material balance by the MD-FPM relationship and by the inclusion of the diffusional component of the solute flux in the MD-FPM relationship that is ignored in the FPM relationship (i.e., the higher the solute flux the lower the separation). In the limit, with a small partition coefficient, K, or large friction factor, b, the MD-FPM and FPM relationships approach each other. Thus for very small pores, where the solute is almost completely rejected, the two models both converge to 100% separation as expected. This limit can also be reached when the membrane potential is very strong which results in a very small partition coefficient for the case of solute exclusion from the membrane. Figure 5.62.b illustrates similar information for the higher feed concentration of $C_{A2} = 0.27151$ kmol/m^3 of NaCℓ in water, keeping the other conditions the same as in Figure 5.62.a. The same trends, as in Figure 5.62.a, are predicted except the separation values are lower for this higher concentration case. The lower separation at the higher concentration is expected due to higher osmotic pressures and higher solute driving force at higher feed

concentrations. Again, the two models approach each other at lower values of K/b and the FPM model overpredicts the separation values due to the reasons stated above.

The following relationship between partition coefficient and membrane potential function, which is identical to Eqn.(3.59),

$$K = 2 \int_0^{1-\lambda} e^{-\Phi(\rho)} \rho \, d\rho \qquad (5.5)$$

is used together with the equation of potential function in MD-SF-PF model, Eqn.(3.44), with $\theta_2 = 1/2$ as determined in Section 5.2.4, to study the effect of membrane pore size on membrane performance as illustrated in Figure 5.63. The operating conditions are: $C_{A2} = 0.04840$ and 0.27151 kmol/m^3 of NaСℓ in water, $\Delta P = 1500$ kPa, T = 25°C and the potential parameter used is $\theta_1 = 53.73 \times 10^{-10}$ m which is a typical value for a reverse osmosis membrane. Figure 5.63.a illustrates how separation varies with pore size; as the pore size is increased the separation decreases. The decrease in separation is more pronounced for the higher feed concentration (i.e., the dashed line). These results are consistent with those in the literature (e.g., Sourirajan, 1970). Figure 5.63.b illustrates how the flux ratio N_T/N_P varies under the same conditions as in Figure 5.63.a. As the pore size is increased the flux ratio increases toward unity, and as the feed concentration is increased the ratio decreases due to osmotic pressure effects.

Figure 5.64 presents typical results for reverse osmosis membrane performance for the usual case of solute exclusion. Figure 5.64.a investigates the multiple effects of operating pressure, ΔP, and membrane pore size, R_W, on the separation, f', and the flux ratio, N_T/N_P, by the MD-FPM-3 relationship. The feed concentration is $C_{A2} = 0.04840$ kmol/m^3 of NaСℓ in water, and T = 25°C. The membrane potential parameter is the same as in Figure 5.63. As the operating pressure is increased the separation and flux ratio increase, and as the pore size is increased the
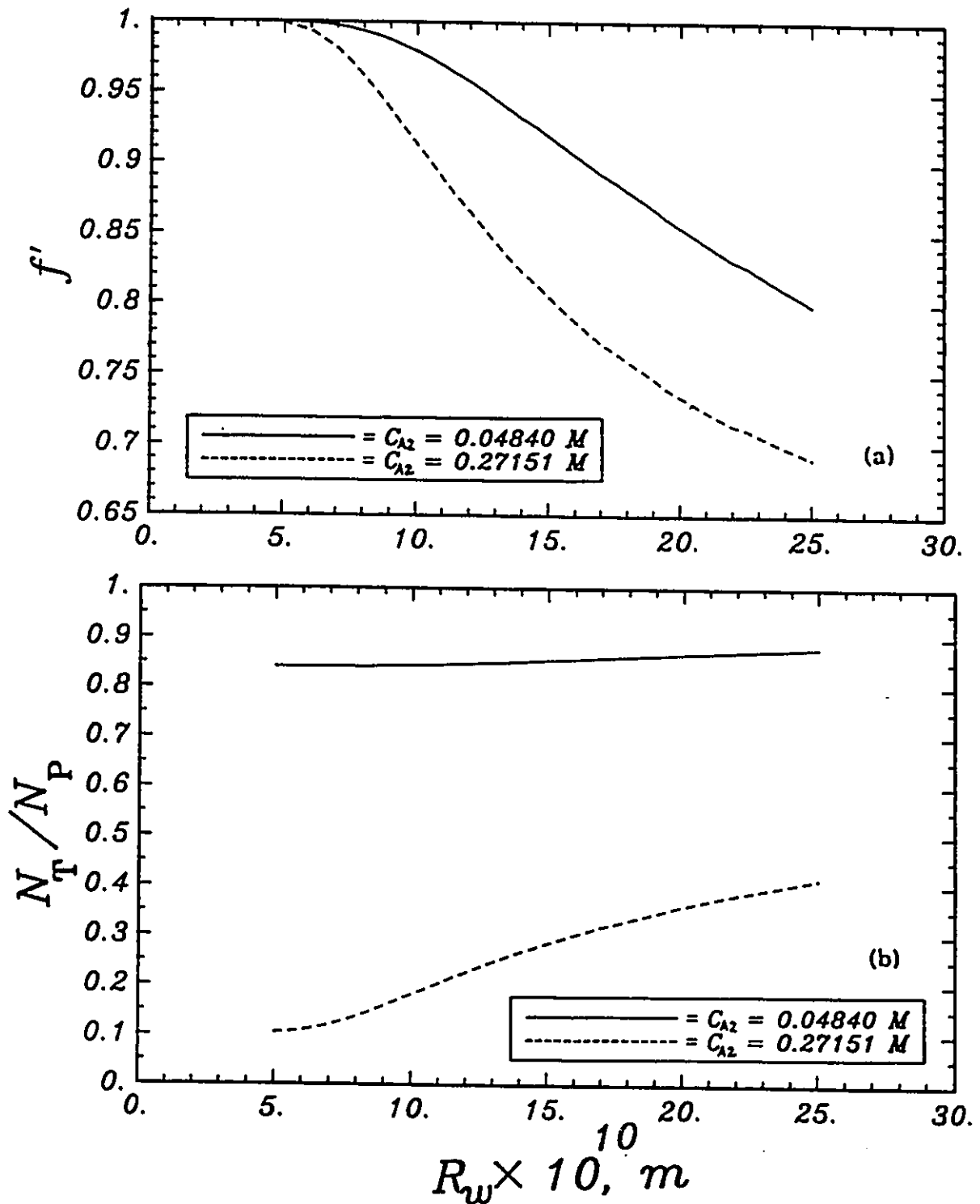
Figure 5.63: Effect of membrane pore size; with feed concentration as aparameter, on membrane performance for NaCℓ-H₂Osystem as predicted by MD-FPM model: (a) separation versus pore size, (b) flux ratio versus pore size. Conditions: $\Delta P = 1500$ kPa, $T = 25°C$, and $\theta_1 = 53.73 \times 10^{-10}$ m.
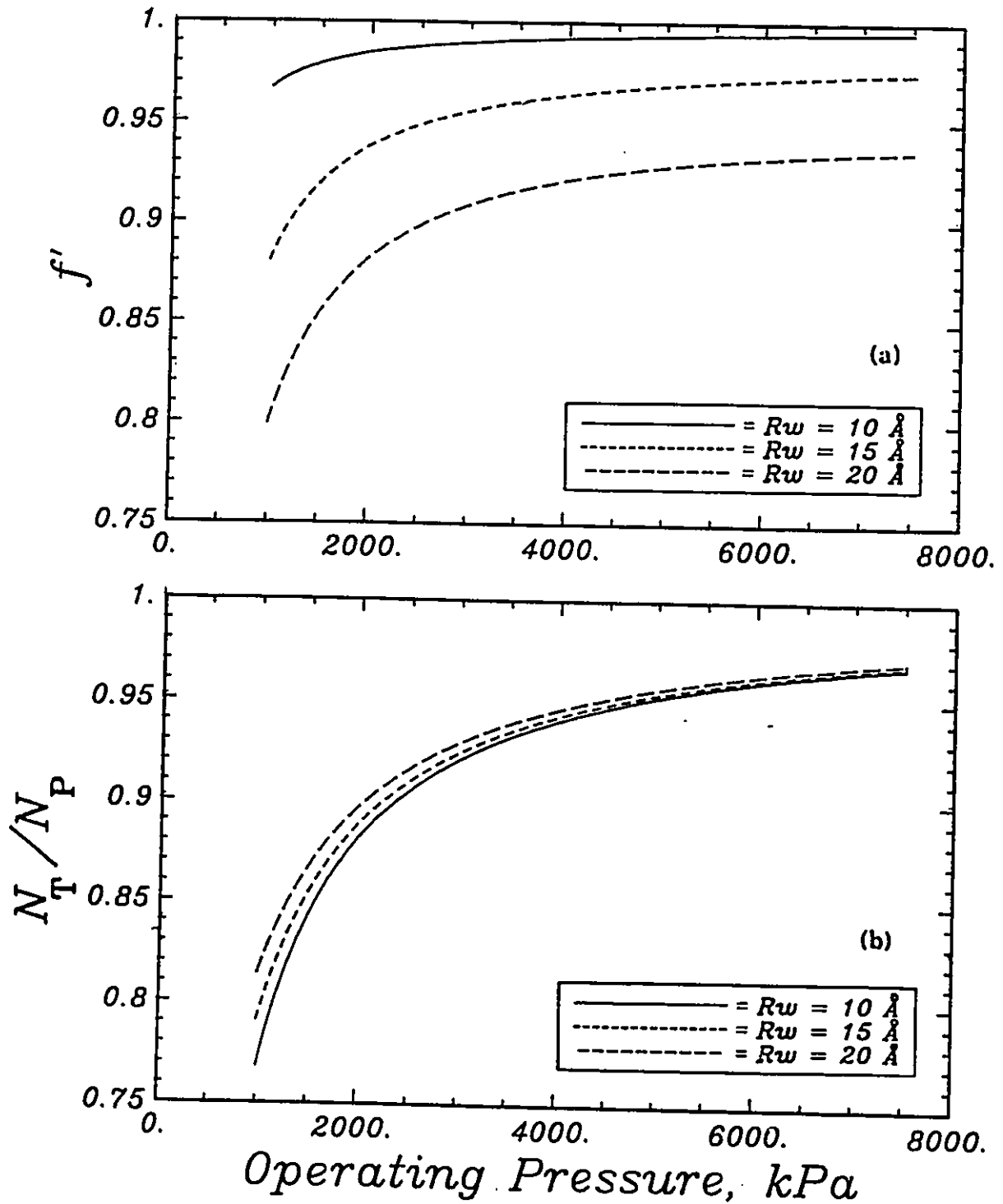
Figure 5.64: Effect of operating pressure, with pore size as a parameter, on membrane performance for NaCℓ-H_2O system as predicted by MD-FPM model: (a) separation versus pressure, (b) flux ratio versus pressure. Conditions: $C_{A2} = 0.04840$ kmol/m³, T = 25°C, and $\theta_1 = 53.73 \times 10^{-10}$ m.

separation decreases and the flux ratio increases. These are expected trends as observed experimentally and are similar to those predicted by MD-SF-PF model.

5.5.2   Concentration Profiles

This section considers the concentration profiles through the membrane as predicted by the MD-FPM-3 and FPM relationships. The concentration profiles are given by Eqn.(3.130) for the MD-FPM-3 relationship and Eqn.(B.II.7) for the FPM-3 relationship. In the MD-FPM model, since the differential equation for solute concentration is restricted to boundary values at the two endpoints of membrane, negative concentrations are never predicted. However, in the FPM relationship, because the differential equation in this model is restricted to only one end point of membrane and the other end point is free, negative values for solute concentration can be predicted, which is physically unrealistic.

To compare the two models in this respect, one set of experimental data from Jonsson and Boesen (1975) are examined as follows.

Choosing the DDS-800 membrane and 1% sucrose-water system, the data are: $C_{A2} = 0.03$ kmol/m^3, $C_{A2}/C_{A3} = 1.3444$, and $J_V = 1. \times 10^{-4}$ m/s. Using FPM-3 relationship, Jonsson and Boesen (1975) estimated: $R_W = 15 \times 10^{-10}$ m, $\tau/\varepsilon = 29.5 \times 10^{-6}$ m, $K = 0.76$, and $b = 1.362$. These data are used to determine the concentration profiles. The diffusivity data for sucrose systems are given in the literature (Cussler, 1984); for a 0.03 molar aqueous solution the value is $D_{AB} = 0.515 \times 10^{-9}$ m^2/s. Equations to determine the α values are Eqn.(3.131) in MD-FPM-3 relationship and Eqn.(3.128) using Eqn.(3.129) in FPM-3 relationship.

The results are shown in Figures 5.65.a and 5.65.b for the MD-FPM-3 and FPM-3 relationships, respectively. The MD-FPM-3 relationship predicts reasonable
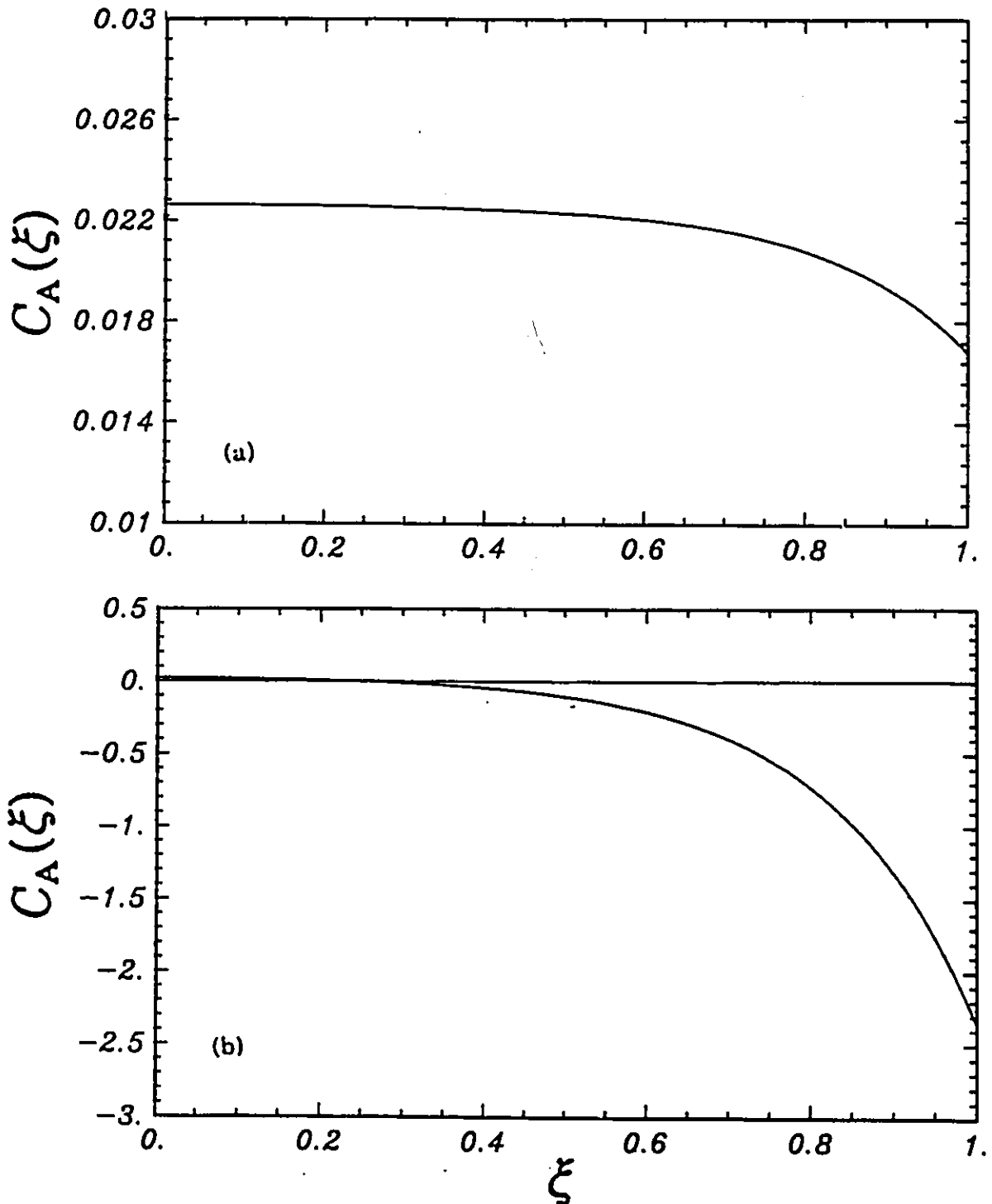
Figure 5.65: Concentration profile inside the pore for sucrose-water system as predicted by: (a) MD-FPM model, and (b) FPM model. Conditions (Jonsson and Boesen, 1975): feed concentration =1% sucrose ($C_{A2}=0.03$ kmol/m^3), $C_{A2}/C_{A3}=1.3444$, $K=0.76$, $R_W=15 \times 10^{-10}$ m, $b=1.362$, and $v/\varepsilon=2.95 \times 10^{-5}$ m.

values that satisfy the boundary conditions. However, the FPM-3 relationship predicts negative values for the concentration after $\xi > 0.2385$ inside the pore so that the boundary condition at $\rho = 1$ is not satisfied. Obviously, this situation is impossible. This result is a reflection of the incorrect form of the material balance used in the derivation of the FPM relationship as discussed in Section 3.4.1. Therefore, the concentration gradient, which drives the solute through the membrane, is calculated incorrectly for the FPM relationship and hence the membrane performance is also incorrectly calculated.

5.6   Concluding Remarks

Since the main results of the present dissertation, both theoretical and experimental, are included in this chapter (Chapter 5), the most important results are presented separately, as the conclusions of the dissertation, in Chapter 6.

CHAPTER 6

CONCLUSIONS

This dissertation has examined, in both theoretical and experimental aspects, the transport phenomena in reverse osmosis (RO) membranes with an emphasis on the role of temperature on RO membrane performance. The major conclusions of this research are summarized here.

A reasonable and powerful transport model has been derived based on the basic laws of transport phenomena which include solute and solution material balances, force balance on solute molecules inside the membrane, momentum balance on fluid inside the membrane, and a condition of thermodynamic equilibrium at the high and low pressure sides of the membrane. The model, called the Modified Surface Force-Pore Flow (MD- SF-PF) model, assumes that the membrane is porous, each pore is modeled as a perfect cylinder, and a potential field exists inside the membrane which is responsible for the solute rejection (or attraction) by the membrane. In order to employ the model to predict the real performance of a RO membrane, experimental data are needed to estimate the model parameters. The MD-SF-PF model, which is a two-dimensional model (in radial and axial pore coordinates), has three parameters: the average membrane pore size, R_W; a potential parameter which describes the interactions between the solute molecules and the polymeric material of the pore wall, θ_1; and a parameter which characterizes the physical structure of the skin layer of the membrane, τ/ϵ. For the case of Extended MD-SF-PF model, there are four parameters to be specified: R_W, θ_1, γ, and τ/ϵ. γ is the second potential parameter which takes the axial variation of the potential into account. To predict for membrane separation, f',

and flux ratio, N_T/N_P, only two parameters are needed for the MD-SF-PF model: R_W, and θ_1. For the case of Extended MD-SF-PF model, the parameters needed to predict for separation and flux ratio are: R_W, θ_1, and γ. These qualitative results are in complete agreement with the preferential sorption-capillary flow mechanism which states that a membrane separation should be determinable once the membrane pore size and the sorption phenomenon are known. In order to predict for absolute values of pure solvent (water) flux, N_P, and total solution flux, N_T, the structure-characterizing parameter, τ/ε, is needed. The models has been tested by simulations and true predictions for real systems, and the novelty and strong ability of the models have been shown. The models, as elucidated later in this chapter, can successfully predict for systems where most transport models fail.

The experimental plan has been designed in a manner to study the effects of temperature on membrane performance; the plan covers a wide range of system pressure and feed concentrations, as well. Three phases of experiments were performed as follows: Phase I includes experiments at the brackish water concentration level of NaCℓ in water (2000 ppm, with a few experiments at 5000-15 000 ppm) in the pressure range of 350-7000 kPa and the temperature range of 5-60°C; Phase II consists of experiments with other 1-1 electrolytes (aqueous solutions of potassium chloride, lithium chloride, and lithium nitrate) at the brackish water concentration level (i.e., 2000 ppm), 25°C temperature, and in the pressure range of 500- 4000 kPa; and Phase III includes experiments at sea water concentration level (i.e., 35 000 ppm) of NaCℓ in water in the pressure range of 4000-7000 kPa and the temperature range of 5-60°C. All of the experiments were done with four thin-film composite, aromatic

polyamide, FT30 commercial RO membranes: two SW30HR (Sea Water-High Rejection) and two BW30 (Brackish Water) membranes.

The experiments reveal that temperature affects the performance of aromatic polyamide FT30 reverse osmosis membranes in a variety of ways. At the brackish water concentration level of 2000 ppm NaCℓ in water (Phase I), separation decreases with temperature at lower operating pressures (i.e., 350-4000 kPa) and becomes independent of temperature at higher operating pressures (i.e., 4000-7000 kPa); the solution flux, however, increases with temperature dramatically. Therefore, higher fluxes can be obtained at temperatures above room temperature with virtually the same separation values as in lower temperatures provided that the system temperature is not too high since the disadvantageous effect of membrane compaction (which is a reduction in permeation flux at high operating pressures and/or temperatures) becomes significant at high temperatures and pressures. Membrane compaction was apparent at all pressures and temperatures, in Phases I and III. In addition to the compaction effect, there seems to be an additional disadvantageous effect at temperatures above 35-40°C, a decline of water permeability. This permeability decline could be caused by some separate change in the mechanism of transport of water at temperatures above 35-40°C or it could be the result of membrane fouling at the higher temperatures.

Similar phenomena happen at sea water concentration level (Phase III): separation decreases, with an increase in temperature, at the lower operating pressures (i.e., 4000 and 7000 kPa) and is temperature independent at the highest operating pressure (i.e., 7000 kPa); the solution flux increases remarkably with

temperature, and compaction is significant at high temperatures and pressures; the additional effect of flux decline also happens at temperatures above 35-40°C.

In both Phases I and III, the BW30 membranes show a larger decrease in flux than the SW30 membranes, which is typical that higher flux membranes (i.e., the BW30 membranes) are more susceptible to changes in permeability. Also, in both Phases I and III, the higher flux membranes (i.e., the BW30 membranes) have lower separations than the lower flux membranes (i.e., the SW30 membranes).

The water permeability coefficient at zero compaction could be described as a function of temperature by an Arrhenius relationship in the two temperature regions of 5-40 and 40-60°C, for all the membranes. The apparent activation energies calculated were larger for the SW30 membranes than for the BW30 membranes, which reflects the higher resistance to water flux in the lower permeable (SW30) membranes. The apparent activation energies were higher in the lower temperature range than in the higher temperature range for both the SW30 and the BW30 membranes.

The Phase I experiments were used to determine the MD-SF-PF model parameters for each of the aromatic polyamide FT30 membranes. This was done based on the minimization of the difference between the experimental and the model values for separation, using the nonlinear optimization routine UWHAUS. In order to solve the differential equation of the model (which, in turn, is used in the optimising code many times), an efficient and precise computer code has been developed, based on the "orthogonal collocation" method of weighted residuals. Once the model parameters are determined for a membrane, the model may be employed to predict RO membrane performance at other operating conditions.

The MD-SF-PF model parameters have been determined for each of the aromatic polyamide FT30 membranes, as described above, and then used in the model to predict membrane performance at other operating conditions in Phases I, II, and III. The agreement between the model predictions and all the experimental data is excellent, as described later in this chapter. The power of the MD-SF-PF model to truly predict RO membrane performance suggests, but does not prove, that the proposed transport mechanism in RO membranes is correct.

The estimated average pores size for the SW30 and BW30 types of FT30 membranes are about 1.0 and 1.2 nm, and the estimated potential parameter values, θ_1, are about 5.4 and 6.2 nm for the SW30 and BW30 membranes, respectively. Therefore, the magnitude of the potential field at the pore centerline is larger for the SW30 membranes than for the BW30 membranes (i.e., $\theta_1/R_W = 5.4$ for SW30 membranes and $\theta_1/R_W = 5.1$ for the BW30 membranes); the stronger potential field in the SW30 membranes is mainly responsible for the higher separations by the SW30 membranes as compared with the BW30 membranes.

The MD-SF-PF model was found to predict the effects of feed concentration and operating pressure, on membrane performance, very well. The SF-PF model, however, failed to predict the effect of feed concentration on membrane performance. The concentration profile inside the pore, by the MD-SF-PF model, was shown to be reasonable while the concentration profile in the SF-PF model was unrealistic.

The MD-SF-PF model, with the model parameters determined under Phase I conditions, were employed to predict for the experimental conditions of Phase II (i.e., different 1-1 electrolytes). The model could reasonably predict the performance for all the new systems of Phase II. The model predicted that, at any

system pressure, the separation varied in the order of $KC\ell < NaC\ell < LiC\ell < LiNO_3$ which is consistent with expectation for the slightly negatively charged FT30 membranes. The potential parameter θ_1 is expected to be different for different solute systems; however, the MD-SF-PF model could predict for the other 1-1 electrolyte systems, based on the potential parameter for $NaC\ell$ system, suggesting the θ_1 parameter might be about the same for all the tested 1-1 electrolytes. The importance of the model predictions is mainly that the MD-SF-PF model can be used to predict for many systems, which can minimize the large expenses of the experimental studies with different solute-membrane systems.

The MD-SF-PF model was extended to a temperature-dependent form by incorporating the temperature dependencies of all the physical properties of the membrane system and assuming that the pore size, R_W, and the potential parameter, θ_1, are temperature independent; the independence of R_W and θ_1 from temperature was theoretically justified. The temperature-extended model has been found to well predict each membrane performance under the experimental conditions of Phases I and III, based on the MD-SF-PF model parameters determined at 25°C and 2000 ppm feed concentration. For the temperature-extended model, the compaction effect has no effect on the separation, f', and the total solution to pure solvent flux ratio, N_T/N_P, so that these two characteristics can be determined independent of the compaction effect; this result was verified experimentally. On the other hand, the compaction effect has been modeled, separately, and the model can be used to determine the absolute values of the fluxes (i.e., N_T and N_P). The compaction effect was modeled in terms of a temperature-dependent compaction coefficient, m, and a temperature-dependent compaction-free permeability coefficient for solvent. The solvent permeability coeffi-

cient was modeled as a linear function of pressure and a nonlinear function of temperature, and the relating coefficients were estimated from experimental results. The nonlinear relationship between the solvent permeability coefficient and temperature was modeled based on independent models for temperature dependency of the compaction coefficient and the compaction-free permeability coefficient of solvent. An alternative approach to modeling the compaction effect was suggested as an Arrhenius type of relationship for the change of the t/ε parameter with temperature. Once the information on the modeling of compaction effect is available, the compaction effect can be predicted and the absolute values of the fluxes (i.e., N_T and N_P) can be determined; such information has been determined for the SW30 and BW30 membranes, and the model predictions for absolute fluxes agree very well with the experimental results.

The MD-SF-PF model predicts the importance of convection and molecular diffusion mechanisms in terms of the dimensionless fluid velocity profile, $\alpha(\rho)$, which is the ratio of fluid convection to molecular diffusion fluxes and may be considered as a kind of Peclet number (i.e., for $\alpha \rightarrow 0$ the fluid transport is mainly by diffusion, and for $\alpha \rightarrow 1$ the transport is mainly by convection). It has been shown by the model that when the system pressure is high (e.g., 7000 kPa), at room temperature, convection becomes as important as diffusion in the fluid transport. However, in most cases, the operating pressure is such that the diffusion mechanism is the dominant phenomenon for the transport of solvent. The solute transport is mainly convective, according to the model. The solute convective flow is mainly induced by the diffusive flow of the solvent phase.

The MD-SF-PF model has been reformulated and extended to a more general form which includes the difficult case of solute-membrane affinity. The model has been extended in three ways: i) the pressure-induced solute transport term has been included in the equation of solute chemical potential; ii) an axial dependency (together with a concentration dependency) to the membrane potential function has been added, which allows for the model to have different partition coefficients at the two sides of the membranes; and iii) the hydrodynamic friction between the solute and the pore wall, b, has been allowed to vary as a function of radial position inside the pore.

The Extended MD-SF-PF model has been employed to describe the performance of cellulose acetate membranes used to separate dilute aqueous solutions of toluene, cumene, and p-chlorophenol. The model describes these data reasonably well. Simulation studies indicate that the model can well describe separations decreasing from positive to negative values as the system pressure is increased (such as for the cumene-water system). Previously, only the 4-parameter version of the finely porous model was found to describe this case; however, as mentioned below, the finely porous model has been found to suffer from serious mistakes which makes the model doubtful to be used any more. Therefore, the Extended MD-SF-PF model is the only model which can be used to describe and/or predict any kind of solute-membrane affinity system of reverse osmosis.

Simulation studies with the Extended MD-SF-PF model indicate that membrane separation is mainly controlled by the potential field inside the membrane, and this potential controls the partitioning effect. Also, this model illustrates that once the organic solute molecules are quickly sorbed by the RO membrane the solute

molecules creep slowly through the membrane pores (close to the pore wall) due to the large attraction forces between the solute molecules and the membrane material; different degrees of solute mobilities are possible inside the membrane pores.

The success of the family of MD-SF-PF model (which includes the original MD-SF-PF model, the Extended MD-SF-PF model, and the temperature-extended MD-SF-PF model) reveals the advantages of these models in describing and predicting the performance of RO membranes and the possible correctness of the transport mechanism suggested by the models. The models, although complex, take into account the interactions between the solute, solvent, and the membrane in a manageable way and use the basic principles of transport phenomena. With the computer code developed, the family of MD-SF-PF models can be easily used to describe and/or predict RO membrane performance for many solute-solvent-membrane systems. This predictive power can be used to reduce the time needed to evaluate experimentally membrane performance for different conditions. Regarding the problem of system design, the family of MD-SF-PF models may be used to describe the performance of RO modules.

As a supplement, the Finely Porous Model (FPM) has been corrected to a form called the Modified Finely Porous Model (MD-FPM). Simulation studies suggest that the corrected model has significant differences from the original FPM relationship. The model needs to be evaluated for different systems. The advantage of the MD-FPM model over the MD-SF-PF model is that the MD-FPM model takes much less CPU time to be solved due to its simplicity of governing equations as compared with the MD-SF-PF model.

CHAPTER 7

RECOMMENDATIONS

Despite the work done in this research and in the literature, more work still needs to be done in order to fully understand the different aspects of transport phenomena in reverse osmosis (RO) membranes. The following is a list of recommendations for further research:

i)   The family of the MD-SF-PF models can be employed to test different solute-membrane systems, to determine the exact behaviour of these models. More experimental data are needed, especially with other kinds of RO membranes, to test the validity of the transport models for different RO membranes.

ii)   One goal in modeling of RO transport phenomena is to predict the membrane performance from the very basic information of the membrane system, such as the surface charge density (for the case of electrolytes) or from van der Waals interaction force (using the Hamaker constant) for the case of neutral organic solutes. Therefore, the relationships between the potential function and the membrane pore size, in the family of MD-SF-PF models, with the physicochemical characteristics of the membrane (such as the surface charge density) need to be determined.

iii)   The real world is usually confronted with multi-solute systems. Therefore, one very useful research program would be the extension of the family of MD-SF-PF models from binary systems to multi-solute systems in a manageable way.

iv) It is recommended to use the family of MD-SF-PF models for RO module design purposes. This needs integrating the governing equations over the length of the RO module considering the fluid dynamics and geometry of the module.

v) Although the present research is a guideline for modeling in reverse osmosis, it is interesting to see how the models behave for the case of ultrafiltration (UF) and microfiltration (MF) membranes. It is expected that, in the case of UF and MF, the pore size should be much larger and the potential function should be much smaller (almost zero) than for the case of reverse osmosis, and the solute size should play a more important role as a steric hindrance by the membrane.

NOMENCLATURE

a'	:	constant in Eqn.(2.8), dimensionless
a_A	:	activity of solute or salt defined in Eqn.(3.62), dimensionless
a_0, a_1, a_2	:	constants in Eqn.(3.88)
a_1, a_2	:	constants in Eqn.(2.61)
A	:	pure solvent permeability coefficient, kmol/m^2 s kPa
A_i	:	pre-exponential factor in Eqn.(2.50), kmol/m^2 s
$A_{i,j}$	:	collocation parameter defined by Eqn.(2.73)
$A_{i,j}{}^\bullet$	:	collocation parameter defined by Eqn.(3.145)
A^0	:	pure solvent permeability coefficient at zero pressure, kmol/m^2 s kPa
$\mathbf{A}$	:	1) potential constant in Eqn.(2.45), m
		2) matrix of first derivatives for orthogonal collocation
b	:	friction parameter defined in Eqn.(2.29), dimensionless
b'	:	constant in Eqn.(2.8), dimensionless
$B_{i,j}$	:	collocation parameter defined by Eqn.(2.74)
$B_{i,j}{}^\bullet$	:	collocation parameter defined by Eqn.(3.144)
$\mathbf{B}$	:	potential parameter in Eqn.(2.46), m^3
C	:	molar density of solution, kmol/m^3
$C_A(r,z)$	:	concentration of solute inside a pore, kmol/m^3
C_{Ai}	:	solute concentration at position i, kmol/m^3
C_{ij}	:	concentration of i at position j, kmol/m^3
$C_{i,j}$	:	collocation parameter defined by Eqn.(3.143)
$C_A(\rho)$	:	parameter defined in Eqn.(2.40), dimensionless

d	:	distance from solute molecule to the pore wall, m
D_{AB}	:	solute diffusivity in free solution, m^2/s
D_{AM}	:	solute diffusivity inside the pore, m^2/s
D_{BM}	:	solvent diffusivity in the membrane, m^2/s
e	:	charge of proton, kC
E	:	apparent activation energy, kJ/kmol
E_i's	:	constants in Eqn.(2.49)
E_t	:	apparent activation energy for τ/ε, in Eqn.(3.90), kJ/kmol
E	:	friction parameter in Eqn.(3.83), m
f	:	separation defined by Eqn.(2.4) or Eqn.(2.5), dimensionless
f'	:	theoretical separation defined by Eqn.(2.6), dimensionless
F	:	objective function defined by Eqn.(5.2)
F_N	:	residual function defined by Eqn.(2.66)
F_A	:	total force driving solute through the pore, kJ/m kmol
F_{AB}	:	frictional force between solute and solvent, kJ/m kmol
F_{AM}	:	frictional force between solute and the pore wall, kJ/m kmol
F_i	:	driving force, in Eqn.(2.11)
g	:	constant of integration in Eqn.(B.II.5), $kmol/m^3$
G	:	1) constant of integration in Eqn.(B.II.1), $kmol/m^3$
		2) objective function defined by Eqn.(5.3)
h	:	distance between two parallel, flat plates, m
H	:	constant of integration in Eqn.(B.II.3), $kmol/m^3$
$I(\xi)$	:	integrating factor defined by Eqn.(B.II.2), dimensionless
J_A	:	vector of solute flux through a single pore, $kmol/m^2$ s
$J_{A,r}$	:	radial component of solute flux through a single pore, $kmol/m^2$ s

$J_{A,z}(r)$:   axial component of solute flux through a single pore, $kmol/m^2 \ s$

J_i .   1)   radially-averaged flux of component i through a single pore, $kmol/m^2 \ s$

           2)   flux of component i through membrane, in Eqn.(2.11)

J_V :   solution volumetric flux through membrane, $m^3/m^2 \ s$

k :   mass transfer coefficient, m/s

k_0 :   Boltzmann's constant, kJ/K

K :   partition coefficient, dimensionless

$K_i(\rho)$:   partition coefficient at position i defined by Eqns.(3.56) and (3.57), dimensionless

K_i :   average partition coefficient at position i defined by Eqns.(3.59) and (3.60), dimensionless

$K^*(\rho)$:   parameter defined by Eqn.(3.70), dimensionless

$\ell_i(x)$:   Lagrange interpolation polynomial, defined by Eqn.(2.70)

ℓ_p :   hydraulic permeability, defined in Eqn.(2.13)

ℓ_π :   osmotic permeability, in Eqn.(2.15)

ℓ_1 :   definite integral defined by Eqn.(3.36), dimensionless

ℓ_2 :   definite integral defined by Eqn.(3.37), dimensionless

ℓ_3 :   definite integral defined by Eqn.(3.77), dimensionless

$L_{i,j}$:   coefficient in Eqn.(2.11)

m :   compaction coefficient defined by Eqn.(3.87), $kmol/m^2 \ s \ kPa^2$

m^*, n^* :   constants in Eqn.(2.63)

m_{ij} :   molality of i at position j, kmol/kg

n :   ionic concentration where double-layer potential is zero, m^{-3}

n_i :   mass flux of component i through membrane, $kg/m^2 \ s$

N	:	number of interior collocation points
N_i	:	molar flux of component i through membrane, $kmol/m^2$ s
p_i	:	permeability of component i, in Eqns.(2.17) and (2.18)
P	:	hydrostatic pressure, kPa
$P_N^{(\alpha,\beta)}$	:	trial function in collocation; see Eqn.(2.68)
$P(\rho,\xi)$	:	hydrostatic pressure inside the pore, kPa
P_i	:	pressure at pore inlet, kPa
P_o	:	pressure at pore outlet, kPa
ΔP	:	pressure difference across the membrane, kPa
ΔP	:	parameter defined by Eqn.(3.26), dimensionless
q_i	:	constant in Eqn.(2.63)
r	:	cylindrical coordinate normal to the pore wall, m
R	:	gas constant, kJ/kmol K
R^i	:	residual in region i
R_i	:	average radius of i, m
Re	:	Reynolds number, in Eqn.(2.8), dimensionless
Sc	:	Schmidt number, in Eqn.(2.8), dimensionless
Sh	:	Sherwood number in Eqn.(2.8), dimensionless
T	:	temperature, K
$u_i(r)$	:	velocity of i inside the pore, m/s
U	:	1) general parameter in Eqn.(2.53)
		2) interaction energy defined by Eqn.(3.84), kJ/m^2
v_i	:	partial molar volume of component i, $m^3/kmol$
x	:	1) coordinate along fluid flow, in Eqns.(2.17) and (2.18)
		2) general independent variable, in Eqns.(2.61) to (2.74)

Δx	:	membrane thickness, m
X_i	:	mole fraction of component i, dimensionless
X_{ij}	:	mole fraction of component i at position j, dimensionless
y	:	general dependent variable
Y	:	general approximating polynomial
z	:	cylindrical coordinate parallel to the pore wall, m
z^+	:	electrochemical valence of cation, dimensionless
z^-	:	electrochemical valence of anion, dimensionless

Greek Letters

α	:	fluid velocity defined in Eqn.(3.100), dimensionless
$\alpha(\rho)$	:	fluid velocity defined in Eqn.(2.37), dimensionless
α_B	:	solvent velocity defined in Eqn.(3.115), dimensionless
β_1	:	parameter defined in Eqn.(3.25), dimensionless
β_1'	:	parameter defined in Eqn.(2.39), dimensionless
β_2	:	parameter defined in Eqn.(2.38), dimensionless
δ_i	:	constant in Eqn.(2.65)
$\delta_{i,N}$	:	Kronecker delta, Eqn.(2.67)
γ	:	potential parameter in Eqn.(3.82), dimensionless
ε	:	fractional pore area of membrane, dimensionless
ε_0	:	free-space permittivity,
ε_r	:	relative permittivity of solvent (water),
η	:	solution viscosity, kPa s
θ_1	:	potential parameter defined in Eqns.(3.44) and (3.82), m
θ_2	:	potential parameter defined in Eqn.(3.44), dimensionless

Θ	:	dimensionless time defined by Eqn.(3.142)
κ	:	Debye length reciprocal, defined by Eqn.(3.85), m^{-1}
λ	:	parameter defined in Eqn.(2.47), dimensionless
μ_A	:	chemical potential of solute, in Eqn.(3.62), kJ/kmol
$\mu_A{}^0$	:	chemical potential of solute at standard state, kJ/kmol
ν^+	:	number of kmol of cations from dissociation of 1 kmol salt, dimensionless
ν^-	:	number of kmol of anions from dissociation of 1 kmol salt, dimensionless
ξ	:	axial coordinate defined by Eqn.(3.19), dimensionless
$\pi(r,z)$	:	osmotic pressure inside the pore, kPa
$\pi(z)$	:	radially-averaged osmotic pressure inside the pore, kPa
π_i	:	osmotic pressure of solution at i, kPa
$\Delta\pi$	:	parameter defined by Eqn.(3.27), dimensionless
ρ	:	1) radial coordinate defined by Eqn.(2.36), dimensionless
		2) mass density of solution, in Eqn.(3.142), kg/m^3
σ	:	1) Staverman coefficient, in Eqn.(2.3), dimensionless
		2) surface charge density, kC/m^2
$\sigma_2(\rho)$	:	parameter defined by Eqn.(3.72), dimensionless
$\sigma_3(\rho)$	:	parameter defined by Eqn.(3.73), dimensionless
τ	:	average pore length taking tortuosity into account, m
τ_{rz}	:	cylindrical-coordinate shear stress, kPa
$\phi(r)$	:	potential function, kJ/kmol
$\phi(r,z)$	:	potential function in Extended MD-SF-PF model, kJ/kmol
$\Phi(\rho)$	:	potential function defined by Eqn.(2.41), dimensionless

$\Phi(\rho,\xi)$:   potential function defined by Eqn.(3.58), dimensionless

X_{ij} :   friction constant, between i and j, kJ s/m^2 kmol

ω :   parameter in Eqn.(2.14)

$\omega(\rho)$:   parameter defined by Eqn.(3.71), dimensionless

Superscripts

S   :   surface

V   :   volume

α, β :   orders of a Jacobi Polynomial

(1)   :   first derivative

(2)   :   second derivative

Subscripts

A   :   solute

B   :   solvent

exp'l   :   experimental

i   :   ith, of ith order

ℓn :   log-mean average

M   :   membrane

model   :   predicted by model

N   :   Nth, of Nth order

P   :   pure solvent

ref   :   reference

T   :   total solution

W   :   pore wall

1   :   feed (bulk) solution

2   :   boundary layer solution

3   :   permeate solution

REFERENCES

Agrawal, J.P., and Sourirajan, S., "Specification, Selectivity, and Performance of Porous Cellulose Acetate Membranes in Reverse Osmosis", Ind. Eng. Chem. Proc. Des. Dev., 8(4), 439-449 (1969).

Anderson, J.E., Hoffman, S.J., and Peters, C.R., "Factors Influencing Reverse Osmosis Rejection of Organic Solutes from Aqueous Solutions", J. Phys. Chem., 76, 4006- 4011 (1972).

Anderson, J.L., and Malone, D.M., "Mechanism of osmotic flow in porous membranes", Biophys. J., 14, 957-982 (1974).

Anderson, J.L., and Quinn, J.A., "Restricted Transport in Small Pores: A Model for Steric Exclusion and Hindered Particle Motion", Biophys. J., 14, 130-150 (1974).

Applegate, L.E., "Membrane Separation Processes", Chem. Eng., June 11, 64-89 (1984).

Banks, W., and Sharples, A., "Studies on Desalination by Reverse Osmosis: III. Mechanism of Solute Rejection", J. Appl. Chem., 16, 153-158 (1966).

Bean, C.P., "The Physics of Porous Membranes: Neutral Pores", in: "Membranes: A Series of Advances", G. Eisenmen, Ed., Vol. 1, Marcel- Dekker, Inc., New York, NY (1972).

Beck, R.E., and Schultz, J.S., "Hindrance of Solute Diffusion within Membranes as Measured with Microporous Membranes of Known Pore Geometry", Biochem. Biophys. Acta, 255, 273-303 (1972).

Belfort, G., "Membrane Modules: Comparison of Different Configurations Using Fluid Mechanics", J. Memb. Sci., 35, 245-270 (1988).

Bhattacharyya, D., Jevtitch., M., Schrodt, J.T., and Fairweather, G., "Prediction of Membrane Separation Characteristics by Pore Distribution Measurements and Surface Force-Pore Flow Model", Chem. Eng. Commun., 42, 111-128 (1986).

Bird, R.B., Stewart, W.E., and Lightfoot, E.N., "Transport Phenomena", John Wiley and Sons, Inc., New York, NY (1960).

Bouchard, C., and Lebrun, R., "Synthesis of Concentration Polarization and Surface Force-Pore Flow Models in Membrane Separation", Proc. Int. Memb. Conf. 25th Anniv. Memb. Res. in Canada, M. Malaiyandi, O. Kutowy, and F. Talbot, Eds., Ottawa, Canada, September 24-26, 295-311 (1986).

Breton, E.J. Jr., "Water and Ion Flow Through Imperfect Osmotic Membranes", Office of Saline Water, U.S. Dept. of the Interior, Res. & Dev. Prog. Rept. 16, April (1957).

Brandon, C.A., and Samfield, M., "Application of High-Temperature Hyperfiltration to Unit Textile Processes for Direct Recycle", Desalination, 24, 97-112 (1978).

Burghoff, H.G., Lee, K.L., and Pusch, W., "Characterization of Transport Across Cellulose Acetate Membranes in the Presence of Strong Solute- Membrane Interactions", J. Appl. Polym. Sci., 25, 323-347 (1980).

Burghoff, H.G., and Pusch, W., "Thermodynamic and Mechanistic Characterization of Water Sorption in Homogeneous and Asymmetric Cellulose Acetate Membranes", J. Appl. Poly. Sci., 20, 789-797 (1976).

Cadotte, J.E., "Evolution of Composite Reverse Osmosis Membranes", in "Material Science of Synthetic Membranes", D.R. Lloyd, Ed., ACS Symposium Series 269, Washington, D.C. (1985).

Cadotte, J.E., and Peterson, R.J., "Thin-Film Composite Reverse-Osmosis Membranes: Origin, Development, and Recent Advances", in "Synthetic Membranes", A.F. Turbak, Ed., Vol. 1, ACS symp. ser., Washington, D.C. (1980).

Cadotte, J.E., Petersen, R.J., Larson, R.E., and Erickson, E.E., "A New Thin-Film Composite Sea Water Reverse Osmosis Membrane", Desalination, 32, 25-31 (1980).

Chan, K., Matsuura, T., and Sourirajan, S., "Interfacial Forces, Average Pore Size and Pore Size Distribution of Ultrafiltration Membranes", Ind. Eng. Chem. Prod. Res. Dev., 21, 605- 612 (1982).

Chen, J.-Y., Nomura, H., and Pusch, W., "Temperature Dependence of Membrane Transport Parameters in Hyperfiltration", Desalination, 46, 437-446 (1983).

Connell, P.J., "Modeling of Reverse Osmosis Transport in the Presence of Strong Solute- Membrane Affinity at Different Temperatures Using the Finely Porous Model", M. Eng. Thesis, McMaster University (1986).

Connell, P., and Dickson, J.M., "Modeling Reverse Osmosis Separations with Strong Solute-Membrane Affinity at Different Temperatures Using the Finely Porous Model", J. Appl. Poly. Sci., 35(5), 1129-1148 (1988).

Cussler, E.L., "Diffusion: Mass Transfer in Fluid Systems", Cambridge University Press, Cambridge (1984).

Dale, M.C., and Okos, M.R., "Reverse Osmosis Membrane Performance as Affected by Temperature and Pressure", Ind. Eng. Chem. Prod. Res. Dev., 22, 452-456 (1983).

Daniels, F., and Alberty, R.A., "Physical Chemistry", 3rd ed., John Wiley and Sons, Inc., New York, NY (1972).

Deen, W.M., Bohrer, M.P., and Epstein, N.B., "Effects of Molecular Size and Configuration on Diffusion in Microporous Membranes", AIChE J., 27, 952-959 (1981).

Dickson, J.M., "Reverse Osmosis Transport Phenomena in the Presence of Strong Solute-Membrane Affinity", Ph.D. Thesis, Virginia Polytechnic Institute and State University (1985).

Dickson, J.M., "Fundamental Aspects of Reverse Osmosis", in "Reverse Osmosis Technology: Application for High-Purity-Water Production", B.S. Parekh, Ed., Marcel Dekker, Inc., New York, NY (1988).

Dickson, J.M., Babai-Pirouz, M., and Lloyd, D.R., "Aromatic Hydrocarbon-Water Separations by a Pressure-Driven Membrane Separation Process", Ind. Eng. Chem. Process Des. Dev., 22, 625-632 (1983).

Dickson, J.M., Matsuura, T., and Sourirajan, S., Unpublished data (1976).

Dickson, J.M., Matsuura, T., and Sourirajan, S., "Transport Characteristics in the Reverse Osmosis System p- Chlorophenol-Water- Cellulose Acetate Membrane", Ind. Eng. Chem. Process Des. Dev., 18, 641-647 (1979).

Dickson, J.M., and Mehdizadeh, H., "Overview of Reverse Osmosis for Chemical Engineers. Part I: Fundamentals of Membrane Mass Transfer", J. Eng. Islamic Rep. Iran, 1(4), 163-179 (1988).

Dickson, J.M., and Mehdizadeh, H., "Overview of Reverse Osmosis for Chemical Engineers. Part II: Applications of Transport Models", J. Eng. Islamic Rep. Iran, accepted with revision (1989).

Dresner, L., "Electrokinetic Phenomena in Charged Microcapillaries", J. Phys. Chem., 67, 1635- 1641 (1963).

Fair, J.C., and Osterle, J.F., "Reverse Electrodialysis in Charged Capillary Membranes", J. Chem. Phys., 54, 3307-3316 (1971).

Faxen, H., "Die Bewegung einer starren Kugel langs der Achse eines mit zahrer Flussigkeit gefullten Rohres", Arkiv. Mat. Astron. Fys., 17(27) (1923).

Ferry, J.D., "Statistical Evaluation of Sieve Constants in Ultrafiltration", J. Gen. Physiol., 20, 95-104 (1936).

Finlayson, B.A., "Nonlinear Analysis in Chemical Engineering", McGraw-Hill, New York, NY (1980).

Glueckauf, E., "On the Mechanism of Osmotic Desalting with Porous Membranes", Proc. First Int. Symp. on Water Desalination, Washington, D.C., U.S. Dept. Interior, Office of Saline Water, 1, 143-156 (1965).

Glueckauf, E., "The Distribution of Electrolytes Between Cellulose Acetate Membrane and Aqueous Solutions", Desalination, 18, 155-172 (1976).

Govindan, T.S., and Sourirajan, S., "Reverse Osmosis Separation of Some Inorganic Salts in Aqueous Solution Using Porous Cellulose Acetate Membranes", Ind. Eng. Chem. Proc. Des. Dev., 5(4), 422-429 (1966).

Gross, R.J., and Osterle, J.F., "Membrane Transport Characteristics of Ultrafine Capillaries", J. Chem. Phys., 49(1), 228-234 (1968).

Hindmarsh, A.C., "ODEPACK, a systematized collection of ODE solvers", in "Scientific Computing", R.S. Stepleman et al., Eds., North-Holland, Amsterdam (1983).

Iberall, A., and Schindler, A., "Physics of Membrane Transport", General Technical Services, Inc., Upper Darby, Pa. (1973).

Jacazio, G., Probstein, R.F., Sonin, A.A., and Yung, D., "Electrokinetic Salt Rejection in Hyperfiltration Through Porous Materials: Theory and Experiment", J. Phys. Chem., 76(26), 4015-4023 (1972).

Jonsson, G., "Methods for Determining the Selectivity of Reverse Osmosis Membranes", Desalination, 24, 19-37 (1978).

Jonsson, G., "Overview of Theories for Water and Solute Transport in UF/RO Membranes", Desalination, 35, 21-38 (1980).

Jonsson, G., and Boesen, C.E., "Water and Solute Transport Through Cellulose Acetate Reverse Osmosis Membranes", Desalination, 17, 145-165 (1975).

Kedem, O., and Katchalsky, A., "Thermodynamic Analysis of the Permeability of Biological Membranes to Non-Electrolytes", Biochem. Biophys. Acta, 27, 229-246 (1958).

Kesting, R.E., "Synthetic Polymeric Membranes: A Structural Perspective", 2nd ed., John Wiley and Sons, New York, NY (1985).

Kimura, S., and Nomura, T., "Purification of High Temperature Water by the Reverse Osmosis Process", Desalination, 38, 373-382 (1981).

Kimura, S., and Sourirajan, S., "Analysis of Data in Reverse Osmosis with Porous Cellulose Acetate Membranes Used", AIChE J., 13(3), 497-503 (1967).

Koh, W.-H., and Anderson, J.L., "Electroosmosis and Electrolyte Conductance in Charged Microcapillaries", AIChE J., 21, 1176-1188 (1975).

Korosi, A., and Fabuss, B.M., "Viscosities of Binary Aqueous Solutions of NaCl, Na_2SO_4, and $MgSO_4$ at Concentrations and Temperatures of Interest in Desalination Processes", J. Chem. Eng. Data, 13(4), 548-552 (1968).

Kurihara, M., Nakagawa, Y., Takeuchi, H., Kanamaru, N., and Tonomura, T., "Single-Stage Sea Water Desalination at High Temperature and Salinity as present in the Middle East Using PEC-1000 Membrane Modules", Desalination, 46, 101-110 (1983).

Lane, J.A., and Riggle, J.W., "Dialysis", Chem. Eng. Prog., Symp. Ser. 55, 127-143 (1959).

Larson, R.E., Cadotte, J.E., and Petersen, R.J., "The FT-30 Seawater Reverse Osmosis Membrane: Element Test Results", Desalination, 38, 473-483 (1981).

Larson, R.E., Petersen, R.J., and Eriksson, P.K., "Test Results on FT-30 Eight-Inch-Diameter Seawater and Brackish Water Reverse Osmosis Elements", Desalination, 46, 81-90 (1983).

Levitt, D.G., "Kinetics of Diffusion and Convection in 3.2 angstrom pores", Biophys. J., 13, 186- 206 (1973).

Loeb, S., "The Loeb-Sourirajan Membrane: How It Came About", in "Synthetic Membranes", A.F. Turbak, Ed., Vol. I, ACS Symposium Series 153, Washington, D.C. (1981).

Loeb, S., and Sourirajan, S., "Sea Water Demineralization by Means of an Osmotic Membrane", Advan. Chem. Ser., 38, 117-132 (1962).

Lonsdale, H.K., Merten, U., and Riley, R.L., "Transport Properties of Cellulose Acetate Osmotic Membranes", J. Appl. Poly. Sci., 9, 1341-1362 (1965).

Lonsdale, H.K., Merten, U., and Tagami, M., "Phenol Transport in Cellulosic Acetate Membranes", J. Appl. Polym. Sci., 11, 1807-1820 (1967).

Marquardt, D.L., "An Algorithm for Least-Squares Estimation of Non-Linear Parameters", J. Soc. Indust. Appl. Math., 2, 431-441 (1963).

Matsuura, T., Blais, P., Dickson, J.M., and Sourirajan, S., "Reverse Osmosis Separation for Some Alcohols and Phenols in Aqueous Solutions Using Aromatic Polyamide Membranes", J. Appl. Polym. Sci., 18, 3671-3684 (1974).

Matsuura, T., and Sourirajan, S., "Physicochemical Criteria for Reverse Osmosis Separation of Alcohols, Phenols, and Monocarboxylic Acids in Aqueous Solutions Using Porous Cellulose Acetate Membranes", J. Appl. Polym. Sci., 15, 2905-2927 (1971).

Matsuura, T., and Sourirajan, S., "Reverse Osmosis Separation of Phenols in Aqueous Solutions Using Porous Cellulose Acetate Membranes", J. Appl. Polym. Sci., 16, 2531-2554 (1972).

Matsuura, T., and Sourirajan, S., "Physicochemical Criteria for Reverse Osmosis Separation of Monohydric and Polyhydric Alcohols in Aqueous Solutions

Using Porous Cellulose Acetate Membranes", J. Appl. Polym. Sci., 17, 1043-1071 (1973a).

Matsuura, T., and Sourirajan, S., "Reverse Osmosis Separation of Hydrocarbons in Aqueous Solutions Using Porous Cellulose Acetate Membranes", J. Appl. Polym. Sci., 17, 3683-3708 (1973b).

Matsuura, T., and Sourirajan, S., "Reverse Osmosis Transport Through Capillary Pores Under the Influence of Surface Forces", Ind. Eng. Chem. Process Des. Dev., 20, 273-282 (1981).

Matsuura, T., Taketani, Y., and Sourirajan, S., "Estimation of Interfacial Forces Governing the Reverse Osmosis System: Nonionized Polar Organic Solute-Water- Cellulose Acetate Membrane", in "Synthetic Membranes", A.F. Turbak, Ed., ACS Symposium Series, Washington, D.C. (1981).

Mehdizadeh, H., Dickson, J.M., and Eriksson, P.K., "Temperature Effects on the Performance of Thin-Film Composite, Aromatic Polyamide Membranes", I&EC Res., 28(6), 814-824 (1989).

Mehdizadeh, H., and Dickson, J.M., "Theoretical Modification of the Surface Force-Pore Flow Model for Reverse Osmosis Transport", J. Memb. Sci., 42, 119-145 (1989a).

Mehdizadeh, H., and Dickson, J.M., "Evaluation of Surface Force-Pore Flow and Modified Surface Force-Pore Flow Models for Reverse Osmosis Transport", Desalination, submitted (1989b).

Mehdizadeh, H., and Dickson, J.M., "Modeling of Reverse Osmosis in the Presence of Strong Solute-Membrane Affinity", Third Annual North American Membrane Society Meeting, Austin, Texas, May 17-19 (1989c).

Mehdizadeh, H., and Dickson, J.M., "Modeling of Temperature Effects on the Performance of Reverse Osmosis Membranes", Chem. Eng. Commun., submitted (1989d).

Mehdizadeh, H., and Dickson, J.M., "Theoretical Modification of the Finely Porous Model for Reverse Osmosis Transport", J. Appl. Polym. Sci., accepted (1989e).

Mehdizadeh, H., and Dickson, J.M., "Solving Nonlinear Differential Equations of Membrane Transport by Orthogonal Collocation", Computers & Chemical Engineering, in press (1989f).

Mehdizadeh, H., and Dickson, J.M., "The Role of Membrane Potential Functions in Determining Reverse Osmosis Transport Phenomena", Proceedings 2nd International Conference on Separations Science and Technology, Hamilton, Ontario, Canada, Oct. 1-4 (1989g).

Mehdizadeh, H., and Dickson, J.M., "Temperature Effects on the Performance of Thin-Film Composite, Aromatic Polyamide Membranes at Seawater-Concentration Level", Chem. Eng. Commun., to be submitted (1989h).

Merten, U., Ed., "Desalination by Reverse Osmosis", MIT Press, Cambridge, MA (1966), pp.15-54.

Merten, U., Lonsdale, H.K., Riley, R.L., and Vos, K.D., "Reverse Osmosis Membrane Research", R&D Progress Report 369, U.S. Department of the Interior, Washington, D.C. (1968).

Morrison, F.A., Jr., and Osterle, J.F., "Electrokinetic Energy Conversion in Ultrafine Capillaries", J. Chem. Phys., 43, 2111-2115 (1965).

Neogi, P., and Ruckenstein, E., "Viscoelectric Effects in Reverse Osmosis", J. Colloid Interface Sci., 79, 159-169 (1981).

Nguyen, T.D., and Matsuura, T., "Design of Aromatic Polyamide Membrane for Reverse Osmosis", Proc. Int. Memb. Conf. 25th Anniv. Memb. Res. Canada, M. Malaiyandi, O. Kutowy, and F. Talbot, Eds., Ottawa, Canada, September 24-26, 99-114 (1986).

Ohya, H., and Taniguchi, Y., "On a Temperature Correction Coefficient for the Water Flux Through Reverse Osmosis Membranes of Large Scale Systems". Desalination, 15, 245-258 (1974).

Onsager, L., "Reciprocal Relations in Irreversible Processes", Phys. Rev., 37, 405-425 (1931).

Orofino, T.A., Hopfenberg, H.B., and Stannett, V., "Characterization of Penetrant Clustering in Polymers", J. Macromol. Sci. Phys., B3, 777-788 (1969).

Petersen, R.J., "Membranes for Desalination", in Synthetic Membranes, Chenoweth M.B., Ed., MMI Press, New York, 129-154 (1986).

Pusch, W., "Determination of Transport Parameters of Synthetic Membranes by Hyperfiltration Experiments; Part I: Derivation of Transport Relationship from the Linear Relations of Thermodynamics of Irreversible Processes", Ber. Bunsenges. Phys. Chem., 81(3), 269- 276 (1977).

Quinn, J.A., Anderson, J.L., Ho W. S., and Petzny W.J., "Model Pores of Molecular Dimension: The Preparation and Characterization of Track-Etched Membranes", Biophys. J., 12, 990- 1007 (1972).

Reid, C.E., and Breton, E.J., "Water and Ion Flow Across Cellulosic Membranes", J. Appl. Polym. Sci., 1, 133-143 (1959).

Renkin, E.M., "Filtration, Diffusion, and Molecular Sieving through Porous Cellulose Membranes", J. Gen. Physiol., 38, 225- 243 (1954).

Reid, R.C., Prausnitz, J.M., and Sherwood, T.K., "The Properties of Gases and Liquids", 3rd ed., McGraw-Hill Book Co., New York, NY (1977).

Rudie, B.J., and Nguyen, T.D., "Calculation of the Pore Size Distribution of PBI Membranes", Proc. Int. Memb. Conf. 25th Anniv. Memb. Res. Canada, M. Malaiyandi, O. Kutowy, and F. Talbot, Eds., Ottawa, Canada, September 24-26, 159-172 (1986).

Saltonstall, C.W., Jr., "Practical Aspects of Sea Water Desalination by Reverse Osmosis", Desalination, 18, 315-320 (1976).

Sasidhar, V., and Ruckenstein, E., "Electrolyte Osmosis Through Capillaries", J. Colloid Interface Sci., 82, 439-457 (1981).

Satterfield, C.N., Colton, C.K., and Pitcher, W.H., Jr., "Restricted Diffusion in Liquids within Fine Pores", AIChE J., 19, 628- 635 (1973).

Sherwood, T.K., Brian, P.L.T., and Fisher, R.E., "Desalination by Reverse Osmosis", I&EC Fund., 6(1), 2-12 (1967).

Soltanieh, M., and Gill, W.N., "Review of Reverse Osmosis Membranes and Transport Models", Chem. Eng. Commun., 12, 279- 363 (1981).

Sourirajan, S., "The Mechanism of Demineralization of Aqueous Sodium Chloride Solutions by Flow, Under Pressure, Through Porous Membranes", Ind. Eng. Chem. Fund., 2, 51-55 (1963).

Sourirajan, S., "Reverse Osmosis", Academic Press, New York, NY (1970).

Sourirajan, S., "Reverse Osmosis and Synthetic Membranes: Theory-Technology-Engineering", National Research Council Canada, Ottawa, Canada (1977).

Sourirajan, S., "Thirty Years of Membrane Research - A Few Highlights", Proc. Int. Memb. Conf. 25th Anniv. Memb. Res. Canada, M. Malaiyandi, O. Kutowy, and F. Talbot, Eds., Ottawa, Canada, September 24-26, 3-32 (1986).

Spiegler, K.S., "Transport Processes in Ionic Membranes", Trans. Faraday Soc., 54, 1408-1428 (1958).

Spiegler, K.S., and Kedem, O., "Thermodynamics of Hyperfiltration (Reverse Osmosis): Criteria for Efficient Membranes", Desalination, 1, 311-326 (1966).

Staverman, A.J., Recueil Trav. Chim. Pays-Bas, 70, 344-352 (1951).

Staverman, A.J., "Structure and Function of Membranes", J. Membr. Sci., 16, 7-20 (1983).

Stoughton, R.W., and Lietzke, M.H., "Calculation of Some Thermodynamic Properties of Sea Salt Solutions at Elevated Temperatures from Data on NaCl Solutions", J. Chem. Eng. Data, 10(3), 254-260 (1965).

Tinghul, L., Chan, K., Matsuura, T., and Sourirajan, S., "Determination of Interaction Forces and Average Pore Size and Pore Size Distribution and their Effects on Fouling of Ultrafiltration Membranes", Ind. Eng. Chem. Prod. Res. Dev., 23, 116-124 (1984).

Usui, S., "Interaction of Electrical Double Layers at Constant Surface Charge", J. Colloid Interface Sci., 44(1), 107-113 (1973).

Verwey, E.J.W., and Overbeek, J.Th.G., "Theory of the Stability of Lyophobic Colloids", Elsevier, New York (1948).

Villadsen, J., and Michelsen, M.L., "Solution of Differential Equation Models by Polynomial Approximation", Prentice-Hall, Englewood Cliffs (1978).

Weast, R.C., "CRC Handbook of Chemistry and Physics", 56th ed., CRC Press (1975).

Westermann-Clark, G.B., and Anderson, J.L., "Experimental Verification of the Space-Charge Model for Electrokinetics in Charged Microporous Membranes", J. Electrochem Soc., 130, 839-847 (1983).

Yang, Y.C., and Dickson, J.M., "Parametric Study of Thin-Film Composite Polyamide-Type Reverse Osmosis Membranes", Proceedings 46th International Water conference, Pittsburgh, PA, 342-348 (1985).

Yuster, S.T., Sourirajan, S., and Bernstein, K., "Sea Water Demineralization by the 'Surface Skimming' Process", University of California (UCLA), Dept. of Engineering, Rept. 58-26, March (1958).

APPENDIX A

THE EXTENDED MD-SF-PF MODEL: BASIC DERIVATIONS

A.I   Derivation of Boltzmann Boundary Conditions

Upon integrating Eqn.(3.45) subject to the following boundary conditions:

$$\int_{C_{A2}}^{C_A(r,0)} \frac{\partial C_A(r,z)}{C_A(r,z)} + \frac{1}{RT} \int_0^{\phi(r,0)} \frac{d\,\phi(r,z)}{dr}\,dr = 0 \tag{A.I.1}$$

one obtains:

$$C_A(r,0) = C_{A2} \exp\left[-\frac{\phi(r,0)}{RT} \right] \tag{A.I.2}$$

On the other hand, using Eqn.(3.47) at $z=0$,

$$C_A(r,0) = C_A(0,0)\ \exp\left[\frac{\phi(0,0)}{RT} \right]\ \exp\left[-\frac{\phi(r,0)}{RT} \right] \tag{A.I.3}$$

Then, comparing Eqns.(A.I.2) and (A.I.3) yields:

$$C_{A2} = C_A(0,0)\ \exp\left[\frac{\phi(0,0)}{RT} \right] \tag{A.I.4}$$

Similarly, integration of Eqn.(3.45) subject to the following boundary conditions:

$$\int_{C_{A3}}^{C_A(r,\tau)} \frac{\partial C_A(r,z)}{C_A(r,z)} + \frac{1}{RT} \int_0^{\phi(r,\tau)} \frac{d\,\phi(r,z)}{dr}\,dr = 0 \tag{A.I.5}$$

yields:

$$C_A(r,\tau) = C_{A3} \exp\left[-\frac{\phi(r,\tau)}{RT} \right] \tag{A.I.6}$$

However, using Eqn.(3.47) at $z=\tau$ gives:

$$C_A(r,\tau) = C_A(0,\tau)\ \exp\left[\frac{\phi(0,\tau)}{RT} \right]\ \exp\left[-\frac{\phi(r,\tau)}{RT} \right] \tag{A.I.7}$$

which, upon comparison with Eqn.(A.I.6) gives:

$$C_{A3} = C_A(0,\tau)\ \exp\left[\frac{\phi(0,\tau)}{RT} \right] \tag{A.I.8}$$

A.II Force Balance on the Solute in a Pore

The force balance on the solute inside a pore, in Figure 3.1, is (Mehdizadeh and Dickson, 1989a):

$$F_A(r, z) = -\{F_{AB}(r, z) + F_{AM}(r, z)\} \tag{A.II.1}$$

where $F_A(r,z)$ is the total force driving the solute through the pore, and $F_{AB}(r,z)$ and $F_{AM}(r,z)$ are the frictional forces between the solute and solvent and between the solute and the pore wall, respectively. $F_{AM}(r,z)$ is given by the definition of friction constant between the solute and the pore wall (Mehdizadeh and Dickson, 1989a):

$$F_{AM}(r, z) = -X_{AM} \frac{J_{A,z}(r)}{C_A(r, z)} \tag{A.II.2}$$

Then, combining Eqns.(A.II.1), (A.II.2), and (3.64) yields:

$$-F_{AB}(r, z) = -\frac{RT}{n(r, z)} \frac{\partial n(r, z)}{\partial z} - v_A \frac{\partial P(r, z)}{\partial z} - X_{AM} J_{A,z}(r) \frac{RT}{n(r, z)} \tag{A.II.3}$$

On the other hand,

$$u_A(r, z) = \frac{J_{A,z}(r)}{C_A(r, z)} \tag{A.II.4}$$

and, by definition (Spiegler, 1958):

$$F_{AB}(r, z) = -X_{AB}[u_A(r, z) - u_B(r)] \tag{A.II.5}$$

so that, using van't Hoff's theorem in Eqn.(3.30), Eqns.(A.II.4) and (A.II.5) are combined as:

$$J_{A,z}(r) = \frac{1}{X_{AB}} \frac{n(r, z)}{RT} [-F_{AB}(r, z)] + \frac{n(r, z) u_B(r)}{RT} \tag{A.II.6}$$

Then, using Eqn.(A.II.3), Eqn.(A.II.6) can be written as:

$$J_{A,z}(\rho) = \frac{1}{\tau X_{AB} b(\rho)} \left\{ -\frac{\partial n(\rho, \xi)}{\partial \xi} - v_A \frac{n(\rho, \xi)}{RT} \frac{\partial P(\rho, \xi)}{\partial \xi} + \alpha(\rho) n(\rho, \xi) \right\} \tag{A.II.7}$$

where ρ and ξ are the dimensionless radial and axial positions defined by Eqns.(2.36) and (3.19), and $\alpha(\rho)$ is the dimensionless solution velocity defined by Eqn.(2.37).

However, from Eqn.(3.68), one can find the axial gradient of osmotic

pressure as:

$$\frac{\partial \pi(\rho, \xi)}{\partial \xi} = -[\pi_2 - K^*(\rho)\,\pi_3][\alpha(\rho) + \omega(\rho)] \; \frac{e^{[\alpha(\rho) + \omega(\rho)]\xi}}{e^{[\alpha(\rho) + \omega(\rho)]} - 1} \; e^{-\Phi(\rho, 0)} \qquad (A.II.8)$$

so that, upon substitution in Eqn.(A.II.7), one will get the axial component of solute

flux as:

$$J_{A,z}(\rho) = \left[\frac{\alpha(\rho) + \omega(\rho)}{\tau X_{AB}\,b(\rho)} \right] \left\{ \pi_2 + \frac{\pi_2 - K^*(\rho)\,\pi_3}{e^{[\alpha(\rho) + \omega(\rho)]} - 1} \right\} e^{-\Phi(\rho, 0)} \qquad (A.II.9)$$

which is the derived Eqn.(3.74).

A.III   Concentration Profile in the Pore

Equation (3.67) can be expanded to the following form:

$$\frac{\partial^2 \pi(\rho, \xi)}{\partial \xi^2} + \frac{v_A}{RT} \left[\frac{\partial \pi(\rho, \xi)}{\partial \xi} \frac{\partial P(\rho, \xi)}{\partial \xi} + \pi(\rho, \xi)\frac{\partial^2 P(\rho, \xi)}{\partial \xi^2} \right] - \alpha(\rho) \frac{\partial \pi(\rho, \xi)}{\partial \xi} = 0 \qquad (A.III.1)$$

However, it is assumed that (Mehdizadeh and Dickson, 1989a):

$$\frac{\partial P(\rho, \xi)}{\partial \xi} = P(\rho, 1) - P(\rho, 0) \qquad (A.III.2)$$

where,

$$P(\rho, 1) - P(\rho, 0) = -\Delta P + \pi_2 \sigma_2(\rho) - \pi_3 \sigma_3(\rho) \qquad (A.III.3)$$

where $\sigma_2(\rho)$ and $\sigma_3(\rho)$ are defined in Eqns.(3.72) and (3.73).

Therefore,

$$\frac{\partial^2 P(\rho, \xi)}{\partial \xi^2} = 0 \qquad (A.III.4)$$

so that Eqn.(A.III.1) becomes:

$$\frac{\partial^2 \pi(\rho, \xi)}{\partial \xi^2} - [\alpha(\rho) + \omega(\rho)] \frac{\partial \pi(\rho, \xi)}{\partial \xi} = 0 \qquad (A.III.5)$$

where $\omega(\rho)$ is defined in Eqn.(3.71). Equation (A.III.5) can be solved analytically

subject to the boundary conditions:

$$n(\rho, 0) = n_2 e^{-\Phi(\rho,0)} \tag{A.III.6}$$

$$n(\rho, 1) = n_3 e^{-\Phi(\rho,1)} \tag{A.III.7}$$

by a method similar to that in the MD-SF-PF model (Mehdizadeh and Dickson, 1989a) to give the following equations for the osmotic pressure and concentration profile inside the pore, as given by Eqns.(3.68) and (3.69).

A.IV   Derivation of Velocity Profile

The force balance on the elemental fluid of Figure 3.1 consists of the following three parts:

1.   The net force due to difference in pressure:

$$(2\pi r\, dr) \left\{ (P|_z - \left[(P|_z + \left(\frac{\partial P}{\partial z} \bigg|_z dz \right) \right] \right\} = -2\pi r\, dr\, dz \frac{\partial P(r, z)}{\partial z} \tag{A.IV.1}$$

2.   The net force due to viscous shear stresses, using Newton's law of viscosity:

$$(2\pi r\, dz) \left\{ (\tau_{rz}|_z - (\tau_{rz}|_{r+dr} \right\} = \eta \left\{ (2\pi r\, dr\, dz) \frac{d^2 u_B(r)}{dr^2} + (2\pi\, dr\, dz) \frac{du_B(r)}{dr} \right\} \tag{A.IV.2}$$

3.   The net force due to the friction force between solute and the pore wall:

$$F_{AM}(2\pi r\, dr\, dz) C_A(r, z) = [-\chi_{AM}(r)\, u_A(r, z)] (2\pi r\, dr\, dz) C_A(r, z)$$

$$= -(2\pi r\, dr\, dz) \chi_{AM}(r) J_{A,z}(r) \tag{A.IV.3}$$

where $\chi_{AM}(r)$ is the proportionality constant defined as:

$$F_{AM}(r, z) = -\chi_{AM}(r)\, u_A(r, z) \tag{A.IV.4}$$

Substituting for $J_{A,z}(r)$ from Eqn.(3.74), Eqn.(A.IV.3) becomes:

$$F_{AM}(r, z)(2\pi r\, dr\, dz) C_A(r, z) = -(2\pi r\, dr\, dz) \chi_{AM}(r) \left| \frac{\alpha(r) + \omega(r)}{\tau \chi_{AB} b(r)} \right|$$

$$\cdot \left\{ n_2 + \frac{n_2 - K^*(r) n_3}{e^{[\alpha(r)+\omega(r)]} - 1} \right\} e^{-\Phi(r,0)} \tag{A.IV.5}$$

Adding up all the three contributions of the force balance, a second-order differential equation is obtained for the velocity profile, as given by Eqn.(3.75), where

the $\sigma_2(\rho)$ and $\sigma_3(\rho)$ terms in this equation are defined by Eqns.(3.72) and (3.73), and

$b(\rho)$ and β_1 are defined by Eqns.(3.13), and (3.25).

APPENDIX B

THE MD-FPM AND FPM MODELS: BASIC DERIVATIONS

B.I   Derivation of Solute Flux Equations in the MD-FPM and FPM Relationships

A balance of applied and frictional forces on the solute molecules inside the pore yields (Jonsson and Boesen, 1975),

$$F_A = -(F_{AB} + F_{AM})$$ (B.I.1)

where,

$$F_{AM} = -X_{AM} u_A = -X_{AM} J_A / C_A(z)$$ (B.I.2)

and,

$$F_{AB} = -X_{AB}(u_A - u_B) = -X_{AM}[J_A / C_A(z) - u_B]$$ (B.I.3)

The driving force for the solute, F_A, is (Mehdizadeh and Dickson, 1989a):

$$F_A = -\frac{d\mu_A(z)}{dz} = -\frac{RT}{n(z)}\frac{dn(z)}{dz}$$ (B.I.4)

Then, using Eqns.(B.I.2) and (B.I.4), Eqn.(B.I.1) becomes:

$$-F_{AB} = (F_A + F_{AM}) = -\frac{RT}{n(z)}\frac{dn(z)}{dz} - X_{AM}\frac{J_A}{n(z)}RT$$ (B.I.5)

On the other hand, from Eqn.(B.I.3),

$$J_A = \frac{1}{X_{AB}}\frac{n(z)}{RT}[-F_{AB}] + \frac{n(z)}{RT}u_B$$ (B.I.6)

Now, using Eqn.(B.I.5), Eqn.(B.I.6) becomes,

$$J_A = \frac{1}{b}\left\{-\frac{1}{X_{AB}}\frac{dn(z)}{dz} + \frac{n(z)u_B}{RT}\right\}$$ (B.I.7)

where b has been defined by Eqn.(3.93). Equation (B.I.7) can be rewritten as,

$$J_A = \frac{1}{b}\left(\frac{1}{\tau X_{AB}}\right)\left\{-\frac{dn(\xi)}{d\xi} + a_B n(z)\right\}$$ (B.I.8)

where ξ and α_B have been defined by Eqns.(3.19) and (3.115).

Now, using Eqn.(3.101) and van't Hoff's law in Eqn.(3.30),

$$n(\xi) = \left\{ n_2 - \left(n_2 - \frac{K_3}{K_2} n_3 \right) \left[\frac{1 - \exp(\alpha\xi)}{1 - \exp(\alpha)} \right] \right\} K_2 \qquad (B.I.9)$$

The derivative dn/dz can be determined from the above equation. Using this derivative and Eqn.(B.I.9), an explicit equation for solute flux is derived, as given by Eqn.(3.102).

Employing Eqn.(3.129), Eqn.(3.102) reduces to the following form, for the MD-FPM-3 relationship,

$$J_A = \frac{\alpha}{\tau X_{AB} b} \left\{ n_2 + \frac{n_2 - n_3}{\exp(\alpha) - 1} \right\} K \qquad (B.I.10)$$

B.II   Derivation of Concentration Profiles and Separation Correlations in the MD-FPM and FPM Relationships

B.II.i   MD-FPM Relationship

Starting with Eqn.(3.98) and the boundary conditions, Eqns.(3.95) and (3.96), Eqn.(3.98) is integrated with respect to ξ to yield:

$$\frac{d C_A(\xi)}{d\xi} - \alpha C_A(\xi) = -\alpha G \qquad (B.II.1)$$

where G is a constant of integration. Multiplying Eqn.(B.II.1) by the following integration factor,

$$I(\xi) = \exp[-\alpha\xi] \qquad (B.II.2)$$

and integrating the resulted equation, one obtains,

$$C_A(\xi) = G + H \exp[\alpha\xi] \qquad (B.II.3)$$

where H is another constant of integration.

In order to determine the constants G and H, the boundary conditions, Eqns.(3.95) and (3.96), are employed. After determining the relationships for G and H,

and substituting these relationships into Eqn.(B.II.3), the concentration profile is obtained (in MD-FPM-4 relationship), as given by Eqn.(3.101).

Using Eqn.(3.129), Eqn.(3.101) reduces to the concentration profile for the MD-FPM-3 relationship, as given by Eqn.(3.130).

B.II.ii   FPM Relationship

Combining Eqns.(3.91) and (3.103), the following first order differential equation is obtained,

$$\frac{d\,C_A(\xi)}{d\xi} - a\,C_A(\xi) = -\,a\,C_{A3} \qquad (B.II.4)$$

where a and ξ have been defined by Eqns.(3.100) and (3.19). Multiplying Eqn.(B.II.4) by the integrating factor in Eqn.(B.II.2), and integrating the resulting equation, one obtains:

$$C_A(\xi) = C_{A3}b + g\exp[a\xi] \qquad (B.II.5)$$

Using Eqn.(3.95), as the boundary condition, the constant g is determined and substituted into Eqn.(B.II.5) to give the concentration profile in FPM-4 relationship as:

$$C_A(\xi) = b\left[C_{A3} + \left(\frac{K_2}{b}C_{A2} - C_{A3}\right)\exp(a\xi)\right] \qquad (B.II.6)$$

which is converted to the following relationship for the FPM-3, when Eqn.(3.129) is employed,

$$C_A(\xi) = b\left[C_{A3} + \left(\frac{K}{b}C_{A2} - C_{A3}\right)\exp(a\xi)\right] \qquad (B.II.7)$$

Now, using Eqn.(3.96), Eqn.(B.II.6) can be employed to derive the following relationships for C_{A3}/C_{A2} ratio:

$$\frac{C_{A3}}{C_{A2}} = \frac{(K_2/K_3)\exp(a)}{1 + (b/K_3)[\exp(a) - 1]} \qquad (B.II.8)$$

Then, using Eqn.(2.6), as the definition of separation, a relationship is derived for separation, in the FPM-4 relationship, as given by Eqn.(3.104).

Using Eqn.(3.129), Eqn.(3.104) reduces to the following form, for the FPM-3 relationship,

$$f' = \frac{(1 - K/b)[\exp(a) - 1]}{[\exp(a) - 1] + K/b}$$

(B.II.9)

APPENDIX C

THE EXPERIMENTAL DATA OF PHASE I

The film numbers 1, 2, 3, and 4 (in the following tables) refer to the membranes SW30-1, SW30-2, BW30-1, and BW30-2, respectively.

Term in Computer Output	Meaning
A * E09	$A \times 10^9$
Avg.	Average
Cl	C
Conc.	Concentration
(D)AM K/Tau * E07	$D_{AM} K/\tau \times 10^7$
f prime	f'
k * E06	$k \times 10^6$
KCL	$KC\ell$
kg/m.m.s	$kg/m^2 s$
kmol/m.m.m	$kmol/m^3$
kmol/m.m.s.kPa	$kmol/m^2 s\,kPa$
LICL	$LiC\ell$
LINO3	$LiNO_3$
NACL	$NaC\ell$
No.	Number
[n]P	n_P
[n]T	n_T
XA1	X_{A1}
XA2 * E04	$X_{A2} \times 10^4$
XA3 * E04	$X_{A3} \times 10^4$

```
Experiment No.          :  176
Operating Pressure      :  1500   kPa
Nominal Solute Conc.    :  2000   ppm
Nominal Feed Flow Rate: 1000   ml/min
Setpoint Temperature    :  25.00  Degree C
Solute                  :  NACL
```

Avg. Feed Conc. (ppm) = 1969. ; XA1 =0.000608 ; Cl = 55.35 kmol/m.m.m

	Film # 1	Film # 2	Film # 3	Film # 4
A * E09, kmol/m.m.s.kPa	189.6482	257.0788	343.4055	317.5891
[n]P , kg/m.m.s	0.005126	0.006949	0.009282	0.008584
[n]T , kg/m.m.s	0.004422	0.006019	0.008015	0.007067
XA2 * E04	7.8986	7.6092	7.4613	7.6159
XA3 * E04	0.1349	0.2212	0.1491	0.2778
f	0.977815	0.963628	0.975489	0.954325
f prime	0.982929	0.970947	0.980033	0.963548
k * E06 , m/s	16.6000	26.0000	38.3500	30.1500
(D)AM K/Tau * E07, m/s	0.7705	1.8069	1.6383	2.6824

```
Experiment No.          :  175
Operating Pressure      :  7000   kPa
Nominal Solute Conc.    :  2000   ppm
Nominal Feed Flow Rate: 1000   ml/min
Setpoint Temperature    :  60.00  Degree C
Solute                  :  NACL
```

Avg. Feed Conc. (ppm) = 2217. ; XA1 =0.000685 ; Cl = 54.56 kmol/m.m.m

	Film # 1	Film # 2	Film # 3	Film # 4
A * E09, kmol/m.m.s.kPa	441.6692	562.2667	848.0902	683.8654
[n]P , kg/m.m.s	0.055712	0.070924	0.106978	0.086263
[n]T , kg/m.m.s	0.051279	0.064993	0.091914	0.076219
XA2 * E04	40.1672	28.5376	24.9872	27.8216
XA3 * E04	0.1406	0.1618	0.7985	0.5189
f	0.979480	0.976383	0.883460	0.924273
f prime	0.996514	0.994346	0.968122	0.981402
k * E06 , m/s	29.1942	45.7259	67.4457	53.0244
(D)AM K/Tau * E07, m/s	1.8329	3.7705	30.8592	14.7336

```
                    Experiment No.          :  174
                    Operating Pressure      :  4000   kPa
                    Nominal Solute Conc.    :  2000   ppm
                    Nominal Feed Flow Rate: 1000    ml/min
                    Setpoint Temperature    :  60.00  Degree C
                    Solute                  :  NACL
```

Avg. Feed Conc. (ppm) = 2057. ; XAl =0.000635 ; Cl = 54.56 kmol/m.m.m

	Film # 1	Film # 2	Film # 3	Film # 4
	********	********	********	********
A * E09, kmol/m.m.s.kPa	495.5572	639.8210	799.8644	757.4970
[n]P , kg/m.m.s	0.035720	0.046118	0.057654	0.054600
[n]T , kg/m.m.s	0.032251	0.041483	0.053129	0.048079
XA2 * E04	19.3442	15.7656	13.9709	15.3750
XA3 * E04	0.0911	0.1406	0.1463	0.3935
f	0.985666	0.977875	0.976985	0.938077
f prime	0.995300	0.991096	0.989546	0.974445
k * E06 , m/s	29.1942	45.7259	67.4457	53.0244
(D)AM K/Tau * E07, m/s	1.5520	3.7966	5.7169	12.8433

```
                    Experiment No.          :  173
                    Operating Pressure      :  350    kPa
                    Nominal Solute Conc.    :  2000   ppm
                    Nominal Feed Flow Rate: 1000    ml/min
                    Setpoint Temperature    :  60.00  Degree C
                    Solute                  :  NACL
```

Avg. Feed Conc. (ppm) = 1934. ; XAl =0.000597 ; Cl = 54.56 kmol/m.m.m

	Film # 1	Film # 2	Film # 3	Film # 4
	********	********	********	********
A * E09, kmol/m.m.s.kPa	558.8334	738.1542	956.4796	820.2938
[n]P , kg/m.m.s	0.003525	0.004656	0.006033	0.005174
[n]T , kg/m.m.s	0.001844	0.002474	0.003362	0.002871
XA2 * E04	6.3329	6.2712	6.2362	6.2674
XA3 * E04	0.5434	0.6947	0.9037	0.7668
f	0.909075	0.883749	0.848771	0.871688
f prime	0.914251	0.889286	0.855167	0.877727
k * E06 , m/s	29.1942	45.7259	67.4457	53.0244
(D)AM K/Tau * E07, m/s	1.7600	3.1337	5.7932	4.0705

Experiment No.   : 172
Operating Pressure   : 1500 kPa
Nominal Solute Conc.   : 2000 ppm
Nominal Feed Flow Rate: 1000 ml/min
Setpoint Temperature   : 60.00 Degree C
Solute   : NACL

Avg. Feed Conc. (ppm) = 2075. ; XA1 =0.000641 ; C1 = 54.56 kmol/m.m.m

	Film # 1	Film # 2	Film # 3	Film # 4
A * E09, kmol/m.m.s.kPa	528.2852	698.9806	873.6140	820.7590
[n]P , kg/m.m.s	0.014280	0.018893	0.023614	0.022185
[n]T , kg/m.m.s	0.011989	0.015859	0.020241	0.017869
XA2 * E04	9.6545	9.0294	8.6072	8.8591
XA3 * E04	0.1477	0.2127	0.2495	0.4150
f	0.976972	0.966825	0.961089	0.935282
f prime	0.984719	0.976460	0.971034	0.953193
k * E06 , m/s	29.1942	45.7259	67.4457	53.0244
(D)AM K/Tau * E07, m/s	1.8941	3.8920	6.1462	8.9319

Experiment No.   : 171
Operating Pressure   : 500 kPa
Nominal Solute Conc.   : 2000 ppm
Nominal Feed Flow Rate: 1000 ml/min
Setpoint Temperature   : 60.00 Degree C
Solute   : NACL

Avg. Feed Conc. (ppm) = 2001. ; XA1 =0.000618 ; C1 = 54.56 kmol/m.m.m

	Film # 1	Film # 2	Film # 3	Film # 4
A * E09, kmol/m.m.s.kPa	564.7918	754.9716	977.2721	853.1678
[n]P , kg/m.m.s	0.005089	0.006802	0.008805	0.007687
[n]T , kg/m.m.s	0.003003	0.004282	0.005621	0.004847
XA2 * E04	6.8189	6.7466	6.6676	6.7272
XA3 * E04	0.3628	0.4828	0.6370	0.5361
f	0.941311	0.921887	0.896936	0.913259
f prime	0.946834	0.928480	0.904516	0.920351
k * E06 , m/s	29.1942	45.7259	67.4457	53.0244
(D)AM K/Tau * E07, m/s	1.7163	3.3570	6.0383	4.2688

```
Experiment No.          :  170
Operating Pressure      :  1500   kPa
Nominal Solute Conc.    :  2000   ppm
Nominal Feed Flow Rate:    1000   ml/min
Setpoint Temperature    :  25.00  Degree C
Solute                  :  NACL
```

Avg. Feed Conc. (ppm) = 2019. ; XA1 =0.000624 ; C1 = 55.35 kmol/m.m.m

	Film # 1	Film # 2	Film # 3	Film # 4
	********	********	********	********
A * E09, kmol/m.m.s.kPa	204.7690	276.7972	376.3519	350.2448
[n]P , kg/m.m.s	0.005535	0.007482	0.010173	0.009467
[n]T , kg/m.m.s	0.004737	0.006384	0.008629	0.007654
XA2 * E04	8.2588	7.9206	7.7674	7.9623
XA3 * E04	0.1250	0.1972	0.1802	0.2764
f	0.979958	0.968394	0.971115	0.955696
f prime	0.984872	0.975124	0.976817	0.965313
k * E06 , m/s	16.6000	26.0000	38.3500	30.1500
(D)AM K/Tau * E07, m/s	0.7406	1.6578	2.0846	2.7996

```
Experiment No.          :  169
Operating Pressure      :  7000   kPa
Nominal Solute Conc.    :  2000   ppm
Nominal Feed Flow Rate:    1000   ml/min
Setpoint Temperature    :  50.00  Degree C
Solute                  :  NACL
```

Avg. Feed Conc. (ppm) = 2075. ; XA1 =0.000641 ; C1 = 54.83 kmol/m.m.m

	Film # 1	Film # 2	Film # 3	Film # 4
	********	********	********	********
A * E09, kmol/m.m.s.kPa	378.3807	478.8857	742.5006	600.2647
[n]P , kg/m.m.s	0.047729	0.060407	0.093659	0.075717
[n]T , kg/m.m.s	0.043535	0.056113	0.081591	0.067383
XA2 * E04	35.8128	26.3154	24.1079	26.6972
XA3 * E04	0.1236	0.1392	0.6832	0.4288
f	0.980722	0.978296	0.893464	0.933125
f prime	0.996560	0.994725	0.971729	0.983979
k * E06 , m/s	25.3709	39.7376	58.6129	46.0803
(D)AM K/Tau * E07, m/s	1.5271	3.0205	24.0843	11.1358

```
Experiment No.          :  168
Operating Pressure      :  350   kPa
Nominal Solute Conc.    :  2000  ppm
Nominal Feed Flow Rate:  1000   ml/min
Setpoint Temperature    :  50.00  Degree C
Solute                  :  NACL
```

Avg. Feed Conc. (ppm) = 1937. ; XA1 =0.000598 ; C1 = 54.83 kmol/m.m.m

	Film # 1	Film # 2	Film # 3	Film # 4
	********	********	********	********
A * E09, kmol/m.m.s.kPa	469.6618	619.4335	835.8177	724.8079
[n]P , kg/m.m.s	0.002962	0.003907	0.005272	0.004571
[n]T , kg/m.m.s	0.001497	0.002149	0.002822	0.002493
XA2 * E04	6.3141	6.2770	6.2311	6.2729
XA3 * E04	0.5650	0.7163	0.9686	0.7927
f	0.905587	0.880295	0.838136	0.867528
f prime	0.910573	0.885947	0.844641	0.873699
k * E06 , m/s	25.3709	39.7376	58.6129	46.0803
(D)AM K/Tau * E07, m/s	1.4887	2.8014	5.2556	3.6498

```
Experiment No.          :  167
Operating Pressure      :  500   kPa
Nominal Solute Conc.    :  2000  ppm
Nominal Feed Flow Rate:  1000   ml/min
Setpoint Temperature    :  50.00  Degree C
Solute                  :  NACL
```

Avg. Feed Conc. (ppm) = 2001. ; XA1 =0.000618 ; C1 = 54.83 kmol/m.m.m

	Film # 1	Film # 2	Film # 3	Film # 4
	********	********	********	********
A * E09, kmol/m.m.s.kPa	460.9462	609.4021	828.8332	721.0696
[n]P , kg/m.m.s	0.004153	0.005491	0.007468	0.006497
[n]T , kg/m.m.s	0.002484	0.003564	0.004960	0.004274
XA2 * E04	6.7830	6.7166	6.6707	6.7309
XA3 * E04	0.3643	0.5016	0.6601	0.5534
f	0.941060	0.918853	0.893201	0.910458
f prime	0.946326	0.925372	0.901105	0.917826
k * E06 , m/s	25.3709	39.7376	58.6129	46.0803
(D)AM K/Tau * E07, m/s	1.4271	2.9105	5.5125	3.8750

```
                    Experiment No.          :  166
                    Operating Pressure      :  4000   kPa
                    Nominal Solute Conc.    :  2000   ppm
                    Nominal Feed Flow Rate:   1000   ml/min
                    Setpoint Temperature    :  50.00  Degree C
                    Solute                  :  NACL
```

Avg. Feed Conc. (ppm) = 2196. ; XA1 =0.000678 ; C1 = 54.83 kmol/m.m.m

	Film # 1	Film # 2	Film # 3	Film # 4
	********	********	********	********
A * E09, kmol/m.m.s.kPa	419.1942	542.1722	695.5278	667.7015
[n]P , kg/m.m.s	0.030216	0.039080	0.050134	0.048128
[n]T , kg/m.m.s	0.026974	0.035237	0.044923	0.041573
XA2 * E04	19.7047	16.4280	14.5478	16.2978
XA3 * E04	0.0953	0.1434	0.1547	0.4027
f	0.985950	0.978863	0.977195	0.940649
f prime	0.995171	0.991283	0.989378	0.975329
k * E06 , m/s	25.3709	39.7376	58.6129	46.0803
(D)AM K/Tau * E07, m/s	1.3273	3.1411	4.8382	10.6597

```
                    Experiment No.          :  165
                    Operating Pressure      :  1500   kPa
                    Nominal Solute Conc.    :  2000   ppm
                    Nominal Feed Flow Rate:   1000   ml/min
                    Setpoint Temperature    :  50.00  Degree C
                    Solute                  :  NACL
```

Avg. Feed Conc. (ppm) = 2086. ; XA1 =0.000644 ; C1 = 54.83 kmol/m.m.m

	Film # 1	Film # 2	Film # 3	Film # 4
	********	********	********	********
A * E09, kmol/m.m.s.kPa	450.8377	591.0794	769.7393	704.6805
[n]P , kg/m.m.s	0.012186	0.015977	0.020806	0.019048
[n]T , kg/m.m.s	0.010191	0.013655	0.017896	0.016281
XA2 * E04	9.6055	9.0345	8.6865	9.0412
XA3 * E04	0.1349	0.2085	0.2425	0.3950
f	0.979065	0.967654	0.962387	0.938714
f prime	0.985965	0.976942	0.972112	0.956345
k * E06 , m/s	25.3709	39.7376	58.6129	46.0803
(D)AM K/Tau * E07, m/s	1.4696	3.2647	5.2002	7.5279

```
Experiment No.          :  164
Operating Pressure      :  1500   kPa
Nominal Solute Conc.    :  2000   ppm
Nominal Feed Flow Rate:    1000   ml/min
Setpoint Temperature    :  25.00  Degree C
Solute                  :  NACL
```

Avg. Feed Conc. (ppm) = 2003. ; XA1 =0.000619 ; Cl = 55.35 kmol/m.m.m

	Film # 1	Film # 2	Film # 3	Film # 4
	********	********	********	********
A * E09, kmol/m.m.s.kPa	211.6363	288.5208	396.9393	342.3602
[n]P , kg/m.m.s	0.005721	0.007799	0.010729	0.009254
[n]T , kg/m.m.s	0.004862	0.006675	0.009185	0.007942
XA2 * E04	8.2580	7.9466	7.8189	8.0191
XA3 * E04	0.1144	0.1873	0.1689	0.1208
f	0.981512	0.969742	0.972713	0.980483
f prime	0.986154	0.976451	0.978416	0.984948
k * E06 , m/s	16.6000	26.0000	38.3500	30.1500
(D)AM K/Tau * E07, m/s	0.6915	1.6304	2.0524	1.2294

```
Experiment No.          :  163
Operating Pressure      :  350    kPa
Nominal Solute Conc.    :  2000   ppm
Nominal Feed Flow Rate:    1000   ml/min
Setpoint Temperature    :  45.00  Degree C
Solute                  :  NACL
```

Avg. Feed Conc. (ppm) = 1916. ; XA1 =0.000592 ; Cl = 54.95 kmol/m.m.m

	Film # 1	Film # 2	Film # 3	Film # 4
	********	********	********	********
A * E09, kmol/m.m.s.kPa	405.9424	559.5238	761.9497	669.2830
[n]P , kg/m.m.s	0.002560	0.003529	0.004806	0.004221
[n]T , kg/m.m.s	0.001385	0.001915	0.002764	0.002345
XA2 * E04	6.2479	6.1996	6.1848	6.2133
XA3 * E04	0.4843	0.6370	0.7985	0.6846
f	0.918179	0.892365	0.865087	0.884328
f prime	0.922537	0.897303	0.870968	0.889878
k * E06 , m/s	23.5406	36.8709	54.3845	42.7560
(D)AM K/Tau * E07, m/s	1.1753	2.2144	4.1365	2.9322

```
Experiment No.          :  162
Operating Pressure      :  7000  kPa
Nominal Solute Conc.    :  2000  ppm
Nominal Feed Flow Rate: 1000  ml/min
Setpoint Temperature    :  45.00  Degree C
Solute                  :  NACL
```

Avg. Feed Conc. (ppm) = 2330. ; XA1 =0.000719 ; C1 = 54.95 kmol/m.m.m

	Film # 1	Film # 2	Film # 3	Film # 4
	********	********	********	********
A * E09, kmol/m.m.s.kPa	336.7895	438.5875	678.4378	548.7390
[n]P , kg/m.m.s	0.042483	0.055323	0.085578	0.069218
[n]T , kg/m.m.s	0.039135	0.050657	0.072500	0.061327
XA2 * E04	38.0659	28.3092	25.5102	29.0677
XA3 * E04	0.1130	0.1675	0.7523	0.4785
f	0.984303	0.976739	0.895501	0.933539
f prime	0.997042	0.994101	0.970581	0.983586
k * E06 , m/s	23.5406	36.8709	54.3845	42.7560
(D)AM K/Tau * E07, m/s	1.1774	3.0451	22.2490	10.3672

```
Experiment No.          :  161
Operating Pressure      :  500   kPa
Nominal Solute Conc.    :  2000  ppm
Nominal Feed Flow Rate: 1000  ml/min
Setpoint Temperature    :  45.00  Degree C
Solute                  :  NACL
```

Avg. Feed Conc. (ppm) = 1966. ; XA1 =0.000607 ; C1 = 54.95 kmol/m.m.m

	Film # 1	Film # 2	Film # 3	Film # 4
	********	********	********	********
A * E09, kmol/m.m.s.kPa	406.7442	551.1316	764.9291	666.6842
[n]P , kg/m.m.s	0.003665	0.004966	0.006892	0.006007
[n]T , kg/m.m.s	0.002292	0.003317	0.004720	0.004045
XA2 * E04	6.6600	6.6010	6.5642	6.6233
XA3 * E04	0.3689	0.4958	0.6846	0.5592
f	0.939266	0.918377	0.887291	0.907936
f prime	0.944642	0.924937	0.895768	0.915620
k * E06 , m/s	23.5406	36.8709	54.3845	42.7560
(D)AM K/Tau * E07, m/s	1.3575	2.7199	5.5493	3.7663

Experiment No.   : 160
Operating Pressure   : 4000   kPa
Nominal Solute Conc.   : 2000   ppm
Nominal Feed Flow Rate: 1000   ml/min
Setpoint Temperature   : 45.00 Degree C
Solute   : NACL

Avg. Feed Conc. (ppm) = 2212. ; XA1 =0.000683 ; Cl = 54.95 kmol/m.m.m

	Film # 1	Film # 2	Film # 3	Film # 4
	********	********	********	********
A * E09, kmol/m.m.s.kPa	375.2054	517.1315	679.2381	655.0576
[n]P , kg/m.m.s	0.027045	0.037275	0.048959	0.047217
[n]T , kg/m.m.s	0.024646	0.032004	0.042356	0.038627
XA2 * E04	19.4804	16.2185	14.7895	16.4090
XA3 * E04	0.0968	0.1378	0.1746	0.4027
f	0.985846	0.979844	0.974464	0.941081
f prime	0.995043	0.991519	0.988215	0.975497
k * E06 , m/s	23.5406	36.8709	54.3845	42.7560
(D)AM K/Tau * E07, m/s	1.2423	2.7690	5.1086	9.8138

Experiment No.   : 159
Operating Pressure   : 1500   kPa
Nominal Solute Conc.   : 2000   ppm
Nominal Feed Flow Rate: 1000   ml/min
Setpoint Temperature   : 45.00 Degree C
Solute   : NACL

Avg. Feed Conc. (ppm) = 2217. ; XA1 =0.000685 ; Cl = 54.95 kmol/m.m.m

	Film # 1	Film # 2	Film # 3	Film # 4
	********	********	********	********
A * E09, kmol/m.m.s.kPa	392.8058	531.5652	716.1673	651.5069
[n]P , kg/m.m.s	0.010618	0.014368	0.019358	0.017610
[n]T , kg/m.m.s	0.008708	0.011984	0.015958	0.014653
XA2 * E04	9.8794	9.4210	9.1092	9.4997
XA3 * E04	0.1519	0.2226	0.2891	0.4335
f	0.977828	0.967506	0.957802	0.936738
f prime	0.984638	0.976389	0.968287	0.954413
k * E06 , m/s	23.5406	36.8709	54.3845	42.7560
(D)AM K/Tau * E07, m/s	1.3733	2.9293	5.2826	7.0744

Experiment No.   : 158
Operating Pressure   : 1500 kPa
Nominal Solute Conc.   : 2000 ppm
Nominal Feed Flow Rate: 1000 ml/min
Setpoint Temperature   : 25.00 Degree C
Solute   : NACL

Avg. Feed Conc. (ppm) = 1998. ; XA1 =0.000617 ; C1 = 55.35 kmol/m.m.m

	Film # 1	Film # 2	Film # 3	Film # 4
	********	********	********	********
A * E09, kmol/m.m.s.kPa	215.3515	293.8619	416.8134	389.5400
[n]P , kg/m.m.s	0.005821	0.007943	0.011266	0.010529
[n]T , kg/m.m.s	0.004990	0.006849	0.009715	0.008603
XA2 * E04	8.2927	7.9671	7.8886	8.1143
XA3 * E04	0.1321	0.2212	0.2226	0.2962
f	0.978598	0.964160	0.963931	0.952014
f prime	0.984082	0.972253	0.971798	0.963524
k * E06 , m/s	16.6000	26.0000	38.3500	30.1500
(D)AM K/Tau * E07, m/s	0.8159	1.9755	2.8494	3.2915

Experiment No.   : 157
Operating Pressure   : 7000 kPa
Nominal Solute Conc.   : 2000 ppm
Nominal Feed Flow Rate: 1000 ml/min
Setpoint Temperature   : 40.00 Degree C
Solute   : NACL

Avg. Feed Conc. (ppm) = 2215. ; XA1 =0.000684 ; C1 = 55.06 kmol/m.m.m

	Film # 1	Film # 2	Film # 3	Film # 4
	********	********	********	********
A * E09, kmol/m.m.s.kPa	300.4419	395.1289	626.8586	505.9315
[n]P , kg/m.m.s	0.037898	0.049842	0.079072	0.063818
[n]T , kg/m.m.s	0.034389	0.045910	0.067583	0.056552
XA2 * E04	33.1610	26.0751	24.5934	27.4393
XA3 * E04	0.1151	0.1717	0.6630	0.4565
f	0.983176	0.974908	0.903120	0.933293
f prime	0.996539	0.993431	0.973107	0.983408
k * E06 , m/s	21.7667	34.0924	50.2863	39.5341
(D)AM K/Tau * E07, m/s	1.2080	3.0679	18.8710	9.6439

Experiment No.   : 156
Operating Pressure   : 500 kPa
Nominal Solute Conc.   : 2000 ppm
Nominal Feed Flow Rate: 1000 ml/min
Setpoint Temperature   : 40.00 Degree C
Solute   : NACL

Avg. Feed Conc. (ppm) = 1942. ; XA1 =0.000600 ; Cl = 55.06 kmol/m.m.m

	Film # 1	Film # 2	Film # 3	Film # 4
	********	********	********	********
A * E09, kmol/m.m.s.kPa	361.4060	493.8543	711.3137	614.0159
[n]P , kg/m.m.s	0.003256	0.004450	0.006409	0.005532
[n]T , kg/m.m.s	0.001957	0.002972	0.004346	0.003698
XA2 * E04	6.5274	6.5002	6.4771	6.5370
XA3 * E04	0.4073	0.5189	0.7235	0.5361
f	0.932118	0.913531	0.879421	0.910649
f prime	0.937635	0.920226	0.888360	0.918032
k * E06 , m/s	21.7667	34.0924	50.2863	39.5341
(D)AM K/Tau * E07, m/s	1.3129	2.5977	5.5069	3.3295

Experiment No.   : 155
Operating Pressure   : 350 kPa
Nominal Solute Conc.   : 2000 ppm
Nominal Feed Flow Rate: 1000 ml/min
Setpoint Temperature   : 40.00 Degree C
Solute   : NACL

Avg. Feed Conc. (ppm) = 2182. ; XA1 =0.000674 ; Cl = 55.06 kmol/m.m.m

	Film # 1	Film # 2	Film # 3	Film # 4
	********	********	********	********
A * E09, kmol/m.m.s.kPa	367.5854	499.6022	727.6147	624.1310
[n]P , kg/m.m.s	0.002318	0.003151	0.004589	0.003936
[n]T , kg/m.m.s	0.001143	0.001632	0.002429	0.002077
XA2 * E04	7.0632	7.0247	7.0111	7.0512
XA3 * E04	0.7855	0.9743	1.3007	1.0118
f	0.883523	0.855519	0.807114	0.849960
f prime	0.888861	0.861382	0.814585	0.856592
k * E06 , m/s	21.7667	34.0924	50.2863	39.5341
(D)AM K/Tau * E07, m/s	1.4407	2.6477	5.5755	3.5068

Experiment No.   :   154
Operating Pressure   :   1500   kPa
Nominal Solute Conc.   :   2000   ppm
Nominal Feed Flow Rate: 1000   ml/min
Setpoint Temperature   :   40.00   Degree C
Solute   :   NACL

Avg. Feed Conc. (ppm) = 2025. ; XA1 =0.000625 ; Cl = 55.06 kmol/m.m.m

	Film # 1	Film # 2	Film # 3	Film # 4
	********	********	********	********
A * E09, kmol/m.m.s.kPa	353.8584	470.2121	647.2628	591.2390
[n]P , kg/m.m.s	0.009565	0.012710	0.017496	0.015981
[n]T , kg/m.m.s	0.007910	0.010821	0.014994	0.013586
XA2 * E04	8.9508	8.5242	8.3407	8.6736
XA3 * E04	0.1491	0.2226	0.2920	0.3996
f	0.976167	0.964407	0.953326	0.936110
f prime	0.983358	0.973902	0.965024	0.953962
k * E06 , m/s	21.7667	34.0924	50.2863	39.5341
(D)AM K/Tau * E07, m/s	1.3504	2.9248	5.4815	6.6134

Experiment No.   :   153
Operating Pressure   :   4000   kPa
Nominal Solute Conc.   :   2000   ppm
Nominal Feed Flow Rate: 1000   ml/min
Setpoint Temperature   :   40.00   Degree C
Solute   :   NACL

Avg. Feed Conc. (ppm) = 2150. ; XA1 =0.000664 ; Cl = 55.06 kmol/m.m.m

	Film # 1	Film # 2	Film # 3	Film # 4
	********	********	********	********
A * E09, kmol/m.m.s.kPa	335.1946	445.2888	593.5502	569.3642
[n]P , kg/m.m.s	0.024161	0.032096	0.042783	0.041040
[n]T , kg/m.m.s	0.021760	0.028952	0.038907	0.035732
XA2 * E04	18.0108	15.4084	14.2745	15.9266
XA3 * E04	0.1010	0.1618	0.1760	0.3935
f	0.984801	0.975647	0.973518	0.940779
f prime	0.994403	0.989514	0.987690	0.975331
k * E06 , m/s	21.7667	34.0924	50.2863	39.5341
(D)AM K/Tau * E07, m/s	1.2367	3.0969	4.8940	9.1224

```
                    Experiment No.          :  152
                    Operating Pressure      :  1500   kPa
                    Nominal Solute Conc.    :  2000   ppm
                    Nominal Feed Flow Rate:  1000   ml/min
                    Setpoint Temperature    :  25.00  Degree C
                    Solute                  :  NACL
```

Avg. Feed Conc. (ppm) = 2017. ; XA1 =0.000623 ; Cl = 55.35 kmol/m.m.m

	Film # 1	Film # 2	Film # 3	Film # 4
	********	********	********	********
A * E09, kmol/m.m.s.kPa	220.4494	299.2283	429.1364	371.1692
[n]P , kg/m.m.s	0.005959	0.008088	0.011600	0.010033
[n]T , kg/m.m.s	0.004926	0.006884	0.009932	0.008581
XA2 * E04	8.3390	8.0613	8.0091	8.2380
XA3 * E04	0.1307	0.1929	0.2156	0.1364
f	0.979023	0.969033	0.965401	0.978115
f prime	0.984340	0.976085	0.973105	0.983461
k * E06 , m/s	16.6000	26.0000	38.3500	30.1500
(D)AM K/Tau * E07, m/s	0.7904	1.7013	2.7688	1.4555

```
                    Experiment No.          :  151
                    Operating Pressure      :  500   kPa
                    Nominal Solute Conc.    :  2000   ppm
                    Nominal Feed Flow Rate:  1000   ml/min
                    Setpoint Temperature    :  35.00  Degree C
                    Solute                  :  NACL
```

Avg. Feed Conc. (ppm) = 1942. ; XA1 =0.000600 ; Cl = 55.18 kmol/m.m.m

	Film # 1	Film # 2	Film # 3	Film # 4
	********	********	********	********
A * E09, kmol/m.m.s.kPa	300.8132	429.9346	627.0288	543.3154
[n]P , kg/m.m.s	0.002710	0.003874	0.005650	0.004895
[n]T , kg/m.m.s	0.001864	0.002589	0.003817	0.003313
XA2 * E04	6.5477	6.4732	6.4556	6.5237
XA3 * E04	0.3827	0.4929	0.6947	0.5044
f	0.936215	0.917855	0.884225	0.915933
f prime	0.941581	0.923899	0.892451	0.922722
k * E06 , m/s	20.0466	31.3984	46.3126	36.4100
(D)AM K/Tau * E07, m/s	1.1637	2.1457	4.6287	2.7921

```
                    Experiment No.          :   150
                    Operating Pressure      :   500   kPa
                    Nominal Solute Conc.    :   2000  ppm
                    Nominal Feed Flow Rate:     1000  ml/min
                    Setpoint Temperature    :   30.00  Degree C
                    Solute                  :   NACL
```

Avg. Feed Conc. (ppm) = 1937. ; XA1 =0.000598 ; C1 = 55.25 kmol/m.m.m

	Film # 1	Film # 2	Film # 3	Film # 4
A * E09, kmol/m.m.s.kPa	264.6334	368.3412	543.3338	468.8332
[n]P , kg/m.m.s	0.002384	0.003319	0.004895	0.004224
[n]T , kg/m.m.s	0.001618	0.002246	0.003399	0.002874
XA2 * E04	6.5011	6.4292	6.4280	6.4810
XA3 * E04	0.3489	0.4785	0.6370	0.4411
f	0.941690	0.920038	0.893544	0.926282
f prime	0.946359	0.925619	0.900954	0.931975
k * E06 , m/s	18.3861	28.7975	42.4763	33.3940
(D)AM K/Tau * E07, m/s	0.9215	1.8141	3.7551	2.1083

```
                    Experiment No.          :   149
                    Operating Pressure      :   500   kPa
                    Nominal Solute Conc.    :   2000  ppm
                    Nominal Feed Flow Rate:     1000  ml/min
                    Setpoint Temperature    :   25.00  Degree C
                    Solute                  :   NACL
```

Avg. Feed Conc. (ppm) = 1905. ; XA1 =0.000588 ; C1 = 55.35 kmol/m.m.m

	Film # 1	Film # 2	Film # 3	Film # 4
A * E09, kmol/m.m.s.kPa	224.4699	311.5701	459.5628	380.9228
[n]P , kg/m.m.s	0.002022	0.002807	0.004141	0.003432
[n]T , kg/m.m.s	0.001367	0.001908	0.002863	0.002416
XA2 * E04	6.3602	6.2963	6.2927	6.3423
XA3 * E04	0.3351	0.4641	0.6082	0.3874
f	0.943066	0.921152	0.896664	0.934189
f prime	0.947343	0.926335	0.903401	0.938962
k * E06 , m/s	16.6000	26.0000	38.3500	30.1500
(D)AM K/Tau * E07, m/s	0.7637	1.5245	3.0769	1.5780

```
                    Experiment No.          :  148
                    Operating Pressure      :  1500   kPa
                    Nominal Solute Conc.    :  2000   ppm
                    Nominal Feed Flow Rate:   1000   ml/min
                    Setpoint Temperature    :  25.00  Degree C
                    Solute                  :  NACL
```

Avg. Feed Conc. (ppm) = 2015. ;   XA1 =0.000622 ; C1 = 55.35 kmol/m.m.m

	Film # 1	Film # 2	Film # 3	Film # 4
A * E09, kmol/m.m.s.kPa	217.9573	299.2154	430.4684	387.1135
[n]P , kg/m.m.s	0.005891	0.008088	0.011636	0.010464
[n]T , kg/m.m.s	0.004974	0.006916	0.009987	0.008882
XA2 * E04	8.3562	8.0614	8.0132	8.2614
XA3 * E04	0.1349	0.2071	0.2212	0.2891
f	0.978327	0.966741	0.964469	0.953563
f prime	0.983864	0.974332	0.972413	0.965030
k * E06 , m/s	16.6000	26.0000	38.3500	30.1500
(D)AM K/Tau * E07, m/s	0.8201	1.8315	2.8478	3.2351

```
                    Experiment No.          :  147
                    Operating Pressure      :  350    kPa
                    Nominal Solute Conc.    :  2000   ppm
                    Nominal Feed Flow Rate:   1000   ml/min
                    Setpoint Temperature    :  25.00  Degree C
                    Solute                  :  NACL
```

Avg. Feed Conc. (ppm) = 1918. ;   XA1 =0.000592 ; C1 = 55.35 kmol/m.m.m

	Film # 1	Film # 2	Film # 3	Film # 4
A * E09, kmol/m.m.s.kPa	232.0499	323.0282	484.7260	414.0298
[n]P , kg/m.m.s	0.001464	0.002037	0.003057	0.002611
[n]T , kg/m.m.s	0.000854	0.001198	0.001852	0.001521
XA2 * E04	6.2092	6.1710	6.1737	6.2009
XA3 * E04	0.5289	0.6918	0.8821	0.5794
f	0.910754	0.883272	0.851166	0.902242
f prime	0.914862	0.887955	0.857200	0.906616
k * E06 , m/s	16.6000	26.0000	38.3500	30.1500
(D)AM K/Tau * E07, m/s	0.7989	1.5195	3.1005	1.5746

```
Experiment No.          :  146
Operating Pressure      :  4000   kPa
Nominal Solute Conc.    :  2000   ppm
Nominal Feed Flow Rate:    1000   ml/min
Setpoint Temperature    :  25.00  Degree C
Solute                  :  NACL
```

Avg. Feed Conc. (ppm) = 2051. ; XA1 =0.000633 ; Cl = 55.35 kmol/m.m.m

	Film # 1	Film # 2	Film # 3	Film # 4
	********	********	********	********
A * E09, kmol/m.m.s.kPa	206.7386	280.4731	388.8257	369.9353
[n]P , kg/m.m.s	0.014902	0.020217	0.028027	0.026665
[n]T , kg/m.m.s	0.013719	0.018552	0.025744	0.023248
XA2 * E04	14.3870	12.7654	12.2679	13.3911
XA3 * E04	0.0925	0.1802	0.1547	0.2849
f	0.985405	0.971568	0.975585	0.955052
f prime	0.993579	0.985901	0.987401	0.978753
k * E06 , m/s	16.6000	26.0000	38.3500	30.1500
(D)AM K/Tau * E07, m/s	0.8917	2.6680	3.3032	5.0755

```
Experiment No.          :  145
Operating Pressure      :  7000   kPa
Nominal Solute Conc.    :  2000   ppm
Nominal Feed Flow Rate:    1000   ml/min
Setpoint Temperature    :  25.00  Degree C
Solute                  :  NACL
```

Avg. Feed Conc. (ppm) = 2100. ; XA1 =0.000648 ; Cl = 55.35 kmol/m.m.m

	Film # 1	Film # 2	Film # 3	Film # 4
	********	********	********	********
A * E09, kmol/m.m.s.kPa	196.1324	261.9339	430.7150	342.3762
[n]P , kg/m.m.s	0.024740	0.033040	0.054330	0.043187
[n]T , kg/m.m.s	0.022979	0.030862	0.046653 ·	0.038446
XA2 * E04	25.6079	20.8526	20.4573	22.2875
XA3 * E04	0.1222	0.2014	0.6269	0.3843
f	0.981162	0.968951	0.903354	0.940763
f prime	0.995240	0.990360	0.969414	0.982796
k * E06 , m/s	16.6000	26.0000	38.3500	30.1500
(D)AM K/Tau * E07, m/s	1.1068	3.0234	14.8129	6.7747

```
Experiment No.          :  144
Operating Pressure      :  7000   kPa
Nominal Solute Conc.    :  2000   ppm
Nominal Feed Flow Rate:    1000   ml/min
Setpoint Temperature    :  35.00  Degree C
Solute                  :  NACL
```

Avg. Feed Conc. (ppm) = 2233. ; XA1 =0.000690 ; Cl = 55.25 kmol/m.m.m

	Film # 1	Film # 2	Film # 3	Film # 4
	********	********	********	********
A * E09, kmol/m.m.s.kPa	266.4975	348.1102	578.8597	454.9702
[n]P , kg/m.m.s	0.033616	0.043911	0.073017	0.057390
[n]T , kg/m.m.s	0.030833	0.040787	0.061416	0.051175
XA2 * E04	31.9385	24.9591	24.1278	26.9163
XA3 * E04	C.1265	0.1929	0.7350	0.4641
f	0.981677	0.972044	0.893490	0.932755
f prime	0.996053	0.992289	0.969606	0.982804
k * E06 , m/s	20.0466	31.3984	46.3126	36.4100
(D)AM K/Tau * E07, m/s	1.2312	3.1916	19.3813	9.0178

```
Experiment No.          :  143
Operating Pressure      :  4000   kPa
Nominal Solute Conc.    :  2000   ppm
Nominal Feed Flow Rate:    1000   ml/min
Setpoint Temperature    :  35.00  Degree C
Solute                  :  NACL
```

Avg. Feed Conc. (ppm) = 2190. ; XA1 =0.000676 ; Cl = 55.25 kmol/m.m.m

	Film # 1	Film # 2	Film # 3	Film # 4
	********	********	********	********
A * E09, kmol/m.m.s.kPa	286.2175	382.3244	522.0102	498.3660
[n]P , kg/m.m.s	0.020631	0.027558	0.037626	0.035922
[n]T , kg/m.m.s	0.018792	0.025193	0.034499	0.031577
XA2 * E04	17.2025	14.9356	14.1325	15.6356
XA3 * E04	0.1067	0.1830	0.1604	0.3950
f	0.984244	0.972960	0.976303	0.941639
f prime	0.993811	0.987763	0.988666	0.974773
k * E06 , m/s	20.0466	31.3984	46.3126	36.4100
(D)AM K/Tau * E07, m/s	1.1775	3.1394	3.9779	8.2201

```
Experiment No.          :  142
Operating Pressure      :  1500   kPa
Nominal Solute Conc.    :  2000   ppm
Nominal Feed Flow Rate:    1000   ml/min
Setpoint Temperature    :  35.00  Degree C
Solute                  :  NACL
```

Avg. Feed Conc. (ppm) = 2116. ;   XA1 =0.000653 ; Cl = 55.25 kmol/m.m.m

	Film # 1	Film # 2	Film # 3	Film # 4
A * E09, kmol/m.m.s.kPa	305.5137	415.0137	584.4057	504.9475
[n]P , kg/m.m.s	0.008258	0.011218	0.015796	0.013649
[n]T , kg/m.m.s	0.006936	0.009508	0.013428	0.011678
XA2 * E04	9.1864	8.7629	8.6484	8.9385
XA3 * E04	0.1590	0.2707	0.2863	0.2156
f	0.975679	0.958583	0.956202	0.967023
f prime	0.982709	0.969130	0.966923	0.975904
k * E06 , m/s	20.0466	31.3984	46.3126	36.4100
(D)AM K/Tau * E07, m/s	1.2269	3.0444	4.6175	2.8987

```
Experiment No.          :  141
Operating Pressure      :  350    kPa
Nominal Solute Conc.    :  2000   ppm
Nominal Feed Flow Rate:    1000   ml/min
Setpoint Temperature    :  35.00  Degree C
Solute                  :  NACL
```

Avg. Feed Conc. (ppm) = 1940. ;   XA1 =0.000599 ; Cl = 55.25 kmol/m.m.m

	Film # 1	Film # 2	Film # 3	Film # 4
A * E09, kmol/m.m.s.kPa	326.0941	450.3411	663.4057	567.0012
[n]P , kg/m.m.s	0.002057	0.002840	0.004184	0.003576
[n]T , kg/m.m.s	0.001121	0.001666	0.002557	0.002125
XA2 * E04	6.2991	6.2729	6.2707	6.3039
XA3 * E04	0.6298	0.8100	1.0551	0.7812
f	0.894892	0.864822	0.823919	0.869633
f prime	0.900070	0.870944	0.831835	0.876150
k * E06 , m/s	20.0466	31.3984	46.3126	36.4100
(D)AM K/Tau * E07, m/s	1.2508	2.4805	5.1932	3.0184

```
Experiment No.          :  140
Operating Pressure      :  7000   kPa
Nominal Solute Conc.    :  2000   ppm
Nominal Feed Flow Rate:  1000   ml/min
Setpoint Temperature    :  30.00  Degree C
Solute                  :  NACL
```

Avg. Feed Conc. (ppm) = 2169. ; XA1 =0.000670 ; C1 = 55.25 kmol/m.m.m

	Film # 1	Film # 2	Film # 3	Film # 4
	********	********	********	********
A * E09, kmol/m.m.s.kPa	231.9614	306.6821	508.0084	405.3347
[n]P , kg/m.m.s	0.029260	0.038685	0.064080	0.051129
[n]T , kg/m.m.s	0.026806	0.035975	0.055214	0.045273
XA2 * E04	28.5270	22.9588	22.6907	24.7094
XA3 * E04	0.1321	0.2113	0.7523	0.4929
f	0.980290	0.968471	0.887750	0.926459
f prime	0.995382	0.990816	0.966916	0.980100
k * E06 , m/s	18.3861	28.7975	42.4763	33.3940
(D)AM K/Tau * E07, m/s	1.2528	3.3569	19.0160	9.2553

```
Experiment No.          :  139
Operating Pressure      :  4000   kPa
Nominal Solute Conc.    :  2000   ppm
Nominal Feed Flow Rate:  1000   ml/min
Setpoint Temperature    :  30.00  Degree C
Solute                  :  NACL
```

Avg. Feed Conc. (ppm) = 2169. ; XA1 =0.000670 ; C1 = 55.25 kmol/m.m.m

	Film # 1	Film # 2	Film # 3	Film # 4
	********	********	********	********
A * E09, kmol/m.m.s.kPa	248.2405	334.6183	460.8637	443.5312
[n]P , kg/m.m.s	0.017893	0.024119	0.033219	0.031970
[n]T , kg/m.m.s	0.016249	0.021969	0.030200	0.027818
XA2 * E04	16.1223	14.1978	13.5216	14.9469
XA3 * E04	0.1052	0.1859	0.1519	0.3950
f	0.984299	0.972270	0.977335	0.941062
f prime	0.993483	0.986927	0.988780	0.973609
k * E06 , m/s	18.3861	28.7975	42.4763	33.3940
(D)AM K/Tau * E07, m/s	1.0723	2.9269	3.4466	7.5844

```
                    Experiment No.          :  138
                    Operating Pressure      :  1500   kPa
                    Nominal Solute Conc.    :  2000   ppm
                    Nominal Feed Flow Rate: 1000   ml/min
                    Setpoint Temperature    :  30.00  Degree C
                    Solute                  :  NACL
```

Avg. Feed Conc. (ppm) = 2017. ;   XA1 =0.000623 ; Cl = 55.25 kmol/m.m.m

	Film # 1	Film # 2	Film # 3	Film # 4
	********	********	********	********
A * E09, kmol/m.m.s.kPa	260.9728	357.5129	513.0273	440.3700
[n]P , kg/m.m.s	0.007054	0.009664	0.013867	0.011903
[n]T , kg/m.m.s	0.006012	0.008289	0.011944	0.010344
XA2 * E04	8.5873	8.2319	8.1746	8.4385
XA3 * E04	0.1547	0.2453	0.2580	0.1661
f	0.975163	0.960632	0.958589	0.973347
f prime	0.981995	0.970228	0.968462	0.980337
k * E06 , m/s	18.3861	28.7975	42.4763	33.3940
(D)AM K/Tau * E07, m/s	1.1081	2.5568	3.9097	2.0856

```
                    Experiment No.          :  137
                    Operating Pressure      :  350    kPa
                    Nominal Solute Conc.    :  2000   ppm
                    Nominal Feed Flow Rate: 1000   ml/min
                    Setpoint Temperature    :  30.00  Degree C
                    Solute                  :  NACL
```

Avg. Feed Conc. (ppm) = 1998. ;   XA1 =0.000617 ; Cl = 55.25 kmol/m.m.m

	Film # 1	Film # 2	Film # 3	Film # 4
	********	********	********	********
A * E09, kmol/m.m.s.kPa	278.6245	386.8718	574.7944	490.3496
[n]P , kg/m.m.s	0.001757	0.002440	0.003625	0.003093
[n]T , kg/m.m.s	0.000991	0.001402	0.002148	0.001781
XA2 * E04	6.4797	6.4393	6.4394	6.4673
XA3 * E04	0.5852	0.7812	0.9830	0.7523
f	0.905204	0.873445	0.840748	0.878116
f prime	0.909749	0.878756	0.847433	0.883737
k * E06 , m/s	18.3861	28.7975	42.4763	33.3940
(D)AM K/Tau * E07, m/s	0.9875	1.9443	3.8851	2.3545

```
Experiment No.          :  136
Operating Pressure      :  1500  kPa
Nominal Solute Conc.    :  2000  ppm
Nominal Feed Flow Rate:  1000  ml/min
Setpoint Temperature    :  25.00  Degree C
Solute                  :  NACL
```

Avg. Feed Conc. (ppm) = 2094. ; XA1 =0.000647 ; Cl = 55.35 kmol/m.m.m

	Film # 1	Film # 2	Film # 3	Film # 4
	********	********	********	********
A * E09, kmol/m.m.s.kPa	221.2796	304.5642	437.3468	374.6634
[n]P , kg/m.m.s	0.005981	0.008232	0.011821	0.010127
[n]T , kg/m.m.s	0.005099	0.007065	0.010221	0.008672
XA2 * E04	8.7442	8.4090	8.3741	8.5757
XA3 * E04	0.1519	0.2651	0.2396	0.1576
f	0.976523	0.959033	0.962968	0.975648
f prime	0.982641	0.968502	0.971409	0.981641
k * E06 , m/s	16.6000	26.0000	38.3500	30.1500
(D)AM K/Tau * E07, m/s	0.9055	2.3098	3.0238	1.6304

```
Experiment No.          :  135
Operating Pressure      :  350  kPa
Nominal Solute Conc.    :  2000  ppm
Nominal Feed Flow Rate:  1000  ml/min
Setpoint Temperature    :  25.00  Degree C
Solute                  :  NACL
```

Avg. Feed Conc. (ppm) = 1953. ; XA1 =0.000603 ; Cl = 55.35 kmol/m.m.m

	Film # 1	Film # 2	Film # 3	Film # 4
	********	********	********	********
A * E09, kmol/m.m.s.kPa	235.7816	330.3700	495.6989	417.1633
[n]P , kg/m.m.s	0.001487	0.002084	0.003126	0.002631
[n]T , kg/m.m.s	0.000864	0.001253	0.001879	0.001534
XA2 * E04	6.3227	6.2876	6.2862	6.3102
XA3 * E04	0.5650	0.8244	0.9397	0.6731
f	0.906356	0.863350	0.844234	0.888438
f prime	0.910695	0.868954	0.850590	0.893396
k * E06 , m/s	16.6000	26.0000	38.3500	30.1500
(D)AM K/Tau * E07, m/s	0.8515	1.8987	3.3173	1.8391

```
Experiment No.          :  134
Operating Pressure      :  7000   kPa
Nominal Solute Conc.    :  2000   ppm
Nominal Feed Flow Rate:    1000   ml/min
Setpoint Temperature    :  25.00  Degree C
Solute                  :  NACL
```

Avg. Feed Conc. (ppm) = 2182. ; XA1 =0.000674 ; Cl = 55.35 kmol/m.m.m

	Film # 1	Film # 2	Film # 3	Film # 4
	********	********	********	********
A * E09, kmol/m.m.s.kPa	197.3599	265.3977	370.8109	353.9617
[n]P , kg/m.m.s	0.024895	0.033477	0.046774	0.044649
[n]T , kg/m.m.s	0.023085	0.031354	0.044323	0.039842
XA2 * E04	26.7710	22.0082	19.9737	24.1574
XA3 * E04	0.1335	0.2439	0.6860	0.4335
f	0.980201	0.963840	0.898271	0.935728
f prime	0.995025	0.988943	0.965719	0.982100
k * E06 , m/s	16.6000	26.0000	38.3500	30.1500
(D)AM K/Tau * E07, m/s	1.1624	3.5286	15.8328	7.3113

```
Experiment No.          :  133
Operating Pressure      :  4000   kPa
Nominal Solute Conc.    :  2000   ppm
Nominal Feed Flow Rate:    1000   ml/min
Setpoint Temperature    :  25.00  Degree C
Solute                  :  NACL
```

Avg. Feed Conc. (ppm) = 2118. ; XA1 =0.000654 ; Cl = 55.35 kmol/m.m.m

	Film # 1	Film # 2	Film # 3	Film # 4
	********	********	********	********
A * E09, kmol/m.m.s.kPa	224.1806	305.0125	424.4180	411.3480
[n]P , kg/m.m.s	0.016159	0.021985	0.030592	0.029650
[n]T , kg/m.m.s	0.014713	0.020126	0.028061	0.025640
XA2 * E04	15.7502	13.9544	13.4873	14.8606
XA3 * E04	0.1095	0.2212	0.1250	0.3597
f	0.983273	0.966200	0.980896	0.945045
f prime	0.993060	0.984168	0.990741	0.975831
k * E06 , m/s	16.6000	26.0000	38.3500	30.1500
(D)AM K/Tau * E07, m/s	1.0344	3.2563	2.6374	6.3876

```
                    Experiment No.          :  132
                    Operating Pressure      :  500   kPa
                    Nominal Solute Conc.    :  2000  ppm
                    Nominal Feed Flow Rate:   1000  ml/min
                    Setpoint Temperature    :  25.00  Degree C
                    Solute                  :  NACL
```

Avg. Feed Conc. (ppm) = 1929. ; XA1 =0.000596 ; C1 = 55.35 kmol/m.m.m

	Film # 1	Film # 2	Film # 3	Film # 4
	********	********	********	********
A * E09, kmol/m.m.s.kPa	227.8545	320.1304	476.5288	412.2189
[n]P , kg/m.m.s	0.002053	0.002884	0.004294	0.003714
[n]T , kg/m.m.s	0.001402	0.001994	0.003008	0.002575
XA2 * E04	6.4504	6.3886	6.3936	6.4501
XA3 * E04	0.3643	0.5477	0.6111	0.4335
f	0.938871	0.908100	0.897458	0.927268
f prime	0.943556	0.914322	0.904476	0.932839
k * E06 , m/s	16.6000	26.0000	38.3500	30.1500
(D)AM K/Tau * E07, m/s	0.8427	1.8778	3.1924	1.8632

```
                    Experiment No.          :  131
                    Operating Pressure      :  1500  kPa
                    Nominal Solute Conc.    :  2000  ppm
                    Nominal Feed Flow Rate:   1000  ml/min
                    Setpoint Temperature    :  25.00  Degree C
                    Solute                  :  NACL
```

Avg. Feed Conc. (ppm) = 2062. ; XA1 =0.000637 ; C1 = 55.35 kmol/m.m.m

	Film # 1	Film # 2	Film # 3	Film # 4
	********	********	********	********
A * E09, kmol/m.m.s.kPa	220.3226	304.4255	440.0293	380.9379
[n]P , kg/m.m.s	0.005955	0.008229	0.011894	0.010297
[n]T , kg/m.m.s	0.005048	0.007070	0.010233	0.008900
XA2 * E04	8.5820	8.2724	8.2479	8.5047
XA3 * E04	0.1547	0.2891	0.2368	0.1618
f	0.975712	0.954619	0.962835	0.974602
f prime	0.981984	0.965076	0.971314	0.980989
k * E06 , m/s	16.6000	26.0000	38.3500	30.1500
(D)AM K/Tau * E07, m/s	0.9310	2.5716	3.0378	1.7338

```
Experiment No.          :  130
Operating Pressure      :  350   kPa
Nominal Solute Conc.    :  2000  ppm
Nominal Feed Flow Rate:  1000  ml/min
Setpoint Temperature    :  20.00  Degree C
Solute                  :  NACL
```

Avg. Feed Conc. (ppm) = 1934. ; XA1 =0.000597 ; C1 = 55.40 kmol/m.m.m

	Film # 1	Film # 2	Film # 3	Film # 4
	********	********	********	********
A * E09, kmol/m.m.s.kPa	194.3663	274.7225	414.9802	356.7242
[n]P , kg/m.m.s	0.001226	0.001733	0.002617	0.002250
[n]T , kg/m.m.s	0.000717	0.001052	0.001614	0.001351
XA2 * E04	6.2364	6.2084	6.2149	6.2445
XA3 * E04	0.5102	0.7523	0.8172	0.5506
f	0.914623	0.874101	0.863245	0.907869
f prime	0.918236	0.878885	0.868580	0.911882
k * E06 , m/s	15.2367	23.8648	35.2005	27.6740
(D)AM K/Tau * E07, m/s	0.6401	1.4533	2.4470	1.3087

```
Experiment No.          :  129
Operating Pressure      :  500   kPa
Nominal Solute Conc.    :  2000  ppm
Nominal Feed Flow Rate:  1000  ml/min
Setpoint Temperature    :  20.00  Degree C
Solute                  :  NACL
```

Avg. Feed Conc. (ppm) = 1940. ; XA1 =0.000599 ; C1 = 55.40 kmol/m.m.m

	Film # 1	Film # 2	Film # 3	Film # 4
	********	********	********	********
A * E09, kmol/m.m.s.kPa	186.2564	260.9770	403.2689	310.2155
[n]P , kg/m.m.s	0.001678	0.002351	0.003633	0.002795
[n]T , kg/m.m.s	0.001147	0.001697	0.002523	0.002169
XA2 * E04	6.4286	6.3807	6.3906	6.4491
XA3 * E04	0.3751	0.6832	0.5938	0.3566
f	0.937410	0.885991	0.900905	0.940487
f prime	0.941693	0.892995	0.907137	0.944736
k * E06 , m/s	15.2367	23.8648	35.2005	27.6740
(D)AM K/Tau * E07, m/s	0.7117	2.0378	2.5885	1.2719

```
Experiment No.          :  128
Operating Pressure      :  7000   kPa
Nominal Solute Conc.    :  2000   ppm
Nominal Feed Flow Rate:    1000   ml/min
Setpoint Temperature    :  20.00  Degree C
Solute                  :  NACL
```

Avg. Feed Conc. (ppm) = 2102. ; XA1 =0.000649 ; C1 = 55.40 kmol/m.m.m

	Film # 1	Film # 2	Film # 3	Film # 4
	********	********	********	********
A * E09, kmol/m.m.s.kPa	163.5657	228.1189	373.5645	304.6137
[n]P , kg/m.m.s	0.020632	0.028775	0.047121	0.038424
[n]T , kg/m.m.s	0.019198	0.026857	0.041337	0.034218
XA2 * E04	22.5625	19.2083	19.4597	21.1235
XA3 * E04	0.1477	0.3996	0.7091	0.5217
f	0.977266	0.938473	0.890828	0.919676
f prime	0.993470	0.979233	0.963629	0.975352
k * E06 , m/s	15.2367	23.8648	35.2005	27.6740
(D)AM K/Tau * E07, m/s	1.2672	5.7167	15.6595	8.6809

```
Experiment No.          :  127
Operating Pressure      :  4000   kPa
Nominal Solute Conc.    :  2000   ppm
Nominal Feed Flow Rate:    1000   ml/min
Setpoint Temperature    :  20.00  Degree C
Solute                  :  NACL
```

Avg. Feed Conc. (ppm) = 1995. ; XA1 =0.000616 ; C1 = 55.40 kmol/m.m.m

	Film # 1	Film # 2	Film # 3	Film # 4
	********	********	********	********
A * E09, kmol/m.m.s.kPa	174.0939	247.1985	336.4858	328.5651
[n]P , kg/m.m.s	0.012549	0.017818	0.0242!4	0.023683
[n]T , kg/m.m.s	0.011469	0.016429	0.023283	0.022481
XA2 * E04	12.9706	11.8851	11.8456	13.4829
XA3 * E04	0.1109	0.3966	0.1123	0.3336
f	0.982011	0.935668	0.981782	0.945888
f prime	0.991461	0.966671	0.990530	0.975292
k * E06 , m/s	15.2367	23.8648	35.2005	27.6740
(D)AM K/Tau * E07, m/s	0.9907	5.6807	2.2325	5.7129

```
                    Experiment No.          :  126
                    Operating Pressure      :  1500   kPa
                    Nominal Solute Conc.    :  2000   ppm
                    Nominal Feed Flow Rate:    1000   ml/min
                    Setpoint Temperature    :  20.00  Degree C
                    Solute                  :  NACL
```

Avg. Feed Conc. (ppm) = 1934. ; XA1 =0.000597 ; C1 = 55.40 kmol/m.m.m

	Film # 1	Film # 2	Film # 3	Film # 4
	********	********	********	********
A * E09, kmol/m.m.s.kPa	178.2713	254.9095	370.8000	313.8311
[n]P , kg/m.m.s	0.004819	0.006890	0.010023	0.008483
[n]T , kg/m.m.s	0.004218	0.006109	0.008687	0.007535
XA2 * E04	7.8318	7.6052	7.5886	7.8037
XA3 * E04	0.1547	0.3874	0.2113	0.1335
f	0.974106	0.935181	0.964637	0.977656
f prime	0.980257	0.949104	0.972172	0.982902
k * E06 , m/s	15.2367	23.8648	35.2005	27.6740
(D)AM K/Tau * E07, m/s	0.8516	3.2835	2.4927	1.3140

```
                    Experiment No.          :  125
                    Operating Pressure      :  1500   kPa
                    Nominal Solute Conc.    :  2000   ppm
                    Nominal Feed Flow Rate:    1000   ml/min
                    Setpoint Temperature    :  25.00  Degree C
                    Solute                  :  NACL
```

Avg. Feed Conc. (ppm) = 1932. ; XA1 =0.000596 ; C1 = 55.35 kmol/m.m.m

	Film # 1	Film # 2	Film # 3	Film # 4
	********	********	********	********
A * E09, kmol/m.m.s.kPa	216.9898	318.9201	437.2615	381.4858
[n]P , kg/m.m.s	0.005865	0.008620	0.011819	0.010312
[n]T , kg/m.m.s	0.004964	0.007621	0.010077	0.008834
XA2 * E04	7.9927	7.7672	7.6959	7.9484
XA3 * E04	0.1632	0.6875	0.2198	0.1547
f	0.972648	0.884797	0.963167	0.974070
f prime	0.979593	0.911552	0.971459	0.980546
k * E06 , m/s	16.6000	26.0000	38.3500	30.1500
(D)AM K/Tau * E07, m/s	1.0367	7.4117	2.9677	1.7570

```
                     Experiment No.        :  124
                     Operating Pressure    :  7000   kPa
                     Nominal Solute Conc.  :  2000   ppm
                     Nominal Feed Flow Rate:  1000   ml/min
                     Setpoint Temperature  :  15.00  Degree C
                     Solute                :  NACL
```

Avg. Feed Conc. (ppm) = 1956. ; XA1 =0.000604 ; C1 = 55.47 kmol/m.m.m

	Film # 1	Film # 2	Film # 3	Film # 4
	********	********	********	********
A * E09, kmol/m.m.s.kPa	136.2953	181.8341	263.8648	256.5602
[n]P , kg/m.m.s	0.017192	0.022937	0.033284	0.032362
[n]T , kg/m.m.s	0.016064	0.021456	0.031201	0.029033
XA2 * E04	19.1370	16.2060	15.8577	18.2507
XA3 * E04	0.1434	0.0996	0.1731	0.4958
f	0.976260	0.983518	0.971343	0.917934
f prime	0.992519	0.993865	0.989099	0.972883
k * E06 , m/s	13.7415	21.5229	31.7463	24.9583
(D)AM K/Tau * E07, m/s	1.2136	1.3271	3.4455	8.1098

```
                     Experiment No.        :  123
                     Operating Pressure    :  4000   kPa
                     Nominal Solute Conc.  :  2000   ppm
                     Nominal Feed Flow Rate:  1000   ml/min
                     Setpoint Temperature  :  15.00  Degree C
                     Solute                :  NACL
```

Avg. Feed Conc. (ppm) = 1990. ; XA1 =0.000614 ; C1 = 55.47 kmol/m.m.m

	Film # 1	Film # 2	Film # 3	Film # 4
	********	********	********	********
A * E09, kmol/m.m.s.kPa	143.0936	194.1963	282.9526	276.5542
[n]P , kg/m.m.s	0.010314	0.013998	0.020395	0.019934
[n]T , kg/m.m.s	0.009441	0.012857	0.018674	0.017248
XA2 * E04	12.0989	11.0897	10.9895	11.8997
XA3 * E04	0.1236	0.1010	0.1010	0.3720
f	0.979892	0.983573	0.983573	0.939494
f prime	0.989794	0.990903	0.990820	0.968776
k * E06 , m/s	13.7415	21.5229	31.7463	24.9583
(D)AM K/Tau * E07, m/s	0.9750	1.1822	1.7328	5.5676

```
Experiment No.          :  122
Operating Pressure      :  350   kPa
Nominal Solute Conc.    :  2000  ppm
Nominal Feed Flow Rate:  1000  ml/min
Setpoint Temperature    :  15.00  Degree C
Solute                  :  NACL
```

Avg. Feed Conc. (ppm) = 1881. ;   XA1 =0.000581 ; Cl = 55.47 kmol/m.m.m

	Film # 1	Film # 2	Film # 3	Film # 4
	********	********	********	********
A * E09, kmol/m.m.s.kPa	158.5121	221.0450	340.2796	295.3483
[n]P , kg/m.m.s	0.001000	0.001394	0.002146	0.001863
[n]T , kg/m.m.s	0.000596	0.000844	0.001344	0.001121
XA2 * E04	6.0442	6.0171	6.0268	6.0538
XA3 * E04	0.5073	0.6082	0.7812	0.4857
f	0.912713	0.895354	0.865593	0.916433
f prime	0.916111	0.898974	0.870451	0.919813
k * E06 , m/s	13.7415	21.5229	31.7463	24.9583
(D)AM K/Tau * E07, m/s	0.5461	0.9488	2.0027	0.9781

```
Experiment No.          :  121
Operating Pressure      :  500   kPa
Nominal Solute Conc.    :  2000  ppm
Nominal Feed Flow Rate:  1000  ml/min
Setpoint Temperature    :  15.00  Degree C
Solute                  :  NACL
```

Avg. Feed Conc. (ppm) = 1937. ;   XA1 =0.000598 ; Cl = 55.47 kmol/m.m.m

	Film # 1	Film # 2	Film # 3	Film # 4
	********	********	********	********
A * E09, kmol/m.m.s.kPa	154.0200	216.5198	333.0400	289.4626
[n]P , kg/m.m.s	0.001388	0.001951	0.003001	0.002608
[n]T , kg/m.m.s	0.000959	0.001361	0.002106	0.001793
XA2 * E04	6.3853	6.3407	6.3536	6.4035
XA3 * E04	0.3874	0.4713	0.5506	0.3105
f	0.935270	0.921243	0.907996	0.948110
f prime	0.939373	0.925715	0.913397	0.951537
k * E06 , m/s	13.7415	21.5229	31.7463	24.9583
(D)AM K/Tau * E07, m/s	0.6193	1.0929	1.9986	0.9140

```
            Experiment No.           :  120
            Operating Pressure       :  1500   kPa
            Nominal Solute Conc.     :  2000   ppm
            Nominal Feed Flow Rate:   1000   ml/min
            Setpoint Temperature     :  15.00  Degree C
            Solute                   :  NACL
```

Avg. Feed Conc. (ppm) = 1958. ; XA1 =0.000605 ; Cl = 55.47 kmol/m.m.m

	Film # 1	Film # 2	Film # 3	Film # 4
	********	********	********	********
A * E09, kmol/m.m.s.kPa	149.5318	206.9432	311.8257	271.7831
[n]P , kg/m.m.s	0.004042	0.005594	0.008429	0.007346
[n]T , kg/m.m.s	0.003485	0.004870	0.007320	0.006349
XA2 * E04	7.7452	7.5387	7.5675	7.7684
XA3 * E04	0.1675	0.1746	0.1859	0.1067
f	0.972317	0.971148	0.969277	0.982371
f prime	0.978393	0.976863	0.975457	0.986281
k * E06 , m/s	13.7415	21.5229	31.7463	24.9583
(D)AM K/Tau * E07, m/s	0.7706	1.1548	1.8439	0.8841

```
            Experiment No.           :  119
            Operating Pressure       :  1500   kPa
            Nominal Solute Conc.     :  2000   ppm
            Nominal Feed Flow Rate:   1000   ml/min
            Setpoint Temperature     :  25.00  Degree C
            Solute                   :  NACL
```

Avg. Feed Conc. (ppm) = 2035. ; XA1 =0.000628 ; Cl = 55.35 kmol/m.m.m

	Film # 1	Film # 2	Film # 3	Film # 4
	********	********	********	********
A * E09, kmol/m.m.s.kPa	215.2037	295.1383	432.3050	382.1680
[n]P , kg/m.m.s	0.005817	0.007978	0.011685	0.010330
[n]T , kg/m.m.s	0.004979	0.006861	0.010073	0.009257
XA2 * E04	8.4233	8.1239	8.1034	8.4178
XA3 * E04	0.1887	0.2127	0.2481	0.3674
f	0.969994	0.966169	0.960546	0.941579
f prime	0.977617	0.973833	0.969406	0.956392
k * E06 , m/s	16.6000	26.0000	38.3500	30.1500
(D)AM K/Tau * E07, m/s	1.1413	1.8458	3.1827	4.2259

```
Experiment No.          :  118
Operating Pressure      :  7000   kPa
Nominal Solute Conc.    :  2000   ppm
Nominal Feed Flow Rate:  1000   ml/min
Setpoint Temperature    :  10.00  Degree C
Solute                  :  NACL
```

Avg. Feed Conc. (ppm) = 1987. ; XA1 =0.000614 ; C1 = 55.48 kmol/m.m.m

	Film # 1	Film # 2	Film # 3	Film # 4
	********	********	********	********
A * E09, kmol/m.m.s.kPa	110.3475	148.0970	261.1220	212.5866
[n]P , kg/m.m.s	0.013919	0.018681	0.032938	0.026816
[n]T , kg/m.m.s	0.012983	0.017474	0.029076	0.024310
XA2 * E04	17.2985	14.9908	15.8959	16.9460
XA3 * E04	0.1689	0.1321	0.6514	0.6370
f	0.972493	0.978483	0.893894	0.896241
f prime	0.990253	0.991200	0.959080	0.962469
k * E06 , m/s	12.3152	19.2889	28.4511	22.3677
(D)AM K/Tau * E07, m/s	1.2804	1.5540	12.4265	9.4965

```
Experiment No.          :  117
Operating Pressure      :  4000   kPa
Nominal Solute Conc.    :  2000   ppm
Nominal Feed Flow Rate:  1000   ml/min
Setpoint Temperature    :  10.00  Degree C
Solute                  :  NACL
```

Avg. Feed Conc. (ppm) = 2035. ; XA1 =0.000628 ; C1 = 55.48 kmol/m.m.m

	Film # 1	Film # 2	Film # 3	Film # 4
	********	********	********	********
A * E09, kmol/m.m.s.kPa	129.1603	178.7615	268.9569	262.1033
[n]P , kg/m.m.s	0.009310	0.012885	0.019386	0.018892
[n]T , kg/m.m.s	0.008529	0.011837	0.017874	0.016398
XA2 * E04	12.4582	11.5325	11.7142	12.7749
XA3 * E04	0.1067	0.0925	0.0769	0.2863
f	0.983040	0.985290	0.987764	0.954472
f prime	0.991450	0.991988	0.993439	0.977617
k * E06 , m/s	12.3152	19.2889	28.4511	22.3677
(D)AM K/Tau * E07, m/s	0.7367	0.9574	1.1822	3.7601

Experiment No.   : 116
Operating Pressure   : 500   kPa
Nominal Solute Conc.   : 2000 ppm
Nominal Feed Flow Rate: 1000 ml/min
Setpoint Temperature   : 10.00 Degree C
Solute   : NACL

Avg. Feed Conc. (ppm) = 1934. ; XA1 =0.000597 ; Cl = 55.48 kmol/m.m.m

	Film # 1	Film # 2	Film # 3	Film # 4
	********	********	********	********
A * E09, kmol/m.m.s.kPa	126.1099	178.0719	284.3379	247.3024
[n]P , kg/m.m.s	0.001136	0.001604	0.002562	0.002228
[n]T , kg/m.m.s	0.000789	0.001123	0.001827	0.001552
XA2 * E04	6.3480	6.3112	6.3386	6.3834
XA3 * E04	0.3047	0.3259	0.4565	0.2566
f	0.949014	0.945467	0.923610	0.957063
f prime	0.952030	0.948394	0.928023	0.959827
k * E06 , m/s	12.3152	19.2889	28.4511	22.3677
(D)AM K/Tau * E07, m/s	0.3981	0.6115	1.4182	0.6501

Experiment No.   : 115
Operating Pressure   : 350   kPa
Nominal Solute Conc.   : 2000 ppm
Nominal Feed Flow Rate: 1000 ml/min
Setpoint Temperature   : 10.00 Degree C
Solute   : NACL

Avg. Feed Conc. (ppm) = 1934. ; XA1 =0.000597 ; Cl = 55.48 kmol/m.m.m

	Film # 1	Film # 2	Film # 3	Film # 4
	********	********	********	********
A * E09, kmol/m.m.s.kPa	127.5714	180.3439	286.2300	251.0085
[n]P , kg/m.m.s	0.000805	0.001137	0.001805	0.001583
[n]T , kg/m.m.s	0.000478	0.000681	0.001101	0.000938
XA2 * E04	6.1939	6.1706	6.1813	6.2108
XA3 * E04	0.3874	0.4641	0.6875	0.4104
f	0.935181	0.922341	0.884955	0.931324
f prime	0.937498	0.924833	0.888841	0.933959
k * E06 , m/s	12.3152	19.2889	28.4511	22.3677
(D)AM K/Tau * E07, m/s	0.3191	0.5537	1.3782	0.6635

```
Experiment No.         :  114
Operating Pressure     :  1500   kPa
Nominal Solute Conc.   :  2000   ppm
Nominal Feed Flow Rate:  1000   ml/min
Setpoint Temperature   :  10.00  Degree C
Solute                 :  NACL
```

Avg. Feed Conc. (ppm) = 1932. ; XA1 =0.000596 ; C1 = 55.48 kmol/m.m.m

	Film # 1	Film # 2	Film # 3	Film # 4
A * E09, kmol/m.m.s.kPa	122.5597	171.8710	270.2833	232.6855
[n]P , kg/m.m.s	0.003313	0.004646	0.007306	0.006289
[n]T , kg/m.m.s	0.002883	0.004052	0.006315	0.005472
XA2 * E04	7.5027	7.3277	7.4087	7.5933
XA3 * E04	0.1349	0.1349	0.1547	0.0897
f	0.977389	0.977389	0.974070	0.984973
f prime	0.982027	0.981598	0.979128	0.988199
k * E06 , m/s	12.3152	19.2889	28.4511	22.3677
(D)AM K/Tau * E07, m/s	0.5282	0.7604	1.3474	0.6542

```
Experiment No.         :  113
Operating Pressure     :  1500   kPa
Nominal Solute Conc.   :  2000   ppm
Nominal Feed Flow Rate:  1000   ml/min
Setpoint Temperature   :  25.00  Degree C
Solute                 :  NACL
```

Avg. Feed Conc. (ppm) = 2001. ; XA1 =0.000618 ; C1 = 55.35 kmol/m.m.m

	Film # 1	Film # 2	Film # 3	Film # 4
A * E09, kmol/m.m.s.kPa	218.9422	304.5553	452.1136	399.5197
[n]P , kg/m.m.s	0.005918	0.008232	0.012221	0.010799
[n]T , kg/m.m.s	0.005121	0.007156	0.010818	0.009245
XA2 * E04	8.3578	8.0887	8.1235	8.3521
XA3 * E04	0.1618	0.1618	0.2226	0.1349
f	0.973819	0.973819	0.963978	0.978168
f prime	0.980654	0.980010	0.972614	0.983856
k * E06 , m/s	16.6000	26.0000	38.3500	30.1500
(D)AM K/Tau * E07, m/s	1.0114	1.4611	3.0490	1.5186

```
                    Experiment No.        :  112
                    Operating Pressure    :  350   kPa
                    Nominal Solute Conc.  :  2000  ppm
                    Nominal Feed Flow Rate:  1000  ml/min
                    Setpoint Temperature  :  5.00  Degree C
                    Solute                :  NACL
```

Avg. Feed Conc. (ppm) = 1940. ; XA1 =0.000599 ; C1 = 55.49 kmol/m.m.m

	Film # 1	Film # 2	Film # 3	Film # 4
	********	********	********	********
A * E09, kmol/m.m.s.kPa	98.5282	140.2382	226.4331	197.0731
[n]P , kg/m.m.s	0.000621	0.000884	0.001428	0.001243
[n]T , kg/m.m.s	0.000352	0.000505	0.000825	0.000706
XA2 * E04	6.1721	6.1547	6.1660	6.1904
XA3 * E04	0.3874	0.4519	0.6514	0.4181
f	0.935359	0.924588	0.891284	0.930230
f prime	0.937278	0.926619	0.894406	0.932501
k * E06 , m/s	10.9448	17.1425	25.2852	19.8787
(D)AM K/Tau * E07, m/s	0.2358	0.4005	0.9744	0.5113

```
                    Experiment No.        :  111
                    Operating Pressure    :  4000  kPa
                    Nominal Solute Conc.  :  2000  ppm
                    Nominal Feed Flow Rate:  1000  ml/min
                    Setpoint Temperature  :  5.00  Degree C
                    Solute                :  NACL
```

Avg. Feed Conc. (ppm) = 2006. ; XA1 =0.000619 ; C1 = 55.49 kmol/m.m.m

	Film # 1	Film # 2	Film # 3	Film # 4
	********	********	********	********
A * E09, kmol/m.m.s.kPa	93.7583	130.2131	191.9688	192.6833
[n]P , kg/m.m.s	0.006758	0.009386	0.013837	0.013889
[n]T , kg/m.m.s	0.006119	0.008566	0.011596	0.010747
XA2 * E04	10.7603	10.1530	9.7586	10.4358
XA3 * E04	0.0968	0.0854	0.0670	0.2778
f	0.984389	0.986215	0.989182	0.955172
f prime	0.991018	0.991594	0.993136	0.973406
k * E06 , m/s	10.9448	17.1425	25.2852	19.8787
(D)AM K/Tau * E07, m/s	0.5552	0.7269	0.8022	2.9392

```
                    Experiment No.          :   110
                    Operating Pressure      :   7000   kPa
                    Nominal Solute Conc.    :   2000   ppm
                    Nominal Feed Flow Rate:  1000   ml/min
                    Setpoint Temperature    :   5.00   Degree C
                    Solute                  :   NACL
```

Avg. Feed Conc. (ppm) = 2019. ; XA1 =0.000624 ; C1 = 55.49 kmol/m.m.m

	Film # 1	Film # 2	Film # 3	Film # 4
	********	********	********	********
A * E09, kmol/m.m.s.kPa	89.5580	123.3902	184.8446	179.7698
[n]P , kg/m.m.s	0.011297	0.015564	0.023316	0.022676
[n]T , kg/m.m.s	0.010586	0.014602	0.021764	0.020359
XA2 * E04	16.2222	14.4975	14.6078	16.7268
XA3 * E04	0.1109	0.0868	0.1010	0.3566
f	0.982225	0.986080	0.983812	0.942839
f prime	0.993175	0.994018	0.993096	0.978715
k * E06 , m/s	10.9448	17.1425	25.2852	19.8787
(D)AM K/Tau * E07, m/s	0.7287	0.8800	1.5152	4.4350

```
                    Experiment No.          :   109
                    Operating Pressure      :   1500   kPa
                    Nominal Solute Conc.    :   2000   ppm
                    Nominal Feed Flow Rate:  1000   ml/min
                    Setpoint Temperature    :   5.00   Degree C
                    Solute                  :   NACL
```

Avg. Feed Conc. (ppm) = 1950. ; XA1 =0.000602 ; C1 = 55.49 kmol/m.m.m

	Film # 1	Film # 2	Film # 3	Film # 4
	********	********	********	********
A * E09, kmol/m.m.s.kPa	97.1352	137.4264	217.2546	189.7715
[n]P , kg/m.m.s	0.002626	0.003715	0.005872	0.005130
[n]T , kg/m.m.s	0.002264	0.003224	0.005075	0.004371
XA2 * E04	7.3827	7.2433	7.3301	7.4845
XA3 * E04	0.0996	0.1180	0.1349	0.0741
f	0.983473	0.980421	0.977604	0.987699
f prime	0.986522	0.983725	0.981604	0.990104
k * E06 , m/s	10.9448	17.1425	25.2852	19.8787
(D)AM K/Tau * E07, m/s	0.3096	0.5338	0.9518	0.4372

```
                    Experiment No.        :  108
                    Operating Pressure    :  500   kPa
                    Nominal Solute Conc.  :  2000  ppm
                    Nominal Feed Flow Rate:  1000  ml/min
                    Setpoint Temperature  :  5.00  Degree C
                    Solute                :  NACL
```

Avg. Feed Conc. (ppm) = 1934. ; XA1 =0.000597 ; C1 = 55.49 kmol/m.m.m

	Film # 1	Film # 2	Film # 3	Film # 4
	********	********	********	********
A * E09, kmol/m.m.s.kPa	98.9560	140.8413	229.0083	196.5759
[n]P , kg/m.m.s	0.000892	0.001269	0.002063	0.001771
[n]T , kg/m.m.s	0.000625	0.000898	0.001458	0.001235
XA2 * E04	6.3185	6.2851	6.3064	6.3442
XA3 * E04	0.0911	0.1618	0.3489	0.1760
f	0.984757	0.972922	0.941610	0.970555
f prime	0.985592	0.974269	0.944702	0.972281
k * E06 , m/s	10.9448	17.1425	25.2852	19.8787
(D)AM K/Tau * E07, m/s	0.0915	0.2373	0.8538	0.3523

```
                    Experiment No.        :  107
                    Operating Pressure    :  1500  kPa
                    Nominal Solute Conc.  :  2000  ppm
                    Nominal Feed Flow Rate:  1000  ml/min
                    Setpoint Temperature  :  25.00 Degree C
                    Solute                :  NACL
```

Avg. Feed Conc. (ppm) = 1987. ; XA1 =0.000614 ; C1 = 55.35 kmol/m.m.m

	Film # 1	Film # 2	Film # 3	Film # 4
	********	********	********	********
A * E09, kmol/m.m.s.kPa	216.7288	300.0373	453.3736	397.3568
[n]P , kg/m.m.s	0.005858	0.008110	0.012255	0.010741
[n]T , kg/m.m.s	0.005055	0.007049	0.010679	0.009397
XA2 * E04	7.7440	7.5553	7.6211	7.8298
XA3 * E04	1.6336	1.5928	1.5255	1.5195
f	0.733890	0.740539	0.751510	0.752484
f prime	0.789172	0.789304	0.799955	0.806055
k * E06 , m/s	16.6000	26.0000	38.3500	30.1500
(D)AM K/Tau * E07, m/s	13.5117	18.8247	26.7170	22.6224

```
Experiment No.          :  106
Operating Pressure      :  350   kPa
Nominal Solute Conc.    :  2000  ppm
Nominal Feed Flow Rate:  1000  ml/min
Setpoint Temperature    :  25.00  Degree C
Solute                  :  NACL
```

Avg. Feed Conc. (ppm) = 1953. ; XA1 =0.000603 ; Cl = 55.35 kmol/m.m.m

	Film # 1	Film # 2	Film # 3	Film # 4
	********	********	********	********
A * E09, kmol/m.m.s.kPa	224.1852	315.5554	494.1137	431.4774
[n]P , kg/m.m.s	0.001414	0.001990	0.003116	0.002721
[n]T , kg/m.m.s	0.000812	0.001154	0.001892	0.001598
XA2 * E04	6.3222	6.2867	6.2961	6.3328
XA3 * E04	0.2184	0.3874	0.7812	0.4785
£	0.963801	0.935797	0.870518	0.920690
£ prime	0.965476	0.938421	0.875995	0.924485
k * E06 , m/s	16.6000	26.0000	38.3500	30.1500
(D)AM K/Tau * E07, m/s	0.2907	0.7577	2.6799	1.3057

```
Experiment No.          :  105
Operating Pressure      :  4000  kPa
Nominal Solute Conc.    :  2000  ppm
Nominal Feed Flow Rate:  1000  ml/min
Setpoint Temperature    :  25.00  Degree C
Solute                  :  NACL
```

Avg. Feed Conc. (ppm) = 2067. ; XA1 =0.000638 ; Cl = 55.35 kmol/m.m.m

	Film # 1	Film # 2	Film # 3	Film # 4
	********	********	********	********
A * E09, kmol/m.m.s.kPa	203.5323	279.7674	402.0858	394.7751
[n]P , kg/m.m.s	0.014671	0.020166	0.028982	0.028455
[n]T , kg/m.m.s	0.013453	0.018543	0.026891	0.025104
XA2 * E04	14.2625	12.9513	12.7790	14.2221
XA3 * E04	0.0996	0.0953	0.1137	0.3751
£	0.984411	0.985076	0.982197	0.941285
£ prime	0.993028	0.992648	0.991112	0.973665
k * E06 , m/s	16.6000	26.0000	38.3500	30.1500
(D)AM K/Tau * E07, m/s	0.9459	1.3752	2.4147	6.7996

```
                Experiment No.          :   104
                Operating Pressure      :   7000   kPa
                Nominal Solute Conc.    :   2000   ppm
                Nominal Feed Flow Rate:     1000   ml/min
                Setpoint Temperature    :   25.00  Degree C
                Solute                  :   NACL
```

Avg. Feed Conc. (ppm) = 2110. ; XA1 =0.000652 ; C1 = 55.35 kmol/m.m.m

	Film # 1	Film # 2	Film # 3	Film # 4
	********	********	********	********
A * E09, kmol/m.m.s.kPa	192.7727	262.2055	373.0614	362.6093
[n]P , kg/m.m.s	0.024316	0.033075	0.047058	0.045740
[n]T , kg/m.m.s	0.022754	0.030971	0.043685	0.041203
XA2 * E04	25.4366	21.2927	20.1030	24.1173
XA3 * E04	0.1081	0.0953	0.1477	0.5217
f	0.983427	0.985379	0.977352	0.919982
f prime	0.995762	0.995532	0.992669	0.978418
k * E06 , m/s	16.6000	26.0000	38.3500	30.1500
(D)AM K/Tau * E07, m/s	0.9709	1.3930	3.2329	9.1103

```
                Experiment No.          :   103
                Operating Pressure      :   1500   kPa
                Nominal Solute Conc.    :   2000   ppm
                Nominal Feed Flow Rate:     1000   ml/min
                Setpoint Temperature    :   25.00  Degree C
                Solute                  :   NACL
```

Avg. Feed Conc. (ppm) = 2014. ; XA1 =0.000622 ; C1 = 55.35 kmol/m.m.m

	Film # 1	Film # 2	Film # 3	Film # 4
	********	********	********	********
A * E09, kmol/m.m.s.kPa	214.6845	300.0194	447.1817	397.4744
[n]P , kg/m.m.s	0.005803	0.008110	0.012087	0.010744
[n]T , kg/m.m.s	0.004980	0.006993	0.010533	0.009350
XA2 * E04	8.3439	8.0918	8.1207	8.4378
XA3 * E04	0.1618	0.1661	0.2184	0.1335
f	0.973994	0.973312	0.964900	0.978540
f prime	0.980622	0.979494	0.973127	0.984188
k * E06 , m/s	16.6000	26.0000	38.3500	30.1500
(D)AM K/Tau * E07, m/s	0.9849	1.4652	2.9111	1.5036

```
                    Experiment No.          :  102
                    Operating Pressure      :  500   kPa
                    Nominal Solute Conc.    :  2000  ppm
                    Nominal Feed Flow Rate:    1000  ml/min
                    Setpoint Temperature    :  25.00  Degree C
                    Solute                  :  NACL
```

Avg. Feed Conc. (ppm) = 1956. ; XA1 =0.000604 ; C1 = 55.35 kmol/m.m.m

	Film # 1	Film # 2	Film # 3	Film # 4
	********	********	********	********
A * E09, kmol/m.m.s.kPa	216.0322	304.6394	469.3647	416.0305
[n]P , kg/m.m.s	0.001946	0.002745	0.004229	0.003748
[n]T , kg/m.m.s	0.001325	0.001882	0.002970	0.002596
XA2 * E04	6.5328	6.4745	6.4805	6.5555
XA3 * E04	0.0982	0.2396	0.5578	0.2990
f	0.983752	0.960338	0.907676	0.950503
f prime	0.984983	0.963013	0.913983	0.954412
k * E06 , m/s	16.6000	26.0000	38.3500	30.1500
(D)AM K/Tau * E07, m/s	0.2021	0.7233	2.7967	1.2407

```
                    Experiment No.          :  101
                    Operating Pressure      :  1500  kPa
                    Nominal Solute Conc.    :  2000  ppm
                    Nominal Feed Flow Rate:    1000  ml/min
                    Setpoint Temperature    :  25.00  Degree C
                    Solute                  :  NACL
```

Avg. Feed Conc. (ppm) = 1895. ; XA1 =0.000585 ; C1 = 55.35 kmol/m.m.m

	Film # 1	Film # 2	Film # 3	Film # 4
	********	********	********	********
A * E09, kmol/m.m.s.kPa	211.4506	298.3601	450.5901	403.1445
[n]P , kg/m.m.s	0.005716	0.008065	0.012179	0.010897
[n]T , kg/m.m.s	0.004962	0.007046	0.010591	0.009378
XA2 * E04	7.8453	7.6290	7.6542	7.9446
XA3 * E04	0.1406	0.1519	0.1944	0.1265
f	0.975979	0.974046	0.966796	0.978396
f prime	0.982092	0.980102	0.974627	0.984095
k * E06 , m/s	16.6000	26.0000	38.3500	30.1500
(D)AM K/Tau * E07, m/s	0.9056	1.4317	2.7593	1.5169

Experiment No.   : 1003
Operating Pressure   : 1500 kPa
Nominal Solute Conc.   : 15 000   ppm
Nominal Feed Flow Rate: 1000 ml/min
Setpoint Temperature   : 25.00 Degree C
Solute   : NACL

Avg. Feed Conc. (ppm) =14612. ;   XA1 =0.004552 ; Cl = 55.35 kmol/m.m.m

	Film # 1	Film # 2	Film # 3	Film # 4
	********	********	********	********
A * E09, kmol/m.m.s.kPa	216.6311	295.3563	417.4327	375.5761
[n]P , kg/m.m.s	0.005856	0.007983	0.011283	0.010152
[n]T , kg/m.m.s	0.001336	0.001937	0.002870	0.002302
XA2 * E04	49.0536	48.6725	48.6864	48.8011
XA3 * E04	3.4221	4.8115	4.8115	4.2066
f	0.925130	0.894719	0.894719	0.907960
f prime	0.930555	0.901580	0.901608	0.914186
k * E06 , m/s	16.6000	26.0000	38.3500	30.1500
(D)AM K/Tau * E07, m/s	1.0015	2.1230	3.1438	2.1693

Experiment No.   : 1002
Operating Pressure   : 1500 kPa
Nominal Solute Conc.   : 10 000   ppm
Nominal Feed Flow Rate: 1000 ml/min
Setpoint Temperature   : 25.00 Degree C
Solute   : NACL

Avg. Feed Conc. (ppm) = 9829. ;   XA1 =0.003051 ; Cl = 55.35 kmol/m.m.m

	Film # 1	Film # 2	Film # 3	Film # 4
	********	********	********	********
A * E09, kmol/m.m.s.kPa	215.7697	294.2067	414.3835	371.6068
[n]P , kg/m.m.s	0.005832	0.007952	0.011201	0.010045
[n]T , kg/m.m.s	0.002530	0.003531	0.004981	0.004275
XA2 * E04	35.3492	34.7092	34.4974	34.9267
XA3 * E04	1.2209	1.7561	1.8704	1.6255
f	0.960107	0.942614	0.938879	0.946883
f prime	0.965581	0.949572	0.945958	0.953615
k * E06 , m/s	16.6000	26.0000	38.3500	30.1500
(D)AM K/Tau * E07, m/s	0.9047	1.8813	2.8544	2.0860

```
Experiment No.          :  1001
Operating Pressure      :  1500   kPa
Nominal Solute Conc.    :  5000   ppm
Nominal Feed Flow Rate:    1000   ml/min
Setpoint Temperature    :  25.00  Degree C
Solute                  :  NACL
```

Avg. Feed Conc. (ppm) = 4906. ;   XA1 =0.001518 ; C1 = 55.35 kmol/m.m.m

	Film # 1	Film # 2	Film # 3	Film # 4
	********	********	********	********
A * E09, kmol/m.m.s.kPa	213.2716	293.3119	413.7097	374.4242
[n]P , kg/m.m.s	0.005765	0.007928	0.011183	0.010121
[n]T , kg/m.m.s	0.003918	0.005468	0.007696	0.006749
XA2 * E04	19.1255	18.5973	18.4211	18.8263
XA3 * E04	0.3996	0.6197	0.6342	0.6846
f	0.973711	0.959232	0.958283	0.954965
f prime	0.979143	0.966736	0.965636	0.963702
k * E06 , m/s	16.6000	26.0000	38.3500	30.1500
(D)AM K/Tau * E07, m/s	0.8362	1.8849	2.7436	2.5465

APPENDIX D

THE EXPERIMENTAL DATA OF PHASE II

The film numbers 1, 2, 3, and 4 (in the following tables) refer to the membranes SW30-1, SW30-2, BW30-1, and BW30-2, respectively.

Term in Computer Output	Meaning
A * E09	$A \times 10^9$
Avg.	Average
C1	C
Conc.	Concentration
(D)AM K/Tau * E07	$D_{AM} K/\tau \times 10^7$
f prime	f'
k * E06	$k \times 10^6$
KCL	$KC\ell$
kg/m.m.s	$kg/m^2 s$
kmol/m.m.m	$kmol/m^3$
kmol/m.m.s.kPa	$kmol/m^2 s\, kPa$
LICL	$LiC\ell$
LINO3	$LiNO_3$
NACL	$NaC\ell$
No.	Number
[n]P	n_P
[n]T	n_T
XA1	X_{A1}
XA2 * E04	$X_{A2} \times 10^4$
XA3 * E04	$X_{A3} \times 10^4$

310

```
                Experiment No.        :  201
                Operating Pressure    :  1500   kPa
                Nominal Solute Conc.  :  2000   ppm
                Nominal Feed Flow Rate:  1000   ml/min
                Setpoint Temperature  :  25.00  Degree C
                Solute                :  NACL
```

Avg. Feed Conc. (ppm) = 1889. ; XA1 =0.000583 ; C1 = 55.35 kmol/m.m.m

	Film # 1	Film # 2	Film # 3	Film # 4
	********	********	********	********
A * E09, kmol/m.m.s.kPa	192.5270	263.0968	356.3105	307.6083
[n]P , kg/m.m.s	0.005204	0.007112	0.009631	0.008315
[n]T , kg/m.m.s	0.004559	0.006208	0.008382	0.006993
XA2 * E04	7.8125	7.6362	7.4818	7.4760
XA3 * E04	0.1293	0.1802	0.1816	0.1434
f	0.977851	0.969126	0.968884	0.975427
f prime	0.983464	0.976418	0.975742	0.980829
k * E06 , m/s	15.3500	22.4900	32.8400	27.6500
(D)AM K/Tau * E07, m/s	0.7692	1.5043	2.0906	1.3715

```
                Experiment No.        :  202
                Operating Pressure    :  1500   kPa
                Nominal Solute Conc.  :  2000   ppm
                Nominal Feed Flow Rate:  1000   ml/min
                Setpoint Temperature  :  25.00  Degree C
                Solute                :  KCL
```

Avg. Feed Conc. (ppm) = 1991. ; XA1 =0.000482 ; C1 = 55.34 kmol/m.m.m

	Film # 1	Film # 2	Film # 3	Film # 4
	********	********	********	********
A * E09, kmol/m.m.s.kPa	191.5888	261.8829	355.9687	294.0262
[n]P , kg/m.m.s	0.005179	0.007079	0.009622	0.007948
[n]T , kg/m.m.s	0.004647	0.006324	0.008594	0.007061
XA2 * E04	6.2021	6.0777	5.9726	5.9560
XA3 * E04	0.1306	0.1816	0.2126	0.1543
f	0.972911	0.962346	0.955903	0.967994
f prime	0.978951	0.970144	0.964419	0.974102
k * E06 , m/s	18.0328	26.4207	38.5797	32.4826
(D)AM K/Tau * E07, m/s	1.0026	1.9530	3.1814	1.8838

```
                    Experiment No.          :  203
                    Operating Pressure      :  7000   kPa
                    Nominal Solute Conc.    :  2000   ppm
                    Nominal Feed Flow Rate:    1000   ml/min
                    Setpoint Temperature    :  25.00  Degree C
                    Solute                  :  KCL
```

Avg. Feed Conc. (ppm) = 2111. ; XA1 =0.000511 ; Cl = 55.34 kmol/m.m.m

	Film # 1	Film # 2	Film # 3	Film # 4
	*******	*******	*******	*******
A * E09, kmol/m.m.s.kPa	181.3432	240.0163	382.6883	294.0923
[n]P , kg/m.m.s	0.022875	0.030276	0.048272	0.037097
[n]T , kg/m.m.s	0.021450	0.028247	0.042607	0.033195
XA2 * E04	16.5631	14.6596	14.3370	13.7584
XA3 * E04	0.1237	0.1418	0.5588	0.2707
f	0.975823	0.972278	0.890730	0.947071
f prime	0.992547	0.990342	0.961076	0.980352
k * E06 , m/s	18.0328	26.4207	38.5797	32.4826
(D)AM K/Tau * E07, m/s	1.6189	2.7678	17.3359	6.6837

```
                    Experiment No.          :  204
                    Operating Pressure      :  4000   kPa
                    Nominal Solute Conc.    :  2000   ppm
                    Nominal Feed Flow Rate:    1000   ml/min
                    Setpoint Temperature    :  25.00  Degree C
                    Solute                  :  KCL
```

Avg. Feed Conc. (ppm) = 2147. ; XA1 =0.000520 ; Cl = 55.34 kmol/m.m.m

	Film # 1	Film # 2	Film # 3	Film # 4
	*******	*******	*******	*******
A * E09, kmol/m.m.s.kPa	185.6697	250.9181	336.6132	303.7889
[n]P , kg/m.m.s	0.013383	0.018086	0.024263	0.021897
[n]T , kg/m.m.s	0.012721	0.017033	0.022760	0.019693
XA2 * E04	10.4604	9.7956	9.3084	9.3046
XA3 * E04	0.0822	0.1390	0.1037	0.2896
f	0.984198	0.973276	0.980054	0.944322
f prime	0.992151	0.985824	0.988865	0.968905
k * E06 , m/s	18.0328	26.4207	38.5797	32.4826
(D)AM K/Tau * E07, m/s	1.0105	2.4592	2.5730	6.3446

```
Experiment No.          :  205
Operating Pressure      :  1500   kPa
Nominal Solute Conc.    :  2000   ppm
Nominal Feed Flow Rate:    1000   ml/min
Setpoint Temperature    :  25.00  Degree C
Solute                  :  KCL
```

Avg. Feed Conc. (ppm) = 2056. ;   XA1 =0.000498 ;   C1 = 55.34 kmol/m.m.m

	Film # 1	Film # 2	Film # 3	Film # 4
	********	********	********	********
A * E09, kmol/m.m.s.kPa	192.8129	262.2839	358.0052	318.9276
[n]P , kg/m.m.s	0.005212	0.007090	0.009677	0.008621
[n]T , kg/m.m.s	0.004613	0.006324	0.008614	0.007348
XA2 * E04	6.3941	6.2745	6.1742	6.1699
XA3 * E04	0.1306	0.1936	0.2066	0.2921
f	0.973768	0.961128	0.958508	0.941339
f prime	0.979584	0.969169	0.966556	0.952685
k * E06 , m/s	18.0328	26.4207	38.5797	32.4826
(D)AM K/Tau * E07, m/s	0.9648	2.0187	2.9911	3.6620

```
Experiment No.          :  206
Operating Pressure      :  500    kPa
Nominal Solute Conc.    :  2000   ppm
Nominal Feed Flow Rate:    1000   ml/min
Setpoint Temperature    :  25.00  Degree C
Solute                  :  KCL
```

Avg. Feed Conc. (ppm) = 1985. ;   XA1 =0.000480 ;   C1 = 55.34 kmol/m.m.m

	Film # 1	Film # 2	Film # 3	Film # 4
	********	********	********	********
A * E09, kmol/m.m.s.kPa	189.9192	264.2909	352.7444	305.9910
[n]P , kg/m.m.s	0.001711	0.002381	0.003178	0.002757
[n]T , kg/m.m.s	0.001239	0.001779	0.002519	0.002037
XA2 * E04	5.1272	5.1151	5.0946	5.0971
XA3 * E04	0.2795	0.3562	0.5140	0.2934
f	0.941848	0.925887	0.893070	0.938966
f prime	0.945511	0.930391	0.899164	0.942474
k * E06 , m/s	18.0328	26.4207	38.5797	32.4826
(D)AM K/Tau * E07, m/s	0.7167	1.3355	2.8338	1.2475

```
                    Experiment No.          :  207
                    Operating Pressure      :  1500   kPa
                    Nominal Solute Conc.    :  2000   ppm
                    Nominal Feed Flow Rate:    1000   ml/min
                    Setpoint Temperature    :  25.00  Degree C
                    Solute                  :  LINO3
```

Avg. Feed Conc. (ppm) = 1928. ; XA1 =0.000505 ; Cl = 55.32 kmol/m.m.m

	Film # 1	Film # 2	Film # 3	Film # 4
	********	********	********	********
A * E09, kmol/m.m.s.kPa	191.8589	261.4074	354.4344	308.0015
[n]P , kg/m.m.s	0.005186	0.007066	0.009580	0.008325
[n]T , kg/m.m.s	0.004639	0.006230	0.008534	0.007271
XA2 * E04	7.0177	6.8105	6.6709	6.6615
XA3 * E04	0.1241	0.1699	0.2105	0.3038
f	0.975426	0.966340	0.958315	0.939823
f prime	0.982333	0.975064	0.968472	0.954422
k * E06 , m/s	13.8076	20.2302	29.5402	24.8717
(D)AM K/Tau * E07, m/s	0.8377	1.5999	2.7893	3.4862

```
                    Experiment No.          :  208
                    Operating Pressure      :  4000   kPa
                    Nominal Solute Conc.    :  2000   ppm
                    Nominal Feed Flow Rate:    1000   ml/min
                    Setpoint Temperature    :  25.00  Degree C
                    Solute                  :  LINO3
```

Avg. Feed Conc. (ppm) = 2071. ; XA1 =0.000542 ; Cl = 55.31 kmol/m.m.m

	Film # 1	Film # 2	Film # 3	Film # 4
	********	********	********	********
A * E09, kmol/m.m.s.kPa	186.5603	250.3495	336.7143	305.2599
[n]P , kg/m.m.s	0.013447	0.018045	0.024270	0.022003
[n]T , kg/m.m.s	0.012557	0.016675	0.022269	0.019348
XA2 * E04	13.3590	12.2201	11.3963	11.4715
XA3 * E04	0.0886	0.1291	0.1291	0.2985
f	0.983672	0.976187	0.976187	0.944953
f prime	0.993380	0.989445	0.988681	0.974005
k * E06 , m/s	13.8076	20.2302	29.5402	24.8717
(D)AM K/Tau * E07, m/s	0.8415	1.7882	2.5625	5.1901

Experiment No.   : 209
Operating Pressure   : 500   kPa
Nominal Solute Conc.   : 2000 ppm
Nominal Feed Flow Rate: 1000 ml/min
Setpoint Temperature   : 25.00 Degree C
Solute   : LINO3

Avg. Feed Conc. (ppm) = 1959. ; XA1 =0.000513 ; Cl = 55.32 kmol/m.m.m

	Film # 1	Film # 2	Film # 3	Film # 4
	********	********	********	********
A * E09, kmol/m.m.s.kPa	192.6645	263.5277	370.4254	301.6601
[n]P , kg/m.m.s	0.001736	0.002374	0.003338	0.002718
[n]T , kg/m.m.s	0.001243	0.001708	0.002424	0.001933
XA2 * E04	5.5849	5.5513	5.5244	5.5227
XA3 * E04	0.2950	0.3398	0.5087	0.2598
f	0.942501	0.933774	0.900858	0.949368
f prime	0.947205	0.938824	0.907971	0.952987
k * E06 , m/s	13.8076	20.2302	29.5402	24.8717
(D)AM K/Tau * E07, m/s	0.6956	1.1174	2.4662	0.9570

Experiment No.   : 210
Operating Pressure   : 500   kPa
Nominal Solute Conc.   : 2000 ppm
Nominal Feed Flow Rate: 1000 ml/min
Setpoint Temperature   : 25.00 Degree C
Solute   : LICL

Avg. Feed Conc. (ppm) = 1974. ; XA1 =0.000840 ; Cl = 55.35 kmol/m.m.m

	Film # 1	Film # 2	Film # 3	Film # 4
	********	********	********	********
A * E09, kmol/m.m.s.kPa	193.4391	263.8180	370.4585	304.9286
[n]P , kg/m.m.s	0.001743	0.002377	0.003338	0.002747
[n]T , kg/m.m.s	0.000953	0.001340	0.001908	0.001519
XA2 * E04	8.9640	8.9342	8.9110	8.8980
XA3 * E04	0.4094	0.5014	0.6420	0.3944
f	0.951299	0.940358	0.923638	0.953087
f prime	0.954365	0.943926	0.928019	0.955713
k * E06 , m/s	14.0204	20.5419	29.9954	25.2549
(D)AM K/Tau * E07, m/s	0.4575	0.7990	1.4847	0.7065

Experiment No.   : 211
Operating Pressure   : 4000   kPa
Nominal Solute Conc.   : 2000   ppm
Nominal Feed Flow Rate: 1000   ml/min
Setpoint Temperature   : 25.00 Degree C
Solute   : LICL

Avg. Feed Conc. (ppm) = 2131. ; XA1 =0.000907 ; Cl = 55.35 kmol/m.m.m

	Film # 1	Film # 2	Film # 3	Film # 4
	********	********	********	********
A * E09, kmol/m.m.s.kPa	184.5651	246.8043	331.2451	299.4015
[n]P , kg/m.m.s	0.013303	0.017790	0.023876	0.021581
[n]T , kg/m.m.s	0.011904	0.015998	0.021375	0.018290
XA2 * E04	21.0927	19.6093	18.4119	18.4964
XA3 * E04	0.1156	0.1632	0.1139	0.2352
f	0.987263	0.982018	0.987450	0.974087
f prime	0.994530	0.991691	0.993824	0.987306
k * E06 , m/s	14.0204	20.5419	29.9954	25.2549
(D)AM K/Tau * E07, m/s	0.6579	1.3465	1.3343	2.3620

Experiment No.   : 212
Operating Pressure   : 1500   kPa
Nominal Solute Conc.   : 2000   ppm
Nominal Feed Flow Rate: 1000   ml/min
Setpoint Temperature   : 25.00 Degree C
Solute   : LICL

Avg. Feed Conc. (ppm) = 2017. ; XA1 =0.000858 ; Cl = 55.35 kmol/m.m.m

	Film # 1	Film # 2	Film # 3	Film # 4
	********	********	********	********
A * E09, kmol/m.m.s.kPa	192.0120	260.6324	353.8031	315.0862
[n]P , kg/m.m.s	0.005190	0.007045	0.009563	0.008517
[n]T , kg/m.m.s	0.004233	0.005727	0.007825	0.006583
XA2 * E04	11.5642	11.2875	11.0890	11.0732
XA3 * E04	0.1496	0.1961	0.1994	0.2450
f	0.982580	0.977169	0.976790	0.971477
f prime	0.987075	0.982644	0.982040	0.977898
k * E06 , m/s	14.0204	20.5419	29.9954	25.2549
(D)AM K/Tau * E07, m/s	0.5564	1.0152	1.4363	1.4934

APPENDIX E

THE EXPERIMENTAL DATA OF PHASE III

The film numbers 1, 2, 3, and 4 (in the following tables) refer to the membranes SW30-1, SW30-2, BW30-1, and BW30-2, respectively.

Term in Computer Output	Meaning
A * E09	$A \times 10^9$
Avg.	Average
C1	C
Conc.	Concentration
(D)AM K/Tau * E07	$D_{AM} K/\tau \times 10^7$
f prime	f'
k * E06	$k \times 10^6$
KCL	$KC\ell$
kg/m.m.s	$kg/m^2 s$
kmol/m.m.m	$kmol/m^3$
kmol/m.m.s.kPa	$kmol/m^2 s\, kPa$
LICL	$LiC\ell$
LINO3	$LiNO_3$
NACL	$NaC\ell$
No.	Number
[n]P	n_P
[n]T	n_T
XA1	X_{A1}
XA2 * E04	$X_{A2} \times 10^4$
XA3 * E04	$X_{A3} \times 10^4$

```
Experiment No.          :  301
Operating Pressure      :  1500   kPa
Nominal Solute Conc.    :  2000   ppm
Nominal Feed Flow Rate:    1000   ml/min
Setpoint Temperature    :  25.00  Degree C
Solute                  :  NACL
```

Avg. Feed Conc. (ppm) = 1969. ; XA1 =0.000608 ; Cl = 55.35 kmol/m.m.m

	Film # 1	Film # 2	Film # 3	Film # 4
	********	********	********	********
A * E09, kmol/m.m.s.kPa	192.5144	261.1295	356.1314	303.1800
[n]P , kg/m.m.s	0.005204	0.007058	0.009626	0.008195
[n]T , kg/m.m.s	0.004450	0.006094	0.008362	0.007058
XA2 * E04	8.0936	7.9381	7.8058	7.8033
XA3 * E04	0.0911	0.1236	0.1420	0.1675
f	0.985024	0.979675	0.976652	0.972466
f prime	0.988761	0.984438	0.981820	0.978554
k * E06 , m/s	15.3500	22.4900	32.8400	27.6500
(D)AM K/Tau * E07, m/s	0.5075	0.9666	1.5536	1.5521

```
Experiment No.          :  302
Operating Pressure      :  4000   kPa
Nominal Solute Conc.    :  35 000 ppm
Nominal Feed Flow Rate:    1000   ml/min
Setpoint Temperature    :  25.00  Degree C
Solute                  :  NACL
```

Avg. Feed Conc. (ppm) =35290. ; XA1 =0.011154 ; Cl = 55.34 kmol/m.m.m

	Film # 1	Film # 2	Film # 3	Film # 4
	********	********	********	********
A * E09, kmol/m.m.s.kPa	184.4239	246.8366	332.1723	299.1936
[n]P , kg/m.m.s	0.013293	0.017792	0.023943	0.021566
[n]T , kg/m.m.s	0.003331	0.004396	0.005562	0.004620
XA2 * E04	137.6813	134.4498	131.3276	131.2113
XA3 * E04	3.9778	5.7109	4.6316	3.6673
f	0.964721	0.949341	0.958920	0.967476
f prime	0.971495	0.958071	0.965179	0.972407
k * E06 , m/s	15.3500	22.4900	32.8400	27.6500
(D)AM K/Tau * E07, m/s	0.9930	1.9531	2.0372	1.3310

```
                      Experiment No.          :   303
                      Operating Pressure      :   7000   kPa
                      Nominal Solute Conc.    :   35 000   ppm
                      Nominal Feed Flow Rate:    1000   ml/min
                      Setpoint Temperature    :   25.00   Degree C
                      Solute                  :   NACL
```

Avg. Feed Conc. (ppm) =35683. ;   XA1 =0.011281 ; C1 = 55.34 kmol/m.m.m

	Film # 1	Film # 2	Film # 3	Film # 4
	********	********	********	********
A * E09, kmol/m.m.s.kPa	182.6897	230.8224	357.3101	279.1960
[n]P , kg/m.m.s	0.023044	0.029116	0.045071	0.035218
[n]T , kg/m.m.s	0.010937	0.013679	0.017017	0.014459
XA2 * E04	225.6105	203.8970	186.6643	188.5506
XA3 * E04	4.6480	4.3864	4.4028	2.9320
f	0.959245	0.961539	0.961396	0.974295
f prime	0.979854	0.978917	0.976844	0.984738
k * E06 , m/s	15.3500	22.4900	32.8400	27.6500
(D)AM K/Tau * E07, m/s	2.3079	3.0167	4.1219	2.2911

```
                      Experiment No.          :   304
                      Operating Pressure      :   5000   kPa
                      Nominal Solute Conc.    :   35 000   ppm
                      Nominal Feed Flow Rate:    1000   ml/min
                      Setpoint Temperature    :   25.00   Degree C
                      Solute                  :   NACL
```

Avg. Feed Conc. (ppm) =34537. ;   XA1 =0.010910 ;   C1 = 55.34 kmol/m.m.m

	Film # 1	Film # 2	Film # 3	Film # 4
	********	********	********	********
A * E09, kmol/m.m.s.kPa	178.7355	237.8165	322.4701	287.4365
[n]P , kg/m.m.s	0.016104	0.021427	0.029055	0.025898
[n]T , kg/m.m.s	0.005978	0.007761	0.009756	0.008312
XA2 * E04	160.0096	152.6683	145.9109	146.6335
XA3 * E04	2.5236	3.7163	3.0137	2.4093
f	0.977116	0.966297	0.972670	0.978153
f prime	0.984477	0.976020	0.979641	0.983806
k * E06 , m/s	15.3500	22.4900	32.8400	27.6500
(D)AM K/Tau * E07, m/s	0.9604	1.9407	2.0623	1.3920

Experiment No.   : 305
Operating Pressure   : 7000 kPa
Nominal Solute Conc.   : 35 000 ppm
Nominal Feed Flow Rate: 1000 ml/min
Setpoint Temperature   : 5.00 Degree C
Solute   : NACL

Avg. Feed Conc. (ppm) =35064. ; XA1 =0.011081 ; Cl = 55.54 kmol/m.m.m

	Film # 1	Film # 2	Film # 3	Film # 4
	********	********	********	********
A * E09, kmol/m.m.s.kPa	84.0115	109.1439	173.9802	133.6737
[n]P , kg/m.m.s	0.010597	0.013767	0.021946	0.016862
[n]T , kg/m.m.s	0.005285	0.006723	0.008889	0.007426
XA2 * E04	182.8134	171.8378	164.6998	164.8455
XA3 * E04	4.5662	3.2097	3.4712	2.1562
f	0.959229	0.971345	0.969010	0.980753
f prime	0.975468	0.981636	0.979264	0.987133
k * E06 , m/s	10.2127	14.9631	21.8492	18.3962
(D)AM K/Tau * E07, m/s	1.3503	1.2768	1.9096	0.9823

Experiment No.   : 306
Operating Pressure   : 4000 kPa
Nominal Solute Conc.   : 35 000 ppm
Nominal Feed Flow Rate: 1000 ml/min
Setpoint Temperature   : 5.00 Degree C
Solute   : NACL

Avg. Feed Conc. (ppm) =34838. ; XA1 =0.011008 ; Cl = 55.54 kmol/m.m.m

	Film # 1	Film # 2	Film # 3	Film # 4
	********	********	********	********
A * E09, kmol/m.m.s.kPa	82.1400	112.0773	156.4777	137.9528
[n]P , kg/m.m.s	0.005921	0.008079	0.011279	0.009944
[n]T , kg/m.m.s	0.001786	0.002404	0.003157	0.002607
XA2 * E04	130.5268	128.5399	126.7594	126.5184
XA3 * E04	3.0954	4.1576	2.7523	2.0990
f	0.972181	0.962631	0.975265	0.981137
f prime	0.976588	0.968058	0.978556	0.983616
k * E06 , m/s	10.2127	14.9631	21.8492	18.3962
(D)AM K/Tau * E07, m/s	0.4333	0.8022	0.6996	0.4393

```
                Experiment No.        :   307
                Operating Pressure    :   5000   kPa
                Nominal Solute Conc.  :   35 000  ppm
                Nominal Feed Flow Rate:   1000   ml/min
                Setpoint Temperature  :   5.00   Degree C
                Solute                :   NACL
```

Avg. Feed Conc. (ppm) =35683. ; XA1 =0.011281 ; Cl = 55.54 kmol/m.m.m

	Film # 1	Film # 2	Film # 3	Film # 4
	********	********	********	********
A * E09, kmol/m.m.s.kPa	80.6722	109.4070	154.1035	134.4000
[n]P , kg/m.m.s	0.007269	0.009858	0.013885	0.012109
[n]T , kg/m.m.s	0.002810	0.003748	0.004914	0.004088
XA2 * E04	147.7151	143.9941	140.7315	140.4382
XA3 * E04	2.5890	3.2588	2.0990	1.7888
f	0.977303	0.971430	0.981600	0.984320
f prime	0.982728	0.977687	0.985292	0.987440
k * E06 , m/s	10.2127	14.9631	21.8492	18.3962
(D)AM K/Tau * E07, m/s	0.5004	0.8664	0.7430	0.5267

```
                Experiment No.        :   308
                Operating Pressure    :   1500   kPa
                Nominal Solute Conc.  :   2000   ppm
                Nominal Feed Flow Rate:   1000   ml/min
                Setpoint Temperature  :   25.00  Degree C
                Solute                :   NACL
```

Avg. Feed Conc. (ppm) = 1982. ; XA1 =0.000612 ; Cl = 55.51 kmol/m.m.m

	Film # 1	Film # 2	Film # 3	Film # 4
	********	********	********	********
A * E09, kmol/m.m.s.kPa	193.3210	259.3145	356.4409	318.8916
[n]P , kg/m.m.s	0.005225	0.007009	0.009635	0.008620
[n]T , kg/m.m.s	0.004432	0.006029	0.008308	0.007054
XA2 * E04	8.1456	7.9707	7.8449	7.8428
XA3 * E04	0.0868	0.1180	0.1448	0.2085
f	0.985817	0.980735	0.976346	0.965951
f prime	0.989346	0.985211	0.981551	0.973436
k * E06 , m/s	15.3500	22.4900	32.8400	27.6500
(D)AM K/Tau * E07, m/s	0.4775	0.9055	1.5623	1.9258

```
                  Experiment No.          :   309
                  Operating Pressure      :   7000   kPa
                  Nominal Solute Conc.    :   35 000   ppm
                  Nominal Feed Flow Rate:     1000   ml/min
                  Setpoint Temperature    :   15.00   Degree C
                  Solute                  :   NACL
```

Avg. Feed Conc. (ppm) =35879. ;   XA1 =0.011345 ; Cl = 55.46 kmol/m.m.m

	Film # 1	Film # 2	Film # 3	Film # 4
	********	********	********	********
A * E09, kmol/m.m.s.kPa	137.7995	161.6098	252.9231	196.7122
[n]P , kg/m.m.s	0.017382	0.020385	0.031904	0.024813
[n]T , kg/m.m.s	0.007736	0.009703	0.012418	0.010513
XA2 * E04	203.0791	187.6116	175.8487	177.2228
XA3 * E04	5.3429	3.8797	4.5662	2.9320
f	0.953414	0.966177	0.960189	0.974441
f prime	0.974211	0.979701	0.974478	0.983744
k * E06 , m/s	12.8223	18.7866	27.4323	23.0969
(D)AM K/Tau * E07, m/s	2.0889	2.0481	3.3084	1.7682

```
                  Experiment No.          :   310
                  Operating Pressure      :   4000   kPa
                  Nominal Solute Conc.    :   35 000   ppm
                  Nominal Feed Flow Rate:     1000   ml/min
                  Setpoint Temperature    :   15.00   Degree C
                  Solute                  :   NACL
```

Avg. Feed Conc. (ppm) =35252. ;   XA1 =0.011142 ; Cl = 55.46 kmol/m.m.m

	Film # 1	Film # 2	Film # 3	Film # 4
	********	********	********	********
A * E09, kmol/m.m.s.kPa	126.3630	170.9008	236.2612	209.1706
[n]P , kg/m.m.s	0.009108	0.012319	0.017030	0.015077
[n]T , kg/m.m.s	0.002539	0.003358	0.004334	0.003618
XA2 * E04	135.1362	132.3243	129.9055	129.8605
XA3 * E04	3.1934	4.7134	3.5039	2.7523
f	0.971649	0.958148	0.968892	0.975566
f prime	0.976681	0.964835	0.973369	0.979075
k * E06 , m/s	12.8223	18.7866	27.4323	23.0969
(D)AM K/Tau * E07, m/s	0.6144	1.2399	1.2012	0.7834

```
                     Experiment No.          :  311
                     Operating Pressure      :  5000   kPa
                     Nominal Solute Conc.    :  35 000   ppm
                     Nominal Feed Flow Rate:  1000   ml/min
                     Setpoint Temperature    :  15.00   Degree C
                     Solute                  :  NACL
```

Avg. Feed Conc. (ppm) =34989. ; XA1 =0.011056 ; C1 = 55.46 kmol/m.m.m

	Film # 1	Film # 2	Film # 3	Film # 4
	********	********	********	********
A * E09, kmol/m.m.s.kPa	123.8535	167.5131	229.4948	204.8013
[n]P , kg/m.m.s	0.011159	0.015093	0.020677	0.018453
[n]T , kg/m.m.s	0.004210	0.005508	0.007054	0.005944
XA2 * E04	152.6237	147.0621	142.2446	142.4311
XA3 * E04	2.4583	3.5365	2.6380	2.0990
f	0.978006	0.968356	0.976398	0.981221
f prime	0.984135	0.976297	0.981714	0.985470
k * E06 , m/s	12.8223	18.7866	27.4323	23.0969
(D)AM K/Tau * E07, m/s	0.6892	1.3568	1.3330	0.8892

```
                     Experiment No.          :  312
                     Operating Pressure      :  1500   kPa
                     Nominal Solute Conc.    :  2000   ppm
                     Nominal Feed Flow Rate:  1000   ml/min
                     Setpoint Temperature    :  25.00   Degree C
                     Solute                  :  NACL
```

Avg. Feed Conc. (ppm) = 1971. ; XA1 =0.000609 ; C1 = 55.47 kmol/m.m.m

	Film # 1	Film # 2	Film # 3	Film # 4
	********	********	********	********
A * E09, kmol/m.m.s.kPa	191.3922	260.1969	356.2613	318.2257
[n]P , kg/m.m.s	0.005173	0.007033	0.009630	0.008602
[n]T , kg/m.m.s	0.004414	0.006049	0.008340	0.007070
XA2 * E04	8.0947	7.9347	7.8108	7.8054
XA3 * E04	0.0798	0.1180	0.1434 .	0.2071
f	0.986902	0.980632	0.976451	0.966000
f prime	0.990153	0.985144	0.981651	0.973489
k * E06 , m/s	15.3500	22.4900	32.8400	27.6500
(D)AM K/Tau * E07, m/s	0.4395	0.9132	1.5608	1.9275

```
                        Experiment No.        :  313
                        Operating Pressure    :  7000  kPa
                        Nominal Solute Conc.  :  35 000  ppm
                        Nominal Feed Flow Rate:  1000  ml/min
                        Setpoint Temperature  :  25.00  Degree C
                        Solute                :  NACL
```

Avg. Feed Conc. (ppm) =35218. ; XA1 =0.011131 ; C1 = 55.46 kmol/m.m.m

	Film # 1	Film # 2	Film # 3	Film # 4
A * E09, kmol/m.m.s.kPa	197.3059	230.4516	345.4421	278.4504
[n]P , kg/m.m.s	0.024888	0.029069	0.043574	0.035124
[n]T , kg/m.m.s	0.010782	0.013459	0.016926	0.014475
XA2 * E04	220.6545	200.1082	183.5225	186.1672
XA3 * E04	4.3537	3.2914	4.5662	2.8503
f	0.961304	0.970748	0.959414	0.974670
f prime	0.980696	0.983876	0.975564	0.984970
k * E06 , m/s	15.3500	22.4900	32.8400	27.6500
(D)AM K/Tau * E07, m/s	2.1696	2.2503	4.3163	2.2503

```
                        Experiment No.        :  314
                        Operating Pressure    :  4000  kPa
                        Nominal Solute Conc.  :  35 000  ppm
                        Nominal Feed Flow Rate:  1000  ml/min
                        Setpoint Temperature  :  25.00  Degree C
                        Solute                :  NACL
```

Avg. Feed Conc. (ppm) =35298. ; XA1 =0.011157 ; C1 = 55.46 kmol/m.m.m

	Film # 1	Film # 2	Film # 3	Film # 4
A * E09, kmol/m.m.s.kPa	184.1232	246.2193	332.0887	298.4630
[n]P , kg/m.m.s	0.013272	0.017747	0.023937	0.021513
[n]T , kg/m.m.s	0.003237	0.004283	0.005488	0.004592
XA2 * E04	136.9412	133.8903	131.0527	131.1164
XA3 * E04	3.7898	5.4656	4.7297	3.6673
f	0.966397	0.951530	0.958059	0.967484
f prime	0.972694	0.959703	0.964366	0.972387
k * E06 , m/s	15.3500	22.4900	32.8400	27.6500
(D)AM K/Tau * E07, m/s	0.9211	1.8219	2.0538	1.3212

```
Experiment No.          :  315
Operating Pressure      :  5000   kPa
Nominal Solute Conc.    :  35 000  ppm
Nominal Feed Flow Rate:    1000   ml/min
Setpoint Temperature    :  25.00  Degree C
Solute                  :  NACL
```

Avg. Feed Conc. (ppm) =35220. ;   XA1 =0.011131 ; Cl = 55.46 kmol/m.m.m

	Film # 1	Film # 2	Film # 3	Film # 4
	********	********	********	********
A * E09, kmol/m.m.s.kPa	180.9746	239.7649	324.6375	290.5956
[n]P , kg/m.m.s	0.016306	0.021603	0.029250	0.026183
[n]T , kg/m.m.s	0.005642	0.007349	0.009198	0.007865
XA2 * E04	159.7865	153.0112	146.2818	147.1808
XA3 * E04	2.5236	3.7490	3.4548	2.6216
£	0.977575	0.966682	0.969297	0.976704
£ prime	0.984455	0.975865	0.976720	0.982445
k * E06 , m/s	15.3500	22.4900	32.8400	27.6500
(D)AM K/Tau * E07, m/s	0.9053	1.8452	2.2245	1.4263

```
Experiment No.          :  316
Operating Pressure      :  4000   kPa
Nominal Solute Conc.    :  35 000  ppm
Nominal Feed Flow Rate:    1000   ml/min
Setpoint Temperature    :  35.00  Degree C
Solute                  :  NACL
```

Avg. Feed Conc. (ppm) =34631. ;   XA1 =0.010941 ; Cl = 55.13 kmol/m.m.m

	Film # 1	Film # 2	Film # 3	Film # 4
	********	********	********	********
A * E09, kmol/m.m.s.kPa	254.4532	337.0183	443.9091	406.8397
[n]P , kg/m.m.s	0.018341	0.024292	0.031997	0.029325
[n]T , kg/m.m.s	0.004486	0.005804	0.007345	0.006199
XA2 * E04	138.2484	134.1256	130.4570	130.7576
XA3 * E04	3.6999	5.3020	5.5964 .	4.3864
£	0.966539	0.952043	0.949379	0.960329
£ prime	0.973597	0.960979	0.957637	0.966878
k * E06 , m/s	18.7057	27.4065	40.0192	33.6946
(D)AM K/Tau * E07, m/s	1.2416	2.4033	3.3115	2.1649

```
                    Experiment No.          :  317
                    Operating Pressure      :  7000  kPa
                    Nominal Solute Conc.    :  35 000  ppm
                    Nominal Feed Flow Rate:  1000  ml/min
                    Setpoint Temperature   :  35.00  Degree C
                    Solute                  :  NACL
```

Avg. Feed Conc. (ppm) =34914. ; XA1 =0.011032 ; C1 = 55.13 kmol/m.m.m

	Film # 1	Film # 2	Film # 3	Film # 4
	********	********	********	********
A * E09, kmol/m.m.s.kPa	261.6229	311.2911	475.8333	376.1858
[n]P , kg/m.m.s	0.033001	0.039266	0.060022	0.047452
[n]T , kg/m.m.s	0.014035	0.017477	0.021370	0.018492
XA2 * E04	230.4306	206.6084	185.2517	189.3942
XA3 * E04	3.7653	3.2588	4.9586	3.0137
f	0.966233	0.970777	0.955526	0.972976
f prime	0.984030	0.984548	0.973716	0.984384
k * E06 , m/s	18.7057	27.4065	40.0192	33.6946
(D)AM K/Tau * E07, m/s	2.3482	2.8206	5.9141	3.0103

```
                    Experiment No.          :  318
                    Operating Pressure      :  5000  kPa
                    Nominal Solute Conc.    :  35 000  ppm
                    Nominal Feed Flow Rate:  1000  ml/min
                    Setpoint Temperature   :  35.00  Degree C
                    Solute                  :  NACL
```

Avg. Feed Conc. (ppm) =34349. ; XA1 =0.010849 ; C1 = 55.13 kmol/m.m.m

	Film # 1	Film # 2	Film # 3	Film # 4
	********	********	********	********
A * E09, kmol/m.m.s.kPa	250.0535	326.5845	463.3479	393.1787
[n]P , kg/m.m.s	0.022530	0.029425	0.041748	0.035425
[n]T , kg/m.m.s	0.007843	0.009998	0.012627	0.010630
XA2 * E04	164.0925	154.8739	146.6744	147.9210
XA3 * E04	2.5236	3.8797	6.2847	2.9320
f	0.976986	0.964614	0.942665	0.973261
f prime	0.984869	0.975328	0.957754	0.980466
k * E06 , m/s	18.7057	27.4065	40.0192	33.6946
(D)AM K/Tau * E07, m/s	1.2333	2.5855	5.6864	2.1640

```
Experiment No.          :  319
Operating Pressure      :  1500   kPa
Nominal Solute Conc.    :  2000   ppm
Nominal Feed Flow Rate:    1000   ml/min
Setpoint Temperature    :  25.00  Degree C
Solute                  :  NACL
```

Avg. Feed Conc. (ppm) = 1934. ; XA1 =0.000597 ; Cl = 55.18 kmol/m.m.m

	Film # 1	Film # 2	Film # 3	Film # 4
	********	********	********	********
A * E09, kmol/m.m.s.kPa	190.9854	261.0509	355.8056	318.8399
[n]P , kg/m.m.s	0.005162	0.007056	0.009617	0.008618
[n]T , kg/m.m.s	0.004510	0.006100	0.008332	0.007104
XA2 * E04	7.9921	7.8035	7.6646	7.6729
XA3 * E04	0.0777	0.1144	0.1314	0.1859
f	0.987006	0.980852	0.978011	0.968898
f prime	0.990291	0.985347	0.982868	0.975794
k * E06 , m/s	15.3500	22.4900	32.8400	27.6500
(D)AM K/Tau * E07, m/s	0.4450	0.9130	1.4616	1.7735

```
Experiment No.          :  320
Operating Pressure      :  5000   kPa
Nominal Solute Conc.    :  35 000 ppm
Nominal Feed Flow Rate:    1000   ml/min
Setpoint Temperature    :  45.00  Degree C
Solute                  :  NACL
```

Avg. Feed Conc. (ppm) =33785. ; XA1 =0.010667 ; Cl = 54.91 kmol/m.m.m

	Film # 1	Film # 2	Film # 3	Film # 4
	********	********	********	********
A * E09, kmol/m.m.s.kPa	328.7674	423.9315	625.6730	502.2214
[n]P , kg/m.m.s	0.029622	0.038196	0.056373	0.045250
[n]T , kg/m.m.s	0.010020	0.012588	0.015602	0.013276
XA2 * E04	167.6434	156.5708	146.3547	148.3418
XA3 * E04	2.4583	3.6346	7.0294	3.3405
f	0.977194	0.966277	0.934757	0.969007
f prime	0.985578	0.977142	0.952640	0.977808
k * E06 , m/s	21.9659	32.1833	46.9942	39.5673
(D)AM K/Tau * E07, m/s	1.5070	3.0219	7.9450	3.0896

```
                    Experiment No.          :  321
                    Operating Pressure      :  4000   kPa
                    Nominal Solute Conc.    :  35 000   ppm
                    Nominal Feed Flow Rate:    1000   ml/min
                    Setpoint Temperature    :  45.00   Degree C
                    Solute                  :  NACL
```

Avg. Feed Conc. (ppm) =35220. ; XA1 =0.011131 ; C1 = 54.91 kmol/m.m.m

	Film # 1	Film # 2	Film # 3	Film # 4
	********	********	********	********
A * E09, kmol/m.m.s.kPa	335.9379	438.5142	564.1376	518.0924
[n]P , kg/m.m.s	0.024214	0.031608	0.040663	0.037344
[n]T , kg/m.m.s	0.005133	0.006713	0.008433	0.007085
XA2 * E04	139.7710	135.9152	132.0132	132.2603
XA3 * E04	4.3701	6.3674	7.1121	5.6128
f	0.961160	0.943397	0.936772	0.950109
f prime	0.969158	0.953759	0.946799	0.958100
k * E06 , m/s	21.9659	32.1833	46.9942	39.5673
(D)AM K/Tau * E07, m/s	1.6729	3.3304	4.8465	3.1699

```
                    Experiment No.          :  322
                    Operating Pressure      :  7000   kPa
                    Nominal Solute Conc.    :  35 000   ppm
                    Nominal Feed Flow Rate:    1000   ml/min
                    Setpoint Temperature    :  45.00   Degree C
                    Solute                  :  NACL
```

Avg. Feed Conc. (ppm) =35486. ; XA1 =0.011218 ; C1 = 54.91 kmol/m.m.m

	Film # 1	Film # 2	Film # 3	Film # 4
	********	********	********	********
A * E09, kmol/m.m.s.kPa	328.5645	400.9885	596.8623	476.8013
[n]P , kg/m.m.s	0.041445	0.050581	0.075288	0.060144
[n]T , kg/m.m.s	0.017167	0.021024	0.025215	0.021919
XA2 * E04	242.7268	213.6310	188.8106	193.7565
XA3 * E04	3.5365	3.5692	5.6128	3.3486
f	0.968816	0.968527	0.950498	0.970473
f prime	0.985779	0.983644	0.970818	0.983047
k * E06 , m/s	21.9659	32.1833	46.9942	39.5673
(D)AM K/Tau * E07, m/s	2.5660	3.6101	7.8027	3.8954

```
Experiment No.          :   323
Operating Pressure      :   1500   kPa
Nominal Solute Conc.    :   2000   ppm
Nominal Feed Flow Rate:     1000   ml/min
Setpoint Temperature    :   25.00  Degree C
Solute                  :   NACL
```

Avg. Feed Conc. (ppm) = 1934. ; XA1 =0.000597 ; Cl = 54.95 kmol/m.m.m

	Film # 1	Film # 2	Film # 3	Film # 4
	********	********	********	********
A * E09, kmol/m.m.s.kPa	189.3091	255.9568	345.9616	310.9078
[n]P , kg/m.m.s	0.005117	0.006919	0.009351	0.008404
[n]T , kg/m.m.s	0.004414	0.005957	0.008042	0.006860
XA2 * E04	7.9419	7.7548	7.5991	7.6070
XA3 * E04	0.0798	0.1137	0.1279	0.1859
f	0.986651	0.980970	0.978603	0.968898
f prime	0.989963	0.985346	0.983186	0.975584
k * E06 , m/s	15.3500	22.4900	32.8400	27.6500
(D)AM K/Tau * E07, m/s	0.4523	0.8954	1.3899	1.7351

```
Experiment No.          :   324
Operating Pressure      :   4000   kPa
Nominal Solute Conc.    :   35 000 ppm
Nominal Feed Flow Rate:     1000   ml/min
Setpoint Temperature    :   60.00  Degree C
Solute                  :   NACL
```

Avg. Feed Conc. (ppm) =34462. ; XA1 =0.010886 ; Cl = 54.54 kmol/m.m.m

	Film # 1	Film # 2	Film # 3	Film # 4
	********	********	********	********
A * E09, kmol/m.m.s.kPa	469.7270	600.2659	745.1145	691.7003
[n]P , kg/m.m.s	0.033858	0.043267	0.053708	0.049858
[n]T , kg/m.m.s	0.007139	0.009219	0.011426	0.009648
XA2 * E04	140.5181	135.7365	130.9268	131.3823
XA3 * E04	5.2039	7.3604	8.8455	7.1121
f	0.952691	0.933072	0.919557	0.935331
f prime	0.963468	0.946471	0.933265	0.946540
k * E06 , m/s	27.2413	39.9125	58.2805	49.0699
(D)AM K/Tau * E07, m/s	2.7909	5.3706	8.4085	5.6107

```
Experiment No.        :  325
Operating Pressure    :  5000  kPa
Nominal Solute Conc.  :  35 000  ppm
Nominal Feed Flow Rate:  1000  ml/min
Setpoint Temperature  :  60.00  Degree C
Solute                :  NACL
```

Avg. Feed Conc. (ppm) =35918. ; XA1 =0.011357 ; Cl = 54.54 kmol/m.m.m

	Film # 1	Film # 2	Film # 3	Film # 4
A * E09, kmol/m.m.s.kPa	441.0686	560.6056	754.4406	652.3888
[n]P , kg/m.m.s	0.039740	0.050511	0.067975	0.058780
[n]T , kg/m.m.s	0.011213	0.014030	0.017070	0.014371
XA2 * E04	170.6605	160.0145	149.7015	151.1999
XA3 * E04	3.7653	5.5146	9.4647	5.1385
f	0.967211	0.951970	0.917534	0.955248
f prime	0.978305	0.966069	0.937664	0.966512
k * E06 , m/s	27.2413	39.9125	58.2805	49.0699
(D)AM K/Tau * E07, m/s	2.5727	5.0910	11.7008	5.1399

```
Experiment No.        :  326
Operating Pressure    :  7000  kPa
Nominal Solute Conc.  :  35 000  ppm
Nominal Feed Flow Rate:  1000  ml/min
Setpoint Temperature  :  60.00  Degree C
Solute                :  NACL
```

Avg. Feed Conc. (ppm) =37253. ; XA1 =0.011791 ; Cl = 54.53 kmol/m.m.m

	Film # 1	Film # 2	Film # 3	Film # 4
A * E09, kmol/m.m.s.kPa	423.8691	511.0872	731.5854	592.7129
[n]P , kg/m.m.s	0.053467	0.064469	0.092282	0.074765
[n]T , kg/m.m.s	0.019984	0.024416	0.028208	0.025111
XA2 * E04	244.6812	215.9243	189.3665	195.6643
XA3 * E04	3.5692	4.3210	5.5473	4.0268
f	0.970075	0.963768	0.953480	0.966236
f prime	0.985765	0.980412	0.971245	0.979814
k * E06 , m/s	27.2413	39.9125	58.2805	49.0699
(D)AM K/Tau * E07, m/s	3.0099	5.0711	8.6548	5.3665

```
                 Experiment No.          :   327
                 Operating Pressure      :   1500   kPa
                 Nominal Solute Conc.     :   2000   ppm
                 Nominal Feed Flow Rate:     1000   ml/min
                 Setpoint Temperature    :   25.00  Degree C
                 Solute                  :   NACL
```

Avg. Feed Conc. (ppm) = 1966. ; XA1 =0.000607 ; Cl = 54.56 kmol/m.m.m

	Film # 1	Film # 2	Film # 3	Film # 4
	********	********	********	**** .*
A * E09, kmol/m.m.s.kPa	172.6827	232.2497	303.7977	274.8328
[n]P , kg/m.m.s	0.004668	0.006278	0.008212	0.007429
[n]T , kg/m.m.s	0.003976	0.005407	0.007080	0.006058
XA2 * E04	7.8472	7.6924	7.5091	7.5187
XA3 * E04	0.0808	0.1222	0.1102	0.1774
f	0.986704	0.979881	0.981860	0.970799
f prime	0.989716	0.984125	0.985337	0.976425
k * E06 , m/s	15.3500	22.4900	32.8400	27.6500
(D)AM K/Tau * E07, m/s	0.4206	0.8879	1.0724	1.4888

```
                 Experiment No.          :   328
                 Operating Pressure      :   4000   kPa
                 Nominal Solute Conc.     :   35 000  ppm
                 Nominal Feed Flow Rate:     1000   ml/min
                 Setpoint Temperature    :   25.00  Degree C
                 Solute                  :   NACL
```

Avg. Feed Conc. (ppm) =35027. ; XA1 =0.011069 ; Cl = 54.54 kmol/m.m.m

	Film # 1	Film # 2	Film # 3	Film # 4
	********	********	********	********
A * E09, kmol/m.m.s.kPa	164.1027	216.3389	281.1647	254.4847
[n]P , kg/m.m.s	0.011829	0.015594	0.020266	0.018343
[n]T , kg/m.m.s	0.002709	0.003570	0.004408	0.003699
XA2 * E04	131.3650	128.8230	126.0258	126.1155
XA3 * E04	3.8715	5.5473	4.1903	3.1934
f	0.965396	0.950409	0.952546	0.971459
f prime	0.970904	0.957469	0.967156	0.974990
k * E06 , m/s	15.3500	22.4900	32.8400	27.6500
(D)AM K/Tau * E07, m/s	0.8366	1.6328	1.5413	0.9772

```
                    Experiment No.          :   329
                    Operating Pressure      :   5000   kPa
                    Nominal Solute Conc.    :   35 000   ppm
                    Nominal Feed Flow Rate:    1000   ml/min
                    Setpoint Temperature    :   25.00   Degree C
                    Solute                  :   NACL
```

Avg. Feed Conc. (ppm) =35447. ; XA1 =0.011205 ; Cl = 54.54 kmol/m.m.m

	Film # 1	Film # 2	Film # 3	Film # 4
	********	********	********	********
A * E09, kmol/m.m.s.kPa	164.3724	215.4946	289.4028	252.1292
[n]P , kg/m.m.s	0.014810	0.019416	0.026075	0.022717
[n]T , kg/m.m.s	0.004940	0.006381	0.007845	0.006660
XA2 * E04	153.7103	147.6565	141.1748	142.0885
XA3 * E04	2.6461	3.8307	4.4191	2.0745
f	0.976642	0.966182	0.960985	0.981689
f prime	0.983045	0.974430	0.969126	0.985604
k * E06 , m/s	15.3500	22.4900	32.8400	27.6500
(D)AM K/Tau * E07, m/s	0.8802	1.7282	2.5773	1.0038

```
                    Experiment No.          :   330
                    Operating Pressure      :   7000   kPa
                    Nominal Solute Conc.    :   35 000   ppm
                    Nominal Feed Flow Rate:    1000   ml/min
                    Setpoint Temperature    :   25.00   Degree C
                    Solute                  :   NACL
```

Avg. Feed Conc. (ppm) =35604. ; XA1 =0.011256 ; Cl = 54.54 kmol/m.m.m

	Film # 1	Film # 2	Film # 3	Film # 4
	********	********	********	********
A * E09, kmol/m.m.s.kPa	168.4720	208.6678	303.9844	244.9969
[n]P , kg/m.m.s	0.021251	0.026321	0.038345	0.030904
[n]T , kg/m.m.s	0.009648	0.012038	0.014602	0.012611
XA2 * E04	208.3823	190.3772	174.0568	176.6264
XA3 * E04	3.4058	2.9974	3.0790	2.0500
f	0.970072	0.973662	0.972944	0.981988
f prime	0.983991	0.984551	0.982613	0.988596
k * E06 , m/s	15.3500	22.4900	32.8400	27.6500
(D)AM K/Tau * E07, m/s	1.6307	1.9589	2.6748	1.5066

APPENDIX F

THE COMPUTER CODE FOR OPTIMISING THE MD-SF-PF MODEL

The program in this appendix uses an integrating package, called LSODE, to integrate the set of ordinary differential equations with respect to time, and an optimising package, called UWHAUS, to best determine the parameters of the MD-SF-PF model. The subroutines LSODE and UWHAUS are not shown in the present dissertation. Some of the most important terms in the computer code are defined as follows.

Term in the code	Meaning
A(I,J)	first derivative of Lagrange interpolation polynomial
AL	the first parameter to determine Jacobi polynomial
AP	solvent permeability coefficient of membrane
B(I,J)	second derivative of Lagrange interpolation polynomial
BE	the second parameter to determine Jacobi polynomial
BETA	a parameter defined in the main program
BETA1	a parameter defined in the main program
BETA2	a parameter defined in the main program
C(I,J)	a parameter defined in the main program
CA(I)	a concentration ratio defined in the main program
CA2(I)	boundary-layer concentration of the feed
CA3(I)	permeate concentration
CA3C(I)	guessed value for permeate concentration

CA3M(I)	calculated value (by MD-SF-PF) for permeate concentration
CMOL(I)	molar density of solution
DAB	free diffusivity of solute in solvent
DIF1	first derivatives of the node polynomial at the roots
DIF2	second derivatives of the node polynomial at the roots
DIF3	third derivatives of the node polynomial at the roots
DIFF(I)	increments used to calculate numerical derivatives
EPS1	a parameter of convergence criterion used by UWHAUS
EPS2	a parameter of convergence criterion used by UWHAUS
FF	frictional drag function, b
FFLOWR(I)	flow rate of pumped feed solution
FLAM	starting value for λ parameter in Marquardt's method
FNU	a parameter in Marquardt's method
FP(I)	experimental values for separation
FPR(I)	model values for separation
JIM	a counter for experimental observations
JV	total volumetric flux of permeation through membrane
MIT	maximum No. of iterations during a current call to UWHAUS
MTC(I)	mass transfer coefficient
N	number of internal collocation points
N0	number of collocation points at pore inlet
N1	number of collocation points at pore outlet
ND	dimension of the vectors DIF1, DIF2, DIF3, and ROOT
NOFILM	number of membrane samples
NPARM	number of model parameters to be optimized

NRUNS	number of experimental runs
nP(I)	mass flux of pure solvent through membrane
nT(I)	total mass flux of permeation through membrane
NT	total molar flux of permeation through membrane
OSMP(I)	osmotic pressure
PDEL(I)	pressure drop across membrane
PHI(I)	dimensionless potential function
PI2(I)	osmotic pressure at the boundary-layer side
PI3(I)	osmotic pressure at the permeate side
PN	molar flux of pure solvent through membrane
RA	average radius of solute molecule
RNTNP	the flux ratio N_T/N_P
ROOT(I)	roots (or zeros) of the node polynomial
RRATIO	the ratio R_A/R_W
RUNNO(I)	run number
SCALE1	scaling factor for first parameter of the model
SCALE2	scaling factor for second parameter of the model
SIGNS(I)	indicates a priori sign restrictions on the parameters
SOLUTE	solute type
SUMD	a definite integral defined in the main program
SUMN	a definite integral defined in the main program
TAUEPS	the ratio τ/ε
TEMP(I)	system temperature in °C
TEMPT(I)	system temperature in K
TH(I)	an array a vector of model parameters values

TH1	the first parameter of the MD-SF-PF model
TH2	the second parameter of the MD-SF-PF model
TIN	initial time
TN	total molar flux of permeation through membrane
TOUT	final time
V1(I)	vector of first derivatives of Lagrange polynomial
V2(I)	vector of second derivatives of Lagrange polynomial
VIS	viscosity of solution
WORK(I)	an array-parameter used for temporary storage for UWHAUS
XA(I)	mole fraction
XA1	mole fraction of bulk feed solution
XA2	mole fraction of boundary-layer solution
XA3	mole fraction of permeate solution
XAB	friction constant xxx_{AB}
Y(I)	fluid velocity $\alpha(\rho)$
YDOT(I)	derivative of $\alpha(\rho)$ with respect to time

```
      PROGRAM MDSFPFOP
C     ==================
C     ***********************************************************
C
C Hussein Mehdizadeh
C
C Subject: This program uses the MD-SF-PF model and the UWHAUS
C          optimization routine to estimate the best parameters
C          of the model (RW and TET1) for one membrane,
C          using the experimental data set of SORTANZ.DAT file
C          and using the integrating package LSODE.
C
C     ***********************************************************
C
C
      IMPLICIT REAL*8 (A-H,O-Z)
C
      REAL*8 JV(90),JVMIN,JVMAX,RESID(90)
     *    ,DIFF(2),SIGNS(2),WORK(415)
     *    ,XA1(90),XA2(90),XA3(90)
     *    ,FP(90),P(90),nP(90),nT(90),TEMP(90),TEMPK(90)
     *    ,FFLOWR(90),MTC(90),XA(36),OSMP(36)
     *    ,TET2,PPI2,PPI3,XA2X,XA3X
C
      INTEGER SOLUTE,NOFILM
      INTEGER NEWNO(90),NEWN(6),INDS(90),RUNNO(90),NFILM(90),NR(90)
C
      EXTERNAL MODEL
C
      CHARACTER*20 ITITLE(2),SALT(10)
C
      COMMON /DATAS/ XO(90),YO(90)
      COMMON /BETAS/ BETA1,BETA2,BETA
      COMMON /AREA1/ C(5,5),ROOT(5)
      COMMON /AREA2/ RA,FF,CMOL(1)
      COMMON /THETA/ TH(2)
      COMMON /AREA3/ PDEL(90),TEMPT(90)
      COMMON /AREA4/ CA(90),CA2(90),CA3(90),CA3M(90),CA3C(90)
      COMMON /SCALE/ SCALE1,SCALE2
      COMMON /TETA1/ TET2,INO
      COMMON /PI23/  PI2(90),PI3(90)
      COMMON /TICLABY/INTIC,FIRVLY,DELVLY,YINC
C
      OPEN (UNIT=2,   FILE='SYS$OUTPUT',    STATUS='UNKNOWN')
      OPEN (UNIT=6,   FILE='MDSFPFOP.DAT',  STATUS='UNKNOWN')
      OPEN (UNIT=15,  FILE='SORTANZ.DAT',   STATUS='OLD')
C
      DATA SALT/'NACL.DAT','KCL.DAT','LINO3.DAT','LICL.DAT',' ',' ',
     *          ' ',' ',' ',' '/
C
C     ***** OPEN AND READ FILES CONTAINING MOLE FRACTION      *****
```

```
C       ***** AND DENSITY DATA, AND READ SOLUTE NO. FROM SCREEN.*****
C
        SCALE1=1.D-10
        SCALE2=1.D-10
C
        TET2=0.5D0
        CMOL(1)=55.35D0
C
  80    LUN=6
        LUN3=3
        LUN4=4
        LUN14=14
        LUN15=15
        LUN16=16
        NINT=41
C
C       Read in the data from SORTANZ.DAT file and store it in vectors
C         for later analysis:
C
        READ (LUN15,*)NRUNS
        NOFILM=6
        NDATA=NRUNS*NOFILM
        READ (LUN15,*)
C
        PRINT*,'**********************************'
        PRINT*,'Data being red from SORTANZ.DAT ...'
        PRINT*,'---------------------------------'
C
        DO 5 I=1,NDATA
           READ(LUN15,12) RUNNO(I),NFILM(I),XA1(I),XA2(I),XA3(I)
     *          ,FP(I),P(I),nP(I),nT(I),TEMP(I),FFLOWR(I),MTC(I)
C       WRITE(6,12)RUNNO(I),NFILM(I),XA1(I),XA2(I),XA3(I)
C    *          ,FP(I),P(I),nP(I),nT(I),TEMP(I),FFLOWR(I),MTC(I)
 12        FORMAT(2X,2(1X,I4),10E12.5)
C
           JV(I)=nT(I)/CMOL(1)/18.02D0
        TEMPK(I)=TEMP(I)+0.27315D03
  5     CONTINUE
C
C    Now, for each model, select and sort the data to be analyzed:
C    Select all experiments at T=25 C and for film J :
C
     DO 120 JIM=2,2
C
        IC=0
        REWIND 3
        REWIND 4
C
        DO 100 I=1,NDATA
           IF(TEMP(I).EQ.25.0.AND.NFILM(I).EQ.JIM) THEN
C
```

```
C              IF(TEMP(I).EQ.25.0.AND.NFILM(I).EQ.JIM.AND.FFLOWR(I).
C      *          EQ.1000.) THEN
               IC=IC+1
               XO(IC)=JV(I)
               YO(IC)=FP(I)
               NR(IC)=RUNNO(I)
                     PDEL(IC)=P(I)
                     CA2(IC)=XA2(I)*CMOL(1)
                     CA3(IC)=XA3(I)*CMOL(1)
                     TEMPT(IC)=TEMPK(I)
                  ELSE
               ENDIF
 100     CONTINUE
C
         NOBS=IC
C
      DO 96 I=1,NOBS
            WRITE(6,97)I,NR(I),XO(I),YO(I),PDEL(I),CA2(I),TEMPT(I)
  97        FORMAT(/,5X,I4,5X,I4,5X,5E20.12)
  96 CONTINUE
C
C*********************************************************
C                                                       *
C                 The MD-SF-PF Model                    *
C                                                       *
C*********************************************************
C
C  Set the initial guesses for the unknown parameters
C  and the parameters for the search routine UWHAUS:
C
C
      NPARM=2
C
C Avg. Pore Size RW, m:
C ( MUST BE MULTIPLIED BY 'SCALE1' )
      TH(1)=10.D0
C
C The Potential Parameter TET1, m:
C ( MUST BE MULTIPLIED BY 'SCALE2' )
      TH(2)=56.D0
C
               EPS1=1.0D-5
               EPS2=1.0D-6
               MIT=100
               FLAM=0.01D0
               FNU=10.D0
                 SIGNS(1)=1.D0
                 SIGNS(2)=1.D0
               DIFF(1)=1.D-7
               DIFF(2)=1.D-7
C     -------------------------------------------------------------
```

```
      CALL UWHAUS(NPROB,MODEL,NOBS,YO,NPARM,TH,DIFF,SIGNS,EPS1,
     *           EPS2,MIT,FLAM,FNU,WORK,LUN)
C     -------------------------------------------------------------
C
      TH1=TH(1)*SCALE1
      TH2=TH(2)*SCALE2
C
      WRITE(6,805) JIM
 805  FORMAT(/,5X,'The followings are the results of the nonlinear',
     *         'optimization search for FILM # ',I1,/)
      WRITE(6,110) TH1,TH2
 110     FORMAT (5X,'TH(1) = RW = ',E30.20,1X,'m',/,5X,'TH(2) =
     *           TET1 = ',E30.20,1X,'m',//////)
C
      REWIND 3               .
      REWIND 4
C
  120 CONTINUE
C
      STOP
      END
C
C *****************************************************************
C     ----------------------------------------------
      SUBROUTINE MODEL (NPROB,TH,F,NOBS,NP)
C     ----------------------------------------------
C
C
      IMPLICIT REAL*8 (A-H,O-Z)
C
      REAL*8 TH(NP),F(NOBS),TET2,PERMSF,PERMIT,FPR(90),JV(90),FP(90),
     *       SUMN,SUMD,SUMN1,SUMN2,SUMN3,SUMD4,SUMD1,SUMD2,SUMD3,MA
C
      INTEGER ZZ,SOLUTE,NCPXA
C
      EXTERNAL FCN,FCNJ
C
      DIMENSION PHI(101),YV(101)
      DIMENSION DIF1(5),DIF2(5),DIF3(5),V1(5),V2(5)
      DIMENSION XINTP(5),A(5,5),B(5,5)
      DIMENSION Y(5),ATOL(5),RWORK(70),IWORK(25)
      DIMENSION RPF(101),YPF(101),ALRO(11)
      DIMENSION XA(30),PA(30),CCA(30),XAX(30),PAX(30),CCAX(30)
C
      CHARACTER*20 SALT(10)
C
      COMMON /DATAS/ XO(90),YO(90)
      COMMON /BETAS/ BETA1,BETA2,BETA
      COMMON /AREA1/ C(5,5),ROOT(5)
      COMMON /AREA2/ RA,FF,CMOL(1)
      COMMON /AREA3/ PDEL(90),TEMPT(90)
```

```
      COMMON /AREA4/ CA(90),CA2(90),CA3(90),CA3M(90),CA3C(90)
      COMMON /SCALE/ SCALE1,SCALE2
      COMMON /TETA1/ TET2,INO
      COMMON /PI23/  PI2(90),PI3(90)
C
      DATA SALT/'NACL.DAT','KCL.DAT','LINO3.DAT','LICL.DAT',' ',' ',
     *            ' ',' ',' ',' '/
      DATA AL,BE/0.D0,0.D0/
      DATA N0,N1/1,1/
C
C     ============================================================
C
C     -Choose a value for SOLUTE (1=NACL, 2=KCL, 3=LINO3, 4=LICL):
      SOLUTE=1
C     SOLUTE=2
C     SOLUTE=3
C     SOLUTE=4
C
C     ------------------------------------------------------------
C
      OPEN (UNIT=LUN25,FILE=SALT(SOLUTE),STATUS='OLD')
C
C     ============================================================
C
C  DATA:
C  -----
      READ(LUN25,*,END=300) NCPXA,MA,(XA(I),PA(I),CCA(I),I=1,24)
C
  300 CONTINUE
C
      IF(SOLUTE.EQ.2) DAB=1.994D-9
      IF(SOLUTE.EQ.3) DAB=1.336D-9
      IF(SOLUTE.EQ.4) DAB=1.367D-9
C
      VIS=0.8965D-06
C
C     ------------------------------------------------
C
C   Solute Free Diffusivity at T=25 C, (m.m/s)
      IF(SOLUTE.EQ.1) DAB25=1.566D-9
      IF(SOLUTE.EQ.2) DAB25=1.994D-9
      IF(SOLUTE.EQ.3) DAB25=1.336D-9
      IF(SOLUTE.EQ.4) DAB25=1.367D-9
C
C   Gas Constant, (kJ/kmol.K)
      R=8.3144D0
C
C   Boltzmann Constant, (kJ/K)
      BOLTZ=1.38066D-26
C
C   Charge of Proton, (kC)
```

```
      ELC=1.60219D-22
C
C    Faraday Constant, (kC/kmol)
      FARAD=96486.7D0
C
C    Avogadro's Number, (ions/m.m.m)
      AVO=6.02205D26
C
C    Free-Space Permittivity, (kC.kC/kJ.m)
      PERMFS=8.8542D-15
C
C    Water Permittivity at 25 degree C, (kC.kC/kJ.m)
      ZPERM25=78.54D0
      PERMIT25=ZPERM25*PERMFS
C
      IF(SOLUTE.NE.1) ZPERM=ZPERM25
C
      PERMIT=ZPERM*PERMFS
C
C    Valence of the Symmetrical Electrolyte
      ZZ=1
C
C    PI Constant
      PI=3.1415926D0
C==========================================================================
C
      DO 1987 INO=1,NOBS
C      -------
C
      DAB=(TEMPT(INO)*TEMPT(INO)/(VIS*1.D06))*(0.181092D-04)*R
     *      /(FARAD*FARAD)
C
C
C ==========================================================================
C
      TH1=TH(1)*SCALE1
      TH2=TH(2)*SCALE2
C
C ==========================================================================
C
C Number of collocation points:
      N=3
C
C ==========================================================================
C
C    -Initially Guessed Permeate Conc., (kmol/m.m.m):
C    -You may change the following guess depending on your system.
C
      CA3M(INO)=5.D-5
      CA3F=CA3M(INO)
C
```

```fortran
      TOL=1.D-6
C
      MH=1
      PRINT*,'-----------------------------'
      PRINT*,'MH = ',MH,'  INO = ',INO
      PRINT*,'CA3M = ',CA3M(INO)
C
      IF(MH.EQ.1) GO TO 1001
C
 1002 MH=MH+1
C
      IF(MH.GT.100.OR.FPR(INO).LT.0.D0) THEN
        WRITE(6,2525) MH,INO,FPR(INO)
 2525   FORMAT(/,'!!! Separation NOT Possible  !!!',/,5X,'MH = ',
     *            I3,5X,'INO = ',I3,'FP = ',E30.20)
        PRINT*,'!!! Separation NOT Possible  !!!'
        PRINT*,'FP = ',FPR(INO)
        GO TO 1988
       ELSE
      ENDIF
C
      IF(CA3C(INO).LT.0D0) CA3C(INO)=1.D-6*MH
C
      CA3M(INO)=CA3C(INO)
      CA(INO)=CA3M(INO)/CA2(INO)
      GO TO 1004
C
C ============================================================
C
C Parameters
C ----------
C
 1001 CA(INO)=CA3M(INO)/CA2(INO)
C
      XAB=R*TEMPT(INO)/DAB
C
      XA2X=CA2(INO)/CCA(1)
      CALL INTER (XA,PA,XA2X,PPI2,NCPXA,SLOPE,STATUS)
      PI2(INO)=PPI2
C
      BETA1=VIS*DAB/(TH1*TH1*PI2(INO))
C
      BETA2=PDEL(INO)/PI2(INO)
C
      BETA=TH1*TH1/(VIS*DAB)
C
      RA=BOLTZ*TEMPT(INO)/(6.D0*PI*VIS*DAB)
C
      RRATIO=RA/TH1
C
 1004 CONTINUE
```

```
C
C ----------------------------------------------
         JV(INO)=XO(INO)
         FP(INO)=YO(INO)
C ================================================================
C
C  COMPUTE ROOTS OF JACOBI POLYNOMIAL :
C  ------------------------------------
C
      CALL JCOBI(ND,N,N0,N1,AL,BE,DIF1,DIF2,DIF3,ROOT)
C
      NT=N+N0+N1
C     WRITE(6,2010) (ROOT(I),I=1,NT)
C2010 FORMAT(5X,'COLLOCATION POINTS',//,8(10X,F13.10,/))
C
C
C  SET UP DISCRETIZED SPATIAL DERIVATIVES :
C  ----------------------------------------
C
      DO 20 I=1,NT
         CALL DFORP(ND,N,N0,N1,I,1,DIF1,DIF2,DIF3,ROOT,V1)
         CALL DFORP(ND,N,N0,N1,I,2,DIF1,DIF2,DIF3,ROOT,V2)
         DO 15 J=1,NT
            A(I,J)=V1(J)
            B(I,J)=V2(J)
   15    CONTINUE
   20 CONTINUE
C
C     WRITE(6,2020)
C2020 FORMAT(//,10X,'DISCRETIZATION MATRIX FOR FIRST DERIVATIVES')
C     WRITE(6,2021)
C2021 FORMAT(7X,'***********************************************')
C
C     DO 24 I=1,NT
C        WRITE(6,2030) (A(I,J),J=1,NT)
C  24 CONTINUE
C
C2030 FORMAT(/,10(E10.4,1X))
C     WRITE(6,2040)
C2040 FORMAT(////,10X,'DISCRETIZATION MATRIX FOR SECOND DERIVATIVES')
C     WRITE(6,2041)
C2041 FORMAT(7X,'***********************************************')
C
C     DO 28 I=1,NT
C        WRITE(6,2030) (B(I,J),J=1,NT)
C  28 CONTINUE
C
C
C  MODIFY DISCRETIZED SPATIAL DERIVATIVES TO ACCOUNT FOR
C  THE BOUNDARY CONDITION AT X=1  :
C  -----------------------------------------------------
```

```
C
      DO 40 I=2,(N+1)
         DO 30 J=2,(N+1)
               A(I,J)=A(I,J)-A(I,1)*A(1,J)/A(1,1)
               B(I,J)=B(I,J)-B(I,1)*A(1,J)/A(1,1)
   30     CONTINUE
   40 CONTINUE
C
C
C  SET UP SYSTEM MATRIX 'C' :
C  -------------------------
C
      DO 60 I=2,(N+1)
        DO 50 J=2,(N+1)
           C(I,J)=B(I,J)+A(I,J)/ROOT(I)
   50     CONTINUE
   60 CONTINUE
C
C
C  INTEGRATE THE DISCRETIZED EQUATIONS IN TIME
C  USING THE ROUTINE 'LSODE'  :
C  -------------------------------------------
C
C     WRITE(6,2100)
C2100 FORMAT(///,5X,'INTEGRATION OF DISCRETIZED EQUATIONS IN',
C    1' TIME',//,5X,'USING THE ROUTINE ''LSODE''  ')
C     CALL TIMER(0)
      NY=N+1
C
      DO 101 I=1,NY
  101 Y(I)=0.01D0
C
      TIN=0.D0
      TOUT=5.D0
C
      ITOL=2
      RTOL=1.D-8
C
      REWIND 7
C
      DO 201 I=1,N
  201 ATOL(I)=1.D-6
C
      ITASK=1
      ISTATE=1
      IOPT=0
      LRW=95
      LIW=25
      MF=22
C
      DO 200 IOUT=1,1
```

```
      REWIND 7
C
C   <><><><><><><><><><><><><><><><><><><><><><><><><><><><><><><><><>
C
      PRINT*,'Calling LSODE ...'
      PRINT*,'================='
C
      CALL LSODE(FCN,NY,Y,TIN,TOUT,ITOL,RTOL,ATOL,ITASK,ISTATE,
     *           IOPT,RWORK,LRW,IWORK,LIW,FCNJ,MF)
C
      PRINT*,'Successful LSODE !!!'
      PRINT*,'===================='
C
C   <><><><><><><><><><><><><><><><><><><><><><><><><><><><><><><><><>
C
C
C  EVALUATE Y AT X=0 :
C  -------------------
C
  111 CONTINUE
C
      Y(N+2)=0.D0
      Y(1)=0.D0
      DO 1205 J=2,N+1
 1205 Y(1)=Y(1)+A(1,J)*Y(J)
      Y(1)=-Y(1)/A(1,1)
C
C     WRITE(6,2210)
C2210 FORMAT(//,5X,'SOLUTION AT COLLOCATION POINTS : ',/,3X,
C    1        '-----------------------------------',//,
C    2        10X,'X',15X,'Y',/)
C     WRITE(6,2220) (ROOT(I),Y(I),I=1,NT)
C2220 FORMAT(3X,F13.10,5X,E13.6)
C     WRITE(6,2230)
C2230 FORMAT(//,5X,'SOLUTION AT FIXED GRID POINTS : ',/,3X,
C    1        '-----------------------------------',//,
C    2        10X,'X',15X,'Y',/)
C
C     WRITE(9,2220) ROOT(1),Y(1)
C     WRITE(21,2220) ROOT(1),Y(1)
C
C
       DO 170 J=1,9
         XGRID=0.1D0*DFLOAT(J)
        CALL INTRP(ND,NT,XGRID,ROOT,DIF1,XINTP)
         YV(J)=0.D0
         DO 160 K=1,NT
  160    YV(J)=YV(J)+XINTP(K)*Y(K)
C
C        WRITE(6,2220) XGRID,YV(J)
C        WRITE(21,2220) XGRID,YV(J)
```

```
C           WRITE(9,2220) XGRID,YV(J)
C             IF(TEND.EQ.TAB(NTAB)) THEN
C                IF (XGRID.EQ.1.D-1) THEN
C                   WRITE(8,2225) ROOT(1),Y(1)
C                  ELSE
C                  ENDIF
C                  WRITE(8,2225) XGRID,YV(J)
C                ELSE
C                ENDIF
C2225 FORMAT(3X,F4.2,5X,E13.6)
C
  170 CONTINUE
C
C      WRITE(6,2220) ROOT(NT),Y(NT)
C      WRITE(21,2220) ROOT(NT),Y(NT)
C      WRITE(9,2220) ROOT(NT),Y(NT)
C      IF (TEND.EQ.TAB(NTAB)) THEN
C         WRITE(8,2225) ROOT(NT),Y(NT)
C         WRITE(8,2226)
C2226    FORMAT(3X,'99999 99999')
C       ELSE
C      ENDIF
C
C      WRITE(6,2240)
C      WRITE(9,2240)
C2240 FORMAT(5X)
C
C
  200 CONTINUE
C
C
C!!!!!!!!!!!!!!!!!!!!!!!!!!!!!!!!!!!!!!!!!!!!!!!!!!!!!!!!!!!!!!!!!!!!!!!!!!!!
C
C
      RRATIO=RA/TH1
C
      DO 169 I=1,99
          XGRID=1.D-2*DFLOAT(I)
          CALL INTRP(ND,NT,XGRID,ROOT,DIF1,XINTP)
          YV(I)=0.D0
        DO 168 J=1,NT
  168   YV(I)=YV(I)+XINTP(J)*Y(J)
          PHI(I)=(TH2/TH1)*DEXP(XGRID*XGRID*TET2)
          IF((1.D0-XGRID).LE.RRATIO) PHI(I)=50.D0
  169 CONTINUE
C
C
      RAT=100.D0*(1.D0-RRATIO)
      LAMB=IDINT(RAT)
      HINC=1.D0/LAMB
C
```

```
C       IF(HM.EQ.2) THEN
C          WRITE(6,666) RRATIO,RAT,LAMB,HINC
C 666    FORMAT(/,3X,'RRATIO = ',E20.12,/,3X,'RAT = ',E20.12,/,
C    *       3X,'LAMB = ',I4,/,3X,'HINC = ',E20.12)
C       ELSE
C       ENDIF
C
C -----------------------------------------------------------
C
      SUMN1=0.D0
      SUMN2=0.D0
      SUMD1=0.D0
      SUMD2=0.D0
C
      XA3X=CA3M(INO)/CCA(1)
      CALL INTER (XA,PA,XA2X,PPI2,NCPXA,SLOPE,STATUS)
      CALL INTER (XA,PA,XA3X,PPI3,NCPXA,SLOPE,STATUS)
        PI2(INO)=PPI2
        PI3(INO)=PPI3
C
C     PRINT*,'PI2 = ',PI2(INO)
C     PRINT*,'PI3 = ',PI3(INO)
C
      DO 167 K=1,(LAMB-3),2
          IF(PHI(K).GT.40.D0) THEN
                SUMD1=SUMD1
              ELSE
          SUMD1=SUMD1+YV(K)*(1.D-2*DFLOAT(K))*(PI2(INO)+(PI2(INO)-
     *          PI3(INO))/(DEXP(YV(K))-1.D0))*DEXP(-PHI(K))/FF
          ENDIF
  167 CONTINUE
C
C
      DO 265 K=1,97,2
          SUMN1=SUMN1+YV(K)*(1.D-2*DFLOAT(K))
  265 CONTINUE
C
C
      SUMN1=4.D0*SUMN1
      SUMD1=4.D0*SUMD1
C
C
      DO 166 K=2,(LAMB-2),2
          IF(PHI(K).GT.40.D0) THEN
                SUMD2=SUMD2
              ELSE
          SUMD2=SUMD2+YV(K)*(1.D-2*DFLOAT(K))*(PI2(INO)+(PI2(INO)-
     *          PI3(INO))/(DEXP(YV(K))-1.D0))*DEXP(-PHI(K))/FF
          ENDIF
  166 CONTINUE
C
```

```fortran
C
      DO 266 K=2,98,2
          SUMN2=SUMN2+YV(K)*(1.D-2*DFLOAT(K))
  266 CONTINUE
C.
C
      SUMN2=2.D0*SUMN2
      SUMD2=2.D0*SUMD2
C
      SUMN0=0.D0
      SUMD0=0.D0
C
      SUMN3=4.D0*YV(99)*(1.D-2*DFLOAT(99))
      SUMN4=0.D0
        IF(PHI(LAMB-1).GT.50.D0) THEN
             SUMD3=0.D0
          ELSE
      SUMD3=4.D0*YV(LAMB-1)*(1.D-2*DFLOAT(LAMB-1))*(PI2(INO)+(PI2(INO)
     *      -PI3(INO))/(DEXP(YV(LAMB-1))-1.D0))*DEXP(-PHI(LAMB-1))/FF
        ENDIF
        IF(PHI(LAMB).GT.50.D0) THEN
             SUMD4=0.D0
          ELSE
           SUMD4=YV(LAMB)*(1.D-2*DFLOAT(LAMB))*(PI2(INO)+(PI2(INO)-
     *        PI3(INO))/(DEXP(YV(LAMB))-1.D0))*DEXP(-PHI(LAMB))/FF
        ENDIF
C
C
      SUMN=SUMN0+SUMN1+SUMN2+SUMN3+SUMN4
      SUMD=SUMD0+SUMD1+SUMD2+SUMD3+SUMD4
C
C
      SUMN=SUMN*0.01D0/3.D0
      SUMD=SUMD*HINC/3.D0
C
C
      CA3C(INO)=CCA(1)/(1.D0+CCA(1)*R*TEMPT(INO)*SUMN/SUMD)
      FPR(INO)=1.D0-CA3C(INO)/CA2(INO)
C     ===============================
C
C
C     WRITE(6,163)CA3M,MH,SUMN,SUMD,FP
C 163 FORMAT(/,5X,'CA3M = ',E30.20,/,5X,'MH = ',I3,/,5X,'SUMN = ',
C    * E30.20,/,5X,'SUMD = ',E30.20,/,5X,'FP = ',E30.20)
C
C
      IF(DABS(CA3M(INO)-CA3C(INO)).GT.TOL) GO TO 1002
      F(INO)=FPR(INO)
C     ================
C
C
```

```
C     WRITE(6,1861) ROOT(1),Y(1)
C1861 FORMAT(//,9X,'r',15X,'Alpha',/,3X,31('-'),/,3X,F13.10,5X,E13.6)
C
      DO 1802 J=1,9
         XGRID=0.1D0*DFLOAT(J)
         CALL INTRP(ND,NT,XGRID,ROOT,DIF1,XINTP)
         YV(J)=0.D0
         DO 1803 K=1,NT
 1803    YV(J)=YV(J)+XINTP(K)*Y(K)
C        WRITE(6,1801) XGRID,YV(J)
 1802 CONTINUE
C
C     WRITE(6,1801) ROOT(NT),Y(NT)
C1801 FORMAT(3X,F13.10,5X,E13.6)
C
C ------------------------------------------------------------------
C
C Effective Membrane Surface Area, m.m :
C     SEFF=15.08D-04
C -------------------------------------------
C
C   -The "Permeate Flux-to-Pure Water Flux" Ratio, (NT / NP)  :
C
      RNTNP=16.D0*(BETA1/BETA2)*SUMN
C     -----------------------------
C
C Tortuosity Factor of the Membrane, m :
      TAUEPS=0.316D-04
C
C
C SW30-1:
      IF(TEMPT(INO).LE.308.15D0) APPTAU=1274.0D0
      IF(TEMPT(INO).GT.308.15D0) APPTAU=575.00D0
C
C SW30-2:
C     IF(TEMPT(INO).LE.308.15D0) APPTAU=1172.0D0
C     IF(TEMPT(INO).GT.308.15D0) APPTAU=391.70D0
C
C BW30-1:
C     IF(TEMPT(INO).LE.308.15D0) APPTAU=828.80D0
C     IF(TEMPT(INO).GT.308.15D0) APPTAU=-78.35D0
C
C BW30-2
C     IF(TEMPT(INO).LE.308.15D0) APPTAU=869.10D0
C     IF(TEMPT(INO).GT.308.15D0) APPTAU=-13.99D0
C
C
      TAUFAC1=APPTAU/R
      TAUFAC2=TAUFAC1/TEMPT(INO)-TAUFAC1/298.15D0
      TAUFAC3=DEXP(TAUFAC2)
C
```

```
      TAUEPS=TAUEPS*TAUFAC3
C
C
C      WRITE(6,6549) APPTAU,R,TAUFAC1,TAUFAC2,TAUFAC3,T,TAUEPS,TET1
C6549 FORMAT(/,20X,'APPTAU =',E30.20,/,20X,'R =',E30.20,/,20X,
C     * 'TAUFAC1 =',E30.20,/,20X,'TAUFAC2 =',E30.20,/,20X,
C     *'TAUFAC3 =',E30.20,/,20X,'T =',E30.20,/,20X,'TAUEPS =',E30.20
C     *,/,20X,'TET1 =',E30.20)
C
C Pure Solvent Permeability Coefficient, kmol/m.m.s.kPa :
      AP=CCA(1)*TH1*TH1/(8.D0*VIS*TAUEPS)
C
C Pure Solvent Permeation Flux, kmol/m.m.s :
      PN=AP*PDEL(INO)
C
C Total Permeation Flux, kmol/m.m.s :
      TN=PN*RNTNP
C
C -----------------------------------------------------------------
C
      IF(MH.GE.99.OR.FPR(INO).LT.0.D0) GO TO 2001
C
      PRINT*,'<><><><><><><><><><><><><><><><><><><><><><><><><><>'
      PRINT*,'***  GOOD NEWS !!!   CONVERGENCE ACHIEVED !!!  ***'
      PRINT*,'<><><><><><><><><><><><><><><><><><><><><><><><><><>'
C
C      WRITE(6,357) SOLUTE,IBEGIN
C 357 FORMAT(/,10X,'SOLUTE =',I2,5X,'IBEGIN =',I3)
C
C
      WRITE(6,356) INO,MH,TH1,TH2,PDEL(INO),CA2(INO),TEMPT(INO),
     *                FPR(INO),RNTNP,PN,TN
  356 FORMAT(/,/,5X,'!!!   GOOD NEWS   !!!   CONVERGENCE ',
     *'ACHIEVED   !!!',//,1X,'INO = ',I3,5X,'MH =',I1,
     *//,10X,'RW = ',E30.20,3X,'m',//,10X,'TET1 = ',E30.20,3X,'m',
     */,10X,'Pdel = ',E20.10,3X,'kPa',//,10X,'CA2 = ',E20.10,3X,
     *'kmol/m.m.m',//,10X,'T = ',E30.20,3X,'K',
     *//,10X,'f prime = ',E20.15,//,10X,'NT / NP = ',
     *E20.15,//,10X,'NP = ',E20.15,//,10X,'NT = ',E20.15,/,35('<>'))
C
C
C      WRITE(4,8888) FP(INO),PDEL(INO)
C8888 FORMAT(E20.15,3X,E7.1)
C
C2002 WRITE(6,256) CA2,RW,PDEL,FP,RNTNP
C 256 FORMAT(/,10X,'CA2 = ',E30.20,2X,'kmol/m.m.m',//,10X,'Rw = ',
C     *E30.20,2X,'m',//,10X,'PDEL = ',E10.2,2X,'kPa',//,10X,'f prime = ',
C     *E30.20,/,10X,'[n]T / [n]P = ',E20.15)
C
C      WRITE(6,1897)BETA1,BETA2,SUMN
C1897 FORMAT(/,7X,'Beta1 = ',E20.12,/,7X,'Beta2 = ',E20.12,/,
```

```
C     *         7X,'SUMN = ',E20.12,/,5X,33('-'))
C
C
 2001 CONTINUE
C
C     GO TO 8891
C
 1988 CONTINUE
C
C 120 CONTINUE
C
C     IF(IBEGIN.LT.NDAT) GO TO 8899
C
 1987 CONTINUE
C
C
      RETURN
      END
C
C ***************************************************************
C
      SUBROUTINE FCN (N,TIN,Y,YDOT)
C     --------------
C
      IMPLICIT REAL*8 (A-H,O-Z)
      REAL*8 TIN,Y,YDOT
C
      DIMENSION Y(N),YDOT(N)
      DIMENSION PHI(101)
C
      COMMON /BETAS/ BETA1,BETA2,BETA
      COMMON /AREA1/ C(5,5),ROOT(5)
      COMMON /AREA2/ RA,FF,CMOL(1)
      COMMON /THETA/ TH(2)
      COMMON /AREA3/ PDEL(90),TEMPT(90)
      COMMON /AREA4/ CA(90),CA2(90),CA3(90),CA3M(90),CA3C(90)
      COMMON /SCALE/ SCALE1,SCALE2
      COMMON /TETA1/ TET2,INO
      COMMON /PI23/  PI2(90),PI3(90)
C
      TH1=TH(1)*SCALE1
      TH2=TH(2)*SCALE2
C
      R=8.3144D0
C
C
      DO 20 I=2,N
           YDOT(I)=C(I,1)
         DO 10 J=2,N
             YDOT(I)=YDOT(I)+C(I,J)*Y(J)
   10     CONTINUE
```

```fortran
         PHI(I)=(TH2/TH1)*DEXP(ROOT(I)*ROOT(I)*TET2)
         RRATIO=RA/TH1
         IF((1.D0-ROOT(I)).LE.RRATIO) PHI(I)=50.D0
      FF=1.D0/(1.D0-2.104D0*RRATIO+2.09D0*RRATIO**3-0.95D0*RRATIO**5)
           IF(PHI(I).GT.40.D0) THEN
             YDOT(I)=YDOT(I)+BETA2/BETA1-BETA*PI2(INO)*(1.D0-CA(INO))
           ELSE
             YDOT(I)=YDOT(I)+(BETA2/BETA1)-(1.D0-DEXP(-PHI(I)))*
     *                 BETA*PI2(INO)*(1.D0-CA(INO))-BETA*PI2(INO)*
     *                 Y(I)*(1.D0-1.D0/FF)*(1.D0+(1.D0-CA(INO))/
     *                 (DEXP(Y(I))-1.D0))*DEXP(-PHI(I))
           ENDIF
   20 CONTINUE
C
      RETURN
      END
C==========================================================================
C
      SUBROUTINE FCNJ (N,TIN,Y,ML,MU,PD,NRPD)
C     ---------------
C
      IMPLICIT REAL*8 (A-H,O-Z)
      REAL*8 PD,TIN,Y
C
      DIMENSION Y(N),PD(N,N)
C
      COMMON /BETAS/ BETA1,BETA2,BETA
      COMMON /AREA1/ C(5,5),ROOT(5)
      COMMON /AREA2/ RA,FF,CMOL(1)
      COMMON /THETA/ TH(2)
      COMMON /SCALE/ SCALE1,SCALE2
C
      RETURN
      END
C==========================================================================
C
      SUBROUTINE JCOBI (ND,N,N0,N1,AL,BE,DIF1,DIF2,DIF3,ROOT)
C     ===============
C
      IMPLICIT REAL*8 (A-H,O-Z)
      DIMENSION DIF1(9),DIF2(9),DIF3(9),ROOT(9)
C
C
C EVALUATION OF ROOTS AND DERIVATIVES OF JACOBI POLYNOMIALS
C P(N) (AL,BE) ; ( MACHINE ACCURACY 16 D )
C -------------------------------------------
C FIRST EVALUATION OF COEFFICIENTS IN RECURSION FORMULAS
C RECURSION COEFFICIENTS ARE STORED IN DIF1 AND DIF2
C
C
      AB=AL+BE
```

```
      AD=BE-AL
      AP=BE*AL
      DIF1(1)=(AD/(AB+2)+1)/2
      DIF2(1)=0.
      IF (N.LT.2) GO TO 15
C
      DO 10 I=2,N
        Z1=I-1
        Z=AB+2*Z1
        DIF1(I)=(AB*AD/Z/(Z+2)+1)/2
        IF (I.NE.2) GO TO 11
        DIF2(I)=(AB+AP+Z1)/Z/Z/(Z+1)
        GO TO 10
   11   Z=Z*Z
        Y=Z1*(AB+Z1)
        Y=Y*(AP+Y)
        DIF2(I)=Y/Z/(Z-1)
   10 CONTINUE
C
C
C ROOT DETERMINATION BY NEWTON METHOD WITH SUPPRESSION
C OF PREVIOUSLY DETERMINED ROOTS
C
   15 X=0.
C
      DO 20 I=1,N
   25 XD=0.
      XN=1.
      XD1=0.
      XN1=0.
C
      DO 30 J=1,N
      XP=(DIF1(J)-X)*XN-DIF2(J)*XD
      XP1=(DIF1(J)-X)*XN1-DIF2(J)*XD1-XN
      XD=XN
      XD1=XN1
      XN=XP
   30 XN1=XP1
C
      ZC=1.
      Z=XN/XN1
      IF (I.EQ.1) GO TO 21
      DO 22 J=2,I
   22 ZC=ZC-Z/(X-ROOT(J-1))
   21 Z=Z/ZC
      X=X-Z
      IF (DABS(Z).GT.1.D-9) GO TO 25
      ROOT(I)=X
      X=X+.0001
   20 CONTINUE
C
```

```
C   ADD EVENTUAL INTERPOLATION POINTS AT X=0 OR X=1
      NT=N+N0+N1
      IF (N0.EQ.0) GO TO 35
C
      DO 31 I=1,N
      J=N+1-I
   31 ROOT(J+1)=ROOT(J)
C
      ROOT(1)=0.
   35 IF (N1.EQ.1) ROOT(NT)=1.
C
C
C   NOW EVALUATE DERIVATIVES OF POLYNOMIAL
C
      DO 40 I=1,NT
      X=ROOT(I)
      DIF1(I)=1.
      DIF2(I)=0.
      DIF3(I)=0.
      DO 40 J=1,NT
      IF (J.EQ.I) GO TO 40
      Y=X-ROOT(J)
      DIF3(I)=Y*DIF3(I)+3.*DIF2(I)
      DIF2(I)=Y*DIF2(I)+2.*DIF1(I)
      DIF1(I)=Y*DIF1(I)
   40 CONTINUE
      RETURN
      END
C
C*****************************************************************
C
      SUBROUTINE DFORP(ND,N,N0,N1,I,ID,DIF1,DIF2,DIF3,ROOT,VECT)
C     ----------------
C
      IMPLICIT REAL*8 (A-H,O-Z)
      DIMENSION DIF1(9),DIF2(9),DIF3(9),ROOT(9),VECT(9)
C
C
C   THIS SUBROUTINE EVALUATES DISCRETIZATION MATRICES AND
C   GAUSSIAN QUADRATURE WEIGHTS , NORMALIZED TO SUM 1
C   ----------------------------------------------------
C   ID = 1  :  DISCRETIZATION MATRIX FOR Y(1) (X)
C   ID = 2  :  DISCRETIZATION MATRIX FOR Y(2) (X)
C   ID = 3  :  GAUSSIAN QUADRATURE WEIGHTS
C
      NT=N+N0+N1
      IF (ID.EQ.3) GO TO 10
C
      DO 20 J=1,NT
      IF (J.NE.I) GO TO 21
      IF (ID.NE.1) GO TO 5
```

```
      VECT(I)=DIF2(I)/DIF1(I)/2
      GO TO 20
    5 VECT(I)=DIF3(I)/DIF1(I)/3
      GO TO 20
   21 Y=ROOT(I)-ROOT(J)
      VECT(J)=DIF1(I)/DIF1(J)/Y
      IF (ID.EQ.2) VECT(J)=VECT(J)*(DIF2(I)/DIF1(I)-2/Y)
   20 CONTINUE
C
      GO TO 50
C
   10 Y=0.
      DO 25 J=1,NT
      X=ROOT(J)
      AX=X*(1-X)
      IF (N0.EQ.0) AX=AX/X/X
      IF (N1.EQ.0) AX=AX/(1-X)/(1-X)
      VECT(J)=AX/DIF1(J)**2
   25 Y=Y+VECT(J)
C
      DO 60 J=1,NT
   60 VECT(J)=VECT(J)/Y
   50 RETURN
      END
C
C*************************************************************
C
      SUBROUTINE INTER(ND,NT,X,ROOT,DIF1,XINTP)
C
      IMPLICIT REAL*8 (A-H,O-Z)
      DIMENSION ROOT(9),DIF1(9),XINTP(9)
C
C
C  EVALUATION OF LAGRANGIAN INTERPOLATION COEFFICIENTS
C  ----------------------------------------------------
      POL=1.
      DO 5 I=1,NT
      Y=X-ROOT(I)
      XINTP(I)=0.
      IF (Y.EQ.0.D0) XINTP(I)=1.
    5 POL=POL*Y
      IF (POL.EQ.0.D0) GO TO 10
      DO 6 I=1,NT
    6 XINTP(I)=POL/DIF1(I)/(X-ROOT(I))
   10 RETURN
      END
C
C.........................................................
```